Ambisonics
(Acoustic Holography and Holophony)

Dr Franz Zotter, Dr Matthias Frank

Graz, February 2, 2017

institut für elektronische musik und akustik

Abstract

What is the audible result of driving several, spherically arranged loudspeakers with amplitude-weighted signals? Which perceived directions, loudnesses, auditory source widths, perceived changes in sound color will there be?

How do we obtain simple predictions of what the audible properties will be like?

How could we formulate mathematically the invariances that desire concerning perceived loudness, auditory source width, accuracy of perceived direction through Ambisonic panning functions? (trigonometric functions for ideal loudspeaker arrangements on the circle, or spherical harmonics for ideal loudspeaker arrangements on the sphere.)? Is the result congruent with our expectations?

How successfully will things turn out on hemispherical loudspeaker arrangements? What is the secret and purpose of separating the encoding and decoding steps, and how does this provide an Ambisonic multi-channel format that makes playback a decent bit independent of the production or recording?

How does the Ambisonic recording technology (spherical arrays, tetrahedral arrays of microphones) work?

Which effects are there in applications to produce Ambisonic audio material?

The IKO is a sound projection instrument. Is it Ambisonic and how does it work?

How do we measure 5D room impulse responses?

How doe we obtain holographic sound images of musical instruments and which kind of information do they contain?

How does acoustical holography and sound field synthesis work in general? What is the Kirchhoff-Helmholtz integal equation, and how far does it bring us when we try to derive Ambisonics, wave field synthesis, planar far and near field holography on its basis? Why does the discrete spatial Fourier transform accross two spatial axes correspond to directions of propagating sound in space, and how? What is a Rayleigh integral?

Why is it necessary for both surrounding spherical microphone or loudspeaker arrays to be open arrays, whereas for both the excitation of exterior sound fields or for the recording of interior fields it seems that rigid spherical surfaces are necessary?

Contents

1 Auditory events of loudspeaker playback

The dedicated goal of amplitude panning is the control of sound impressions in freely adjustable directions using just a few loudspeakers, as known from two-channel stereophony.

However, it would too small a requirement and insufficient, to just desire a well-controllable perceived direction. Of course, sounds should also be largely stay unchanged when undergoing this kind of control. Change should neither affect loudness, spectrum, temporal structure, nor the perceived width of the sound (auditory source width). All variations in these aspects should stay as small as possible during motion of the panning direction.

Which properties does our perception yield considering these aspects?

1.1 Loudness

At a measurement point in the free field, the same signal fed to equalized loudspeakers of exactly the same acoustic distance would superimpose constructively ($+6$ dB).

In a room with early reflections and a less strict equality of the incoming pair of sounds (inaccurate loudspeaker positioning, different mounting situations, different directions in the directivities of ears and loudspeakers), the superposition can be regarded as stochastically constructive, only ($+3$ dB), in particular at frequencies that aren't very low.

For the above reasoning, typical amplitude panning rules try to keep the weights to distribute a signal to the loudspeakers normalized by root of squares instead of normalizing to the linear sum, in order to obtain constant loudness ([Pul97], VBAP):

$$g_l = \frac{g_l}{\sqrt{\sum_{l=1}^{\mathrm{L}} g_l^2}}. \tag{1}$$

1.2 Perceived direction

In the early ages of stereophony researchers investigated the differences in delay times and amplitudes required to gain control of the perceived direction. Below, only such research examples are considered that did not use fixation of the listeners head.

1.2.1 Time differences on horizontal $\pm 30^\circ$ front loudspeaker pair

The dissertation of K. Wendt in 1963 [Wen63] shows notably accurate listening experiments done on $\pm 30^\circ$ two-channel stereophny using time delays, in which listeners indicated from where they heard the sounds for each of the tested time differences. H. Lee revisited the properties in 2013 [LR13], but with musical sound material and an experiment, in which the listener adjusted the time differences until they could match the perceived direction to the one of a corresponding reference loudspeaker, Fig. 1.

The time differences are seldom used for auditory event placement: auditory imags are strongly frequency-dependent (not shown here) and therefore unstable with narrow-band

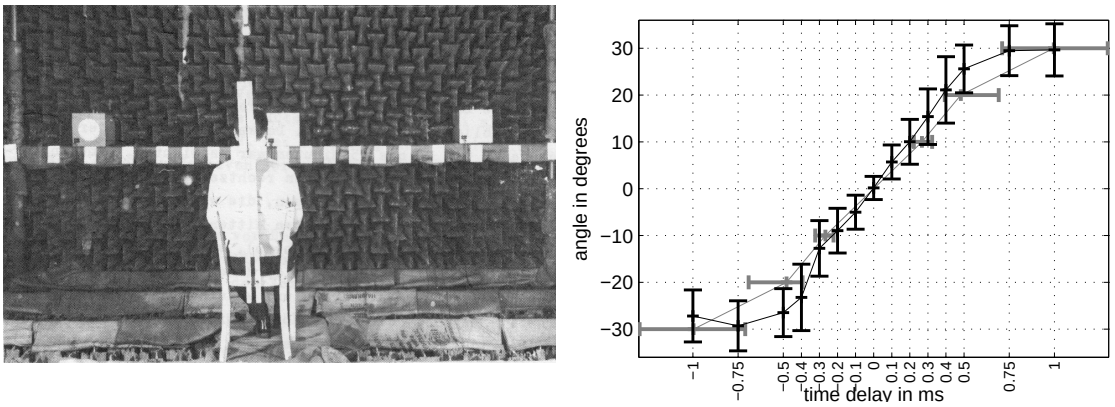

Figure 1 – K. Wendts experiment [Wen63] using an angular scale to read off, and the results for time differences between the loudspeakers using impulse signals, without head fixation (standard deviation was interpolated for this figure). In gray: Results of the time-difference adjustment experiment of Lee [LR13] using musical material (25%,50%,75% quartiles, symmetrized diagram).

sounds. Leakey and Cherry showed 1957 [LC57] that time delay stereophony looses its effect under the presence of background noise.

1.2.2 Level differences on horizontal $\pm 30°$ front loudspeaker pair

K. Wendt's [Wen63] and H. Lee's [LR13] experiments again deliver insights in sound source positioning with $\pm 30°$ two-channel stereophony, however this time with level differences.

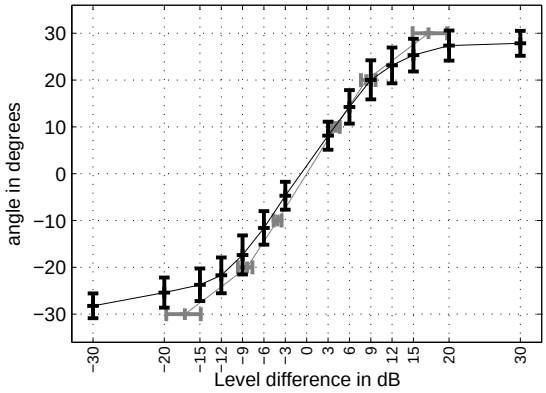

Figure 2 – Wendt's [Wen63] results to crack (impulsive) signals with level differences and without head fixation (standard deviation interpolate for this illustration). In gray: Results of Lee's [LR13] level-difference adjustment exeperiment with musical sounds (25%,50%,75% quartiles, symmetrized diagram).

As opposed to Figure 1, in which auditory image panning with time differences were characterized by statistical spreads of up to $15°$, level-difference-based panning is clearly smaller in the spread of perceived directions than $10°$, Fig. 2.

1.2.3 Level differences on horizontally surrounding loudspeaker pairs

A pairwise control of neighboring loudspeakers is useful for panning auditory events along the horizon.

As shown in Appendix A, the classical research done specifically targeted at such applications was contributed by Theile und Plenge 1977 [TP77]. They used a mobile reference loudspeaker with some reference sound that could be moved to match the perceived direction of a loudspeaker pair playing pink noise with level differences at different orientations with respect to the listener's head. There is also the experiment of Pulkki [Pul03] usign level-adjustment task, in which levels were adjusted as to match the auditory event to one of a reference loudspeaker for three reference loudspeaker directions and several head orientations. A comprehensive experiment was done by Simon et al. [SMR09], who used a graphical user interface displaying the floorplan of a $0° + k \cdot 45°$-loudspeaker ring to have the listeners specify the perceived direction, the experiment of Martin et al. in 1999 [MWCQ99] used a graphical user interface showing the floorplan of a 5.1 ring, and last but not least, Matthias Frank investigated this as a part of one experiment in his PhD thesis using a direct pointing method to enter the preceived direction [Fra13b], see Fig. 47.

As all these classical experiments were not able to give a consistent result that could easily be summarized, also methodically, in 2015 Zotter undertook a level-difference adjustment experiment with 24 la arranged as a horizontal ring [ZF15]. In the experiment, each thinkable loudspeaker pair was used that enclosed at least 1, 2, or 3 loudspeakers between that served as reference directions to play a reference sound for each of which the level difference was adjusted by the listeners to move the auditory event to the respective reference direction. The level adjustment task used amplitude-panned pink noise with pulsed envelope and the reference sound was a complex of sinusoids to avoid adjustments by similar coloration.

From the sum of the experiments in Fig. 3 and 47 it becomes obvious that the auditory event for equal levels is not necessarily the middle of the loudspeaker pair. For lateral loudspeaker pairs, such auditory rather appear shifted towards the front. Also the slope of the curves increase at the sides, so that for lateral loudspeaker pairs smaller changes of the level difference are sufficient to modify the direction of the resulting auditory event.

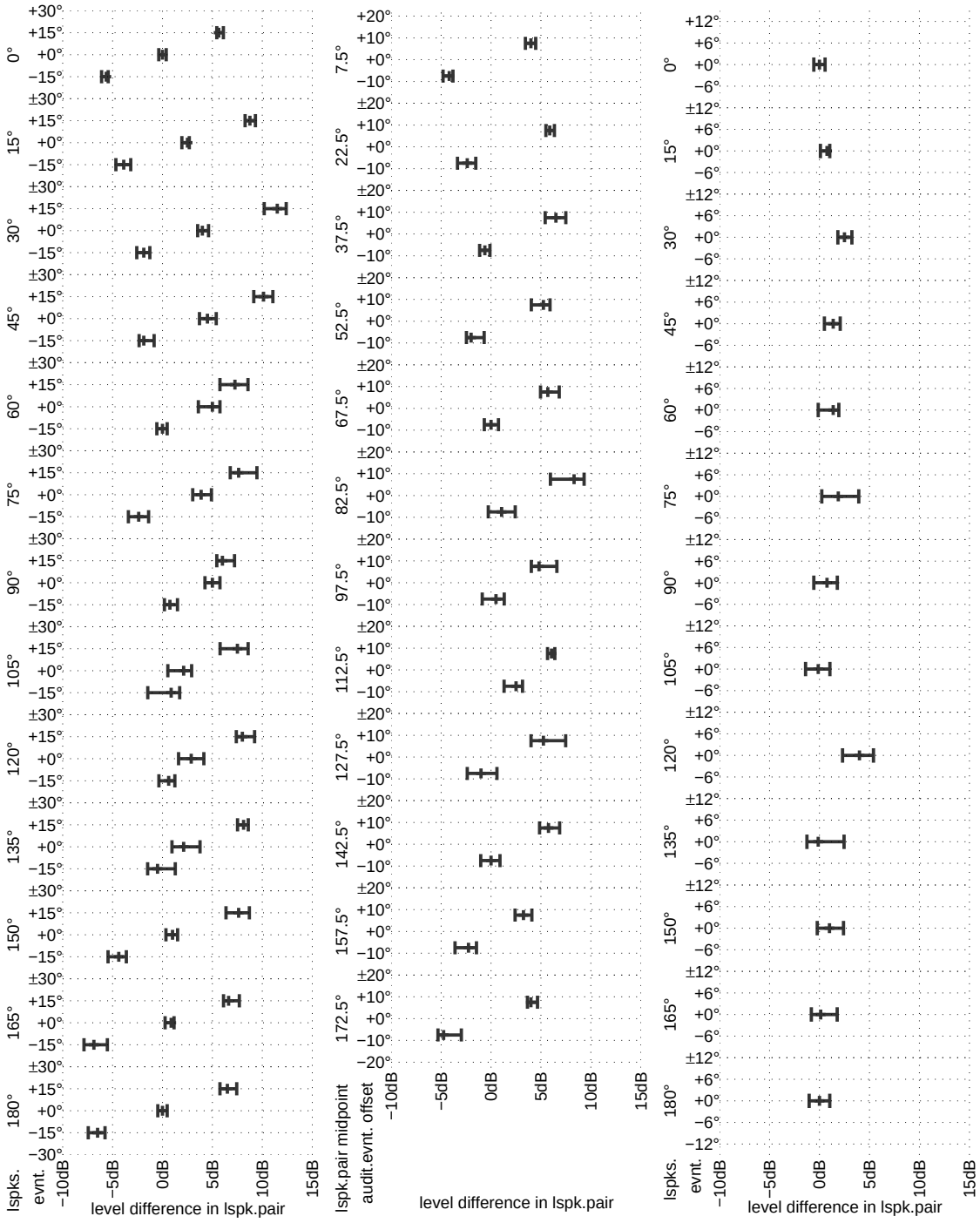

Figure 3 – Level-difference adjustment experiment presented at ICSA 2015 [ZF15] used each loudpeaker pair enclosing at least 1, 2, or 3 loudspeakers, within a 24-channel ring arrangement, and the enclosed loudspeakers served as reference directions. Loudspeaker pairs of $\pm 30°$, $\pm 22.5°$, $\pm 15°$ were used in any $15°$ orientation relative to the look direction.

1.2.4 Level differences on frontal loudspeaker pairs, horizontal to vertical

Quite extensively, T. Kimura investiates the localization of auditory events between frontal, vertical $\pm 13.5^\circ$ loudspeaker pairs in 2012 [KA12, KA14]. The work of F. Wendt in 2013 [Wen13, WFZ13] also investigates a slant and vertical loudspeaker pair, Fig. 4. Kimura uses pulsed white, Wendt uses pulsed pink noise.

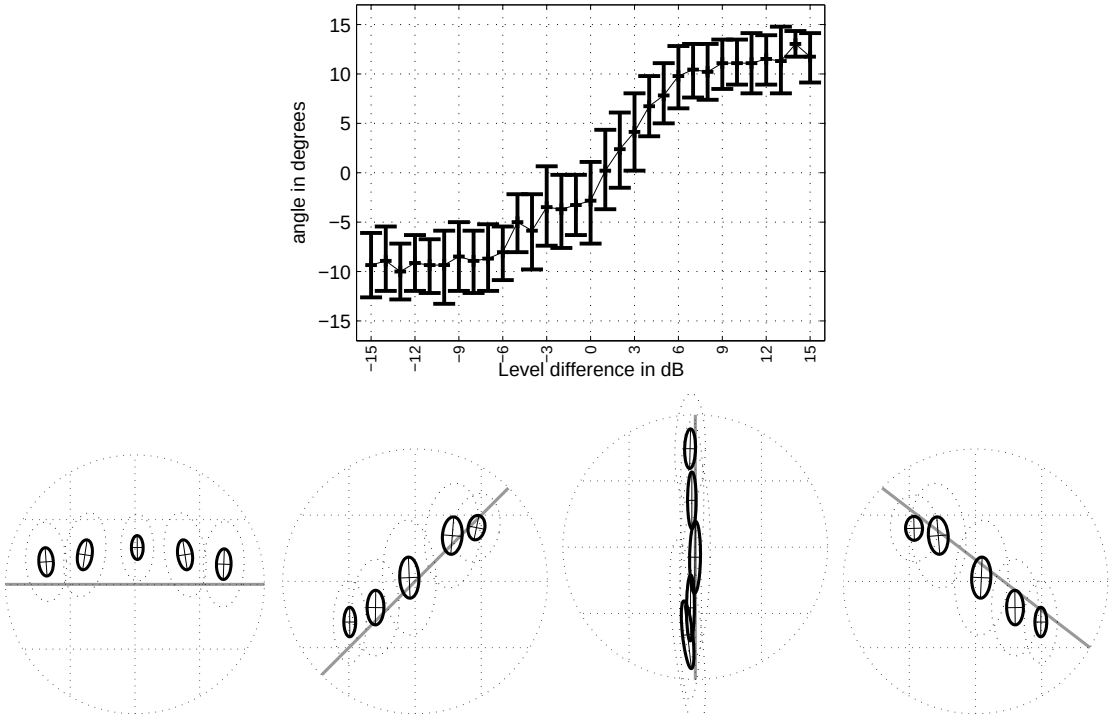

Figure 4 – Mean values and 95% confidence intervals of the direct-pointing experiments of Kimura (top) with level differences on a vertical $\pm 13.5^\circ$ loudspeaker pair and results of F. Wendt (bottom) on frontally arranged horizontal, slant, and vertical $\pm 20^\circ$ luodspeaker pairs showing two-dimensional 95% confidence (solid) and standard deviation ellipses (dotted).

Obviously, the horizontal spread is always smaller than the vertical spread and the spread does not align with the direction of the loudspeaker pair. The largest vertical spread appears for the vertical loudspeaker pair.

1.2.5 Frontal loudspeaker triangles

V. Pulkki [Pul01] and F. Wendt [Wen13, WFZ13] investigated localization properties for frontal loudspeaker triplets with level differences, see Fig. 5. Both used pulsed pink noise in their experiments. While V. Pulkki used an indirect adjustment task to evaluate VBAP

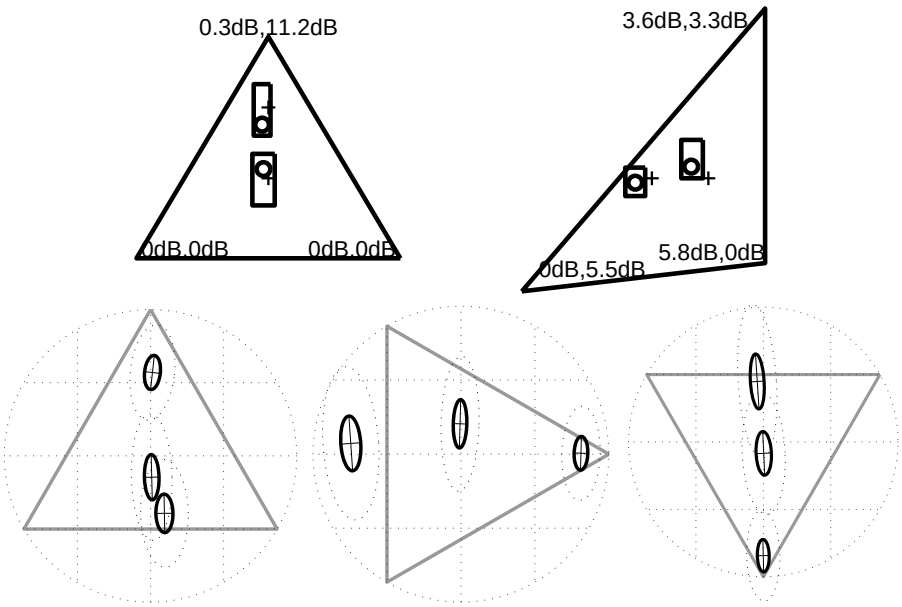

Figure 5 – Indirect level-adjustment experiment of Pulkki [Pul01] shows the spread and mean of the adjusted VBAP angles for frontal loudspeaker triplets, adn the experiments of F. Wendt [Wen13, WFZ13] use a direct pointing method to obtain results in the shape of two-dimensional 95% confidence (solid) and standard deviation ellipses (dotted)for $\{-\infty,\, 0,\, +11.71\}$ dB for the top loudspeaker (left diagram), or the right loudspeaker (center diagram) respectively, or $\{-\infty,\, 0,\, +11.51\}$ dB for the bottom loudspeaekr (right).

control angles to obtain auditory events directioally matching the respective reference loudspeakers, F. Wendt uses a direct pointing method.

Wendt's experiments indicate that loudspeaker triplets with three different azimuthal positions yield a smaller spread in the indicated direction than such with vertical loudspeaker pairs (not the case in Pulkki's experiments).

1.2.6 Frontal loudspeaker rectangles

F. Wendt [Wen13, WFZ13] moreover presents experiments about frontal loudspeaker rectangles, again using a pointer method and pulsed pink noise, Fig. 6.

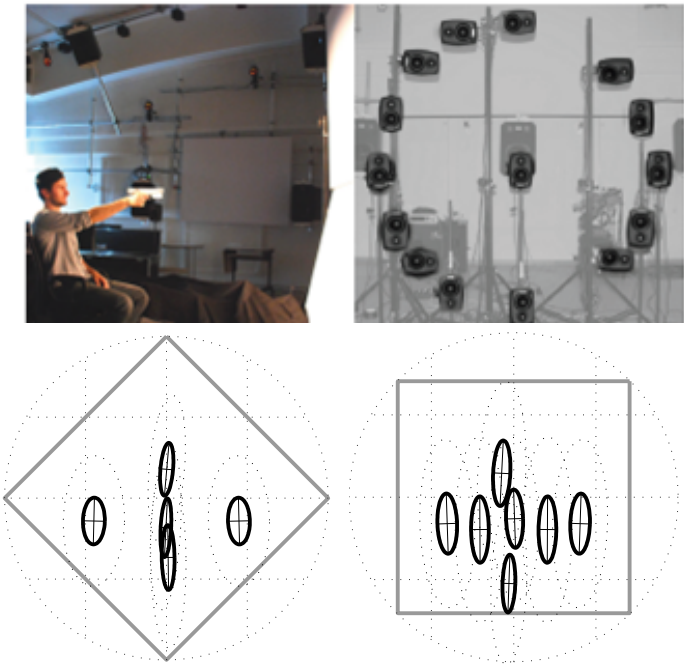

Figure 6 – Wendt's experiments about frontal loudspeaker rectangles showing two-dimensional 95% confidence (solid) and standard deviation ellipses (dotted). The experimental setup of this and above-mentioned experiments is shown. Left: each of the corner loudspeakers is raised once by $+6$ dB in level, right: both left/right loudspeaker levels are raised once by $\{+3, +6\}$ dB, and both top/bottom pairs are once raised by $+6$ dB.

Again it seems that arrangements avoiding vertical loudspeaker pairs exhibit a smaller statistical spread in the responses.

1.3 Width of two or three frontal loudpeakers on the horizon

M. Frank [Fra13b] investigated the auditory source width for frontaler loudspeaker pairs with 0 dB level difference and various aperture angles, as well as the influence of an additional center loudspeaker on the auditory source width. The response was given by reading numbers off a left-right symmetric scale written on the loudspeaker arrangement.

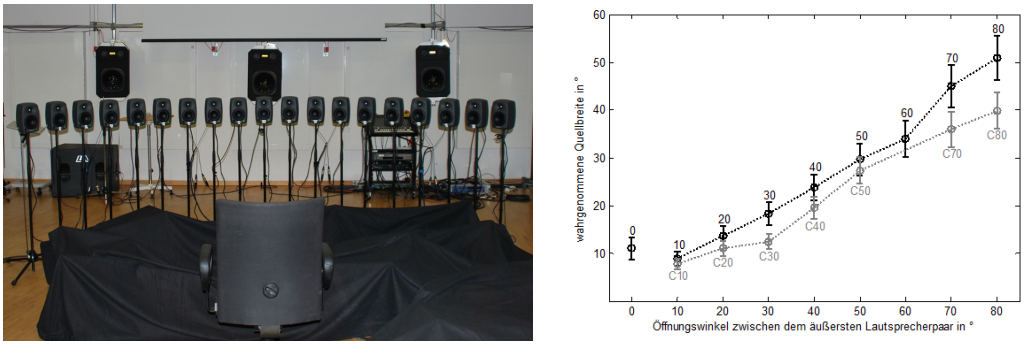

Figure 7 – Experimental setup and results of experiments of M. Frank (confidence intervals) about auditory source width of frontal stereo pairs of the angles $\pm 5°, \ldots, \pm 40°$ and with an additional center loudspeaerk (C).

Obviously the additional center loudspeaker decreases the auditory source width clearly.

Auditory source with is difficult to compare for different directions and also single loudspeakers yield auditory source widths that vary with direction. Anyway, for moving auditory events, a relatively constant auditory source width is desirable. For static auditory events, often the narrowest-possible extent is desirable.

1.4 Number of active loudspeakers and coloration

Loudspeakers in a studio or performance space are often characterized by different colorations that are caused by different reflection patterns (most often the back wall behind the loudspeaker). When changing the active loudspeakers, or their number, these differences become audible.

Despite it is unfavorable to play back with many loudspeakers activated with the same level, because this can, e.g., yield in-head localization or annoying phasing effects, it is anyway beneficial to activate always a few loudspeaker to stabilize the coloration, as opposed to using just one loudspeaker and moving the playback to another one.

Far less pronounced, but in some cases relevant: the auditory source width also changes with a varying number of active loudspeakers when panning to a different direction.

2 Model of loudness, direction, width

2.1 Loudness

If each of the loudspeakers is dirven with the same signal, located equidistantly to the receiver, and equalized, but weighted with differently in amplitude by g_l, so a constructive interference could be assumed so that the amplitude becomes [Ger92]

$$P = \sum_{l=1}^{\mathrm{L}} g_l. \tag{2}$$

However, the interference stops to be strictly constructive as soon as the room is not entirely anechoic, the seating position is not exactly centered, or even for anechoic and centered conditions at high frequencies, when the superposition at the ears cannot be assumed to be purely constructive anymore. Then it is better to assume a less well-defined, stochastic superposition in which the squared amplitude is determiend by the squares of the weights [Ger92]:

$$E = \sum_{l=1}^{\mathrm{L}} g_l^2. \tag{3}$$

Therefore, the most common amplitude panning rules use RMS-normalized gains to obtain a loudness impression that is as constant as possible.

2.2 Vector models for horizontal loudspeaker pairs

A weighted sum of the loudspeakers direction vectors $\boldsymbol{\theta}_1$, $\boldsymbol{\theta}_2$ could be conceived as simple linear model of the perceived direction, using a linear blending parameter $0 \le q \le 1$

$$\boldsymbol{r} = (1-q)\,\boldsymbol{\theta}_1 + q\,\boldsymbol{\theta}_2. \tag{4}$$

The parameter q adjust where the resulting vector $\boldsymbol{r}$ is located on the connecting line between $\boldsymbol{\theta}_1$ and $\boldsymbol{\theta}_2$. On frontal loudspeaker pairs, localization curves typically run through the middle direction $q = \frac{1}{2}$ for level differences of 0 dB. If only one loudspeakers is active, the result is either of the loudspeaker directions, thus the parameter is $q = 0$ or $q = 1$.

Classical definitions. As the simplest choice for q, one could insert $q = \frac{g_2}{g_1+g_2}$ or $q = \frac{g_2^2}{g_1^2+g_2^2}$ to get the vector definitions according to [Ger92]:

$$\boldsymbol{r}_{\mathrm{V}} = \frac{g_1\,\boldsymbol{\theta}_1 + g_2\,\boldsymbol{\theta}_2}{g_1+g_2}, \qquad \boldsymbol{r}_{\mathrm{E}} = \frac{g_1^2\,\boldsymbol{\theta}_1 + g_1^2\,\boldsymbol{\theta}_1}{g_1^2+g_2^2}. \tag{5}$$

For both models, equal gains $g_1 = g_2$ yield $q = \frac{1}{2}$, and also the endpoints with $g_2 = 0$ or $g_1 = 0$ correspond to $q = 0$ or $q = 1$, respectively. However, the slope of the $\boldsymbol{r}_{\mathrm{E}}$ vector is

steeper than the one of the $\boldsymbol{r}_\mathrm{V}$. For instance, if $g_2 = 2\,g_1$, the vector $\boldsymbol{r}_\mathrm{V}$ lies on $q = 2/3$ of the line between $\boldsymbol{\theta}_1$ and $\boldsymbol{\theta}_2$, while $\boldsymbol{r}_\mathrm{E}$ lies at $q = 4/5$ of the connecting line.

The $\boldsymbol{r}_V$ vector for the $\pm\alpha$ loudspeaker pair at the directions $\boldsymbol{\theta}_{1,2}^\mathrm{T} = (\cos\alpha, \pm\sin\alpha)$ corresponds to the tangent law [CDV58], whose formal origin lies in a model of a summing localization based on a simple model of the ear signals, cf. Appendix B. The equivalence of this law to the vector model follows from the tangent $\tan\varphi$ as ratio of y divided by x component of the $\boldsymbol{r}_V$ vector, $\tan\varphi = \frac{g_1\,\sin(\alpha)+g_2\,\sin(-\alpha)}{g_1\,\cos(\alpha)+g_2\,\cos(\alpha)} = \frac{g_1-g_2}{g_1+g_2}\tan\alpha$.

Possible refinements. The increased slope of lateral loudspeaker pairs in Fig. 3 can be modeled by increasing the exponent $q = \frac{g_2^\gamma}{g_1^\gamma+g_2^\gamma}$ yielding $\tan\varphi = \frac{g_1^\gamma-g_2^\gamma}{g_1^\gamma+g_2^\gamma}\tan\alpha$, cf. [ZF15]. Moreover, a shift of the localization curve to the front can be involved by reinforcing the frontal loudspeaker with a weight $w > 1$, e.g. using $q = \frac{g_2^\gamma}{w\,g_1^\gamma+g_2^\gamma}$, cf. [Pul03, Fra13b].

Both strategies were involed in [ZF15] to arrive at this form

$$\boldsymbol{r}_\gamma^w = \frac{(g_1\,w(\boldsymbol{\theta}_1))^\gamma\,\boldsymbol{\theta}_1 + (g_2\,w(\boldsymbol{\theta}_2))^\gamma\,\boldsymbol{\theta}_2}{(g_1\,w(\boldsymbol{\theta}_1))^\gamma + (g_2\,w(\boldsymbol{\theta}_2))^\gamma}, \tag{6}$$

which corresponds to a generalized tangent law

$$\tan\varphi = \frac{(g_1\,w(\boldsymbol{\theta}_1))^\gamma - (g_2\,w(\boldsymbol{\theta}_2))^\gamma}{(g_1\,w(\boldsymbol{\theta}_1))^\gamma + (g_2\,w(\boldsymbol{\theta}_2))^\gamma}\tan\alpha \tag{7}$$

involving a frontal directivity $w(\varphi) = -4.8 + 4.2\cos\varphi + 0.3\cos 2\varphi + 0.3\cos 3\varphi$ in dB and an increased exponent for lateral middle directions $\gamma(\varphi_\mathrm{mid}) = 2 - \frac{1}{\sqrt{2}}\cos(2\varphi_\mathrm{mid})$.

2.3 Vector model for more than 2 loudspeakers

For more than two active loudspeakers and in 3D, a vector model with varying exponents would be problematic and unstable. It is therefore more reasonable to choose the average exponent $\overline{\gamma} = 2$ to arrive at a weighted $\boldsymbol{r}_\mathrm{E}$ vector

$$\boldsymbol{r}_\mathrm{E} = \frac{\sum_{l=1}^\mathrm{L} g_l^2\,\boldsymbol{\theta}_l}{\sum_{l=1}^\mathrm{L} g_l^2}, \qquad \text{or} \qquad \boldsymbol{r}_\mathrm{E}^w = \frac{\sum_{l=1}^\mathrm{L}(g_l\,w(\boldsymbol{\theta}_l))^2\,\boldsymbol{\theta}_l}{\sum_{l=1}^\mathrm{L}(g_l\,w(\boldsymbol{\theta}_l))^2}. \tag{8}$$

These models were excellent in modeling the perceived direction in the listening experiments of Frank's thesis [Fra13b].

2.4 Model of the perceived width

The following estimator of the width can be interpreted geometrially: The expression $2\arccos\|\boldsymbol{r}_\mathrm{E}\|$ can be seen as aperture angle of a cap cut off the unit sphere at a plane with the distance $\|\boldsymbol{r}_\mathrm{E}\|$ from the origin. The $\boldsymbol{r}_\mathrm{E}$ vector can achive the length 1 at most. A width of 0° is therefore only achievable if exactly one louspeaker is active.

In the experiments of M. Frank [Fra13b, Fra13a] about the auditory source width, stereo pairs of large half angle α were heard as wider. The length of the $\boldsymbol{r}_\mathrm{E}$ vector gets shorter with the half angle α. In a symmetrical loudspeaker pair $\boldsymbol{\theta}_{12}^\mathrm{T} = (\cos\alpha, \pm\sin\alpha)$ with $g_1 = g_2 = 1$, the y coordinate of the $\boldsymbol{r}_\mathrm{E}$ vector cancels and its length becomes

$$\|\boldsymbol{r}_\mathrm{E}\| = r_\mathrm{E,x} = \cos\alpha.$$

The corresponding spherical cap is of the same size as the loudspeaker pair $2\arccos\|\boldsymbol{r}_\mathrm{E}\| = 2\alpha$. However, only $\frac{5}{8}$ of this size was indicated by the listeners of the experiments, which yields to the following estimator of the perceived width :

$$W = \tfrac{5}{8}\cdot\tfrac{180^\circ}{\pi}\cdot 2\arccos\|\boldsymbol{r}_\mathrm{E}\|. \tag{9}$$

With the additional center loudspeaker $g_3 = 1$, $\boldsymbol{\theta}^\mathrm{T} = (1, 0)$ in the listening experiment, this estimator woudl be

$$\|\boldsymbol{r}_\mathrm{E}\| = r_\mathrm{E,x} = \frac{1}{3} + \frac{2}{3}\cos\alpha,$$

which is consistent and also yields a smaller value for W, as $\arccos\|\boldsymbol{r}_\mathrm{E}\| < \alpha$.

3 Amplitude panning using vector bases

3.1 VBAP

Assuming the $\boldsymbol{r}_\mathrm{V}$ model to predict the perceived direction, an intended auditory event at a panning direction $\boldsymbol{\theta}$, we call it the *virtual source*, can theoretically be created by the criterion according to V. Pulkki [Pul97]

$$\boldsymbol{\theta} = \sum_{l=1}^{\mathrm{L}} \tilde{g}_l \, \boldsymbol{\Theta}_l.$$

Here, $\boldsymbol{\Theta}_l$ are the direction vectors of the loudspeakers involved and the amplitude weights $\tilde{g}_l$ need to be normalized for constant loudness

$$g_l = \frac{\tilde{g}_l}{\sqrt{\sum_{l=1}^{\mathrm{L}} \tilde{g}_l^2}}.$$

Moreover, the weights g_l should always stay positive to avoid in-head localization or other annoying listening experiences. For loudspeaker arrangements along the horizon, always $1 \ldots 2$ loudspeakers will be contributing to the auditory event, for loudspeakers arranged in a sphere, always $1 \ldots 3$ loudspeakers will be used, whose directions must enclose the direction of the desired auditory event, the virtal source. For the diretional stability of the auditory event, the angle enclosed between the loudspeakers should stay smaller than $90°$.

The system of equations for Vector-Base Amplitude Panning [Pul97] using 3 loudspeakers is denoted as

$$\boldsymbol{\theta} = [\boldsymbol{\Theta}_1,\, \boldsymbol{\Theta}_2,\, \boldsymbol{\Theta}_3] \begin{bmatrix} \tilde{g}_1 \\ \tilde{g}_2 \\ \tilde{g}_3 \end{bmatrix} = \mathbf{L} \cdot \tilde{\boldsymbol{g}} \qquad \Rightarrow \tilde{\boldsymbol{g}} = \mathbf{L}^{-1}\, \boldsymbol{\theta}, \qquad \boldsymbol{g} = \frac{\tilde{\boldsymbol{g}}}{\|\tilde{\boldsymbol{g}}\|}. \tag{10}$$

The selection of the loudspeakers involved in creating the auditory event at the direction $\boldsymbol{\theta}$ is dony via forming the loudspeaker triplets of a convex hull spread by all given playback loudspeakers. To find the correct triplet, the list of all triplets is being searched for the one with all-positive weights, $\tilde{g}_1 \geq 0$, $g_2 \geq 0$, $g_3 \geq 0$.

3.2 VBIP

With nearly the same set of equations, but for the squares of the weights, the auditory event can be controlled corresponding to the direction of the $\boldsymbol{r}_\mathrm{E}$ vector

$$\boldsymbol{\theta} = [\boldsymbol{\Theta}_1,\, \boldsymbol{\Theta}_2,\, \boldsymbol{\Theta}_3] \begin{bmatrix} \tilde{g}_1^2 \\ \tilde{g}_2^2 \\ \tilde{g}_3^2 \end{bmatrix} = \mathbf{L} \cdot \tilde{\boldsymbol{g}}_\mathrm{sq} \;\; \Rightarrow \tilde{\boldsymbol{g}}_\mathrm{sq} = \mathbf{L}^{-1}\, \boldsymbol{\theta}, \;\; \tilde{\boldsymbol{g}} = \begin{bmatrix} \sqrt{\tilde{g}_\mathrm{sq1}} \\ \sqrt{\tilde{g}_\mathrm{sq2}} \\ \sqrt{\tilde{g}_\mathrm{sq3}} \end{bmatrix}, \;\; \boldsymbol{g} = \frac{\tilde{\boldsymbol{g}}}{\|\tilde{\boldsymbol{g}}\|}. \tag{11}$$

This formulation might appears more contemporary due to the excellent match of the $\boldsymbol{r}_\mathrm{E}$ model to predict experimental results of Frank [Fra13b, Fra14b].

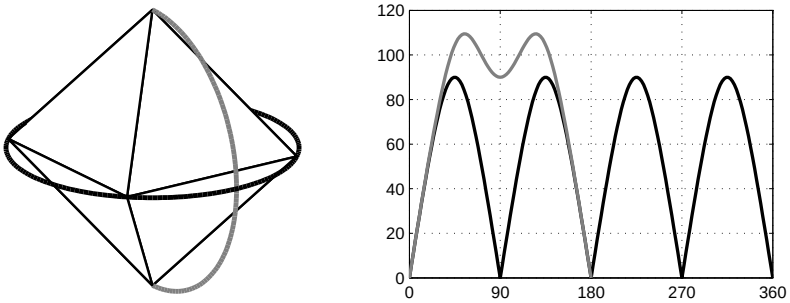

Figure 8 – The width measure $2\arccos\|\boldsymbol{r}_\mathrm{E}\|$ for a virtual source on a horizontal and a vertical trajectory ($45°$ azimuth) using VBAP on an octahedral arrangement.

3.3 MDAP

If one of the loudspeakers is exactly aligned with the virtual source for either VBAP or VBIP, e.g. $\vartheta_1 = \boldsymbol{\theta}$, the resulting gains are $g_{1,2,3} = (1, 0, 0)$, and therefore only 1 loudspeaker will be activated. For a virtual source between the 2 loudspeakers, e.g. $\vartheta_1 + \vartheta_2 \propto \boldsymbol{\theta}$, then we obtain $g_{1,2,3} = (1, 1, 0)/\sqrt{2}$, and hereby only 2 loudspekers will be active. This behavior in particular yields audible variation in the perceived width and coloration. For virtual source movements that cross a common edge of neighboring loudspeaker triplets, there will often be unexpectedly intense jumps that are quite pronounced.

Fig. 8 illustrates the variation of the perceived width with VBAP on an octahedral arrangements of loudspeakers in the directions $\vartheta_l^\mathrm{T} \in \{[\pm1, 0, 0], [0, \pm1, 0], [0, 0, \pm1]\}$.

In order to adjust the $\boldsymbol{r}_\mathrm{E}$ or $\boldsymbol{r}_\mathrm{V}$ vector not only directionally but also in length, and thus to control the number of active loudspeakers for moving sound objects, Pulkki extended VBAP to multi-direction amplitude panning (MDAP [Pul99]). Hereby not only the perceived width but also the coloration can be held constant.

MDAP uses several virtual source directions instead of just one, in a fixed constellation around the intended direction of the auditory event. For horizontal loudspeaker rings, this

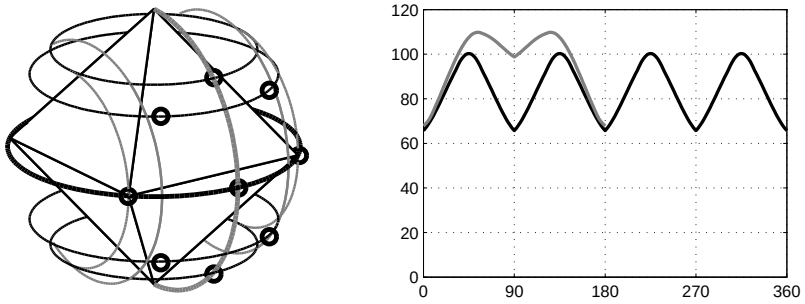

Figure 9 – The width measure $2\arccos\|\boldsymbol{r}_\mathrm{E}\|$ for virtual sources on a horizontal and vertical path on an octahedron setup using MDAP with additional 8 half-amplitude virtual sources at $45°$ distance to the main virtual source.

is an arrangement of equally loud virtual sources distributed on the interval $[\varphi-\alpha;\varphi+\alpha]$, e.g., at three positions $\varphi-\alpha$, φ, $\varphi+\alpha$. For more arbitrary loudspeaker 3D arrangements, this could be a ring-like arrangement of virtual sources, see Fig. 9. This ring arrangement uses 8 additional virtual sources in a 45° angle wrt. the main virtual source.

At least mathematically, however, it requires to post optimize the amplitudes and angles of the virtual sources in order to accurately match the desired $\boldsymbol{r}_\mathrm{V}$ or vector in direction and length, as discussed in [EJZ14]. Primarily, this is caused by the fact that $\boldsymbol{r}_\mathrm{V}$ vectors resulting individually from of the virtual sources involved match in direction, but not in length. Their resultant superposition therefore gets distorted towards those virtual source directions with the longest $\boldsymbol{r}_\mathrm{V}$ vectors. Epain's article [EJZ14] therfore proposes a non-linear optimization to finds the optimal orientation and weighting of the vritual sources involved, for any panning angle.

3.4 Loudspeaker rectangles and large holes

Surrounding loudspeaker hemispheres typically exhibit the following two problems, in most cases:

- Loudspeaker rectangles at the sides of standard setups (ITU-R BS.2051-0) with height can be decomposed ambiguously into triangles at the sides, back, and top. This yields causes there being a characteristic direction in which auditory events are just created by two of the loudspeakers.
- Signals of virtual sources below the horizon usually get lost.

The problem of the unfavorable or ambiguous triangulations into loudspeaker triplets appears subtle, however, it can cause clearly audible deficiencies. Above all, when ambiguous triangulation yield unsymmetric behavior between left and right, e.g., for the top, rear, and lateral directions, see [RFZN16].

As surrounding loudspeaker hemispheres are typically open by 180° towards below, VBAP/ VBIP/ MDAP is numerically unstable and theoretically useless for any panning direction below. Despite, not having any loudspeakers below the horizon renders amplitude panning downwards infeasible, it is still necessary to reasonably preserve signals of virtual sources that meant for playback on complete loudspeaker setups.

In the case of the unsymmetric loudspeaker rectangles, see Fig. 10, and a missing lower hemisphere of surrounding loudspeakers, the insertion of one or more *imaginary loudspeakers* in the vertical direction (nadir) or in the middle of the rectangle (the average direction vector) has proven to be a useful strategy, e.g. in [ZF12]. Any imaginary loudspeaker aims at either extending the admissible triangulation towards open parts of the surround loudspeaker setup, or to cover for parts with potential asymmetry, see [RFZN16].

The signal of the imaginary loudspeaker can be dealt with in two ways

- it can be dismissed, e.g., for loudspeaker below at nadir, this would still yield a signal near the closest horizontal pair of loudspeakers for virtual sources panned to directions below the horizon, unless panned directly to nadir
- it can be distributed to the neighboring M loudspeakers by a factor of $\frac{1}{\sqrt{\mathrm{M}}}$, or less as in Fig. 10, or be entirely re-normalized to maintain loudness.

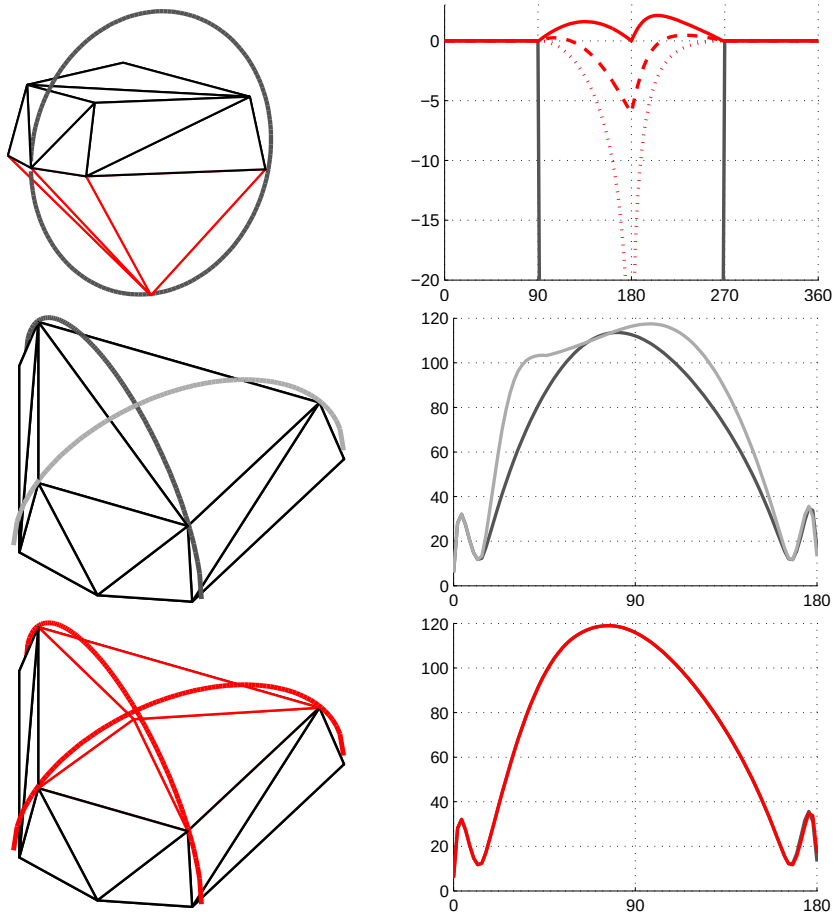

Figure 10 – VBAP on the ITU D (4+5+0) setup. *Top row:* Insertion of imaginary loudspeaker at nadir preserves loudness of downward-panned signals, shown for vertical path and E values in dB for factors $\{\frac{1}{\sqrt{5}}, \frac{1}{2\sqrt{5}}, 0\}$ to re-distribute the signal to the 5 existing horizontal loudspeakers. *Middle row:* Due to typical triangulation, two left-right mirrored vertical paths ($45°$ azimuth) yield unsymmetric behavior, as shown by the $2\arccos\|\boldsymbol{r}_\mathrm{E}\|$ measure. *Bottom row:* Insertion of imaginary loudspeaker at $65°$ fixes symmetry and feeds the signal with a factor $\frac{1}{\sqrt{4}}$ to the 4 existing neightbor loudspeakers.

4 Panning functions for a circularly and spherically surrounding loudspeaker arrays

In the seventies, Cooper [CS72] described the idea of using angular amplitude functions to control the auditory event, which could be thought of as an extension to mid/side decompositions, or as recording with figure-of-eight and omnidirectional directivity patterns. Stemming from this approach and from this time, the notion and technology of Ambisonics was developed by Felgett [Fel74], Gerzon [Ger75], and Craven [CG77]. Since then, the term Ambisonics became common for technology using angular harmonic functions to express surround sound.

The previous section required that direction and length of the $\boldsymbol{r}_\mathrm{E}$ and $\boldsymbol{r}_\mathrm{V}$ vectors resulting from amplitude panning on loudspeakers matched the desired auditory event direction and width. Harmonic functions with strict symmetry around a panning direction $\boldsymbol{\theta}_\mathrm{s}$ will help us in achieving this goal and in defining good sampling.

Appendix C shows how 2D Ambisonic panning can be expressed in terms of a finite-order Fourier series using the exponentials $e^{\mathrm{i}m\phi}$ with real coefficients, i.e., a finite-order cosine $\cos m\phi$ series in the azimuthal distance $\phi = \varphi - \varphi_s$ between loudspeaker angles $\varphi = \varphi_l$ and the panning angle φ_s. For this symmetric finite-resolution function, a regular circular polygon of sufficiently many loudspeakers would automatically yield correct aiming of the vector measures $\boldsymbol{r}_\mathrm{E}$ and $\boldsymbol{r}_\mathrm{V}$ towards the panning direction $\boldsymbol{\theta}_\mathrm{s}$ and panning-invariant loudness and width magnitudes E, P, $\|\boldsymbol{r}_\mathrm{E}\|$, $\|\boldsymbol{r}_\mathrm{V}\|$,

To arrive at a more general goal which holds for both circular and spherical arrangements of loudspeakers, we tread a more general path in deriving Ambisonic panning. After this, we will see in the results from listening experiments that the concept largely achieves the desired perceptual goals.

We therefore desire to define axisymmetric functions around the panning direction $\boldsymbol{\theta}_\mathrm{s}$ and their decomposition into suitable order-limited harmonic functions. The projection of the variable loudspeaker direction vector $\boldsymbol{\theta}$ on the panning direction $\boldsymbol{\theta}_\mathrm{s}$ yields the cosine of the enclosed angle to the axis $\boldsymbol{\theta}_\mathrm{s}^\mathrm{T}\boldsymbol{\theta} = \cos\phi$, and hereby expresses the only dimension of the axisymmetric function, $\mu = \cos\phi$. As the m^th power thereof, $\cos^m\phi$, can be expressed in terms of a cosine series up to the m^th order, a power series in μ is a reasonable representation of the panning functon on the sphere.

To do this properly, we will first learn about the term harmonics, solve for axisymmetric harmonics, establish the panning function on the circle using these harmonics, and then finally come to the spherical panning function.

4.1 Axisymmetric harmonics: Gegenbauer polynomials

The Laplacian is defined in the D-dimensional Cartesian space as

$$\triangle = \sum_{j=1}^{\mathrm{D}} \frac{\partial^2}{\partial x_j^2}. \tag{12}$$

Solving the Eigenvalue problem $\triangle = -m^2\, f = 0$ for one dimension $\frac{\partial^2}{\partial x^2} f = -m^2 f$yields with the exponential Ansatz $f = e^{ax}$, inserted and differentiated to $a^2\, f = -m^2\, f$, *harmonic functions* $f = e^{\pm \mathrm{i} m x}$ with $m \in \mathbb{Z}$ if the function should be periodic $f(x) = f(x + 2\pi\, k)$, $k \in \mathbb{Z}$. If only a limited number of Eigenvalues $m \le K$ is used, this yields a limited-order expansion into *harmonics*, a band-limited Fourier series. It is useful to limit the resolution of a represented function.

For 2 dimensions appendix C defines panning function with limited m, defined using a series of real part of this complex exponential $e^{\mathrm{i}m\phi} = \cos(m\phi)$ with the polar angle $\phi = \arctan\frac{y}{x}$ enclosed with the x axis. For 3 dimensions this is not useful anymore. Beneficial properties get lost, $\cos(m\phi)$ is not orthogonal when integrated over the sphere.

Generally, eigensolutions $\triangle f = -\lambda\, f$ to the Laplacian are called *harmonics*. For suitable Eigenvalues λ, these solutions span an orthogonal set of basis functions that are typically used for Fourier expansion on a finite interval.

Chosing the last Cartesian coordinate axis as panning direction $\boldsymbol{\theta}_\mathrm{s} = [\ldots,\, 0,\, 1]^\mathrm{T}$, and writing the direction vector as $\boldsymbol{\theta} = \frac{[x_1,\ldots,x_\mathrm{D}]^\mathrm{T}}{\sqrt{\sum_j x_j^2}} = \frac{[x_1,\ldots,x_\mathrm{D}]^\mathrm{T}}{r}$, i.e. $\boldsymbol{\theta}_\mathrm{s}^\mathrm{T}\boldsymbol{\theta} = \frac{x_\mathrm{D}}{r} = \cos\phi := \mu$, the purely axisymmetric panning function

$$f = f(\mu)$$

only depends on μ. Sec. 11.1 describes the formalism of re-writing the Laplacian to general coordinate systems. Here, we re-write it to the axial dimension $-1 \le \mu \le 1$ in order to find *axisymmetric harmonics* useful to represent limited-resolution patterns of rotational symmetry around x_D. As derived in the appendix D, the Laplacian with regard to the single axial coordinate $\mu = \cos\phi$ becomes:

$$r^2 \triangle_\mu = (1-\mu^2)\frac{\mathrm{d}^2}{\mathrm{d}\mu^2} - (\mathrm{D}-1)\,\mu\,\frac{\mathrm{d}}{\mathrm{d}\mu}. \tag{13}$$

Solving the Laplacian differential equation for axisymmetric functions. With the above, we establish the Laplace differential equation $(r^2\, \triangle_\mu + \lambda) f = 0$ with the Eigenvalue λ

$$(1-\mu^2)\frac{\mathrm{d}^2 f}{\mathrm{d}\mu^2} - (\mathrm{D}-1)\,\mu\,\frac{\mathrm{d}f}{\mathrm{d}\mu} + \lambda\, f = 0, \tag{14}$$

in the hope that if a limited set of discrete eigenvalues $\lambda_n \le K$ is used, then we obtain harmonics orthogonal on the interval $-1 \le \mu \le 1$ that contain only limited powers of μ^n with $n \le \mathrm{N}$, given a suitable of K and λ_n. We know trigonometrically that such functions can only contain oscillations up to $\cos(\mathrm{N}\phi)$, thus have limited angular resolution.

We solve the equation with the Frobenius (power series) Ansatz $f = \sum_k c_k\, \mu^k$, see Appendix F, and get an interrelation of its coefficients $c_{k+2} = \frac{k^2+k(\mathrm{D}-2)-\lambda}{(k+1)(k+2)}\; c_k$. Choosing $\lambda = \lambda_n = n^2 + (\mathrm{D}-2)n$, the power series terminates at $k = n$, so that $c_{k>n} = 0$, hence it becomes polynomial $f = \mathcal{P}_n$, and the relation between the coefficients of $\mathcal{P}_n$ remains

$$c^{(n)}_{k+2} = \frac{(k-n)(k+n+\mathrm{D}-2)}{(k+1)(k+2)}\; c^{(n)}_k. \tag{15}$$

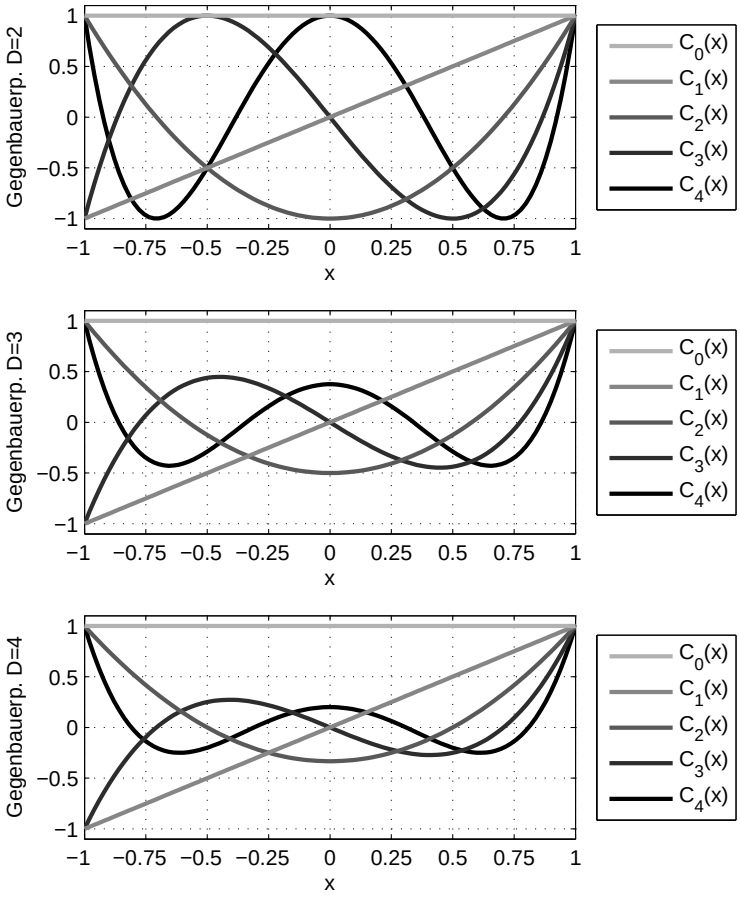

Figure 11 – Gegenbauer polynomials $\mathcal{P}_n(\mu)$ for $\mathrm{D} = 2, 3, 4$, i.e. Chebyshev polynomials $T_n(\mu)$ for $\mathrm{D} = 2$, and Legendre polynomials $P_n(\mu)$ for $\mathrm{D} = 3$. Due to their shape, they are orthogonal with regard to the weight $w(\mu) = \sqrt{1-\mu^2}^{\mathrm{D}-3}$.

We re-write the above equation accordingly:

$$(1-\mu^2)\frac{\mathrm{d}^2\mathcal{P}_n}{\mathrm{d}\mu^2} - (\mathrm{D}-1)\,\mu\,\frac{\mathrm{d}\mathcal{P}_n}{\mathrm{d}\mu} + n(n+\mathrm{D}-2)\,\mathcal{P}_n = 0. \tag{16}$$

This equation is called the *ultraspherical* or *Gegenbauer* differential equation, and they can be constructed from $\mathcal{P}_0(\mu) = 1$, and $\mathcal{P}_1(\mu) = 1$ with the recurrence derived in Appendix H.3, here with the normalization $\mathcal{P}_n(1) = 1$, therefore a bit differently defined as in textbooks:

$$\mathcal{P}_{n+1}(\mu) = \frac{2n+\mathrm{D}-2}{n+\mathrm{D}-2}\;\mu\,\mathcal{P}_n(\mu) - \frac{n}{n+\mathrm{D}-2}\mathcal{P}_{n-1}(\mu). \tag{17}$$

Fig. 11 shows the Gegenbauer polynomials for $\mathrm{D} = 2, 3$, i.e., the Chebyshev polynomials and the Legendre polynomials.

Orthogonality. The Gegenbauer polynomials $\mathcal{P}_n$ are orthogonal according to the integral $\iiint \mathcal{P}_n \mathcal{P}_m \delta(r-1) \prod_j \mathrm{d}x_j = N_n^2 \delta_{nm}$. We re-write the integration elements to get the orthogonality relation in μ, see Appendix E, yielding

$$\int_{-1}^{1} \mathcal{P}_n(\mu)\mathcal{P}_m(\mu) \sqrt{1-\mu^2}^{\mathrm{D}-3} \,\mathrm{d}\mu = N_n^2 \,\delta_{nm}, \tag{18}$$

with the squared norm $N_n^2 = \int_{-1}^{1} \mathcal{P}_n^2(\mu) \sqrt{1-\mu^2}^{\mathrm{D}-3} \,\mathrm{d}\mu = \frac{n!}{(2n+\mathrm{D}-2)(n+\mathrm{D}-3)!} \frac{S_{\mathrm{D}-1}}{S_{\mathrm{D}-2}}$ of the polynomial, see Appendix H.6, H.9. Orthogonality can be shown by integrating Eq. (16) over $\mathcal{P}_m$ using the corresponding integration element, and by inegration by parts, as shown in Appendix G.

Orthogonality has the benefit of enabling a transform integral to find the coefficients γ_n of a function decomposed into the polynomials $\mathcal{P}_n$, see Appendix H,

$$g(\mu) = \sum_{n=0}^{\infty} \gamma_n \,\mathcal{P}_n(\mu), \qquad \gamma_n = \frac{1}{N_n^2} \int_{-1}^{1} g(\mu)\,\mathcal{P}_n(\mu) \sqrt{1-\mu^2}^{\mathrm{D}-3} \,\mathrm{d}\mu. \tag{19}$$

4.2 Axisymmetric panning function

The axisymmetric panning function is based on the decomposition of a Dirac delta pointing towards the panning direction $\boldsymbol{\theta}_\mathrm{s}$,

$$\delta(1-\boldsymbol{\theta}_\mathrm{s}^\mathrm{T}\boldsymbol{\theta}) = \begin{cases} \infty, & \text{for } \boldsymbol{\theta} = \boldsymbol{\theta}_\mathrm{s} \\ 0, & \text{otherwise} \end{cases}, \qquad \text{with } \int_{\mathbb{S}^{\mathrm{D}-1}} \delta(1-\boldsymbol{\theta}_\mathrm{s}^\mathrm{T}\boldsymbol{\theta}) \,\mathrm{d}\boldsymbol{\theta} = 1, \tag{20}$$

into infinitely many axisymmetric harmonics

$$\delta(1-\boldsymbol{\theta}_\mathrm{s}^\mathrm{T}\boldsymbol{\theta}) = \frac{1}{S_{\mathrm{D}-2}} \sum_{n=0}^{\infty} \gamma_n \,\mathcal{P}_n(\boldsymbol{\theta}_\mathrm{s}^\mathrm{T}\boldsymbol{\theta}), \tag{21}$$

where the factor $\frac{1}{S_{\mathrm{D}-2}}$ accounts for normalization with regard to the integrals over the independent, axisymmetric coordinates, whose value corresponds to the surface of the next lesser order unit sphere $\mathbb{S}^{\mathrm{D}-2}$.

The desired axisymmetric panning function is based on the representation of the Dirac delta, but with limited order and involving a sidelobe-suppressing weight a_n,

$$g(\boldsymbol{\theta}) = \frac{1}{S_{\mathrm{D}-2}} \sum_{n=0}^{\mathrm{N}} a_n \,\gamma_n \,\mathcal{P}_n(\boldsymbol{\theta}_\mathrm{s}^\mathrm{T}\boldsymbol{\theta}). \tag{22}$$

Finding γ_n decomposing the Dirac delta at $\mu = 1$. Given a Dirac delta located at $\mu = 1$ as $\frac{\delta(1-\mu)}{\sqrt{1-\mu^2}^{\mathrm{D}-3}}$ which is correctly normalized to the axial coordinate to fulfill $\int_{-1}^{1} \delta(1-\mu) \,\mathrm{d}\mu = 1$, we use the transform integral Eq. (19) to find its coefficients γ_m:

$$\frac{\delta(1-\mu)}{\sqrt{1-\mu^2}^{\mathrm{D}-3}} = \sum_{n=0}^{\infty} \gamma_n \,\mathcal{P}_n(\mu), \quad \gamma_n = \frac{1}{N_n^2} \int_{-1}^{1} \delta(1-\mu)\,\mathcal{P}_n(\mu) \,\mathrm{d}\mu = \frac{\mathcal{P}_n(1)}{N_n^2}. \tag{23}$$

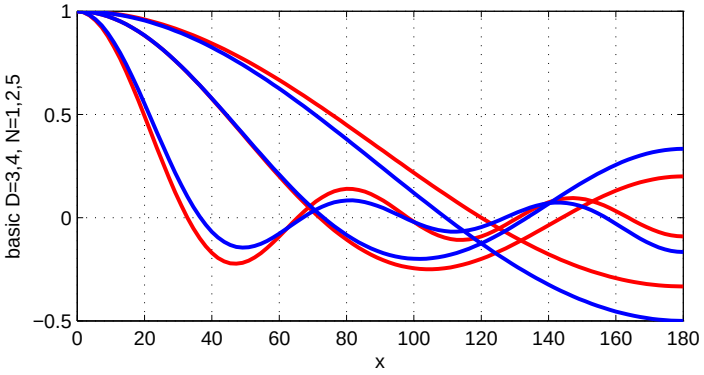

Figure 12 – Basic patterns for $\mathrm{D} = 2, 3$ (red,blue), and $\mathrm{N} = 1, 2, 5$.

The Gegenbauer polynomials as defined here are normalized to $\mathcal{P}_m(1) = 1$, therefore the expansion coefficient simplifies to

$$\gamma_m = \frac{1}{N_m^2}. \tag{24}$$

Measures P, E, $\boldsymbol{r}_\mathrm{V}$, $\boldsymbol{r}_\mathrm{V}$ of finite-order axisymmetric panning functions. As derived in Appendix I, the metrics of the continuous, limited-order axisymmetric panning function can be found by solving integrals over the continuous loudspeaker direction $\boldsymbol{\theta}$. The measures only depend on the order-suppressing weight a_n; here with the integration measure is abbreviated as $w(\mu) = \sqrt{1-\mu^2}^{\mathrm{D}-3}$,

$$P = S_{\mathrm{D}-2} \int_{-1}^{1} g(\mu)\, w(\mu) \mathrm{d}\mu = a_0, \tag{25}$$

$$E = S_{\mathrm{D}-2} \int_{-1}^{1} g^2(\mu)\, w(\mu) \mathrm{d}\mu = \sum_{n=0}^{\mathrm{N}} \frac{|a_n|^2}{S_{\mathrm{D}-2} N_n^2}, \tag{26}$$

$$\boldsymbol{r}_\mathrm{V} = \frac{\int_{-1}^{1} g(\mu)\, \mu\, w(\mu) \mathrm{d}\mu}{P}\, \boldsymbol{\theta}_\mathrm{s} = \frac{a_1}{a_0}\, \boldsymbol{\theta}_\mathrm{s}, \tag{27}$$

$$\boldsymbol{r}_\mathrm{E} = \frac{\int_{-1}^{1} g^2(\mu)\, \mu\, w(\mu) \mathrm{d}\mu}{E}\, \boldsymbol{\theta}_\mathrm{s} = \frac{\sum_{n=0}^{\mathrm{N}} \frac{2\beta_{n+1}}{N_n^2}\, a_n a_{n+1}}{\sum_{n=0}^{\mathrm{N}} \frac{1}{N_n^2} |a_n|^2}\, \boldsymbol{\theta}_\mathrm{s}. \tag{28}$$

Obviously, the measures P and $\boldsymbol{r}_\mathrm{V}$ only depend on the weights a_0 and a_1, while the quadratic measures E and $\boldsymbol{r}_\mathrm{E}$ involve weights of all the orders.

Basic weights. With the weights $a_n = 1$, there is no sidelobe suppression but the narrowest main lobe and highest directivity that can be represented using the limited orders $n \le \mathrm{N}$.

Fig. 12 shows the limited-order panning functions for $\mathrm{D} = 2, 3$ and $\mathrm{N} = 1, 2, 5$.

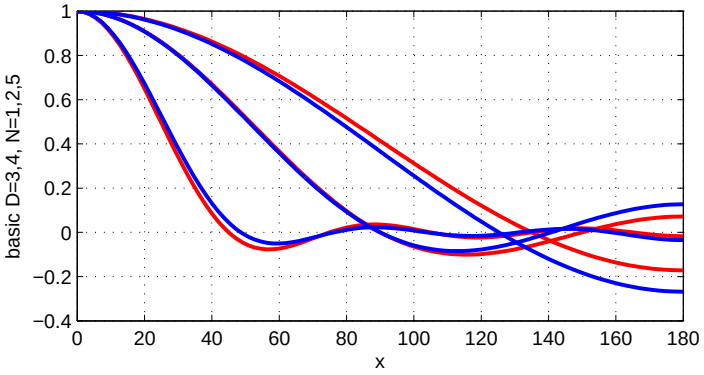

Figure 13 – Max-re patterns for $\mathrm{D} = 2, 3$ (red,blue), and $\mathrm{N} = 1, 2, 5$.

Max$-\boldsymbol{r}_\mathrm{E}$ weights. To shape the finite-order axisymmetric panning function, we choose max-$\boldsymbol{r}_\mathrm{E}$ weights [DRP99] a_n that maximize the magnitude r_E of the $\boldsymbol{r}_\mathrm{E}$ vector, cf. Appendix J. They consist of Gegenbauer polynomials evaluated at the greatest root $r_{\mathrm{E,max}}$ of the polynomial $\mathcal{P}_{\mathrm{N}+1}$ of the next higher order,

$$a_n = \mathcal{P}_n(r_{\mathrm{E,max}}), \qquad r_{\mathrm{E,max}} = \arg\max_{r_\mathrm{E}}\{\mathcal{P}_{\mathrm{N}+1}(r_\mathrm{E}) = 0\}. \tag{29}$$

This requires a root finder or an approximation of the location of the greatest root.

Fig. 13 shows max-rE patterns for $\mathrm{D} = 2, 3$ and $\mathrm{N} = 1, 2, 5$.

In-phase weights. According to [DRP99], it is also convenient to define weights that entirely suppress the side lobes by causing an N^{th} order zero at $\mu = -1$, which is often referred to as higher-order cardioid, and which is a max-flat design at $\mu = -1$

$$g(\mu) \propto (1+\mu)^\mathrm{N}. \tag{30}$$

Without a finished derivation yet in Appendix J.1, according to [Dan00], in-phase weighting is done by

$$a_n = \frac{\mathrm{N}!}{(\mathrm{N}-n)!}\frac{(\mathrm{N}+\mathrm{D}-2)!}{(\mathrm{N}+n+\mathrm{D}-2)!}. \tag{31}$$

Fig. 14 shows in-phase patterns for $\mathrm{D} = 2, 3$ and $\mathrm{N} = 1, 2, 5$.

Solutions in 2 and 3 dimensions. For $\mathrm{D} = 2$ we get the Chebyshev differential equation and the Chebyshev polynomials T_n as solutions, and for $\mathrm{D} = 3$ the Legendre differential equation with Legendre polynomials P_n as solutions

$$\mathrm{D} = 2: \qquad (1-\mu^2)\frac{\mathrm{d}^2 T_n}{\mathrm{d}\mu^2} - \mu\,\frac{\mathrm{d}T_n}{\mathrm{d}\mu} + n^2\,T_n = 0, \tag{32}$$

$$\mathrm{D} = 3: \qquad (1-\mu^2)\frac{\mathrm{d}^2 P_n}{\mathrm{d}\mu^2} - 2\,\mu\,\frac{\mathrm{d}P_n}{\mathrm{d}\mu} + n(n+1)\,P_n = 0. \tag{33}$$

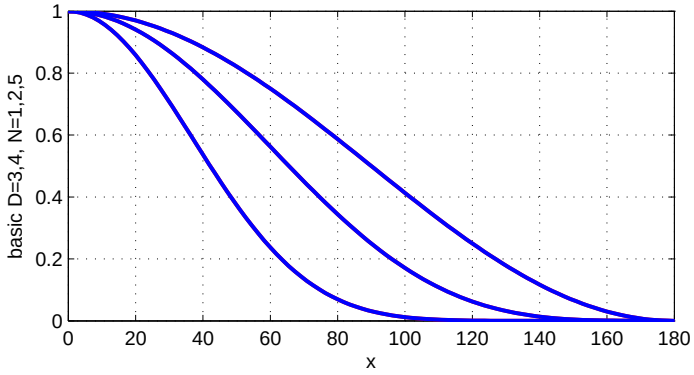

Figure 14 – In-phase patterns for $\mathrm{D} = 2, 3$ (red,blue), and $\mathrm{N} = 1, 2, 5$.

These polynomials and their three-term recurrences are listed in Tables 1,2, yielding polynomials normalized at $\mu = 1$, i.e., $T_n(1) = 1$ and $P_n(1) = 1$ for all n, and they fulfill the orthogonality relations

$$\mathrm{D} = 2: \quad \int_{-1}^{1} T_n(\mu) T_m(\mu) \frac{\mathrm{d}\mu}{\sqrt{1-\mu^2}} = \frac{2}{2-\delta_{m,0}} \delta_{nm}, \quad \text{with } N_n^2 = \frac{2-\delta_{m,0}}{2}, \tag{34}$$

$$\mathrm{D} = 3: \quad \int_{-1}^{1} P_n(\mu) P_m(\mu) \, \mathrm{d}\mu = \frac{2}{2n+1} \delta_{nm}, \quad \text{with } N_n^2 = \frac{2n+1}{2}. \tag{35}$$

and recurrences

$$\mathrm{D} = 2: \quad T_{m+1}(\mu) = (2-\delta_{m,0}) \mu \, T_m(\mu) - T_{m-1}(\mu), \tag{36}$$

$$\mathrm{D} = 3: \quad P_{n+1}(\mu) = \frac{2n+1}{n+1} \mu P_n(\mu) - \frac{n}{n+1} P_{n-1}(\mu). \tag{37}$$

The Dirac delta $\delta(1 - \boldsymbol{\theta}_\mathrm{s}^\mathrm{T} \boldsymbol{\theta})$ pointing to $\boldsymbol{\theta}_\mathrm{s}$ is represented by the coefficients

$$\mathrm{D} = 2: \quad \gamma_n = \frac{2-\delta_{n,0}}{2\pi}, \qquad \mathrm{D} = 3: \quad \gamma_n = \frac{2n+1}{4\pi}. \tag{38}$$

4.3 Circular panning function in Chebyshev polynomials

On the circle, the equivalence of a Dirac delta evaluated at the projection of the variable direction $\boldsymbol{\theta}$ on the panning direction $\boldsymbol{\theta}_\mathrm{s}$ is given in terms of an infinte sum of Chebyshev polynomials, see Tab. 1, cf. [ZF12],

$$\sum_{m=0}^{\infty} \frac{2-\delta_{m,0}}{2\pi}\, T_m(\boldsymbol{\theta}_\mathrm{s}^\mathrm{T}\boldsymbol{\theta}) = \delta(1-\boldsymbol{\theta}_\mathrm{s}^\mathrm{T}\boldsymbol{\theta}),$$

with $\int_{\mathbb{S}^1} \delta(1-\boldsymbol{\theta}_\mathrm{s}^\mathrm{T}\boldsymbol{\theta})\,\mathrm{d}\boldsymbol{\theta} = 1$, and $\delta(1-\boldsymbol{\theta}_\mathrm{s}^\mathrm{T}\boldsymbol{\theta}) = \begin{cases}\infty, & \text{for } \boldsymbol{\theta}=\boldsymbol{\theta}_s,\\ 0, & \text{otherwise.}\end{cases}$

The limited-order panning function should involve the sidelobe-suppressing weights a_m

$$g(\boldsymbol{\theta}) = \sum_{m=0}^{\mathrm{N}} \frac{2-\delta_{m,0}}{2\pi}\, a_m\, T_m(\boldsymbol{\theta}_\mathrm{s}^\mathrm{T}\boldsymbol{\theta}),$$

for which we may insert $\max-\boldsymbol{r}_\mathrm{E}$ weights [DRP99] as derived above, $a_m = T_m\Big(\cos\frac{90^\circ}{\mathrm{N}+1}\Big)$.

Table 1 – Coefficients of the Chebyshev polynomials that are orthogonal for integration on the interval $[-1,1]$ with the integration element $\frac{\mathrm{d}\mu}{\sqrt{1-x^2}}$. The Chebyshev polynomials obey the recurrence $T_{m+1}(\mu) + T_{m-1}(\mu) - (2-\delta_{m,0})\mu\, T_m(\mu) = 0$ for $m > 1$.

$T_m(\mu) = \sum_{k=0}^{m} c_k\,\mu^k$	Coefficients of the Chebyshev polynomials									
$n=$	c_9	c_8	c_7	c_6	c_5	c_4	c_3	c_2	c_1	c_0
0										1
1									1	
2								2		−1
3							4		−3	
4						8		−8		1
5					16		−20		5	
6				32		−48		18		−1
7			64		−112		56		−7	
8		128		−256		160		−32		1
9	256		−576		432		−120		9	

Measures. The function is of limited angular resolution N and allows to be sampled correctly. The E, P, $\boldsymbol{r}_\mathrm{V}$, and $\boldsymbol{r}_\mathrm{E}$ measures of the continuous function can be derived, see Appendix I,

$$P = a_0, \qquad \boldsymbol{r}_\mathrm{V} = \frac{a_1}{a_0}\,\boldsymbol{\theta}_\mathrm{s}, \tag{39}$$

$$E = \sum_{n=0}^{\mathrm{N}} \frac{|a_n|^2}{2\pi}, \qquad \boldsymbol{r}_\mathrm{E} = \frac{\sum_{n=0}^{\mathrm{N}} 2\Re\{a_n a_{n+1}^*\}}{\sum_{n=0}^{\mathrm{N}} |a_n|^2}\,\boldsymbol{\theta}_\mathrm{s}. \tag{40}$$

4.4 Optimal circular loudspeaker layout: circular t design

Assume that we sample a polynomial in $\left(\boldsymbol{\theta}_\mathrm{s}^\mathrm{T}\boldsymbol{\theta}\right)^m$ limited in the order by $m \leq t$, $t \in \mathrm{N}$. The discretization uses the directions $\{\boldsymbol{\theta}_l\}$ at L points and that this is called t design whenever discrete summation and integral are equivalent, i.e., discrete summation accurately determines the direct component (DC) of the polynomial despite the variable orientation of $\boldsymbol{\theta}_s$, according to the definition in [DGS77],

$$\int_{-\pi}^{\pi} T_m\left(\boldsymbol{\theta}_\mathrm{s}^\mathrm{T}\boldsymbol{\theta}\right)\,\mathrm{d}\boldsymbol{\theta} = \tfrac{2\pi}{\mathrm{L}}\sum_{l=1}^{\mathrm{L}} T_m\left(\boldsymbol{\theta}_\mathrm{s}^\mathrm{T}\boldsymbol{\theta}_l\right). \tag{41}$$

This simplistic criterion of just estimating the DC correctly is relevant for all models:

- In the calculation of P, an integral over the N^{th}-order panning function $g(\boldsymbol{\theta})$ is evaluated, which is why at least
  a $t \geq \mathrm{N}$ design
  should be used for loudpseaker placement to obtain optimal results for P from the discrete panning gains.
- In the calculation of $\boldsymbol{r}_\mathrm{V}$, the N^{th}-order pattern $g(\boldsymbol{\theta})$ is multiplied by $\boldsymbol{\theta}_\mathrm{s}^\mathrm{T}\boldsymbol{\theta}$, causing an integral over an $(\mathrm{N}+1)^{\mathrm{th}}$-order polynomial, which is why the loudspeaker placement should at least correspond to
  a $t \geq \mathrm{N}+1$ design
  to obtain optimal results for $\boldsymbol{r}_\mathrm{V}$ from the discrete panning gains.
- For calculating E, the squared continuous panning function is integrated, hence a $2\mathrm{N}^{\mathrm{th}}$-order function, thus the loudspeaker setup should at least be
  a $t \geq 2\mathrm{N}$ design
  to achieve optimal results or $\boldsymbol{r}_\mathrm{E}$ from the discrete panning gains.
- In the calculation of $\boldsymbol{r}_\mathrm{E}$, the squared panning function multiplied by $\boldsymbol{\theta}_\mathrm{s}^\mathrm{T}\boldsymbol{\theta}$ is integrated, a $(2\mathrm{N}+1)^{\mathrm{th}}$-order function, so the loudspeaker setup should at least be
  a $t \geq 2\mathrm{N}+1$ design
  to get optimal results for $\boldsymbol{r}_\mathrm{E}$ from the discrete panning gains.

Now we know that we should at least be a $t \geq 2\mathrm{N}+1$ design to ensure results of the E, P, $\boldsymbol{r}_\mathrm{V}$, and $\boldsymbol{r}_\mathrm{E}$ for discrete panning gains that are equally optimal than those for the continuous panning function.

On the circle, every equiangular sampling $\varphi_l = \frac{2\pi}{\mathrm{L}}(l-1)$ is a t-design if the number of samples fulfills the sampling criterion $t \leq \mathrm{L}+1$. There should be equally many sampling points than zero crossings of $\cos(m\varphi)$ or $\sin(m\varphi)$, or two samples per oscillation (equivalent to Whittaker/Kotelnikov/Shannon sampling theorem).

Our knowledge about t designs, equiangular sampling on the circle, and the polynomial orders of the various integrals involved in the models allow the following conclusion: We need

$$\mathrm{L} \geq 2\mathrm{N}+2 \tag{42}$$

equiangularly spaced loudspeakers on the horizon to obtain an optimally placed Ambisonic playback system of the order N. The $\boldsymbol{r}_\mathrm{E}$ vector is the strictest of the criteria.

4.5 Spherical panning function in Legendre polynomials

On the sphere, the equivalence of a Dirac delta evaluated at the projection of the variable direction $\boldsymbol{\theta}$ on the panning direction $\boldsymbol{\theta}_\mathrm{s}$ is given in terms of an infinte sum of Legendre polynomials, see Tab. 2, cf. [ZF12],

$$\sum_{n=0}^{\infty} \frac{2n+1}{4\pi}\, P_n(\boldsymbol{\theta}_\mathrm{s}^\mathrm{T}\boldsymbol{\theta}) = \delta(1-\boldsymbol{\theta}_\mathrm{s}^\mathrm{T}\boldsymbol{\theta}),$$

for which $\int_{\mathbb{S}^2} \delta(1-\boldsymbol{\theta}_\mathrm{s}^\mathrm{T}\boldsymbol{\theta}),\, \mathrm{d}\boldsymbol{\theta} = 1$ and $\delta(1-\boldsymbol{\theta}_\mathrm{s}^\mathrm{T}\boldsymbol{\theta}) = \begin{cases}\infty, & \text{for } \boldsymbol{\theta}=\boldsymbol{\theta}_s,\\ 0, & \text{otherwise.}\end{cases}$

The limited-order summation of the panning function involves the coefficients a_n

$$g(\boldsymbol{\theta}) = \sum_{n=0}^{\mathrm{N}} \frac{2n+1}{4\pi}\, a_n\, P_n(\boldsymbol{\theta}_\mathrm{s}^\mathrm{T}\boldsymbol{\theta}), \tag{43}$$

and it may use $\max \boldsymbol{r}_\mathrm{E}$ weights according to [ZF12, DRP99], as derived in Appendix J,

$$a_n = P_n\Big(\cos\frac{137.9^\circ}{\mathrm{N}+1.51}\Big). \tag{44}$$

Table 2 – Coefficients of the Legendre polynomials that are orthogonal for the integration on the interval $[-1,1]$ with the integration element $\mathrm{d}\mu$. The recurrence to obtain these coefficients is $(n+1)P_{n+1}(\mu) - (2n+1)\mu P_n(\mu) + nP_{n-1}(\mu) = 0$.

$P_n(\mu) = \sum_{k=0}^{n} c_k\, \mu^i$	Coefficients of the Legendre polynomials									
$n=$	c_9	c_8	c_7	c_6	c_5	c_4	c_3	c_2	c_1	c_0
0										1
1									1	
2								$\frac{3}{2}$		$-\frac{1}{2}$
3							$\frac{5}{2}$		$-\frac{3}{2}$	
4						$\frac{35}{8}$		$-\frac{30}{8}$		$\frac{3}{8}$
5					$\frac{63}{8}$		$-\frac{70}{8}$		$\frac{15}{8}$	
6				$\frac{231}{16}$		$-\frac{315}{16}$		$\frac{105}{16}$		$-\frac{5}{16}$
7			$\frac{429}{16}$		$-\frac{693}{16}$		$\frac{315}{16}$		$-\frac{35}{16}$	
8		$\frac{6435}{128}$		$-\frac{12012}{128}$		$\frac{6930}{128}$		$-\frac{1260}{128}$		$\frac{35}{128}$
9	$\frac{12155}{128}$		$-\frac{25740}{128}$		$\frac{18018}{128}$		$-\frac{4620}{128}$		$\frac{315}{128}$	

Measures. The function is of limited angular resolution N and allows to be sampled correctly. The E, P, $\boldsymbol{r}_\mathrm{V}$, and $\boldsymbol{r}_\mathrm{E}$ measures of the continuous function can be derived, see Appendix I,

$$P = a_0, \qquad \boldsymbol{r}_\mathrm{V} = \frac{a_1}{a_0}\,\boldsymbol{\theta}_\mathrm{s}, \tag{45}$$

$$E = \sum_{n=0}^{\mathrm{N}} \frac{2n+1}{4\pi}|a_n|^2, \qquad \boldsymbol{r}_\mathrm{E} = \frac{\sum_{n=0}^{\mathrm{N}}(n+1)2\Re\{a_n a_{n+1}^*\}}{\sum_{n=0}^{\mathrm{N}}(2n+1)|a_n|^2}\,\boldsymbol{\theta}_\mathrm{s}. \tag{46}$$

4.6 Optimal spherical loudspeaker layout: spherical t-design

Spherical t-designs are L sampling nodes $\{\boldsymbol{\theta}_l\}$ on the sphere that allow to replace the integration over any spherical polynomial of limited order $n \leq t$ to be evaluated correctly using a summation over the sampled polynomials. Note that the direction $\boldsymbol{\theta}_\mathrm{s}$ stays arbitrary, and a t-design establishes the exact equivalence

$$\int_{\mathbb{S}^2} P_n(\boldsymbol{\theta}_\mathrm{s}^\mathrm{T}\boldsymbol{\theta})\,\mathrm{d}\boldsymbol{\theta} = \tfrac{4\pi}{\mathrm{L}} \sum_{l=1}^{\mathrm{L}} P_n(\boldsymbol{\theta}_\mathrm{s}^\mathrm{T}\boldsymbol{\theta}_l). \tag{47}$$

The evaluation of the measures P, E, $\boldsymbol{r}_\mathrm{V}$, and $\boldsymbol{r}_\mathrm{E}$ from the continuous functions, as shown in the Appendix I, require integration over N^th, $(\mathrm{N}+1)^\mathrm{th}$, $2\mathrm{N}^\mathrm{th}$, and $(2\mathrm{N}+1)^\mathrm{th}$ order polynomials, respectively. To obtain the exact equivalence between the metrics for continuous and discretized panning functions on the sphere, we require the discrete sampling nodes $\{\boldsymbol{\theta}_l\}$ to be at least a

$$t \geq 2\mathrm{N}+1 \text{ design.} \tag{48}$$

On the sphere, there are only the following geometrically regular polyhedra

- Tetrahedron, (2-design),
- Octahedron, $\mathrm{L}=6$, (3-design),
- Hexahedron/Cube, $\mathrm{L}=8$, (3-design),
- Icosahedron, $\mathrm{L}=12$, (5-design),
- Dodecahedron, $\mathrm{L}=20$, (5-design).

For instance, for $\mathrm{N}=1$, the octahedron is a suitable spherical design, for $\mathrm{N}=2$, the icosahedral or octahedral layouts are suitable.

Exceeding those spherical designs, there arrangements found by optimization by Hardin and Sloane [HS96] and Gräf and Potts [GP11] available on the following websites
http://neilsloane.com/sphdesigns/dim3/ and
http://homepage.univie.ac.at/manuel.graef/quadrature.php
(Chebyshev-type Quadratures on $\mathbb{S}^2$).

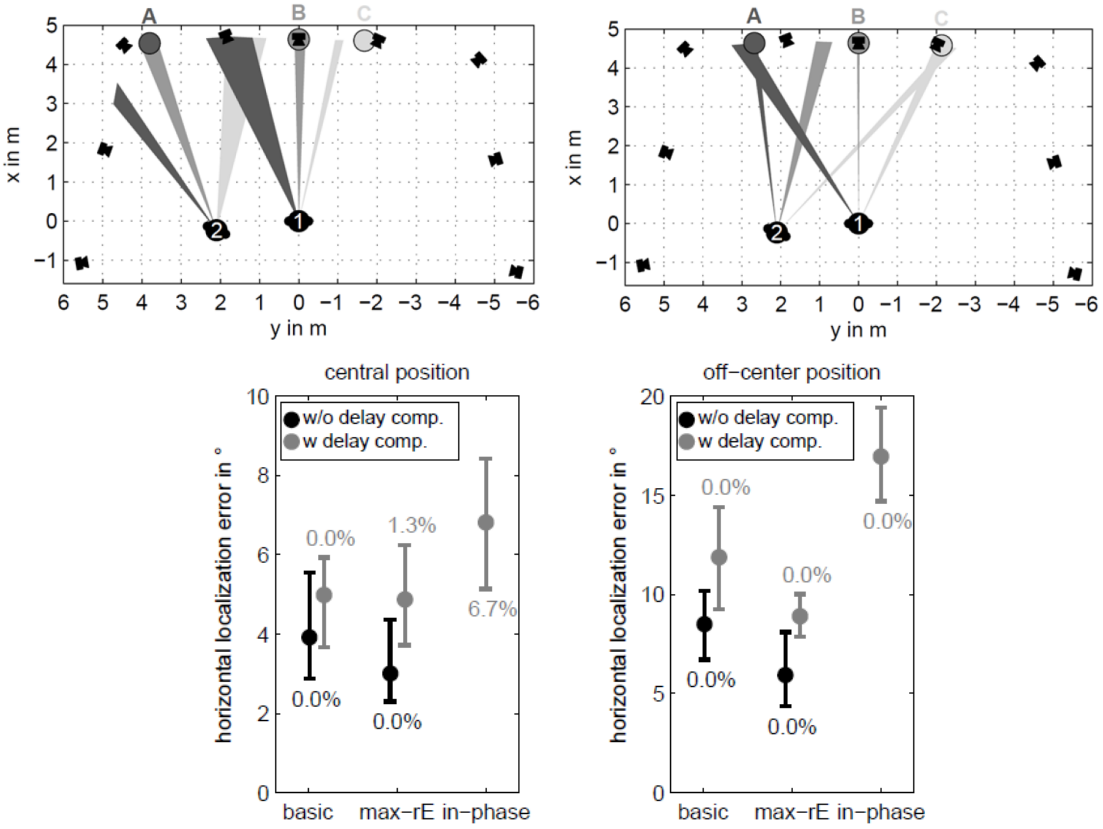

Figure 15 – In Frank's 2008 pointing experiment [FSZ08] on center and off-center listening seats for 3 virtual sources (A, B, C) using 1^{st}-order (left) and 5^{th}-order (right) Ambisonics on 12 loudspeakers of the IEM CUBE indicate a more stable localization with high orders. Moreover $\max - \boldsymbol{r}_{\text{E}}$ weighting and omission of delay compensation were favorized, while the recangular weighting "basic" and one that entirely suppresses sidelobes "inphase" are less precisely localized off-center.

4.7 Listening experiments on circular Ambisonics

There are several listening experiments discussing the features of Ambisonics, most of which are summarized in [Fra14a].

The first of the investigations deals with center and off-center listening seats as shown in Fig. 15. It illustrates that $\max - \boldsymbol{r}_{\text{E}}$ with the highest order achieves the best stability with regard to localization at off-center listening seats. Astonishingly, the delay compensation due to the different delay times deteriorated the results, most probably because of the nearly linear frontal arrangement of loudspeakers that is more robust to lateral shifts of the listening positions as a circular arrangement.

Fig. 16(a) shows the direction histogram for two different weightings a_m, and it illustrates that proper sidelobe suppression of the panning function by using $\max - \boldsymbol{r}_{\text{E}}$ is decisive at shifted listening positions to avoid splitting of the auditory image.

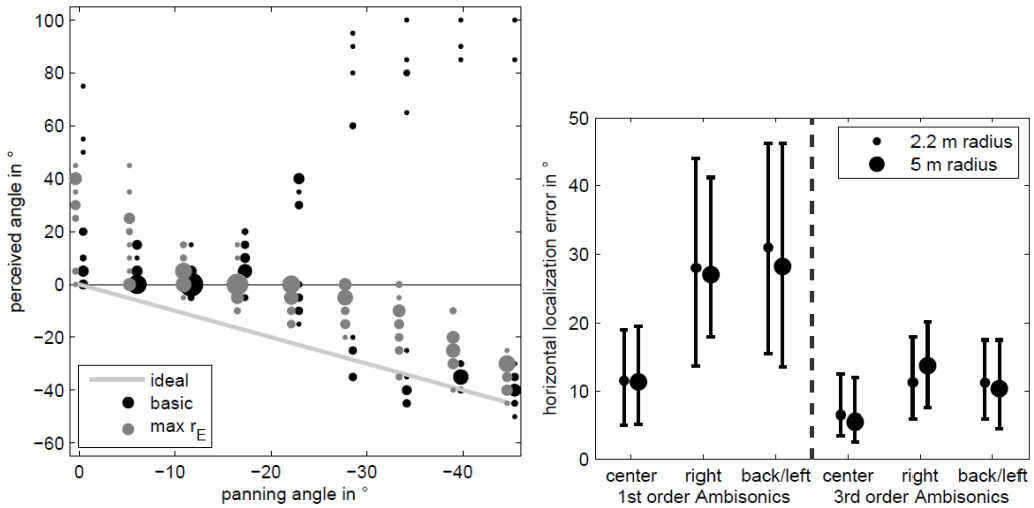

(a) Frank 2013 off-center experiment (b) Stitt 2014 off-center experiments

Figure 16 – Experiments on an off-center position in (a) show that $\max - \boldsymbol{r}_\mathrm{E}$ outperforms the basic, rectangularly truncated Fourier series at off-center listening positions, where it can avoid splitting of the auditory event. Stitt's experiments (b) imply that localization with higher orders is more stable and that the localization deficiency at off-centre listening seats seems to be proportional to the ratio between distance to the center divided by radius of the loudspeaker ring, and not the specifc time-delays that are larger for large loudspeaker rings, cf. [SBvW14].

Peter Stitt's work shows that the localization offsets at off-center listening seats do not increase with the radius of the loudspeaker arrangement as long as the off-center seat stays in proportion to the radius, Fig. 16(b). Frank's 2016 experments [FZ17] showed that a sweet spot size measuring the perceptually plausible playback area is around $\frac{2}{3}$ of the radius of the lousdpeaker setup.

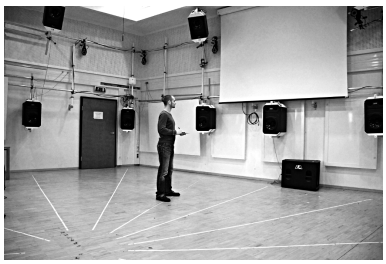

(a) Listening area size experiment

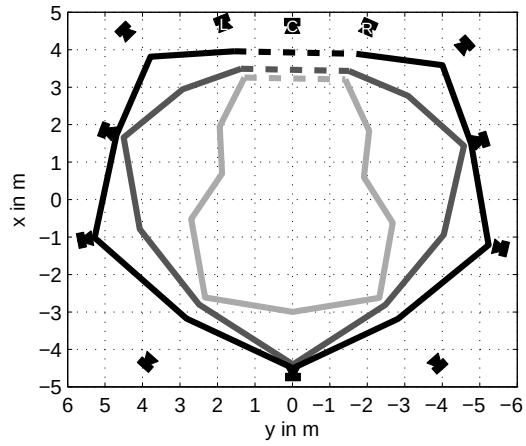

(b) Frontal sound

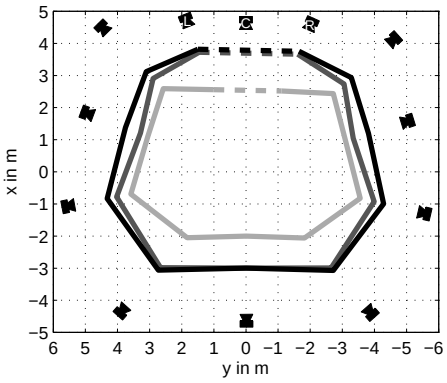

(c) Diffuse sound

Figure 17 – The perceptual sweet spot size as investigated by Frank [FZ17] is nearly covering the entire area enclosed by the IEM CUBE as a playback setup (black=5th, gray=3rd, light gray=1st order Ambisonics). It is smallest for 1st-order Ambisonics (slightly bigger when playing diffuse sounds), and largest for higher orders (for diffuse sound scenes, one should keep some distance to the loudspeakers).

The perceived width of auditory events is investigated in the experimental results of Fig. 18, [Fra14a], in which pink noise was placed frontally panned in different orientations of the loudspeaker ring (with one lousdpeaker in front, with front direction lying quarter- and half-spaced wrt loudspeaker spacing). Listeners compared the width of multiple stimuli and the results were meant to show indicate constant width for the differently rotated loudspeaker ring, because the optimally sampled arrangement with $\mathrm{L} = 2\mathrm{N} + 2$ should achieve a constant $\boldsymbol{r}_\mathrm{E}$ vector. While the panning-invariant length of the optimally sampled $\boldsymbol{r}_\mathrm{E}$ vector is not perfectly reflected in the perceived widths of low-order experiment using 3^rd order on 8 lousdpeakers, for which the on-loudspeaker position is perceived as being significantly wider, the high-order exeriment with 7^th order on 16 loudspeakers perfectly validates the model assumption.

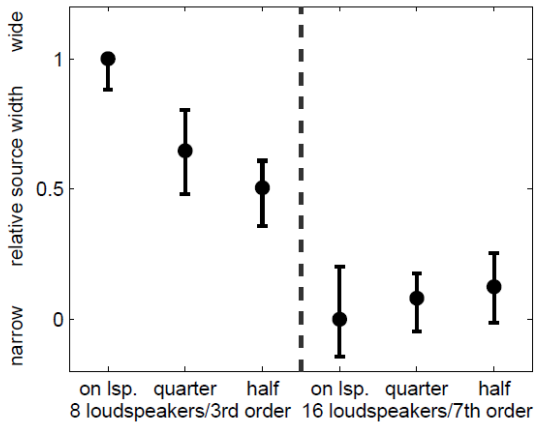

Figure 18 – Frank's 2013 experiments showed for $\max - \boldsymbol{r}_\mathrm{E}$ Ambisonics on three frontal loudspeakers that large perceived widths are not entirely accurately modeled by the optimally-sampled, therefore constant $\boldsymbol{r}_\mathrm{E}$ vector for low orders, however reasonably well, and significantly for high orders/narrow width.

Fig. 19 shows experiments investigating the time-variant change in sound coloration for a pink noise virtual source rotating at a speed of $100°$/s, and for different Ambisonic panning setups. There is an obvious andvantage at both listening positions, centered and off-center, in using the sidelobe suppressing "$\max - \boldsymbol{r}_\mathrm{E}$" weighting instead of the "basic" rectangular truncation of the Fourier series to keep the coloration constant. At the off-center listening position, this weighting scheme achieves good results with regard to constant coloration for both 3^rd and 7^th order arrangements with 8 and 16 loudspeakers that were investigated.

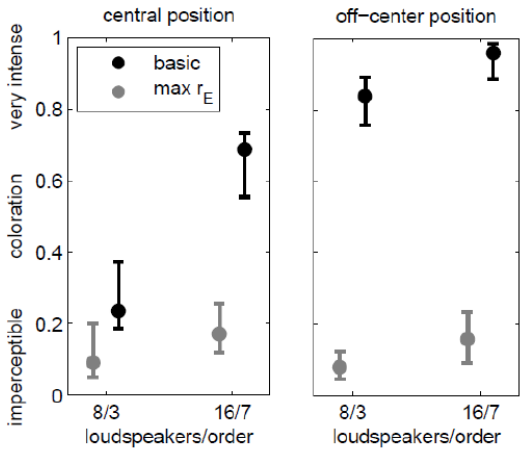

Figure 19 – Frank's 2013 experiments on the variation of the sound coloration of virtual sources rotating at a speed of $100°/\mathrm{s}$ imply that $\max - \boldsymbol{r}_\mathrm{E}$ weighting outperforms the "basic" weighting with $a_m = 1$, and that adjusting the number of louspeakers to the Ambisonic order seems to be reasonable.

5 Encoding/Decoding for surrounding rings and hemispheres

Both axisymmetric sets of orthogonal polynomials used for Ambisonic panning, Chebyshev for the circle and Legendre for the sphere, allow for addition theorems that embed them into a function space without specific axial symmetry. This permits to superimpose several panning functions symmetric wrt. different axes, which is the basis of Ambisonic encoding and the geometry-agnostic Ambisonic signal format. To arrive at the mathematical description, the Laplacian is solved without symmetry constraint.

5.1 Angular harmonics for circle and sphere

A unit direction vector for two dimensions depends on the polar azimuth angle, while in three dimensions, there is also the dependency on the zenith angle ϑ, see Fig. 36,

$$\boldsymbol{\theta} = \begin{pmatrix}\cos\varphi\\ \sin\varphi\end{pmatrix} = \begin{pmatrix}\sqrt{1-\mu^2}\\ \mu\end{pmatrix}, \qquad \boldsymbol{\theta} = \begin{pmatrix}\cos\varphi\,\sin\vartheta\\ \sin\varphi\,\sin\vartheta\\ \cos\vartheta\end{pmatrix}. \tag{49}$$

This means that these harmonics are not only variable in terms of the direction vector's last coordinate.

Square-integrable functions only depending on the direction, not having any symmetry restriction therefore could be expressed in harmonics with regard to those coordinates. The following two sections derive those angular harmonics.

5.1.1 Circular harmonics

Appendix K re-writes the Laplacian $\triangle = \frac{\partial^2}{\partial x^2} + \frac{\partial^2}{\partial y^2}$ for $\mathrm{D} = 2$ to a single depencency on the polar angle $\varphi = \arctan\frac{y}{x}$. We obtain

$$\triangle_\varphi = \frac{\partial^2}{\partial x^2} + \frac{\partial^2}{\partial y^2} = \frac{x^2+y^2}{r_{xy}^4}\frac{\partial^2}{\partial\varphi^2} = \frac{1}{r_{xy}^2}\frac{\partial^2}{\partial\varphi^2}. \tag{50}$$

Eigensolutions to this Laplacian $r_{xy}^2\triangle_\varphi\Phi = -\lambda\,\Phi$ are solved by the guessing an exponential solution $\Phi = e^{a\phi}$ and yield, e.g., $\Phi = e^{\pm\mathrm{i}\sqrt{\lambda}\varphi}$. The only way to obtain a necessarily geometrically periodic solution in the azimuth angle is to set $\lambda = m^2$ with $m \in \mathbb{Z}$, yielding $\Phi = e^{\mathrm{i}m\varphi}$. As this is more convenient in most cases, we could also choose real-valued trigonometric solutions as normalized circular harmonics :

$$\Phi_m(\varphi) = \sqrt{\frac{2-\delta_{m,0}}{2\pi}}\begin{cases}\cos(m\varphi_\mathrm{s}), & m \geq 0,\\ \sin(|m|\varphi_\mathrm{s}), & m < 0.\end{cases} \tag{51}$$

5.1.2 Spherical harmonics

Appendix K re-writes the Laplacian $\triangle = \frac{\partial^2}{\partial x^2} + \frac{\partial^2}{\partial y^2} + \frac{\partial^2}{\partial z^2}$ for $\mathrm{D} = 3$ is to its angular dependencies on azimuth $\varphi = \arctan\frac{y}{x}$ and cosine $\mu = \arccos\frac{z}{r}$ of the zenith angle $\mu = \cos\vartheta$. We get

$$r^2 \triangle_{\varphi,\mu} = (1-\mu^2)\frac{\partial^2}{\partial \mu^2} - 2\mu\frac{\partial}{\partial\mu} + \frac{1}{1-\mu^2}\frac{\partial^2}{\partial\varphi^2}. \tag{52}$$

We search for spherical harmonics by solving

$$r^2 \triangle_{\varphi,\mu} Y = -\lambda Y.$$

We guess a product as suitable eigensolution $Y = \Theta(\mu)\,\Phi(\varphi)$, and we desire periodic harmonics Φ_m in φ with the eigenvalue $\frac{1}{1-\mu^2}\frac{\partial\Phi_m}{\partial\varphi} = -\frac{m^2}{1-\mu^2}\Phi_m$. We also desire convergent solutions in μ and so use $(1-\mu^2)\frac{\partial^2}{\partial\mu^2}\Theta - 2\mu\frac{\partial}{\partial\mu}\Theta = n(n+1)\Theta$, with the eigenvalues of the axisymmetric polynomials from Eq. (17) for $\mathrm{D} = 3$. Inserted into the equation above, and after division by Φ_m, we obtain a modified equation for the missing function Θ depending on the cosine of the zenith angle in $\mu = \cos\vartheta$

$$(1-\mu^2)\frac{\partial^2}{\partial\mu^2}\Theta - 2\mu\frac{\partial}{\partial\mu}\Theta + \left[n(n+1) - \frac{m^2}{1-\mu^2}\right]\Theta = 0. \tag{53}$$

With $-n < m < n$, the equation is the *associated* or *shifted Legendre differential equation*, and it is solved by the *associated Legendre functions* $\Theta = P_n^m(\mu)$. They are called functions as they involve a factor $\sqrt{1-\mu^2} = \sin\vartheta$ for every odd m besides the polynomial part in μ. With $m = 0$ this equation is called *Legendre differential equation* and the solutions are the Legendre polynomials $\Theta = P_n(\mu)$ as above.

The fully normalized spherical harmonics are shown in Fig. 20 for orders n up to 3, and they are written as:

$$Y_n^m(\boldsymbol{\theta}) = \sqrt{\frac{2n+1}{2}\frac{(n-|m|)!}{(n+|m|)!}}\,P_n^m(\cos\vartheta)\;\Phi_m(\varphi). \tag{54}$$

Note that while the above N3D normalization $\int_{\boldsymbol{\theta}\in\mathbb{S}^2} |Y_n^m(\boldsymbol{\theta})|^2\,\mathrm{d}\boldsymbol{\theta} = 1$ *defines the magnitude of the spherical harmonics, but its sign or complex phase can be arbitrary. Legendre functions are defined differently in literature, and it can be* $\sin(m\varphi)$ *instead of* $\sin(|m|\varphi)$. *In Ambisonics, real-valued functions and the SN3D normalization* $\sqrt{\frac{1}{2}\frac{(n-|m|)!}{(n+|m|)!}}$ *are prefered, and positive signs of the first-order dipole components in the directions of the respective coordinate axes,* x, y, z, *which might require to involve the Condon-Shortley phase* $(-1)^m$ *fixing the signs of the Legendre functions or* $1-2u[m+1]$ *to fix the phase of the sinusoids, depending on the implementation of the respective functions.*

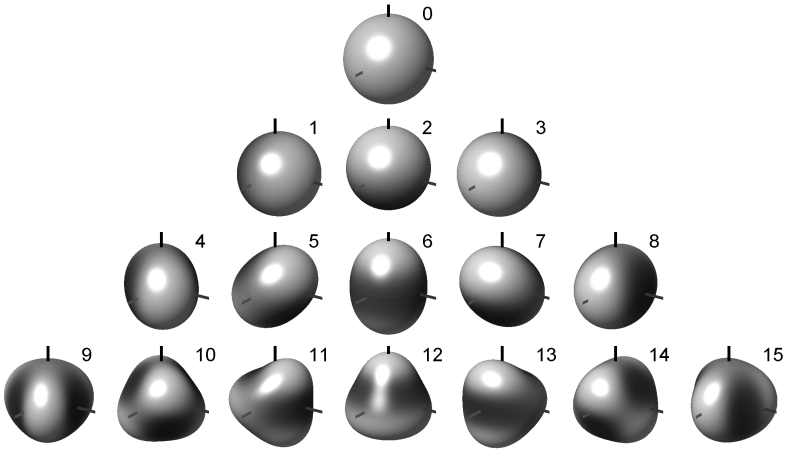

Figure 20 – Spherical harmonics (Kugelflächenfunktionen) indexed by Ambisonic channel number $ACN = n^2 + n + m$; rows show spherical harmonics for the order $0 \leq n \leq 3$ with the $2n + 1$ harmoncis of the degree $-n \leq m \leq n$. What is plotted is a surface of the radius $R = 0.8 + 0.2\, Y_n^m(\boldsymbol{\theta})$ with the magnitude coded in color: gray signifies zero, with black negative excursion, white positive excursion. The order n counts the circular zero crossings, and $|m|$ counts those running through zenith and nadir.

5.2 Encoding and Decoding

The relations called addition theorems embed the polynomial axisymmetric harmonics $T_m(\cos\varphi) = \cos m\varphi$ for $\mathrm{D} = 2$ and $P_n(\cos\vartheta)$ for $\mathrm{D} = 3$ in the more general solutions Φ_m and Y_n^m, respectively. for For the Chebyshev polynomials, the addition theorem is

$$\cos[m(\varphi - \varphi_\mathrm{s})] = \sin(m\varphi)\sin(m\varphi_\mathrm{s}) + \cos(m\varphi)\cos(m\varphi_\mathrm{s}) = \frac{2\pi\Phi_m(\varphi_s)\Phi_m(\varphi)}{2 - \delta_{m,0}}, \quad (55)$$

and for the Legendre polynomials, the addition theorem is

$$\frac{2n+1}{4\pi} P_n(\boldsymbol{\theta}_\mathrm{s}^\mathrm{T}\boldsymbol{\theta}) = \sum_{m=-n}^{n} Y_n^m(\boldsymbol{\theta}) Y_n^m(\boldsymbol{\theta}_\mathrm{s}). \quad (56)$$

Both of these addition theorems Eqs. (55) (56) have in common that while the direction φ_s or $\boldsymbol{\theta}_\mathrm{s}$ is used to shift the argument of the axisymmetric harmonic to a desired symmetry axis (virtual source direction) on their left-hand equation side, the right-hand side uses more general functions evaluated at the variables φ or $\boldsymbol{\theta}$, respectively, and seperately at the virtual source direction φ_s or $\boldsymbol{\theta}_\mathrm{s}$, respectively. This splits up the calculation of the Ambisonic panning gains into two parts, encoding and decoding.

In mixing and production, encoding represents the directional composition of the audio scene, and decoding expresses the surround directions represented by the loudspeaker playback facility.

5.3 Encoding and continuous decoding for 2D

Taking a signal $s(t)$ that is to be represented at the direction φ_s, the encoding to obtain the $2\mathrm{N}+1$ order-limited 2D Ambisonic signals, $-\mathrm{N} \le m \le \mathrm{N}$, in *full normalization* can be written as

$$\chi_m(t) = a_m \, \Phi_m(\varphi_\mathrm{s}) \; s(t), \tag{57}$$

including the weights a_m (e.g. $\max - \boldsymbol{r}_\mathrm{E}$). The surround signal could be expanded over the variable direction φ using a continuous decoding (without discretization)

$$s(\varphi, t) = \sum_{m=-\mathrm{N}}^{\mathrm{N}} \Phi_m(\varphi) \; \chi_m(t). \tag{58}$$

5.4 Encoding and continuous decoding for 3D

Taking a signal $s(t)$ that is to be represented at the direction $\boldsymbol{\theta}_\mathrm{s}$, the encoding to obtain the $(\mathrm{N}+1)^2$ order-limited 3D Ambisonic signals, $0 \le n \le \mathrm{N}$, $-n \le m \le n$, in *full normalization* can be written as

$$\chi_n^m(t) = a_n \, Y_n^m(\boldsymbol{\theta}_\mathrm{s}) \; s(t), \tag{59}$$

including the weights a_n (e.g. $\max - \boldsymbol{r}_\mathrm{E}$), and the surround signal can be expanded over the variable direction $\boldsymbol{\theta}$ using a continuous decoding (without discretization, if SN3D normalization is used instead of N3D, an additional factor $(2n+1)$ is required)

$$s(\boldsymbol{\theta}, t) = \sum_{n=0}^{\mathrm{N}} \sum_{m=-n}^{n} Y_n^m(\boldsymbol{\theta}) \; \chi_n^m(t). \tag{60}$$

5.5 Decoder matrix design

Continuous surround loudspeaker distributions are infeasible, and there will always be the necessity to discretize to the playable set of discrete directions ϑ_l or φ_l, which are represented by the surrounding loudspeakers' directions.

As the directional distribution of the surrounding loudspeakers can be non-uniform or for other purposes, the equations related to encoding and discrete decoding were formulated in terms of matrices and vectors:

$$\boldsymbol{\chi}_\mathrm{N}(t) = \mathrm{diag}\{\boldsymbol{a}_\mathrm{N}\} \; \boldsymbol{y}_\mathrm{N}(\boldsymbol{\theta}_\mathrm{s}) \, s(t), \tag{61}$$

$$\boldsymbol{s}(t) = \mathbf{D} \, \boldsymbol{\chi}_\mathrm{N}(t). \tag{62}$$

Hereby, the decoding matrix $\mathbf{D}$ can be defined in various ways.

5.5.1 Sampling

The first and natural definition of $\mathbf{D}$ uses the fact that one could also use sampling of the harmonic functions with suitable t designs. Using the playback loudspeakers' directions ϑ_l, we can define a matrix of the encoding vectors $\boldsymbol{y}_{\mathrm{N}}(\vartheta_l)$ that would be used to represent each of the loudspeakers in Ambisonics:

$$\mathbf{Y}_{\mathrm{N}} = [\boldsymbol{y}_{\mathrm{N}}(\vartheta_1), \ldots, \boldsymbol{y}_{\mathrm{N}}(\vartheta_1)]. \tag{63}$$

Sampling decoding would get the loudspeaker signals as

$$\boldsymbol{s}(t) = \frac{4\pi}{\mathrm{L}} \mathbf{Y}_{\mathrm{N}}^{\mathrm{T}} \boldsymbol{\chi}_{\mathrm{N}}(t), \tag{64}$$

where the factor $\frac{4\pi}{\mathrm{L}}$ takes into account that the number of loudspeakers should not increase the level and should represent the unit sphere. This defines the sampling decoder

$$\mathbf{D} = \frac{4\pi}{\mathrm{L}} \mathbf{Y}_{\mathrm{N}}^{\mathrm{T}}. \tag{65}$$

Other important decoder design techniques such as mode matching [Pol05, Dan00] and energy-preserving [ZPN12] decoding are left out here for brevity.

5.5.2 AllRAD

Despite its simplicity, the All-Round Ambisonic Decoder (AllRAD [ZF12]) is the most versatile decoding technique so far. It combines the flexibility of vector-base amplitude panning with the smoothness advantage of Ambisonic panning, and allows for always relatively well-behaved playback of Ambisonic content on any non-uniform surround loudspeaker arrangements.

AllRAD uses sampling decoding to a virtual, high-resolution t design loudspeaker layout, e.g. a 5200 pts. design from [GP11], in order to obtain optimal $\boldsymbol{r}_{\mathrm{E}}$, $\boldsymbol{r}_{\mathrm{V}}$, E, P measures, virtually. To obtain signals and still quite optimal measures on the available physical loudspeakers, the 5200 virtual-loudspeaker signals are fed through a static VBAP matrix $\boldsymbol{G}$ that supplies the available loudspeakers

$$\mathbf{D} = \boldsymbol{G} \, \frac{4\pi}{\mathrm{L}'} \boldsymbol{Y}_{\mathrm{N}}^{\mathrm{T}}. \tag{66}$$

Note that the insertion of *imaginary* loudspeakers as described in Sec. 3.4 is a necessary step to prevent signal loss when panning a virtual source close to the boundaries of the available surround loudspeaker array, as described in [ZF12].

6 Intensity-based stereo recording

Classical coincident recording considers capturing a mid and side component. The technique dates back to Blumlein in the 1930s [Blu33]. This can be done by using a pair of coincident directional microphones, be it an omnidirectional micropohone or two cardioid microphones opposing each other, both is possible. The pickup pattern obtained is

$$\boldsymbol{g}(\varphi) = \begin{bmatrix} 1 \\ \cos(\varphi) \end{bmatrix}. \tag{67}$$

and by modifying the strength of mid vs. side channel of both channels before stereo playback with a blending parameter $0.5 \leq \alpha \leq 1$,

$$\begin{bmatrix} L \\ R \end{bmatrix} = \begin{bmatrix} 1 & 1 \\ 1 & -1 \end{bmatrix} \begin{bmatrix} a & 0 \\ 0 & (1-a) \end{bmatrix} \begin{bmatrix} 1 \\ \cos(\varphi) \end{bmatrix} \boldsymbol{g}(\varphi), \tag{68}$$

one can modify the stereo width of an M/S recording.

7 Ambisonic recording

After Cooper and Shiga [CS72] worked on expressing panning strategies for arbitrary surround loudspeaker setups in terms of Fourier series, the notion and technology of Ambisonics was developed by Felgett [Fel74], Gerzon [Ger75], and Craven [CG77]. In particular, Craven, Felgett, and Gerzon were also considering a suitable recording technology.

While this idea of representing the directional information surround sound signals might still be obvious for one omnidirectional microphone, one front-back-oriented and one left-right-oriented figure-of-eight microphone, the question is: what would be the mathematical advantage of doing Fourier expansions of the surround sound when we might not be able to capture it in this way with the classical recording technology?

7.1 First order (encoding)

Assuming 3 coincident cardioid microphones that point into a set of balanced directions ϑ_1, ϑ_2, ϑ_3 on the horizontal plane ($0°$, $\pm 120°$) can be denoted by the following set of pickup patterns depending on the variable direction $\boldsymbol{\theta}$ of the incoming sound

$$\boldsymbol{g}(\boldsymbol{\theta}) = \frac{1}{2} + \frac{1}{2} \begin{bmatrix} \vartheta_1^{\mathrm{T}} \\ \vartheta_2^{\mathrm{T}} \\ \vartheta_3^{\mathrm{T}} \end{bmatrix} \boldsymbol{\theta} = \frac{1}{2} + \frac{1}{2} \begin{bmatrix} 1 & 0 \\ -\frac{1}{2} & \frac{\sqrt{3}}{2} \\ -\frac{1}{2} & -\frac{\sqrt{3}}{2} \end{bmatrix} \boldsymbol{\theta} = \frac{1}{2} + \frac{1}{2} \begin{bmatrix} \cos(\varphi) \\ \cos(\varphi + 120°) \\ \cos(\varphi - 120°) \end{bmatrix}.$$

Combining all the three microphone signals by $\frac{2}{3}\mathbf{1}^{\mathrm{T}}\boldsymbol{g}(\varphi)$ yields an omnidirectional pickup pattern

$$\frac{2}{3}\mathbf{1}^{\mathrm{T}}\boldsymbol{g}(\varphi) = 1, \tag{69}$$

as $\sum_{k=0}^{N-1} \cos(\varphi + \frac{2\pi}{N}k) = 0$. Moreover, combining the microphone signals by the following matrix yields omnidirectional characteristics and dipole characterisitcs into the x and y directions

$$\frac{2}{3}\begin{bmatrix} 1 & 1 & 1 \\ 1 & -1 & -1 \\ -1 & 1 & 1 \end{bmatrix} \boldsymbol{g}(\varphi) = \begin{bmatrix} 1 \\ \cos(\varphi) \\ \sin(\varphi) \end{bmatrix}. \tag{70}$$

It is not surprising that the same principle also works for a coincident tetrahedron microhone array of cardioids with the aiming directions FLU-FRD-BLD-BRU

$$\boldsymbol{g}(\boldsymbol{\theta}) = \frac{1}{2} + \frac{1}{2}\begin{bmatrix} \boldsymbol{\theta}_1^{\mathrm{T}} \\ \boldsymbol{\theta}_2^{\mathrm{T}} \\ \boldsymbol{\theta}_3^{\mathrm{T}} \\ \boldsymbol{\theta}_4^{\mathrm{T}} \end{bmatrix} \boldsymbol{\theta} = \frac{1}{2} + \frac{1}{2}\frac{1}{\sqrt{3}}\begin{bmatrix} 1 & 1 & 1 \\ 1 & -1 & -1 \\ -1 & 1 & -1 \\ -1 & -1 & 1 \end{bmatrix} \boldsymbol{\theta}. \tag{71}$$

Encoding is achieved there by the matrix that adds all microphone signals in the first line, subtracts back from front microphone signals in the second line, subtracts right from left microphone singals in the third line, and subtracts down from up microphone signals in the last line

$$\frac{1}{2}\begin{bmatrix} 1 & 1 & 1 & 1 \\ 1 & 1 & -1 & -1 \\ 1 & -1 & 1 & -1 \\ 1 & 1 & -1 & -1 \end{bmatrix} \boldsymbol{g}(\varphi). \tag{72}$$

As for higher frequencies, where typical capsules cannot be considered coincident anymore, there will be besides directional error a loss of presence, a shelving filter that slightly boosts high frequencies above the spatial aliasing limit is typical. Roughly, an up to 3 dB boost can be done for frequencies above which the microphone spacing reaches half a wavelength.

Upmixing. As first-order recorcdings are not highly resolved, there are several works on algorithms with resolution enchancement strategies that re-assign time-frequency bins more sharply to directions. A good summary has been given by Politis [Pol16]. Technologies are called DirAC, HOA-DirAC, Harpex.

Higher order. Higher-order microphones require more of the acoustic holophonic and holographic basics than presented above. Higher-order recording is dealt with after the derivation of the wave equation, Kirchhoff-Helmholtz integral equation, and soluitions in the spherical coordinate system.

8 The Helmholtz equation (Derivation, Cartesian coordinates)

The holophony and holography discussed in this lecture is based on the lossless linear wave equation in the frequency domain, the Helmholtz equation. It is the fundamental relation underlying any practical implementation to solve holographic or holophonic problems, and this chapter presents a derivation based on Cartesian coordinates and known Newtonian equation of motion (mass $F = m\,\ddot{\xi}$, spring $F = s\,\xi$). The derivation starts out with a differential mechanical segment whose repetition to a chain yields a wave-propagating system. Changing the forces stretching the segments into area-related forces pressing the segment, i.e. pressures, and re-writing the spring equations with regard to the adiabatic stiffnes of air yields the Helmholtz equation.

8.1 Differential Mass and Spring Segment

The most compact derivation of the wave equation considers a differentially small mass spring structure as its basic element. Fig. 21 describes the dimension x as a position on

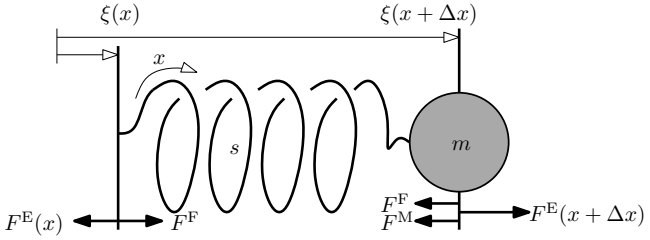

Figure 21 – Differential mass and spring segment.

the spring, e.g. its third winding. The coordinate $\xi(x)$ by contrast describes the deflected location in space, cf. [Mös09].

Spring and mass. A spring reacts with a force, opposing deformation from the relaxed state, which is described by a deflection $\xi_{\mathrm{entsp}}(x) = x$. The spring length $\xi(x+\Delta x) - \xi(x)$ therefore equals Δx for the relaxed spring. Upon deformation, the spring force is proportional to the length difference $\xi(x+\Delta x) - \xi(x) - \Delta x$ and the stiffness s of the spring. A mass element at the location $\xi(x+\Delta x)$ in space reacts with a force proportional to its mass m and acceleration $\ddot{\xi}(x+\Delta x)$ of its location. The equations for both forces are

$$F^{\mathrm{F}} = s\Big[\xi(x+\Delta x) - \xi(x) - \Delta x\Big] \qquad \xrightarrow{\frac{\partial}{\partial t}} \dot{F}^{\mathrm{F}} = s\Big[v(x+\Delta x) - v(x)\Big],$$

$$F^{\mathrm{M}} = m\,\ddot{\xi}(x+\Delta x) \qquad \xrightarrow{\frac{\partial}{\partial t}} \dot{F}^{\mathrm{M}} = m\,\dot{v}(x+\Delta x).$$

The opportunity was used to derive both equations with regard to time, so that we could get rid of the term Δx in the first equation. The deflection ξ hereby always appears derived at least once, so that we may exchange its letter $\dot{\xi} = v$, $\ddot{\xi} = \dot{v}$, $\dddot{\xi} = \ddot{v}$ by the velocity and

its derivatives. At the left and right end of the segment we have different equations for an equilibrium of the internal and the external forces $F^{\mathrm{E}}(x)$ and $F^{\mathrm{E}}(x+\Delta x)$, due to the right-sided location of the mass:

$$\begin{aligned} \text{left end:} \qquad & F^{\mathrm{E}}(x) = F^{\mathrm{F}} \\ & \xrightarrow{\frac{\partial}{\partial t}} \dot{F}^{\mathrm{E}}(x) = s\,[v(x+\Delta x) - v(x)]\,, \qquad (73) \\ \text{right end:} \qquad & F^{\mathrm{E}}(x+\Delta x) = F^{\mathrm{F}} + F^{\mathrm{M}} \\ & \xrightarrow{\frac{\partial}{\partial t}} \dot{F}^{\mathrm{E}}(x+\Delta x) = s\,[v(x+\Delta x) - v(x)] + m\,\ddot{v}(x+\Delta x). \qquad (74) \end{aligned}$$

Appendix M solves a 0D wave equation, inwhich the end at $x = 0$ is clamped so that $v(0) = 0$.

8.2 1D Wave equation (longitudinal medium with specific mass and spring)

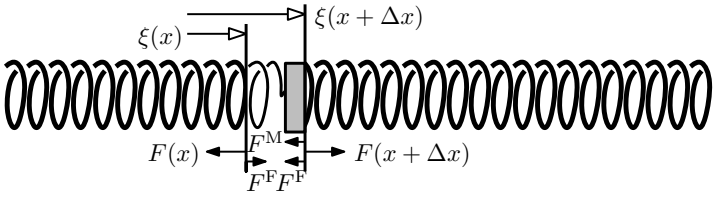

Figure 22 – Continuous spring with specific mass.

A one-dimensional medium is characterized by a chain of infinitesimally small mass and spring segments as described by Figs. 21, 22. There are length-related parameters specific for the material: specific mass ρ, bulk modulus K. The effective mass increases with material length $m = \rho\,\Delta x$, while the effectiv stiffness decreases with length: $s = K/\Delta x$.

Subtracting Eqs. (74)(73) and taking the limit $\Delta x \to 0$, we obtain a differential quotient, i.e. a partial spatial derivative:

$$\begin{aligned} F(x+\Delta x) - F(x) &= \rho\,\Delta x\;\dot{v}(x+\Delta x), \qquad \Big|\ \text{mit } \frac{1}{\Delta x} \text{ und } \lim_{\Delta x\to 0} \\ \frac{\partial}{\partial x} F &= \rho\;\dot{v}. \qquad (75) \end{aligned}$$

The same is true for Eq. (74) derived wrt. time

$$\begin{aligned} \dot{F}(x) &= K\;\frac{v(x+\Delta x) - v(x)}{\Delta x}, \qquad \Big|\ \lim_{\Delta x\to 0} \\ \dot{F}(x) &= K\;\frac{\partial}{\partial x}\;v. \qquad (76) \end{aligned}$$

The spatially derived Eq. (76) yields eith the temporally derived Eq. (75) $K\,\frac{\partial^2}{\partial x^2} v = \rho\,\ddot{v}$. After division by K and replacing $c^2 = \frac{\rho}{K}$, the following compact notation is common

$$\left(\frac{\partial^2}{\partial x^2} - \frac{1}{c^2}\,\frac{\partial^2}{\partial t^2}\right) v = 0. \qquad (77)$$

We call this equation *wave equation*.

It obviously involves a factor $\frac{1}{c^2}$ to combine an oscillatory equation with regard to time with one in terms of location.

Homogeneous solution. We guess the solution to be a product of two exponential functions: $e^{\mathrm{i}\,\omega\,t}$, $e^{\mathrm{i}k\,x}$. This solution $v_\mathrm{h} = e^{\mathrm{i}\,\omega\,t}\,e^{\mathrm{i}k\,x}$ is expected to separate into parts upon insertion. In doing so, Eq. (77) delivers us the *characteristic equation*:

$$\begin{aligned}(\mathrm{i}k)^2\,v_\mathrm{h} - \frac{(\mathrm{i}\omega)^2}{c^2}\,v_\mathrm{h} = 0 \qquad &\left|\frac{1}{v_\mathrm{h}}\right.\\ k^2 = \frac{\omega^2}{c^2}.\end{aligned} \tag{78}$$

Consequently the required $k = \pm\omega/c$ yields the homogeneous solution at any frequency ω:

$$v_\mathrm{h} = a\,e^{\mathrm{i}\omega t+\mathrm{i}kx} + b\,e^{\mathrm{i}\omega t-\mathrm{i}kx}. \tag{79}$$

Since negative phase corresponds to delay, the solution $e^{\mathrm{i}\omega t+\mathrm{i}kx}$ arrives later at negative x, therefore propagates backwards. The other wave $e^{\mathrm{i}\omega t-\mathrm{i}kx}$ arrives later at positive x, therefore corresponds to the forwards-traveling wave.

Inhomogeneous Solution. If there is an excitation of the wave equation at the instant $t = 0$ and location $x = 0$,

$$\left(\frac{\partial^2}{\partial x^2} - \frac{1}{c^2}\frac{\partial^2}{\partial t^2}\right) v = \delta(t)\,\delta(x), \tag{80}$$

we can give the solution in terms of an integral

$$v_\mathrm{in} = \int_{-\infty}^{\infty}\int_{-\infty}^{\infty} \nu(\omega,k)\,e^{\mathrm{i}\,\omega\,t}\,e^{\mathrm{i}k\,x}\,\mathrm{d}k\,\mathrm{d}\omega \tag{81}$$

and get upon insertion

$$\int_{-\infty}^{\infty}\int_{-\infty}^{\infty}\left[(\mathrm{i}k)^2 - \frac{(\mathrm{i}\omega)^2}{c^2}\right]\nu(\omega,k)\,e^{\mathrm{i}\,\omega\,t}\,e^{\mathrm{i}k\,x}\,\mathrm{d}k\,\mathrm{d}\omega = \delta(t)\,\delta(x) \tag{82}$$

and two-fold application of the Fourier integral $\iint e^{\mathrm{i}k'x}e^{\mathrm{i}\omega' t}\,\mathrm{d}x\,\mathrm{d}t$ and orthogonalities $\int e^{\mathrm{i}(k-k')x}\mathrm{d}x = 2\pi\delta(k-k')$, $e^{\mathrm{i}(\omega-\omega')t}\mathrm{d}t = 2\pi\delta(t-t')$,

$$\nu(\omega,k) = \frac{1}{(2\pi)^2}\frac{c^2}{\omega^2 - k^2c^2} = \frac{1}{(2\pi)^2}\frac{c^2}{(\omega-kc)(\omega+kc)}. \tag{83}$$

Causality $v_\mathrm{in}(t<0) = 0$ in the Fourier integral constructing the time-domain response requires a shift of poles to $\lim_{\epsilon\to+0}\frac{c^2}{(\omega-\mathrm{i}\epsilon-kc)(\omega-\mathrm{i}\epsilon+kc)}$. The knowledge of this physically required shift is sufficient to describe the physical solution in the frequency domain. We

only transform the spectral coefficient $\nu(\omega, k)$ of Eq. (81) back into the space domain and skip the transformation to the time domain. Partial fraction expansion with regard to k yields:

$$\nu(\omega, k) = \lim_{\epsilon \to +0} \frac{c}{2\omega} \left[\frac{1}{k - \frac{\omega - \mathrm{i}\epsilon}{c}} - \frac{1}{k + \frac{\omega - \mathrm{i}\epsilon}{c}} \right]. \tag{84}$$

$$v(\omega, x) = \lim_{\epsilon \to +0} \frac{1}{2\pi} \frac{c}{2\omega} \int_{-\infty}^{\infty} \left[\frac{e^{\mathrm{i}kx}}{k - \frac{\omega - \mathrm{i}\epsilon}{c}} - \frac{e^{\mathrm{i}kx}}{k + \frac{\omega - \mathrm{i}\epsilon}{c}} \right] \mathrm{d}\omega. \tag{85}$$

Using Jordan's lemma for the integrand $e^{\mathrm{i}kx}$ excluding the pole, then for $x \geq 0$ it is

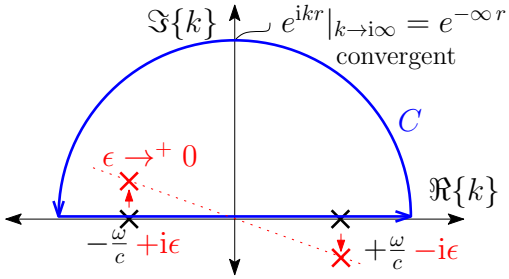

Figure 23 – Causality-enforcing regularization of the polse of the inhomogeneous solution of the wave equation with regard to the wave number k. Closure of the improper integration path is required to run on a semicircle on the positive imaginary half space C_+ for $x \geq 0$, or the negative imaginary half-space C_- for $x < 0$.

required to close the integral by an infinite semicircle over the positive imaginary axis, and hereby the integration only contains the second pole $kc = -\omega + \mathrm{i}\epsilon$, cf. Fig. 23. For $x < 0$ the mathematically negatively oriented path C_- is required that contains $kc = \omega - \mathrm{i}\epsilon$. The sign change of the differently oriented paths C_+ and C_- cancels with the signs of the partial fractions:

$$v_{\mathrm{in}}(\omega, x) = -\frac{1}{2\pi} \frac{c}{2\omega} 2\pi\mathrm{i}\, e^{-\mathrm{i}\frac{\omega}{c}|x|} = \frac{c}{2\mathrm{i}\omega} e^{-\mathrm{i}\frac{\omega}{c}|x|}.$$

It is common to simplify $\frac{\omega}{c}$ by the letter k

$$v_{\mathrm{in}} = \frac{e^{-\mathrm{i}k|x|}}{2\mathrm{i}k}. \tag{86}$$

8.3 1D Helmholtz equation

One-diensional, longitudinal sound propagation in air is equivalent to the one on the mass-loaded spring described before, by the only change that instead of the negative force (=tensile strain) per surfacce, we insert $p = -F/A$ in the equations. As propagation in the air usually does not produce heat convection (at high-enough frequencies, *adiabatic change*, i.e. only short-time and local heat oscillation), the equation is lossless. Adiabatic changes are characterized by

$$p\,V^\kappa = \text{const.}, \tag{87}$$

for which the adiabatic index (heat capacity ratio) of the air is $\kappa = 1.4$. Even after a change $(p_0, V_0) \to (p_0 + \Delta p, V_0 + \Delta V)$ the result of the above equation must be equal to the same constant. Pulling out the original state simplifies linearization for small volume changes:

$$p_0\,V_0^\kappa = p_0\,V_0^\kappa \underbrace{(1+\frac{\Delta p}{p_0})\,(1+\frac{\Delta V}{V_0})^\kappa}_{=1} \qquad \Rightarrow 1+\frac{\Delta p}{p_0} = \underbrace{(1+\frac{\Delta V}{V_0})^{-\kappa}}_{\approx 1-\kappa\frac{\Delta V}{V_0}+\frac{\kappa(\kappa-1)}{2!}\cancel{\frac{\Delta V^2}{V_0^2}\ldots}}$$

$$\Longrightarrow \Delta p = -\kappa\,p_0\frac{\Delta V}{V_0}.$$

The adiabatic equation is now linearized for small volume changes [1] $\Delta V = V - \Delta x\Delta y\Delta z$ and we describe the volume change in terms of deflection wrt. the x direction

$$V = [\xi(x+\Delta x) - \xi(x)]\Delta y\Delta z = \Delta\xi\Delta y\Delta z = \frac{\Delta\xi}{\Delta x}\,V_0, \;\; \Rightarrow \Delta p = -\kappa\,p_0\left(\frac{\Delta\xi}{\Delta x} - 1\right).$$

Differentiating in time, $\frac{\partial\Delta p}{\partial t} = \frac{\partial(p-p_0)}{\partial t} = \dot p$, sowie $\frac{\partial}{\partial t}\left(\frac{\Delta\xi}{\Delta x} - 1\right) = \frac{\Delta v}{\Delta x}$, and taking the limit $\lim_{\Delta x\to 0}$, we obtain the compression equations:

$$\dot p = -\kappa\,p_0\,\frac{\partial v}{\partial x},$$

and the constants yield the bulk modulus $K = \kappa\,p_0 \approx 1.4\cdot 10^5$Pa. Euler's equation of motion is similar to Eq. (75), $\Delta F = \rho\Delta x\Delta y\Delta z\frac{\partial v}{\partial t}$, only that we replace the external tensile strain by the negative pressure loading on the exterior surface $F = -p\,\Delta y\Delta z$ and get $-\Delta p\Delta y\Delta z = \rho\Delta x\Delta y\Delta z\frac{\partial v}{\partial t}$. Division by $\Delta x\Delta y\Delta z$ and $\lim_{\Delta x\to 0}$ yields the equation of motion. Together with the compression equation this becomes ($c = \sqrt{\frac{K}{\rho}}$),

$$\begin{aligned} \rho\,\dot v &= -\frac{\partial}{\partial x}p, \\ -\dot p &= K\,\frac{\partial}{\partial x}v, \\ \Longrightarrow \left(\frac{\partial^2}{\partial x^2} - \frac{1}{c^2}\frac{\partial^2}{\partial t^2}\right)p &= 0. \end{aligned}$$

1. Volume changes are sufficiently small as long as the second-order term vanishes wrt. the first-order term $\frac{\kappa(\kappa-1)}{2!}\frac{\Delta V^2}{V_0^2} \ll \kappa\frac{\Delta V}{V_0}$. Equality $\frac{\Delta V}{V_0} = \frac{2}{\kappa-1} \approx 7$ would require a changing pressure of $|\Delta p| = \kappa\,p_0\frac{\Delta V}{V_0} = 7\cdot 10^5$ Pa; related to $2\cdot 10^-5$ Pa this amounts to astonishing 210 dB.

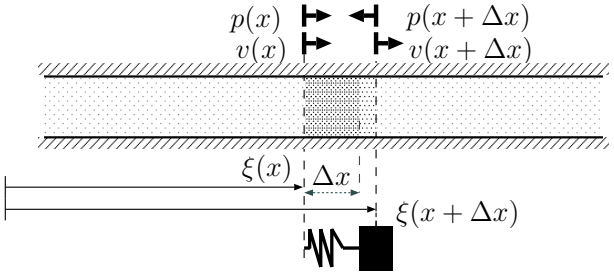

Figure 24 – Model of linear lossless wave propagation.

According to the first equation, a particle starts to move into the direction of pressure decrease. According to the second equation, it yields a pressure decrease inside the volume segment, whenever the end oriented leading into the direction of motion is moving faster than the one behind.

We guess an exponential solution wrt. time and write in the Fourier deomain $p(t) = p(\omega)e^{\mathrm{i}\omega t}$, which uses the somewhat jaunty convention in acoustics to use same letters for quantities in frequency or time domain.

The resulting linearl lossless wave equation in the frequency domain is called *Helmholtz* equation:

$$\frac{\partial}{\partial x}\, p = -\mathrm{i}\,\omega\,\rho\,v \qquad \text{equation of motion,} \tag{88}$$

$$\mathrm{i}\,\omega\, p = -K\,\frac{\partial}{\partial x}\, v \qquad \text{equation of compression,} \tag{89}$$

$$\left(\frac{\partial^2}{\partial x^2} + \frac{\omega^2}{c^2}\right)\, p = 0, \qquad \underline{\text{1D Helmholtz equation}} \tag{90}$$

To recognize equations in the frequency domain, it is often sufficient to find ω or k as dependencies, or to recognize the absence of time or temporal derivatives.

8.4 Helmholtz equation in higher dimensions

In a multidimensional space, the equations for linear air-bourne sound nearly look identical. A scheme for the differential air element in 2D is shown in Fig. 25. All relations are free from torque.

The interior increase of the pressure of the volume element over time now involves the spatial decreases of the pressure in all spatial dimensions (the gradient is denoted by *del* $\boldsymbol{\nabla}^{\mathrm{T}} = [\frac{\partial}{\partial x}, \frac{\partial}{\partial y}, \dots])$

$$\dot{p} = -K\,\left[\frac{\partial}{\partial x}\, v_x + \frac{\partial}{\partial y}\, v_y + \dots\right] = -K\,\boldsymbol{\nabla}^{\mathrm{T}}\boldsymbol{v}, \qquad \text{equation of compression,} \tag{91}$$

and the spatial decrease of the pressure in each of the spatial dimensions now starts to

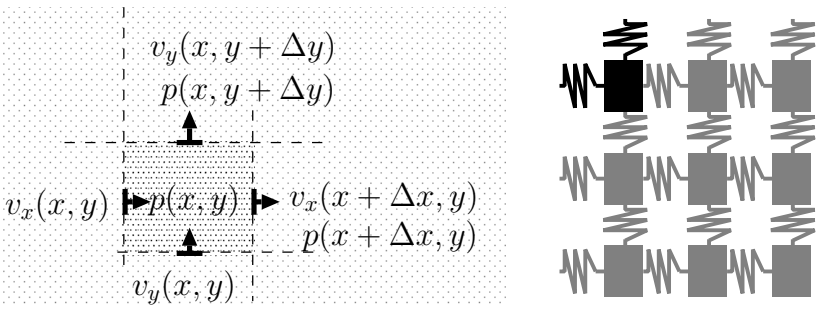

Figure 25 – Scheme for differential 2D air element.

move the volume element into each of the respective dimensions

$$\begin{pmatrix} \frac{\partial}{\partial x} \\ \frac{\partial}{\partial y} \\ \vdots \end{pmatrix} p = \boldsymbol{\nabla}\, p = -\rho\, \dot{\boldsymbol{v}}, \qquad \text{equation of motion.} \tag{92}$$

Component-wise insertion into each other yields the 2D Helmholtzg equation in the Fourier domain (the *Laplacian* is $\triangle = \boldsymbol{\nabla}^{\mathrm{T}}\boldsymbol{\nabla} = \frac{\partial^2}{\partial x^2} + \frac{\partial^2}{\partial y^2} + \ldots$, and the wave number $k = \omega/c$)

$$\left(\triangle + k^2\right)\, p = 0, \qquad \underline{\text{Helmholtz equation}}. \tag{93}$$

The Helmholtz equation denotes the law after which sound waves must propagate in a free and lossless medium such as air. After its solution we will see how useful it is to predict sound propagation. In the first attempt, we will solve it by plane waves, which cannot be caused in all the space by a finite physical effort, however they can be a quite useful description for waves in a finite space.

8.4.1 Homogeneous solution: plane waves

We set $k = \frac{\omega}{c}$ and guess the exponential product solution $p_{\mathrm{h}} = e^{\mathrm{i}\, k_x\, x}\; e^{\mathrm{i}\, k_y\, y}$ for two dimensions.

This solution inserted into Eq. (93) and divided by p_{h} yields the characteristic equation

$$-k_x^2 - k_y^2 = -k^2. \tag{94}$$

Its k_x and k_y parameters are called wave numbers.

In arbitrarily many dimensions, this equals

$$p_{\mathrm{h}} = e^{\mathrm{i}k_x x} e^{\mathrm{i}k_y y} e^{\mathrm{i}k_z z} \cdots = e^{\mathrm{i}\boldsymbol{k}^{\mathrm{T}}\boldsymbol{r}}, \tag{95}$$

which uses the notation of the observaion position as $\boldsymbol{r} = [x,\, y,\, \ldots]^{\mathrm{T}}$ and the wave numbers as *wave vector* $\boldsymbol{k} = [k_x,\, k_y,\, \ldots]^{\mathrm{T}}$. The charakteristisc equation is

$$k_x^2 + k_y^2 + k_z^2 + \cdots = \boldsymbol{k}^{\mathrm{T}}\boldsymbol{k} = k^2. \tag{96}$$

The wave vector lies in the so-called *k space* [Wil99]. Its components must fulfill the characteristic equation.

Superimposed homogeneous solutions. With the above knowledge, we restrict the solution to all physical homogeneous solutions, [Cap69]:

$$p_h = e^{\mathrm{i}\,\boldsymbol{k}^{\mathrm{T}}\,\boldsymbol{r}}\;\delta(\boldsymbol{k}^{\mathrm{T}}\boldsymbol{k} - k^2). \tag{97}$$

A homogeneous sound field can be written as superimoposed homogeneous solutions using the coefficients $\psi\,(\boldsymbol{k})$:

$$p\,(\boldsymbol{r}) = \int \psi\,(\boldsymbol{k}) \cdot \delta\left(\boldsymbol{k}^{\mathrm{T}}\boldsymbol{k} - k^2\right)\, e^{\mathrm{i}\boldsymbol{k}^{\mathrm{T}}\boldsymbol{r}}\mathrm{d}\boldsymbol{k}. \tag{98}$$

Therefore, the homogeneous sound field is a Fourier expansion. In general, the k space is not restricted to real values $\boldsymbol{k} \in \mathbb{C}^{\mathrm{D}}$, and $\psi\,(\boldsymbol{k})$ is called *wave number spectrum* of the sound pressure [Mös88].

Real-valued k space. Taking purely real values $\boldsymbol{k} \in \mathbb{R}^{\mathrm{D}}$ for a start, the wave numbers $\boldsymbol{k}$ must lie on a hypersphere [2] of radius k in the k space, cf. Eq. (96). Therefore $\boldsymbol{k}$ corresponds to a unit direction vector $\boldsymbol{\theta} \in \mathbb{R}^{\mathrm{D}}$ with $\boldsymbol{\theta}^{\mathrm{T}}\boldsymbol{\theta} = 1$ times the wave number k

$$\boldsymbol{k} = k \cdot \boldsymbol{\theta}. \tag{99}$$

Writing also the observation point $\boldsymbol{\theta}_r$ as a direction vector $\boldsymbol{\theta}$ times radius r,

$$\boldsymbol{r} = r \cdot \boldsymbol{\theta}_r, \tag{100}$$

each solution only depends on the distance $kr = 2\pi\frac{r}{\lambda}$ of the point of observation to the coordinate orgin times $\boldsymbol{\theta}^{\mathrm{T}}\boldsymbol{\theta}_r = \cos\vartheta$ of the enclosed angle ϑ between position vector and plane-wave direction:

$$p_{\mathrm{h}} = e^{\mathrm{i}kr\,\boldsymbol{\theta}^{\mathrm{T}}\boldsymbol{\theta}_r} = e^{\mathrm{i}kr\,\cos\vartheta}. \tag{101}$$

The absolute value $|p_{\mathrm{h}}| = 1$ obviously equals 1 everywhere. The phase change equals kr for enclosed angles $0°$, while it is constant at a plane with the $90°$ angles wrt. the direction of the wave. Each shift of the coordiante origin along the propagation direction of the plane wave $\boldsymbol{r} \leftarrow \boldsymbol{r} + \frac{\phi}{k}\boldsymbol{\theta}$ yields a phase shift ϕ

$$p_{\mathrm{h}} = e^{\mathrm{i}k\,\boldsymbol{\theta}^{\mathrm{T}}\left(\boldsymbol{r}+\frac{\phi}{k}\,\boldsymbol{\theta}\right)} = e^{\mathrm{i}k\,\boldsymbol{\theta}^{\mathrm{T}}\boldsymbol{r}+\mathrm{i}\phi\,\boldsymbol{\theta}^{\mathrm{T}}\boldsymbol{\theta}} = e^{\mathrm{i}\phi}\,e^{\mathrm{i}k\,\boldsymbol{\theta}^{\mathrm{T}}\boldsymbol{r}}, \tag{102}$$

jast as shifts in time would yield, $e^{-\mathrm{i}\omega\Delta t}$.

The phase progression $k\,\boldsymbol{\theta}^{\mathrm{T}}\boldsymbol{r}$ corresponds to the projection of the observation point $\boldsymbol{r}$ onto the radial $\boldsymbol{\theta}$, cf. Fig. 26. Since negative phase corresponds to delay, the wave number vevtor $\boldsymbol{k}$, or its direction $\boldsymbol{\theta}$ points to where the plane wave is approaching from.

A single plane wave represents a *far field approximation* of a source field and the equation of motion Eq. (92) $\boldsymbol{\nabla}\,p = -\rho\,\dot{\boldsymbol{v}}$ yields $\boldsymbol{\nu}(k\,\boldsymbol{\theta}) = \boldsymbol{\theta} \cdot \psi(k\,\boldsymbol{\theta})/\rho\,c$, hence:

2. The hyper unit sphere $\boldsymbol{\theta}^{\mathrm{T}}\boldsymbol{\theta} = 1$ in 1D ($\theta_x^2 = 1$) consists of two points $\theta_x = \pm 1$, in 2D ($\theta_x^2 + \theta_y^2 = 1$) of a unit circle, $\theta_x = \cos\varphi$, $\theta_y = \sin\varphi$ and in 3D $\theta_x^2 + \theta_y^2 + \theta_z^2 = 1$ of a unit sphere $\theta_x = \cos\varphi\sin\vartheta$, $\theta_y = \sin\varphi\sin\vartheta$, $\theta_z = \cos\vartheta$.

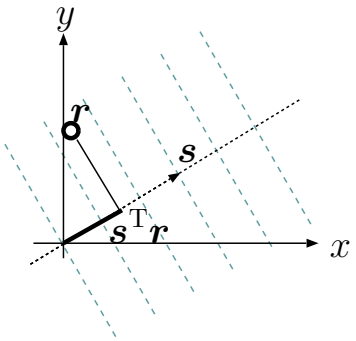

Figure 26 – Vector projection determining the phase of a plane wave (magnitude=1).

In the far field, sound pressure and particle velocity are in phase and related by the characteristic sound impedance $\rho\, c$.

Example: wave vecctor and plane-wave superposition in 2D. Using a real-valued 2D wave vector $\boldsymbol{k} \in \mathbb{R}^2$ determined by polar angle φ on the unit circle $\boldsymbol{\theta} \in \mathbb{S}^1 \subset \mathbb{R}^2$ and wave number k, we get

$$\boldsymbol{k} = \begin{pmatrix} k_x \\ k_y \end{pmatrix} = k \cdot \boldsymbol{\theta} = k \cdot \begin{pmatrix} \cos(\varphi) \\ \sin(\varphi) \end{pmatrix}. \tag{103}$$

In a finite volume, any homogeneous sound field can be described in terms of superimposed plane waves (i.e. by real-valued $\boldsymbol{k}$) from all polar angles, which is mathematically described as a circular integral

$$p(\boldsymbol{r}) = \frac{1}{2\pi} \iint_{\mathbb{S}^1 \subset \mathbb{R}^2} \psi(\boldsymbol{k})\, e^{\mathrm{i}k\boldsymbol{\theta}^{\mathrm{T}}\boldsymbol{r}}\, \mathrm{d}^2\boldsymbol{\theta} = \frac{1}{2\pi} \int_0^{2\pi} \psi(\boldsymbol{k})\, e^{\mathrm{i}k\boldsymbol{\theta}(\varphi)^{\mathrm{T}}\boldsymbol{r}}\, \mathrm{d}\varphi. \tag{104}$$

Example: wave vecctor and plane-wave superposition in 3D. For $\boldsymbol{k} \in \mathbb{R}^3$, the wave vector $\boldsymbol{k}$ is determined by a direction vector using the spherical angles $\varphi \ldots$ azimuth and $\vartheta \ldots$ zenith on the unit sphere $\boldsymbol{\theta} \in \mathbb{S}^2 \subset \mathbb{R}^3$ times the wave number$k$

$$\boldsymbol{k} = \begin{pmatrix} k_x \\ k_y \\ k_z \end{pmatrix} = k \cdot \boldsymbol{\theta} = k \cdot \begin{pmatrix} \cos(\varphi)\sin(\vartheta) \\ \sin(\varphi)\sin(\vartheta) \\ \cos(\vartheta) \end{pmatrix}. \tag{105}$$

The corresponding plane-wave sound field representation that superimposes plane waves from all directions $\boldsymbol{\theta}$ becomes an integral over a sphere

$$p(\boldsymbol{r}) = \frac{1}{4\pi} \iiint_{\mathbb{S}^2 \subset \mathbb{R}^3} \psi(\boldsymbol{k})\, e^{\mathrm{i}k\boldsymbol{\theta}^{\mathrm{T}}\boldsymbol{r}}\, \mathrm{d}\boldsymbol{\theta} = \frac{1}{4\pi} \int_0^{\pi} \int_0^{2\pi} \psi(\boldsymbol{k})\, e^{\mathrm{i}k\boldsymbol{\theta}^{\mathrm{T}}\boldsymbol{r}}\, d\varphi\, \sin(\vartheta)\, \mathrm{d}\vartheta. \tag{106}$$

8.4.2 Elementary inhomogeneous solution: Green's function (free field)

The Green's function is an elementary prototype for solutions to inhomogeneous propblems $(\triangle - \frac{1}{c^2}\frac{\partial^2}{\partial t^2})p = -q$, which is defined as

$$(\triangle - \frac{1}{c^2}\frac{\partial^2}{\partial t^2})G = -\delta.$$

The solution to a general excitation q of the equation can be obtained by convolution of the Delta distribution with the respective source phenomenon $\int q(\boldsymbol{s})\,\delta(\boldsymbol{r}-\boldsymbol{s})\,\mathrm{d}V(\boldsymbol{s}) = q(\boldsymbol{r})$. As the wave equation is linear, the general solution is the convolution of the Green's function with the excitation function $p(\boldsymbol{r}) = \int q(\boldsymbol{s})\,G(\boldsymbol{r}-\boldsymbol{s})\,\mathrm{d}V(\boldsymbol{s})$ over space, and if formulated in the time domain: also over time. The integral superimposes acoustical responses of any point in time and space of the source phenomenon weighted by the corresponding source strength in space and time.

The complex exponential in space, $e^{\mathrm{i}\boldsymbol{k}^{\mathrm{T}}\boldsymbol{r}}$, are valid solutions for any wave vector fulfilling $\boldsymbol{k}^{\mathrm{T}}\boldsymbol{k} = \left(\frac{\omega}{c}\right)^2$. In general, the wave vector need not be restricted to real values $\boldsymbol{k} \in \mathbb{C}^{\mathrm{D}}$. As in the example with the continuous spring, we can compose Green's function as an inhomogeneous solution from spatial and temporal complex exponentials weighted by a coefficient γ:

$$G = \iint \gamma\; e^{\mathrm{i}\boldsymbol{k}^{\mathrm{T}}\boldsymbol{r}}\, e^{\mathrm{i}\omega\, t}\,\mathrm{d}\omega\,\mathrm{d}\boldsymbol{k} \tag{107}$$

Because of $\triangle e^{\mathrm{i}\,\boldsymbol{k}^{\mathrm{T}}\boldsymbol{r}} = (-k_x^2 - k_y^2 - k_z^2 - \dots)e^{\mathrm{i}\,\boldsymbol{k}^{\mathrm{T}}\boldsymbol{r}} = -k^2 e^{\mathrm{i}\,\boldsymbol{k}^{\mathrm{T}}\boldsymbol{r}}$ and $\frac{\partial^2}{\partial t^2}e^{\mathrm{i}\omega t} = -\omega^2 e^{\mathrm{i}\omega t}$, insertion into the wave equation yields

$$-\iint \gamma\,\left[k^2 - \tfrac{\omega^2}{c^2}\right] e^{\mathrm{i}\,\boldsymbol{k}^{\mathrm{T}}\boldsymbol{r}}\, e^{\mathrm{i}\,\omega\, t}\,\mathrm{d}\omega\,\mathrm{d}\boldsymbol{k} = -\delta(t)\,\delta(\boldsymbol{r}).$$

Multiple transformations $e^{-\mathrm{i}\,\hat{\boldsymbol{k}}^{\mathrm{T}}\boldsymbol{r}}e^{-\mathrm{i}\hat{\omega}t}\,\mathrm{d}\boldsymbol{r}\,\mathrm{d}t\iint$ remove the integrals by orthogonality

$$-\iint \gamma(k^2-\tfrac{\omega^2}{c^2})\,\underbrace{[\int e^{\mathrm{i}\,(\boldsymbol{k}-\hat{\boldsymbol{k}})^{\mathrm{T}}\boldsymbol{r}}\mathrm{d}\boldsymbol{r}]}_{(2\pi)^{\mathrm{D}}\delta(\boldsymbol{k}-\hat{\boldsymbol{k}})}\,\underbrace{[\int e^{\mathrm{i}(\omega-\omega')t}\mathrm{d}t]}_{2\pi\delta(\omega-\omega')}\,\mathrm{d}\omega\,\mathrm{d}\boldsymbol{k} = -\underbrace{\int \delta(t)e^{-\mathrm{i}\omega' t}\mathrm{d}t}_{1}\,\underbrace{\int \delta(\boldsymbol{r})e^{-\mathrm{i}\,\hat{\boldsymbol{k}}^{\mathrm{T}}\boldsymbol{r}}\mathrm{d}\boldsymbol{r}}_{1},$$

and the unknown coefficient remains $\gamma = \frac{1}{(2\pi)^{\mathrm{D}+1}}\frac{1}{k^2-\frac{\omega^2}{c^2}}$. Letting G in the frequency domain, one $\frac{1}{2\pi}$ in γ and the integral $e^{\mathrm{i}\omega t}\mathrm{d}\omega\int$ are omitted. We transform γ only back via $\boldsymbol{k}$

$$G = \frac{1}{(2\pi)^{\mathrm{D}}}\iint \frac{e^{\mathrm{i}\boldsymbol{k}^{\mathrm{T}}\boldsymbol{r}}}{k^2-\frac{\omega^2}{c^2}}\,\mathrm{d}\boldsymbol{k} = \frac{1}{(2\pi)^{\mathrm{D}}}\iint \frac{e^{\mathrm{i}kr\mu}}{k^2-\frac{\omega^2}{c^2}}\,\mathrm{d}\boldsymbol{k}.$$

By re-expressing $\boldsymbol{k}^{\mathrm{T}}\boldsymbol{r} = kr\,\boldsymbol{\theta}_{\mathrm{k}}^{\mathrm{T}}\boldsymbol{\theta}_{\mathrm{r}} = kr\cos\vartheta = kr\mu$ we simplify the integral. *Now we already see formally that Green's function can only depend on the distance r between source and receiver location $G = G(\omega, r)$.*

The book [Duf01, S.110-112] shows a notably conpact derivation for $\mathrm{D} = 3$, which we will use below; see also Appendix O for arbitrary dimensions.

Derivation for D=3 by transforming back from the Fourier domain: For $\mathrm{D}=3$, the transformation back from the Fourier domain is similarly simple to accomplish as for $\mathrm{D}=1$, see Eq. (86). Before going into details, we recognize that the substitution of $\boldsymbol{k}^{\mathrm{T}}\boldsymbol{r}$ by $kr\cos\vartheta$ contains the radius of the wave vector $k=\|\boldsymbol{k}\|$ and the cosine of the angle between $\boldsymbol{r}$ und $\boldsymbol{k}$. In k space, we can always define a correspondingly oriented coordinate system for any $\boldsymbol{r}$ as to simplify the integral $\iiint_{-\infty}^{\infty}\mathrm{d}\boldsymbol{k}=\int_0^\infty\int_0^{2\pi}\int_0^\pi k^2\,\mathrm{d}k\,\mathrm{d}\varphi\,\mathrm{d}\cos\vartheta=\int_0^\infty\int_0^{2\pi}\int_{-1}^1 k^2\,\mathrm{d}k\,\mathrm{d}\varphi\,\mathrm{d}\mu$. After re-arranging the integrals, we get

$$\begin{aligned}
G&=\frac{\int_0^{2\pi}\mathrm{d}\varphi}{(2\pi)^3}\int_0^\infty\frac{\int_{-1}^1 e^{\mathrm{i}kr\mu}\,\mathrm{d}\mu}{k^2-\frac{\omega^2}{c^2}}\,k^2\,\mathrm{d}k=\frac{1}{(2\pi)^2}\int_0^\infty\frac{1}{\mathrm{i}kr}\frac{e^{\mathrm{i}kr}-e^{-\mathrm{i}kr}}{k^2-\frac{\omega^2}{c^2}}\,k^2\,\mathrm{d}k\\
&=\frac{1}{(2\pi)^2}\frac{1}{\mathrm{i}r}\int_0^\infty\frac{e^{\mathrm{i}kr}-e^{-\mathrm{i}kr}}{k^2-\frac{\omega^2}{c^2}}\,k\,\mathrm{d}k=\frac{1}{(2\pi)^2}\frac{1}{\mathrm{i}r}\left[\int_0^\infty\frac{e^{\mathrm{i}kr}\,k}{k^2-\frac{\omega^2}{c^2}}\,\mathrm{d}k-\int_0^\infty\frac{e^{-\mathrm{i}kr}\,k}{k^2-\frac{\omega^2}{c^2}}\,\mathrm{d}k\right]\\
&=\frac{1}{(2\pi)^2}\frac{1}{\mathrm{i}r}\left[\int_0^\infty\frac{e^{\mathrm{i}kr}\,k}{k^2-\frac{\omega^2}{c^2}}\,\mathrm{d}k-\int_0^{-\infty}\frac{e^{-\mathrm{i}(-k)r}\,(-k)}{(-k)^2-\frac{\omega^2}{c^2}}\,\mathrm{d}(-k)\right]\\
&=\frac{1}{(2\pi)^2}\frac{1}{\mathrm{i}r}\left[\int_0^\infty\frac{e^{\mathrm{i}kr}\,k}{k^2-\frac{\omega^2}{c^2}}\,\mathrm{d}k+\int_{-\infty}^0\frac{e^{-\mathrm{i}kr}\,k}{k^2-\frac{\omega^2}{c^2}}\,\mathrm{d}k\right]\\
&=\frac{1}{(2\pi)^2}\frac{1}{\mathrm{i}r}\int_{-\infty}^\infty\frac{e^{\mathrm{i}kr}}{k^2-\frac{\omega^2}{c^2}}\,k\,\mathrm{d}k.
\end{aligned}\tag{108}$$

The remaining improper integral is solved by applying Jordan's Lemma, after partial fraction expansion $\frac{1}{k^2-\frac{\omega^2}{c^2}}=\frac{1}{2k}\frac{1}{k-\frac{\omega}{c}}+\frac{1}{2k}\frac{1}{k+\frac{\omega}{c}}$ and regularization for causal solutions, cf. Eq. (85),

$$\begin{aligned}
G&=\frac{1}{(2\pi)^2}\frac{1}{2\mathrm{i}r}\lim_{\epsilon\to+0}\left[\oint_{C_+}\frac{e^{\mathrm{i}kr}}{k-\frac{\omega-\mathrm{i}\epsilon}{c}}\,\mathrm{d}k+\oint_{C_+}\frac{e^{\mathrm{i}kr}}{k+\frac{\omega-\mathrm{i}\epsilon}{c}}\,\mathrm{d}k\right]\\
&=\frac{2\pi}{(2\pi)^2}\frac{\mathrm{i}}{2\mathrm{i}r}\lim_{\epsilon\to+0}e^{-\mathrm{i}kr-\frac{\epsilon}{c}r}=\frac{e^{-\mathrm{i}kr}}{4\pi\,r}.
\end{aligned}\tag{109}$$

Green's function for arbitrarily many dimensions: Appendix N shows how a direction-independent coordinate system can be used to obtain Green's functions if the number D of dimensions is arbitrary, cf. [Som92]. Accordingly, in the far field, Green's function must always be proportional to

$$\lim_{r\to\infty}G=a\,\frac{e^{-\mathrm{i}kr}}{\sqrt{r}^{\mathrm{D}-1}}.\qquad\text{(for D = 1 and D = 3 even exactly for small radii).}\tag{110}$$

Even a general form of the Green's function can be given as

$$G=\frac{1}{4\mathrm{i}}\sqrt{\frac{2\pi}{kr}}^{\mathrm{D}-2}H^{(2)}_{\frac{\mathrm{D}-2}{2}}(kr).\tag{111}$$

With the simplified special cases for $\mathrm{D} = 1, 3$, the Green's functions in the free field are defined as:

$$\left[\frac{\partial^2}{\partial r^2} + k^2\right] G_{1\mathrm{D}}(r) = -\delta_{1\mathrm{D}}(r), \qquad \Rightarrow G_{1\mathrm{D}} = \frac{e^{-\mathrm{i}kr}}{2\mathrm{i}k}, \tag{112}$$

$$\left[\frac{\partial^2}{\partial r^2} + \frac{1}{r}\frac{\partial}{\partial r} + k^2\right] G_{2\mathrm{D}}(r) = -\delta_{2\mathrm{D}}(r), \qquad \Rightarrow G_{2\mathrm{D}} = \frac{1}{4\mathrm{i}} H_0^{(2)}(kr), \tag{113}$$

$$\left[\frac{\partial^2}{\partial r^2} + \frac{2}{r}\frac{\partial}{\partial r} + k^2\right] G_{3\mathrm{D}}(r) = -\delta_{3\mathrm{D}}(r), \qquad \Rightarrow G_{3\mathrm{D}} = \frac{e^{-\mathrm{i}kr}}{4\pi r}. \tag{114}$$

How is a Green's function related to a plane wave? The radius coordinate of the Green'schen function consists of a distance of two Cartesian position vectors $\boldsymbol{r}_1$ and $\boldsymbol{r}_2$, of which one is the source location, the other is the observation point. Letting one of them become large, we could re-write it in terms of length and direction vector $\boldsymbol{r}_1 = r_1\boldsymbol{\theta}$. This permits far-field approximation

$$\begin{aligned}\lim_{r_1\to\infty} r &= \|\boldsymbol{r}_1 - \boldsymbol{r}_2\| = \lim_{r_1\to\infty} \sqrt{(r_1\boldsymbol{\theta} - \boldsymbol{r}_2)^{\mathrm{T}}(r_1\boldsymbol{\theta} - \boldsymbol{r}_2)} = \lim_{r_1\to\infty} \sqrt{r_1^2 - 2r_1\boldsymbol{\theta}^{\mathrm{T}}\boldsymbol{r}_2 + r_2^2} \\ &= \lim_{r_1\to\infty} r_1\sqrt{1 - \frac{2\boldsymbol{\theta}^{\mathrm{T}}\boldsymbol{r}_2}{r_1} + \frac{r_2^2}{r_1^2}} \quad \underset{\to 1-x}{\overset{\sqrt{1-2x}}{=}} \quad r_1 - \boldsymbol{\theta}^{\mathrm{T}}\boldsymbol{r}_2.\end{aligned} \tag{115}$$

For the *phase approximation* we notice, for instance at a wave-length of 30 cm, we notice even a relatively small distance difference, e.g. between 15 m und 15 m+15 cm: it changes the sign of the wave. For this reason, to approximate the phase of the Green's function, we must at least use the approximation $r_1 - \boldsymbol{\theta}^{\mathrm{T}}\boldsymbol{r}_2$. By contrast, this level of precision is irrelevant for the *magnitude approximation*, e.g., if we use instead of the magnitude $\frac{1}{\sqrt{15\,m+15\,cm}^{\mathrm{D}-1}}$ the magnitude $\frac{1}{\sqrt{15\,m}^{\mathrm{D}-1}}$. At large distance r_1, assuming r_1 to be constant, the Green's function is therefore proportional to a plane wave from the respective direction $\boldsymbol{\theta}$ of the source

$$\lim_{r_1\to\infty} G \propto e^{\mathrm{i}\,k\,\boldsymbol{\theta}^{\mathrm{T}}\boldsymbol{r}_2}. \tag{116}$$

9 Theoretical Holography and Holophony

This section describes the theoretical basics behind sound field holography and holophony (sound field synthesis) based on considerations that were presented in [ZS13] and [SZ15].

The Kirchhoff-Helmholtz Integral (KHI) or Helmholtz integral equation (HIE) is considered as the most generic basis of any holographic or holophonic attempt. It was found in the independent efforts of Hermann von Helmholtz (1860) and Gustav Robert Kirchhoff (1883), whose intention was to apply the new analytic methods introduced by the third integral identity for the Laplace/Poisson equation in George Green's essay (1828) to linear lossless wave equations. The researchers found the equation for Huygens' principle [Huy90], which had been searched for for more than 100 years which only resulted in mathematically less elegant and less accurate formulations [BC39, Jes73].

To see how this integral works, we first deal with the divergence theorem for vector fields, the definition of the Green's function in potential theory (Laplace/Poisson equation) and the skilld formulation of Green's third integral identity, as well as its transcription to the wave equation.

Divergence of vector fields (Gauß' integral theorem). To determine the source strength of a vector field (e.g. gravitation field of the earth) there are two alternative integrals.

Let $\boldsymbol{a}(\boldsymbol{r}) = [a_x(\boldsymbol{r}), a_y(\boldsymbol{r}), a_z(\boldsymbol{r})]^{\mathrm{T}}$ be a field yielding at every location $\boldsymbol{r} = [x, y, z]^{\mathrm{T}}$ a vector $\boldsymbol{a}$. The divergence theorem states:

$$Q = \oint_{\partial V} \boldsymbol{a}(\boldsymbol{r})^{\mathrm{T}} \,\mathrm{d}\boldsymbol{S}(\boldsymbol{r}) = \int_V \boldsymbol{\nabla}^{\mathrm{T}} \boldsymbol{a}(\boldsymbol{r}) \,\mathrm{d}V(\boldsymbol{r}). \tag{117}$$

This means that the source strength Q within a volume V is know to correspond to a surface integral that balances the whole flux of field lines running out of the hull of the volume, perpendicularly. Would field lines just transit through this hull, the source strength would be $Q = 0$. The integration element is $\mathrm{d}\boldsymbol{S}(\boldsymbol{r}) = \mathrm{d}S(\boldsymbol{r})\,\boldsymbol{n}(\boldsymbol{r})$, within which $\mathrm{d}S(\boldsymbol{r})$ is a surface element and $\boldsymbol{n}(\boldsymbol{r})$ its unit vector pointing outwards, perpendicularly. The balance of the flux though the hull yields the same result as if one would cut the volume in the hull into smaller volumes, balance the fluxes through their hulls, and sum up the results. In the limit to infinitely many and infinitesimally small portions, the partitioned flux integrals can be first-order approximated by the divergence $\boldsymbol{\nabla}^{\mathrm{T}}\,\boldsymbol{a}(\boldsymbol{r})$ at no loss in accuracy. In doing so and integrating over the divergences in all the volume, we obtain the alternative integral yielding the source strength. The operator nabla or del $\boldsymbol{\nabla}^{\mathrm{T}} = \left[\frac{\partial}{\partial x}, \frac{\partial}{\partial y}, \frac{\partial}{\partial z}\right]$ is a vector of derivatives.

How the divergence theorem works: We regard the flux balance of a small rectangular box at the coordinates x_i and $x_i + \Delta x_i$ for all the dimensions. The flux balance for surfaces at the coordinates x_i and $x_i + \Delta x_i$ for a certain i only regards vector components aligned with the respective coordinate axis x_i, hence considering that at x_i the normal

vector is pointing into the negative x_i direction, and at $x_i + \Delta x_i$ to the positive x_i one, we obtain $\Delta Q_i = [a_i(x_i+\Delta x_i, x_{j\neq i}) - a_i(x_i, x_{j\neq i})] \prod_{j\neq i} \Delta x_j$. Small position changes are approximated by a first-order Taylor series $a_i(x_i+\Delta x_i, x_{j\neq i}) = a_i(x_i, x_{j\neq i}) + \frac{\partial a_i(x_i, x_{j\neq i})}{\partial x_i} \Delta x_i$, and so the flux becomes $\Delta Q_i = [\frac{\partial a_i(x_i, x_{j\neq i})}{\partial x_i} \Delta x_i] \prod_{j\neq i} \Delta x_j = \frac{\partial a_i(\boldsymbol{r})}{\partial x_i} \Delta V$. Summing up the contributions of all dimensions equals $\Delta Q = \sum_i \Delta Q_i = \boldsymbol{\nabla}^{\mathrm{T}} \boldsymbol{a} \Delta V$, and with $\lim_{\Delta x_i \to 0}$, $\forall i$, we obtain $\mathrm{d}Q = \boldsymbol{\nabla}^{\mathrm{T}} \boldsymbol{a} \mathrm{d}V$ which is then integrated over the respective volume.

Potentialtheorie. Although most physical fields are vector fields, the potential theory introduced a fundamental novelty: conservative, non-vortical vector fields can be represented as gradient of a scalar potential field $u(\boldsymbol{r})$,

$$\boldsymbol{a}(\boldsymbol{r}) = \boldsymbol{\nabla}\, u(\boldsymbol{r}), \tag{118}$$

what simplifies a lot of calculations. The gradient is a vector (column vector) of all partial spatial derivatives. Physically, in a conservative vector field the potential difference $u(\boldsymbol{a}) - u(\boldsymbol{b})$ is proportional to the work required, path-independently [3], to move a unit mass from $\boldsymbol{a}$ to $\boldsymbol{b}$:

$$W = [u(\boldsymbol{b}) - u(\boldsymbol{a})] = \int_{\boldsymbol{a}}^{\boldsymbol{b}} \boldsymbol{F}(\boldsymbol{r})\, \mathrm{d}\boldsymbol{r}. \tag{119}$$

Potential fields in electrostatics fulfill the Laplace/Poisson differential equation

$$\text{without excitation} \quad \triangle\, u(\boldsymbol{r}) = 0, \qquad \text{with extitation} \quad \triangle\, u(\boldsymbol{r}) = \rho(\boldsymbol{r}). \tag{120}$$

Green'sche Funktion. In 1828 George Green [Gre28] published an essay on his own, in the humble hope that his integral theorems might help poeple doing calculations in potential theory. A new concept was to define a Laplace/Poisson differential equation with vanishingly small excitation and to define its solution as a function. Today we call G,

$$\triangle G(\boldsymbol{r}, \boldsymbol{s}) = -\delta(\boldsymbol{r} - \boldsymbol{s}), \tag{121}$$

the *Green's function* and we use the Dirac delta symbol as a compact notation (here in 3D) of the normalized, point-shaped excitation,

$$\delta(\boldsymbol{r} - \boldsymbol{s}) = \lim_{\epsilon \to 0} \begin{cases} \frac{3}{4\pi\epsilon^3}, & \text{for } \|\boldsymbol{r} - \boldsymbol{s}\| < \epsilon, \\ 0, & \text{otherwise.} \end{cases} \tag{122}$$

Integrating this distribution over a volume V yields a result depending on the location of $\boldsymbol{s}$ inside the volume V, on its boundary ∂V, or the disjoint volume $\overline{V}$, $V \cup \partial V \cup \overline{V} = \mathbb{R}^{\mathrm{D}}$:

$$\int_V \delta(\boldsymbol{r} - \boldsymbol{s})\, \mathrm{d}V(\boldsymbol{s}) = \begin{cases} 1, & \text{if } \boldsymbol{r} \in V, \\ 1/2, & \text{if } \boldsymbol{r} \in \partial V, \\ 0, & \text{if } \boldsymbol{r} \in \overline{V}. \end{cases} \tag{123}$$

The second value is only half, because only the half of the vanishingly small spherical excitation can be inside the integral over V, while the other hemisphere lies outside.

3. The path-independence corresponds to analyticity of functions defined on the complex number plane. *remark.: poles in $\mathbb{C}$ correspond to two-dimensional vortex fields.*

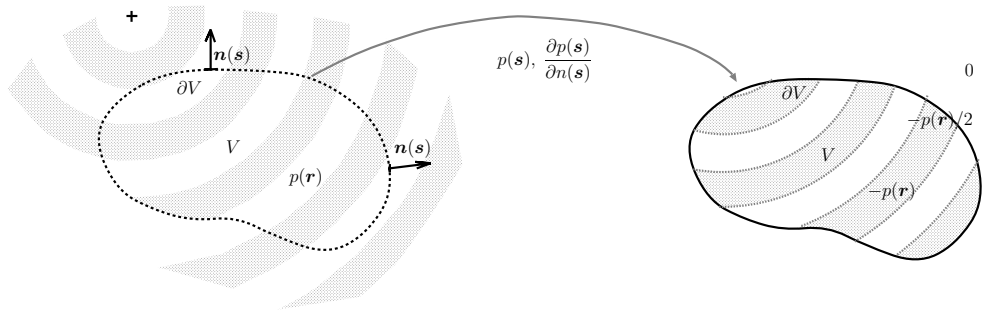

Figure 27 – Mit Randwerten $p(\boldsymbol{s})$ und $\frac{\partial p(\boldsymbol{s})}{\partial n(\boldsymbol{s})}$ am Rand von ∂V eines homogenen (anregungs- und hindernisfreien) Feldes, ergibt das Kirchhoff-Helmholtz-Integral $-p(\boldsymbol{r})$ innerhalb von V, $p(\boldsymbol{r})/2$ am Rand ∂V und 0 sonst.

Green's second/third identity. In the same contribution in 1828 [Gre28], Green specified a couple of integration theorems. One of it inserts into the divergence theorem a playfully composed equation from two fields, G and p

$$\boldsymbol{u} = p\boldsymbol{\nabla}G - G\boldsymbol{\nabla}p, \tag{124}$$

and it yields Green's second identity with $\cancel{\boldsymbol{\nabla}^{\mathrm{T}}p\boldsymbol{\nabla}G} + p\boldsymbol{\nabla}^{\mathrm{T}}\boldsymbol{\nabla}G - \cancel{\boldsymbol{\nabla}^{\mathrm{T}}G\boldsymbol{\nabla}p} - G\boldsymbol{\nabla}^{\mathrm{T}}\boldsymbol{\nabla}p$,

$$\oint_{\partial V} \big[p\,\boldsymbol{\nabla}G - G\,\boldsymbol{\nabla}p\big]^{\mathrm{T}}\,\mathrm{d}\boldsymbol{S} = \int_V \big[p\ \triangle G - G\ \triangle p\big]\,\mathrm{d}V. \tag{125}$$

Assuming that p fulfilles the Laplace differential equation $\triangle p = 0$ and G is Green's function $\triangle G = -\delta$, the right hand side reduces to the Green's third identity

$$\oint_{\partial V} \big[p(\boldsymbol{s})\,\boldsymbol{\nabla}G(\boldsymbol{r},\boldsymbol{s}) - G(\boldsymbol{r},\boldsymbol{s})\,\boldsymbol{\nabla}p(\boldsymbol{s})\big]^{\mathrm{T}}\,\mathrm{d}\boldsymbol{S}(\boldsymbol{s}) = \begin{cases} -p(\boldsymbol{r}), & \text{for } \boldsymbol{r} \in V, \\ -p(\boldsymbol{r})/2, & \text{for } \boldsymbol{r} \in \partial V, \\ 0, & \text{for } \boldsymbol{r} \in \overline{V}. \end{cases} \tag{126}$$

The meaning of the equation is enormous: we can completely describe the scalar potential $p(\boldsymbol{r})$ of the Laplace/Poisson differential equation (e.g. in electrostatics) within a homogeneous volume V by only knowing its boundary values that are used inside the Integral.

Does this also work in acoustics: in sound fields instead of potential fields?

9.1 Kirchhoff-Helmholtz Integral (KHI)

Helmholtz [vH60] and Kirchhoff [Kir83] applied the same procedure to the linear lossless wave equation. Now p and G are defined by the equations

$$(\triangle + k^2)p = 0, \qquad (\triangle + k^2)G = -\delta(\boldsymbol{r} - \boldsymbol{s}), \tag{127}$$

in which k is the wave number ω/c. We immediately obtain from Green's second identity Eq. (125) by replacing with the adapted definitions of the symbols p and G the Kirchhoff-Helmholtz integral (KHI), cf. Fig. 30. Even with the adapted defintions for p and G,

volume integration is performed over the same quantities as with Green's third identity, because $p \triangle G - G \triangle p = p(-\delta - k^2 G) - G(-k^2 p) = -p\,\delta$, cf. Eq. (126),

$$\oint_{\boldsymbol{s}\in\partial V} \left[p(\boldsymbol{s}) \frac{\partial G(\boldsymbol{r},\boldsymbol{s})}{\partial n(\boldsymbol{s})} - G(\boldsymbol{r},\boldsymbol{s}) \frac{\partial p(\boldsymbol{s})}{\partial n(\boldsymbol{s})} \right] \mathrm{d}S(\boldsymbol{s}) = \begin{cases} -p(\boldsymbol{r}), & \boldsymbol{r}\in V, \\ -p(\boldsymbol{r})/2, & \boldsymbol{r}\in\partial V, \\ 0, & \boldsymbol{r}\in\overline{V}. \end{cases} \tag{128}$$

The implications of the KHI are powerful: the KHI is capable of fully equivalently representing homogeneous acoustic fields (of negated sign) bounded inside a volume V, alone on the basis of the boundary values $p(\boldsymbol{s})$ and $\frac{\partial p(\boldsymbol{s})}{\partial n(\boldsymbol{s})}$ on ∂V.

9.1.1 The KHI as ideal sound absorber

Let's assume the incident sound field p_{in}, e.g. from a point source 10m away.

Now we superimpose with this sound field $p_{\mathrm{in}}(\boldsymbol{r})$ a KHI driven by the boundary values $p_{\mathrm{in}}(\boldsymbol{s})$ and $\frac{\partial p_{\mathrm{in}}(\boldsymbol{s})}{\partial n(\boldsymbol{s})}$ that would be observed in the incident field. We get cf. Eq. (128),

$$p_{\mathrm{in}}(\boldsymbol{r}) + \oint_{\boldsymbol{s}\in\partial V} \left[p_{\mathrm{in}}(\boldsymbol{s}) \frac{\partial G(\boldsymbol{r},\boldsymbol{s})}{\partial n(\boldsymbol{s})} - G(\boldsymbol{r},\boldsymbol{s}) \frac{\partial p_{\mathrm{in}}(\boldsymbol{s})}{\partial n(\boldsymbol{s})} \right] \mathrm{d}S(\boldsymbol{s}) = \begin{cases} 0, & \boldsymbol{r}\in V, \\ p_{\mathrm{in}}(\boldsymbol{r})/2, & \boldsymbol{r}\in\partial V, \\ p_{\mathrm{in}}(\boldsymbol{r}), & \boldsymbol{r}\in\overline{V}. \end{cases} \tag{129}$$

Finite: An interesting result: obviously the KHI produces from the observed boundary values (pressure and normal sound particle velocity) of the original field the ihrer Normalableitungen the opposing field inside the finite volume V, which in sum yields a perfect quiet zone $p = 0$. The source field in the infinite exterior domain $\overline{V}$ remains unchanged. It is crucial for the cancellation in V to choose the directional derivatives $\frac{\partial}{\partial n(\boldsymbol{s})}$ (sign-determining!) pointing towards the source domain $\overline{V}$.

Infinite: We can even apply the KHI if instead of the source domain, the source-free domain is infinitely large. The definition of the synthesis volume (and the volume integral to which it corresponds) always implicitly falls into the source-free domain V because of the underlying assumptions made. However, as before: a perfect quiet zone in the source-free domain V is only achieved whenever the sign-determining directional derivatives point into $\frac{\partial}{\partial n(\boldsymbol{s})}$ the source domain $\overline{V}$.

:-) small hint: Hence do not forget to take the KHI with you whenever you are going to enter a room of annoying loudness. Its application is childishly simple: put up early-enough for everybody, or apply it inside-out to stow the acoustic disturber inside! (-:

Works of Maurice Jessel [Jes73] and his patents in fact attempted to build active wall absorbers using omnidirectional and figure-of-eight microphones as well as omnidirectional and figure-of-eight loudspeakers. However, with the current technologies, the frequency range for the desired effects is strongly limited.

9.1.2 The KHI to calculate diffraction/scattering/reflection

Placement of a rigid body inside a homogeneous sound field causes reflection, scattering, and diffraction of the impinging sound waves.

The KHI offers the most general mathematical description of such scatterers. The sound pressure outside the scatterer must be composed of two fields: $p = p_{\text{in}} + p_{\text{sc}}$, the homogeneous field p_{in} that was present before inserting the scatterer, and for which the KHI is not necessarily needed, and the component p_{sc} describing the scattered field that gets scattered/diffracted/reflected by the body inserted into the homogeneous field. The scattered field outside of the scattering object is described by the KHI.

The boundary condition of the rigid surface requires that the sound particle velocity normal to the surface must vanish. By its proportionality to the normal derivative of the sound pressure, we may write $\frac{\partial p_{\text{in}}(\boldsymbol{s}) + \partial p_{\text{sc}}(\boldsymbol{s})}{\partial n(\boldsymbol{s})} = 0$. Hereby, the term with the Green's function without derivative vanishes and what remains is:

$$-p_{\text{in}}(\boldsymbol{r}) + \oint_{\boldsymbol{s}\in\partial V} \left[p_{\text{in}}(\boldsymbol{s}) + p_{\text{sc}}(\boldsymbol{s})\right] \frac{\partial G(\boldsymbol{r},\boldsymbol{s})}{\partial n(\boldsymbol{s})}\,\mathrm{d}S(\boldsymbol{s}) = \begin{cases} -[p_{\text{in}}(\boldsymbol{r}) + p_{\text{sc}}(\boldsymbol{r})], & \boldsymbol{r}\in V, \\ -\frac{p_{\text{in}}(\boldsymbol{r}) + p_{\text{sc}}(\boldsymbol{r})}{2}, & \boldsymbol{r}\in\partial V, \\ 0, & \boldsymbol{r}\notin V. \end{cases} \tag{130}$$

We know the homogeneous original field $p_{\text{in}}(\boldsymbol{s})$ on the surface, and we are required to calculate the scattered field Randwert $p_{\text{sc}}(\boldsymbol{s})$ from the integral equation.

The boundary elemenet method (BEM, [Juh93]) decomposes the integral, e.g. into small triangular integrals of the dipole (or monopole) source over the triangle weighted by the sound pressure (or normal velocity) that is assumed to be constant on the triangle. If the evaluation of the sound pressure is done directly on all of the surface elements' center points (discretized case two of the integral equation), this is called collocation method. Note that while single sources get singular if evaluated at their location, a surface integral of sources typically yields finite values. The collocation method results a square matrix problem with equally many constraints as there are parameters. With $\boldsymbol{H} = [\int_{S_i} \frac{\partial}{\partial n} G(\boldsymbol{s}, \boldsymbol{r}_j)\,\mathrm{d}\,S_i(\boldsymbol{s})]_{i,j}$ this yields:

$$\begin{aligned} -\boldsymbol{p}_{\text{in}} + \boldsymbol{H}\,(\boldsymbol{p}_{\text{in}} + \boldsymbol{p}_{\text{sc}}) &= -(\boldsymbol{p}_{\text{in}} + \boldsymbol{p}_{\text{sc}})/2 \\ (\boldsymbol{I}/2 + \boldsymbol{H})\boldsymbol{p}_{\text{sc}} &= (\boldsymbol{I}/2 - \boldsymbol{H})\boldsymbol{p}_{\text{in}} \\ \boldsymbol{p}_{\text{sc}} &= (\boldsymbol{I}/2 + \boldsymbol{H})^{-1}(\boldsymbol{I}/2 - \boldsymbol{H})\,\boldsymbol{p}_{\text{in}}. \end{aligned}$$

9.1.3 Sommerfeld's radiation condition

The KHI encloses the homogeneous field. For radiating fields, we may use two nested KHIs, an inner one enclosing the source and having its surace at a small radius r_0, and the outer enclosing the KHI at r_0 has its surface at a large radius r_∞

$$p = \int_{r_0} (G\frac{\partial}{\partial n}p - p\frac{\partial}{\partial n}G)\,\mathrm{d}S_0 + \int_{r_\infty} (G\frac{\partial}{\partial n}p - p\frac{\partial}{\partial n}G)\,\mathrm{d}S_\infty. \tag{131}$$

Desiring that no field should be originating from the far field, the second integral must vanish. For an arbitrary number of spatial dimensions D (we typically have 3), the proportionality of the Green's function in the far field is $\lim_{r\to\infty} G = \alpha\ r^{-\frac{D-1}{2}}\, e^{-\mathrm{i}\,k\,r}$ and its derivative $\lim_{r\to\infty} \frac{\partial}{\partial r} G \approx \left(-\mathrm{i}\,k - \cancel{\frac{D-1}{2} r^{-1}}\right)\ \alpha\, r^{-\frac{D-1}{2}}\, e^{-\mathrm{i}\,k\,r}$, see Appendix N. By this setting, we obtain the important *radiation condition* that Sommerfeld introduced. It must not only be fulfilled by G, but by any phyiscal radiating field p in D dimensions:

$$\lim_{r\to\infty} r^{\frac{D-1}{2}} \left(\frac{\partial}{\partial r} + \mathrm{i}k\right) p = 0. \tag{132}$$

The condition is a finiteness constraint important to ensure physical solutions that are convergent, causal, and which are of finite energy. Plane waves or standing waves do generally not fulfill the radiation condition.

The condition causes a radial sound intensity $I_r = p\, v_r^*$ with $\frac{\partial}{\partial r} p = -\mathrm{i}\omega\rho\, v_r$ that is strictly real and radially pointing outwards at large radii $I_r = p\left[\frac{1}{\mathrm{i}\omega\,(-\rho)} \frac{\partial}{\partial r} p\right]^* = p\left[\frac{-\mathrm{i}k\,p}{\mathrm{i}\omega\,(-\rho)}\right]^* = \frac{|p|^2}{\rho\, c}$. This ensures that all sound energy is dissipated towards infinity.

9.2 Theoretic holophony using the single-layer potential

For sound field resynthesis in an elegant theory according to Fazi [Faz10], we assume an *equivalent scattering problem*. By this trick, the synthesized secondary field p_{sc} constrains the sound pressure of the virtual, primary field p_{in} to vanish on the surface ∂V of an *ideally sound soft scatterer* $(p_{\mathrm{sc}} + p_{\mathrm{in}})|_{\partial V} = 0$, when superimposing the primary with the secondary field. This discards the dipole sources of the KHI, yielding the benefit that only one source type needs to be constructed. Moreover, it is generally preferred to work with the omnidirectional source type, because they are considered to be approximated more easily by common physical loudspeakers, as opposed to dipole sources.

Despite the obvious differences between a physical loudspeaker array for playback in a room and a continuous integral of monopole sources in the free field, the integral equation of a *single-layer potential* integrated over monopole sources is the solid theoretical basis from which the *driving function* (what is fed to the loudspeakers) of any sound field synthesis approach can be derived; typically requiring reasonable approximation.

Sound field synthesis in the finite volume $\overline{V}$: Be V the infinite exterior volume of a sound soft scatterer, ∂V its surface, and $\overline{V}$ the finite interior of the scatterer, we get

$$-p_{\mathrm{in}}(\boldsymbol{r}) + \oint_{\boldsymbol{s}\in\partial V} \underbrace{\left[\frac{\partial p_{\mathrm{in}}(\boldsymbol{s})}{\partial n(\boldsymbol{s})} + \frac{\partial p_{\mathrm{sc}}(\boldsymbol{s})}{\partial n(\boldsymbol{s})}\right]}_{:=g(\boldsymbol{s})} G(\boldsymbol{r},\boldsymbol{s})\,\mathrm{d}S(\boldsymbol{s}) = \begin{cases} -[p_{\mathrm{in}}(\boldsymbol{r}) + p_{\mathrm{sc}}(\boldsymbol{r})], & \boldsymbol{r}\in V, \\ -\cancel{\frac{p_{\mathrm{in}}(\boldsymbol{r}) + p_{\mathrm{sc}}(\boldsymbol{r})}{2}}^{0}, & \boldsymbol{r}\in\partial V, \\ 0, & \boldsymbol{r}\in\overline{V}. \end{cases}$$

Adding p_{in} at both sides yields the integral equation in 3 cases:

$$\oint_{\boldsymbol{s}\in\partial V} g(\boldsymbol{s})\, G(\boldsymbol{r},\boldsymbol{s})\,\mathrm{d}S(\boldsymbol{s}) = \begin{cases} -p_{\mathrm{sc}}(\boldsymbol{r}), & \boldsymbol{r}\in\ V \quad \text{case 1,} \\ p_{\mathrm{in}}(\boldsymbol{r}), & \boldsymbol{r}\in\partial V \quad \text{case 2,} \\ p_{\mathrm{in}}(\boldsymbol{r}), & \boldsymbol{r}\in\ \overline{V} \quad \text{case 3.} \end{cases} \tag{133}$$

The primary field $p_{\mathrm{in}}(\boldsymbol{r})$ is known everywhere. The challenge of sound field synthesis obviously lies in determining the driving function $g(\boldsymbol{s})$ (*single-layer potential*) fulfilling the conditions of the three cases. Case 1 is not helpful because p_{sc} is unknown. It seems useful to focus on case 2, as both the single-layer potential and the primary field are evaluated over the same set $\boldsymbol{r},\boldsymbol{s}\in\partial V$.

As discussed in the works [FN12, ZS13], this yields uniqueness problems whenever one or more modes $p_l^{\mathrm{res}}(\boldsymbol{r})$ exist in the interior $\overline{V}$ of the scatterer, at the regarded freuqency (there are always special frequencies at which modes exist). Otherwise, if no modes exist, the integral equation of case 2 is fully determined [Juh93]. For the special modal frequencies, the integral over ∂V degenerates, despite the non-zero contribution of any mode $\frac{\partial p_l^{\mathrm{res}}(\boldsymbol{s})}{\partial n(\boldsymbol{s})} \neq 0$ to the single layer potential, since:

$$\oint_{\boldsymbol{s}\in\partial V} \frac{\partial p_l^{\mathrm{res}}(\boldsymbol{s})}{\partial n(\boldsymbol{s})}\, G(\boldsymbol{r},\boldsymbol{s})\,\mathrm{d}S(\boldsymbol{s}) = 0, \quad \forall \boldsymbol{r}\in\partial V. \tag{134}$$

This means that if modes exist, arbitrarily much of each one of them can be added to the single-layer potential $g(\boldsymbol{s})$ that we search, without any influence on the constraints imposed by cases 1 and 2:

$$\oint_{\partial V} \Big[g(\boldsymbol{s}) + \alpha_l \frac{\partial p_l^{\mathrm{res}}(\boldsymbol{s})}{\partial n(\boldsymbol{s})}\Big]\, G(\boldsymbol{r},\boldsymbol{s})\,\mathrm{d}S(\boldsymbol{s}) = \begin{cases} -p_{\mathrm{sc}}(\boldsymbol{r}) + 0, & \boldsymbol{r}\in\ V \quad \text{case 1,} \\ p_{\mathrm{in}}(\boldsymbol{r}) + 0, & \boldsymbol{r}\in\partial V \quad \text{case 2,} \\ p_{\mathrm{in}}(\boldsymbol{r}) + \alpha_l p_l^{\mathrm{res}}(\boldsymbol{r}), & \boldsymbol{r}\in\ \overline{V} \quad \text{case 3.} \end{cases}$$

Case 2: Assuming modes exist at the regarded frequency, the single-layer potential $g(\boldsymbol{s})$ is not uniquely defined anymore by the constraint of the integral to $p_{\mathrm{in}}(\boldsymbol{r})|_{\partial V}$ in case 2, because $g(\boldsymbol{s}) + \sum_l \alpha_l \frac{\partial p_l^{\mathrm{res}}(\boldsymbol{s})}{\partial n(\boldsymbol{s})}$ for arbitrary α_l is still a valid solution.

Case 1 of the KHI remains unaltered because modes (standing waves) do not create a radiating field outside $\overline{V}$: However, the scattered field p_{sc} is required to obey the radiation condition, which is granted by the compliance of the monopole and dipole sorces of the KHI with the radiation condition. By contrast, modes are standing waves and as such always violate the radiation condition. They do not exist outside $\overline{V}$.

Case 3: The addition of modes to the single-layer potential only changes the result in case 3, inside $\overline{V}$. To obtain the desired unique solutions of synthesis also at the special, modal frequencies, in addition to the constraints of case 2, one needs to impose constraints to the integral equation relating to case 3, see [Juh93]:

— either constraints of case 3 are added at few, suitable interior points (CHIEF points [Sch68]), which renders the equation system overdetermined,

— or the integral equation of case 2 is derived with regard to $n(\boldsymbol{r})|_{\partial V}$ and added to the original integral quation of case 2 by a suitable real constant (Burton-Miller method [BM71]). This involves the transition between case 2 and 3.

Conclusion 1 on synthesis: *It is always possible to uniquely define a complete synthesis problem for any arbitrary homogeneous sound field within a finite volume $\overline{V}$ (case 3) by single-layer-potential-controlled monopole sources on the surface ∂V, i.e. by the normal velocity $g(\boldsymbol{s}) = \frac{\partial[p_{\mathrm{in}}(\boldsymbol{s})+p_{\mathrm{sc}}(\boldsymbol{s})]}{\partial n(\boldsymbol{s})}$ by an ideally sound-soft scattering problem that is equivalent to sound field synthesis.*

Conclusion 2 on analysis: *At special frequencies it is insufficient for sound field synthesis within $\overline{V}$ to only know exclusively one of the free-field sound field quantities on the surface ∂V. The primary sound field might contain standing waves vanishing for either $p_{\mathrm{in}}(\boldsymbol{s})$ or $\frac{\partial p_{\mathrm{in}}(\boldsymbol{s})}{\partial n(\boldsymbol{s})}$. For a sound field identification problem using sensors on ∂V there are the following strategies:*

* *If there is no scatterer (free field), it either helps to know both, sound pressure or sound particle velocity on ∂V, or suitable mixtures thereof (cardioid microphones) to uniquely define the sound field in $\overline{V}$,*
* *Or alternatively knowing only either the free-field quantities $p_{\mathrm{in}}(\boldsymbol{s})$ or $\frac{\partial p_{\mathrm{in}}(\boldsymbol{s})}{\partial n(\boldsymbol{s})}$ can still yield full knowledge of the sound field within $\overline{V}$ if the quantity is known at supporting control points inside $\overline{V}$.*
* *The most pracitcal solution to uniquely and entirely identify a field within $\overline{V}$ relates to equivalent scattering: if $\overline{V}$ is filled by a scatter enforcing either vanishing pressure $p(\boldsymbol{s}) = 0$ (sound soft) or paticle velocity $\frac{\partial p(\boldsymbol{s})}{\partial n(\boldsymbol{s})} = 0$ (sound hard). The remaining quantity must be non-vanishing for any non-vanishing primary field $p_{\mathrm{in}}(\boldsymbol{r}) \neq 0$. This follows from synthesis by equivalent scattering, or abstractly from the Helmholtz equation being a second-order differential equation: There can't be any non-trivial field of both vanishing zeroth- and first-order derivatives.*

Sound field synthesis for the infinite volume V: The single-layer potential is not always suitable for the synthesis of infinitely large sound fields radiating towards infinity. The equivalent scattering problem for synthesis to a finite volume $\overline{V}$ in Eq. (133) indicates the reason:

If the primary field exclusively consists of standing-wave components $p_{\mathrm{in}} = p^{\mathrm{res}}$ at or near special frequencies, which are suited in shape to already fulfill the condition $p_{\mathrm{in}}(\boldsymbol{s}) = p^{\mathrm{res}}(\boldsymbol{s}) = 0$ of the sound soft scatterer, then the scatterer cannot cause a scattered exterior field $p_{\mathrm{sc}}(\boldsymbol{r}) = 0$ in V:

$$\oint_{\partial V} \frac{\partial p^{\mathrm{res}}(\boldsymbol{s})}{\partial n(\boldsymbol{s})}\, G(\boldsymbol{r},\boldsymbol{s})\, \mathrm{d}S(\boldsymbol{s}) = \begin{cases} 0, & \boldsymbol{r} \in V, \\ 0, & \boldsymbol{r} \in \partial V, \\ p^{\mathrm{res}}(\boldsymbol{r}), & \boldsymbol{r} \in \overline{V}. \end{cases}$$

This equation with $p_{\mathrm{in}}(\boldsymbol{r})$ subtracted from Eq. (133) expresses the deficiency we get with the single-layer potential when attempting to synthesize sound fields into the infinite volume V:

Obvisously at or near special frequencies, single-layer potentials exist that do cause exterior, radiating fields. Those shapes will be missing when aiming at a full control of arbitrarily-shaped far-field radiation patterns.

Conclusion 3 on synthesis towards infinity: *The single-layer potential is not suitable for the synthesis of arbitrarily-shaped radiation patterns, as the single-layer potentials corresponding to modes do not radiate. There are the following strategies:*

* *Either the synthesis for the exterior volume needs to employ both monopole sources $G(\boldsymbol{s})$ and dipole sources $\frac{\partial G(\boldsymbol{s})}{\partial n(\boldsymbol{s})}$ on the contour ∂V in the free fied, or a suitable combination of both, to enable controlling any directivity pattern.*
* *An implict combination of $G(\boldsymbol{s})$ and $\frac{\partial G(\boldsymbol{s})}{\partial n(\boldsymbol{s})}$ achieves full radiation control by formulating radiation control as boundary condition on the normal sound particle velocity pattern $\frac{\partial p(\boldsymbol{s})}{\partial n(\boldsymbol{s})}$ on ∂V. This rigid boundary condition at ∂V isolates the modes of the interior volume $\overline{V}$ from the radiation control in V. Any pattern $\frac{\partial p(\boldsymbol{s})}{\partial n(\boldsymbol{s})}$ then produces radiation.*
* *Alternatively, a free-field single-layer potential formulation using only $G(\boldsymbol{s})$ on the contour ∂V could be used, which is modified by adding suitable sources $G(\boldsymbol{r})$ within $\overline{V}$ to establish full control.*

9.3 Wave field synthesis

The article [ZS13, Sec.6] and AES tutorial [SZ15] gives a depictive introduction on sound field synthesis and shows the approximations done for wave field synthesis in detail.

The attempt of getting rid of the sources type $\frac{\partial}{\partial n}G$, i.e. the synthesis using a single-layer potential is solved approximately in wave field synthesis, which is done as follows.

The derivative of a Green's function wrt. a direction $\boldsymbol{n}$ is given as

$$\frac{\partial}{\partial n}G = \boldsymbol{n}^{\mathrm{T}}\boldsymbol{\nabla}G = \boldsymbol{n}^{\mathrm{T}}(\boldsymbol{\nabla}r)\,\frac{\partial G}{\partial r} = \boldsymbol{n}^{\mathrm{T}}\frac{\boldsymbol{r}}{r}\,\frac{\partial G}{\partial r} = \boldsymbol{n}^{\mathrm{T}}\boldsymbol{\theta}\,\left(-\mathrm{i}k - \frac{1}{r}\right)G. \tag{135}$$

Assuming the frequency to be large, the expression simplifies to

$$\lim_{kr\gg 1}\frac{\partial}{\partial n}G = -\mathrm{i}k\;\boldsymbol{n}^{\mathrm{T}}\boldsymbol{\theta}\,G = -\mathrm{i}k\;\cos\phi\;G. \tag{136}$$

Letting now the incident field be the primary source $p_{\mathrm{in}}(\boldsymbol{s}) = G(\boldsymbol{r}_0, \boldsymbol{s})$ at the location $\boldsymbol{r}$, evaluated at the surface of the KHI, we get as a syntesis integral

$$\begin{aligned} p_{\mathrm{in}}(\boldsymbol{r}) &= \oint_{\boldsymbol{s}\in\partial V}\left[\frac{\partial G(\boldsymbol{r}_0,\boldsymbol{s})}{\partial n(\boldsymbol{s})}\,G(\boldsymbol{s},\boldsymbol{r}) - G(\boldsymbol{r}_0,\boldsymbol{s})\,\frac{\partial G(\boldsymbol{s},\boldsymbol{r})}{\partial n(\boldsymbol{s})}\right]\mathrm{d}S(\boldsymbol{s}) \\ &= -\mathrm{i}k\oint_{\boldsymbol{s}\in\partial V}(\cos\phi_0 + \cos\phi)\,G(\boldsymbol{r}_0,\boldsymbol{s})\,G(\boldsymbol{s},\boldsymbol{r})\,\mathrm{d}S(\boldsymbol{s}). \end{aligned} \tag{137}$$

Understandably, what the secondary sources $G(\boldsymbol{s},\boldsymbol{r})$ play depends on the angle enclosed by the connection line between the primary source at $\boldsymbol{r}$ and the secondary source at $\boldsymbol{s}$,

related to the surface normal $\boldsymbol{n}$ at the secondary source. Astonishingly, there is also a term depending on the angle ϕ describing the angle enclosed by the connection line to the listener and the surface normal. However, a common synthesis for all listening spots is desired.

Fig. 28 illustrates the angular simplification that is made. For sources that contribute to the waves approaching the listener, it is assumed that the listener is located along the connecting line of every secondary source to the primary source, for approximation. By contrast, every secondary source is muted which is not contributing to the waves running from the primary source to the listener (right in Fig. 28). The resulting equation uses the unit step function:

$$p_{\text{in}}(\boldsymbol{r}) = -\mathrm{i}k \oint_{\boldsymbol{s}\in\partial V} \underbrace{2\cos\phi_0\, u(-\cos\phi_0) G(\boldsymbol{r}_0, \boldsymbol{s})}_{g(\boldsymbol{s})}\, G(\boldsymbol{s}, \boldsymbol{r})\, \mathrm{d}S(\boldsymbol{s}), \tag{138}$$

and driving the loudspeaker arrangement obviously consists of the delay and attenuation of $G(\boldsymbol{r}_0, \boldsymbol{s})$ of the spound propagating from primary to secondary source, the amplitude factor $2\cos\phi_0$ related to the angle enclosed between surface normal at $\boldsymbol{s}$ wrt. the direction of the primary source, and the step function $u(-\cos\phi_0)$ selecting those secondary sources at whose surface segments the sound waves from the primary source enter the synthesis volume, while muting those where they leave.

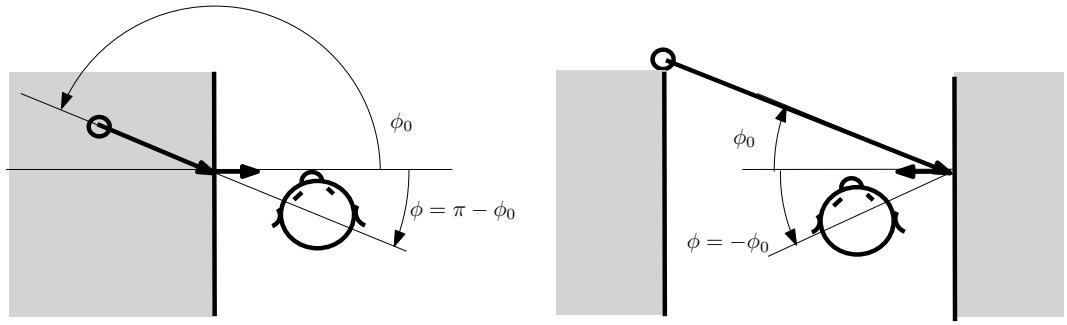

Figure 28 – Approximation of a listening-position-independent anglular constellation in wave-field synthesis (left), and fading out of boundaries opposing the direction of sound incidence.

Fig. 30 illustrates the original KHI with monopoles and dipoles that obviously cancel leaving sound waves that would otherwise propagate througout the volume. As the respective part of the surface radiates to the exterior and not the interior, it can be removed from the integration range without much disturbance (see “left side” as opposed to “right side” in Fig. 30), see also [SRA08].

Moreover, it is not necessary that the KHI only creates such waves that exclusively propagate into the interior of the synthesis volume (imagine there being a free field or absorbing material). *For this reasons, it is not necessary to use dipole sources*, see Fig. 31.

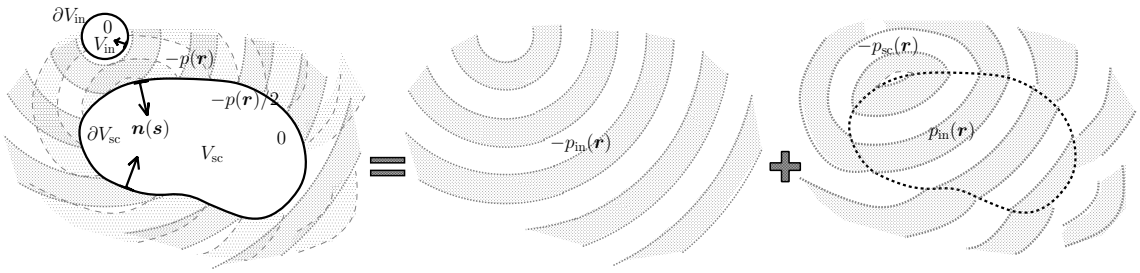

Figure 29 – Kirchhoff-Helmholtz-Integral angewendet, um schallweiche Beugung an ∂V_{sc}, die der Schallfeldsynthese äquivalent ist, zu verdeutlichen. Hier wird denkbare Interaktion des gebeugten Schallfeldes mit denkbaren Randbedingungen der virtuellen Quelle an ∂V_{in} vernachlässigt. Das dargestellte Feld muss außerhalb von V_{sc} dem negativen oritinalen Schallfeld $-p_{\text{in}}(\boldsymbol{r})$ und dem gebeugten Schallfeld äquivalent sein, und der perfekten Schallfeldresynthese $p_{\text{in}}(\boldsymbol{r})$ innerhalb von V_{sc}.

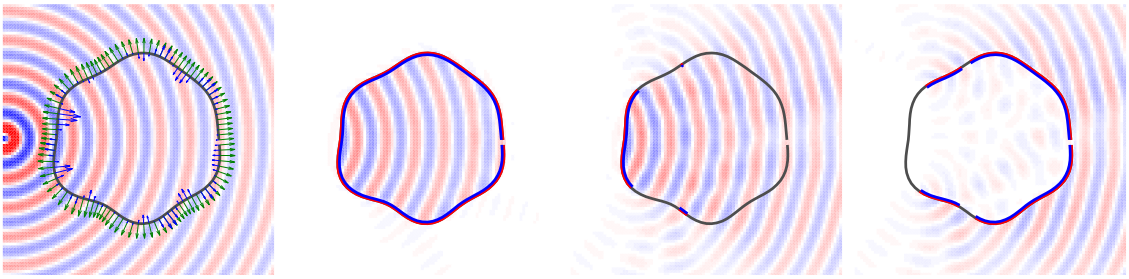

(a) Feld der Punktquelle. (b) Ganzes KHI. (c) Linke Seite (einl.). (d) Rechte Seite (ausl.).

Figure 30 – Um das innere alleine korrekt nachzubilden, muss nicht das gesamte KHI gerechnet werden. Gebiete mit einlaufendem Schall genügen.

9.4 Rayleigh Integrals

Regarding the xy plane as one part of the surface integration of the Kirchhoff-Helmholtz integral, while the rest of the integration is done over an infinitely large hemisphere over the positive z axis, then the radiation condition requires that only the Rayleigh integral over x, y is non-zero:

$$p = -\iint_{-\infty}^{\infty} (G \frac{\partial}{\partial z'} p|_{z'=0} - p|_{z'=0} \frac{\partial}{\partial z'} G)\, \mathrm{d}x' \mathrm{d}y', \qquad \text{Rayleigh-Integral.} \qquad (139)$$

The negative sign corresponds to a surface normal to z^-. With the equation of motion (92) $\frac{\partial}{\partial z} p|_{z'=0} = -\mathrm{i}\,\rho\,\omega\,v_z|_{z'=0}$ it remains

$$p = \iint_{-\infty}^{\infty} (\mathrm{i}\,\rho\,\omega\,G\,v_z|_{z'=0} + p|_{z'=0} \frac{\partial}{\partial z} G)\, \mathrm{d}x' \mathrm{d}y'.$$

The benefit of this description lies in a strong simplification of planar acoustic holography.. The following paragraph shows how syntheis in terms of particle velocity or pressure boundary conditions (or the source strength distribution) work.

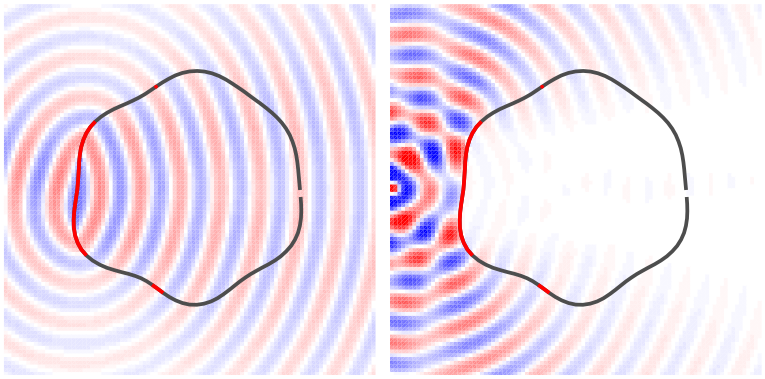

(a) left: monopole sources (b) Synthesis error: synthesized minus orig. field

Figure 31 – The KHI also works approximately after its reduction to monopoles in surface parts with incoming waves, cf. [SRA08]. The hull should be convex to avoid visible disturbances.

Particle velocity as boundary condition. Imposing the constraint of a rigid normal velocity at $z' = 0$ can be described as follows: The sources of the Rayleigh integral are shifted slightly to z^+ and mirrored by the image source principle around $z = 0$ to z^-. While the terms $\frac{\partial}{\partial z'} p|_{z'=0}$ and $p|_{z'=0}$ are just amplitude patterns in x, y, the dipole for z^- of course mirrors and changes its sign:

$$p = \iint_{-\infty}^{\infty} \left[(G^- + G^+) \frac{\partial}{\partial z'} p|_{z'=0} + p|_{z'=0} (\frac{\partial}{-\partial z'} G^- + \frac{\partial}{\partial z'} G^+) \right] \mathrm{d}x' \mathrm{d}y'. \tag{140}$$

The sign change causes the second bracket to vanish in the limit $\lim_{z^+ - z^- \to 0}$, leaving the equation

$$p(x, y, z > 0) = 2 \iint_{-\infty}^{\infty} G(x - x', y - y', z) \frac{\partial}{\partial z'} p(x', y', 0) \, \mathrm{d}x' \mathrm{d}y'. \tag{141}$$

The equation is only true for $z > 0$, because the rigid boundary condition at $z = 0$ is only simulated there by mirroring.

Sound pressure as a boundary condition. Imposing the constraint of a sound pressure pattern at $z = 0$ uses a similar approach as the above. The main difference is that the image source principle uses odd mirroring with sign change, in order to obtain an ideally sound soft boundary condition for the sound pressure. The remaining integral only uses dipole sources:

$$p(x, y, z > 0) = 2 \iint_{-\infty}^{\infty} p(x', y', 0) \frac{\partial}{\partial z} G(x - x', y - y', z) \, \mathrm{d}x' \mathrm{d}y'. \tag{142}$$

Monopole source distributions. It is interesting that the boundary condition for the normal velocitiy is structurally equivalent: Point sources are superimposed by an ampli-

tude distribution f (*here it is not used to express frequency*)

$$p(x,y,z) = \iint_{-\infty}^{\infty} G(x-x',y-y',z)\ f(x',y')\ \mathrm{d}x'\mathrm{d}y'. \tag{143}$$

This formally expresses sound field synthesis to a half-space, when the loudspeakers can be modeled as omnidirectional sources.

9.4.1 What can we learn from the Rayleigh Integrals

We can learn an interesting aspect from the Rayleigh-Integral imposing a boundary condition on the normal velocity at $z = 0$. Calculating the right-sided limit of the particle velocity $v_z|_{z=0^+} = \frac{1}{\mathrm{i}\,\rho\,\omega}\frac{\partial}{\partial z}p|_{z=0^+}$ from Eq. (141), we find

$$v(x,y,0^+) = \iint_{-\infty}^{\infty} \frac{\partial G(x-x',y-y',z)}{\partial z}|_{z=0^+}\ v_z(x',y',0)\ \mathrm{d}x'\mathrm{d}y' = v(x,y,0). \tag{144}$$

This happens as $\frac{\partial}{\partial z}$ is a tangential derivative of the Green's function and hence 0 anywhere, except when evaluated at the Green's function itself $x = x'$ and $y = y'$, so consequently $\frac{\partial G(x-x',y-y',z)}{\partial z}|_{z=0^+} = \delta(x-x',y-y')$. Green's function in the integral therefore only delivers a contribution to the normal velocity at its own position, locally.

This is not anymore true with curved surfaces, where Green's function of the free field also delivers a contribution to the surface normal velocity at remote points, non-locally. This is because the derivative is not necessarily tangential anymore. Wave field synthesis disregards the loss of the purely local excitation and hence approximates arbitrary surfaces by what the planar Rayleighintegral would do.

10 Planar Holography / Holophony

10.1 Planar near-field Holography with

We search the continuous sound particle velocity pattern of a planar surface by recording M sound pressure samples at a distance d from the surface. For this purpose, we utilize the Rayleigh integral to describe a system of equations between known sound pressure samples and the unknown velocity distribution v_z

$$\begin{aligned} p(x_1, y_1, d) = &\quad 2\,\mathrm{i}\,\rho\,\omega \iint_{-\infty}^{\infty} G(x_1 - x', y_1 - y', d)\; v_z(x', y', 0)\; \mathrm{d}x'\mathrm{d}y' \\ \vdots \qquad = &\qquad \vdots \\ p(x_\mathrm{M}, y_\mathrm{M}, d) = &\quad 2\,\mathrm{i}\,\rho\,\omega \iint_{-\infty}^{\infty} G(x_\mathrm{M} - x', y_\mathrm{M} - y', d)\; v_z(x', y', 0)\; \mathrm{d}x'\mathrm{d}y'. \end{aligned}$$

In practice, the equation system cannot be inverted to obtain a continuous pattern $v_z(x, y)$. The integral is discretized into small parts with the discretization intervals Δx and Δy. If the discretization is fine enough, it is a good approximation to use monopoles times surface element, what delivers the matrix

$$\begin{bmatrix} p(x_1, y_1, d) \\ \vdots \\ p(x_\mathrm{M}, y_\mathrm{M}, d) \end{bmatrix} = \quad 2\,\mathrm{i}\,\rho\,\omega \sum_{l_x, l_y} \begin{bmatrix} G(x_1 - l_x\Delta x, y_1 - l_y\Delta y, d) \\ \vdots \\ G(x_\mathrm{M} - l_x\Delta x, y_\mathrm{M} - l_y\Delta y, d) \end{bmatrix} v_z(l_x\Delta x, l_y\Delta y, 0)\; \Delta x\Delta y.$$

Using matrix-vector notation this becomes $\boldsymbol{p} = \boldsymbol{G}\,\boldsymbol{v}_z$. Typically, we have only access to only a few measured sound pressure samples M for $\boldsymbol{p}$ when comparted to the wishes of a high-resolution $\mathrm{L}_x, \mathrm{L}_y$ that we desire for the resulting $v_z(x, y)$. Just to give an example: Using $8 \times 8 = 64$ microphones and desiring an image having $\mathrm{L}_x \times \mathrm{L}_y = 100 \times 100$ pixels for the normal velocity yields a system with 9936 undetermined degrees of freedom. To uniquely define those degrees of freedom, it is typical to find the least-squares $\boldsymbol{v}_z$

$$\begin{aligned} &\min \|\boldsymbol{v}_z\|_2^2 \\ &\text{subject to: } \boldsymbol{p} = \boldsymbol{G}\,\boldsymbol{v}_z \end{aligned}$$

The conclusion that this is not an exact solution, different sampling and a different kind of metric might yield other solutions was utilized in Philipp Schmidt's master's thesis [Sch12a]. For instance, we can write down a minimization problem for the L_p norm $\|\boldsymbol{x}\|_p = \sqrt[p]{|x_1|^p + |x_2|^p + \ldots}$

$$\begin{aligned} &\min \|\boldsymbol{v}_z\|_p \\ &\text{subject to: } \boldsymbol{p} = \boldsymbol{G}\,\boldsymbol{v}_z. \end{aligned}$$

For the value $p = 1$, the solution image for $\boldsymbol{v}_z$ contains as few as possible non-zero pixels fulfilling the imposed condition $\boldsymbol{p} = \boldsymbol{G}\,\boldsymbol{v}_z$. This obviously is a *sparsity enforcing* metric. Large values for $p \to \infty$ enforce smeared solutions, with the attempt of finding a $\boldsymbol{v}_z$ fulfilling the conditions with the most equal magnitude at each pixel.

Regularization. The matrix $\boldsymbol{G}$ can be *ill-conditioned*. This means that some entries or vectors have a vanisihngly representation. In particular, such patterns corresponding to a high spatial variation, i.e. patterns like $\begin{bmatrix} + & - & + & - \\ - & + & - & + \end{bmatrix}$, across the microphone array are often not strongly attenuated in the propagation from $\boldsymbol{v}_z$ to $\boldsymbol{p}$ described by $\boldsymbol{G}$. This problem is entirely independent of the paricular holographical minimization task. These patterns are often not easy to produce with magnitudes in the dynamic range of the transducers on the measurement surface. Consequently, they are under-represented in the model $\boldsymbol{G}$ of sound propagation. While analytically this might still seem unproblematic, the practical errors are not only measurement noise, but also achievable equalization accuracy of the microphones and other slight deficiencies that lie in the same magnitude as the expected, vanishingly small acoustical patterns. Regularization is a means to boost these under-represented patterns so that their inversion stops trying too hard on their reconstruction. To this end, the diagonal of the singular value decomposition can be loaded by a small contribution α:

$$\boldsymbol{G} = \boldsymbol{U}\,\boldsymbol{S}\,\boldsymbol{V}^{\mathrm{T}}, \qquad \Longrightarrow \boldsymbol{G}_{\mathrm{reg}} = \boldsymbol{U}\,[\boldsymbol{S} + \alpha \boldsymbol{I}]\,\boldsymbol{V}^{\mathrm{T}}. \tag{145}$$

The inverse of $\boldsymbol{G}_{\mathrm{reg}}$ will hereby gradually omit components whose propagation is expected to fall below the order of magnitude of α.

10.1.1 Least-square error and least-squares problems

The rectangular $(n \times m)$ model matrix $\boldsymbol{A}$ should together with the m parameters $\boldsymbol{x}$ yield the n measured values $\boldsymbol{b}$,

$$\boldsymbol{A}\boldsymbol{x} = \boldsymbol{b}. \tag{146}$$

There are a couple of classical solution options (inverse, left/right inverse, generalized inverse) depending on the size relations. Both assume that $\boldsymbol{A}$ is well-conditioned (numerically invertible).

Inversion: $\boldsymbol{x}$ bestimmt, $n = m$. The matrix is square and possesses an inverse

$$\boldsymbol{x} = \boldsymbol{A}^{-1}\boldsymbol{b}. \tag{147}$$

Least-square error solution: $\boldsymbol{x}$ is over-determined, $n > m$. As there are more conditions n than the m parameters, and it is unknown how precisely model and measurement match, we have to assume that there can be a mismatch in the modeled measurements. As a cost function, we minimize the square error of the mismatch

$$J(\boldsymbol{x}) = (\boldsymbol{A}\boldsymbol{x} - \boldsymbol{b})^{\mathrm{H}} (\boldsymbol{A}\boldsymbol{x} - \boldsymbol{b}), \tag{148}$$

equating its derivative to zero yields

$$\frac{\partial J}{\partial \boldsymbol{x}} = 2\boldsymbol{A}^{\mathrm{H}} (\boldsymbol{A}\boldsymbol{x} - \boldsymbol{b}) = \boldsymbol{0}, \qquad \Rightarrow \boldsymbol{x} = \left(\boldsymbol{A}^{\mathrm{H}}\boldsymbol{A}\right)^{-1} \boldsymbol{A}^{\mathrm{H}}\boldsymbol{b}. \tag{149}$$

Obviously $\left(\boldsymbol{A}^{\mathrm{H}}\boldsymbol{A}\right)^{-1} \boldsymbol{A}^{\mathrm{H}}$ is left-inverse to $\boldsymbol{A}$, but it does not invert $\boldsymbol{A}$ from the right.

Least squares solution: $\boldsymbol{x}$ is under-determined, $n < m$. With the multitude of parameters m the n can be fulfilled in many non-unique ways. Solutions of constrant L_2 norm lie on a m-dimensional hyper sphere, whereas the constraint $\boldsymbol{A}\boldsymbol{x} = \boldsymbol{b}$ spans a hyper plane on which all solutions must lie. The solution of the minimum L_2 norm delivers the contact point between the smallest-possible sphere centered at $\boldsymbol{0}$ with the hyper plane described by the constraints. The norm plus the deviation from constraints multiplied by the Lagrange multipliers $\boldsymbol{\lambda}$ yields the cost function

$$J(\boldsymbol{x}, \boldsymbol{\lambda}) = \boldsymbol{x}^{\mathrm{H}}\boldsymbol{x} + \boldsymbol{\lambda}^{\mathrm{H}}(\boldsymbol{A}\boldsymbol{x} - \boldsymbol{b}). \tag{150}$$

The minimum is found reached by zeroing both derivatives to $\boldsymbol{x}$ and $\boldsymbol{\lambda}$

$$\begin{aligned}
\frac{\partial J}{\partial \boldsymbol{x}} &= 2\boldsymbol{x}^{\mathrm{H}} + \boldsymbol{\lambda}^{\mathrm{H}}\boldsymbol{A} = \boldsymbol{0}, & &\Rightarrow \boldsymbol{x} = -\frac{1}{2}\boldsymbol{A}^{\mathrm{H}}\boldsymbol{\lambda}. \\
\frac{\partial J}{\partial \boldsymbol{\lambda}^{\mathrm{H}}} &= \boldsymbol{A}\boldsymbol{x} - \boldsymbol{b} = \boldsymbol{0}, \overset{\text{with the above}}{\Rightarrow} -\frac{1}{2}\boldsymbol{A}\boldsymbol{A}^{\mathrm{H}}\boldsymbol{\lambda} = \boldsymbol{b}, & &\overset{\text{inverse}}{\Rightarrow} \boldsymbol{\lambda} = -2\left(\boldsymbol{A}\boldsymbol{A}^{\mathrm{H}}\right)^{-1}\boldsymbol{b}, \\
\Longrightarrow \boldsymbol{x} &= \boldsymbol{A}^{\mathrm{H}}\left(\boldsymbol{A}\boldsymbol{A}^{\mathrm{H}}\right)^{-1}\boldsymbol{b}.
\end{aligned} \tag{151}$$

Obvisously $\boldsymbol{A}^{\mathrm{H}}\left(\boldsymbol{A}\boldsymbol{A}^{\mathrm{H}}\right)^{-1}$ is right-inverse to $\boldsymbol{A}$.

Generalized inverse: pseudo inverse. Singular decomposition of $\boldsymbol{A}$

$$\boldsymbol{A} = \boldsymbol{U}\,\boldsymbol{S}\,\boldsymbol{V}^{\mathrm{H}}$$

yields two matrices $\boldsymbol{U}_{(n\times n)}$ and $\boldsymbol{V}_{(m\times m)}$ that are unitary, $\boldsymbol{U}^{\mathrm{H}}\boldsymbol{U} = \boldsymbol{U}\boldsymbol{U}^{\mathrm{H}} = \boldsymbol{I}$ and $\boldsymbol{V}^{\mathrm{H}}\boldsymbol{V} = \boldsymbol{V}\boldsymbol{V}^{\mathrm{H}} = \boldsymbol{I}$, and an $(n \times m)$ diagonal matrix $\boldsymbol{S} = \mathrm{diag}_{(n\times m)}\{[s_i]_i\}$ of descendingly sorted, real-valued, positive singular values $s_i \in \mathbb{R}^+;\ s_1 \geq s_2 \geq \cdots \geq 0$. The generalized inverse or pseudo-inverrse is

$$\boldsymbol{A}^{\dagger} = \boldsymbol{V}\,\boldsymbol{S}^{\dagger}\,\boldsymbol{U}^{\mathrm{H}}, \qquad \text{with } \boldsymbol{S}^{\dagger} = \mathrm{diag}_{(m\times n)}\{[1/s_i]_i\}. \tag{152}$$

It is easy to regularize by limiting the singular values s_i with a floor value. Moreover, the generalization of this inversion is that we obtain the inverse matrix for $n = m$, the left-inverse matrix for $n > m$, and the right-inverse matrix for $n < m$.

According to [GK65], the pseudo-inverse $\boldsymbol{A}^{\dagger}$ finds the shortest-possible solution vector $\boldsymbol{x}$ (minimum L_2 norm) with the shortest-possible error vector $\boldsymbol{A}\,\boldsymbol{x} - \boldsymbol{b}$ (minimum L_2 norm).

10.1.2 Conditioning of a matrix

The condition number of a matrix defines the relation between the largest and smallest singular value:

$$\kappa(\boldsymbol{A}) = \frac{s_{\max}}{s_{\min}}, \tag{153}$$

and it lies in the range $1 \leq \kappa \leq \infty$. It tells us something about the dynamic range of possible scaling properties the matrix $\boldsymbol{A}$ has on input vectors, and hence, how error tolerant it is to work with the (pseudo-)inverse of $\boldsymbol{A}$.

Explanation: The left-multiplication of the parameter vector $\boldsymbol{x}$ by a unitary matrix $\hat{\boldsymbol{x}} = \boldsymbol{V}^{\mathrm{H}}\boldsymbol{x}$, i.e. $\boldsymbol{V}^{\mathrm{H}}\boldsymbol{V} = \boldsymbol{V}\boldsymbol{V}^{\mathrm{H}} = \boldsymbol{I}$, does not change its norm:

$$\|\hat{\boldsymbol{x}}\|_2^2 = \|\boldsymbol{V}^{\mathrm{H}}\boldsymbol{x}\|_2^2 = \boldsymbol{x}^{\mathrm{H}}\cancel{\boldsymbol{V}\boldsymbol{V}^{\mathrm{H}}}\boldsymbol{x} = \|\boldsymbol{x}\|_2^2.$$

By contrast, the norm of the image $\boldsymbol{b} = \boldsymbol{A}\boldsymbol{x}$ throuh the matrix $\boldsymbol{A} = \boldsymbol{U}\boldsymbol{S}\boldsymbol{V}^{\mathrm{H}}$ is scaled

$$\|\boldsymbol{b}\|_2^2 = \|\boldsymbol{A}\boldsymbol{x}\|_2^2 = \|\boldsymbol{U}\boldsymbol{S}\boldsymbol{V}^{\mathrm{H}}\boldsymbol{x}\|_2^2 = \|\boldsymbol{U}\boldsymbol{S}\hat{\boldsymbol{x}}\|_2^2 = \|\boldsymbol{S}\hat{\boldsymbol{x}}\|_2^2.$$

Assuming that $\boldsymbol{S}$ has at least as many rows as columns, the norm lies within the range

$$s_{\min}\,\|\boldsymbol{x}\|_2 \leq \|\boldsymbol{b}\|_2 \leq s_{\max}\,\|\boldsymbol{x}\|_2.$$

Assuming that $\boldsymbol{x}$ contains uncorrelated errors $\boldsymbol{\epsilon}$ of a norm $\|\boldsymbol{\epsilon}\|_2 = \frac{\|\boldsymbol{x}\|_2}{\kappa(\boldsymbol{A})}$ depending on the norm of $\boldsymbol{x}$ divided by the condition number, the norm of the error in the image $\boldsymbol{b}_\epsilon = \boldsymbol{A}\boldsymbol{\epsilon}$ is

$$\frac{s_{\min}^2}{s_{\max}}\,\|\boldsymbol{x}\|_2 \leq \|\boldsymbol{b}_\epsilon\|_2 \leq s_{\min}\,\|\boldsymbol{x}\|_2.$$

which means that the worst-case error (maximum) meets the image that is scaled-down the most, $\|\boldsymbol{b}_\epsilon\|_2 \leq \|\boldsymbol{b}\|_2$. For the biggest error tolerance, the condition number should therefore be as small as possible, $\kappa \to 1$, so that only large parameter errors in the range of magnitude of the parameters $\|\boldsymbol{\epsilon}\|_2 \approx \|\boldsymbol{x}\|_2$ yield large image errors in the range of magnitude of the image. Then, the mapping of small errors $\|\boldsymbol{\epsilon}\|_2 \ll \|\boldsymbol{x}\|_2$ stays small $\|\boldsymbol{b}_\epsilon\|_2 \ll \|\boldsymbol{b}\|_2$ without exception.

In our under-determined holographical case, in which $\boldsymbol{S}$ has fewer columns as rows, the same considerations are true as for the right-inverse system. However, the measurement errors are present in $\boldsymbol{b}$, and the holographical image appears in the parameters $\boldsymbol{x}$.

10.1.3 L_p Norm Minimization

Software packages for convex optimization allow to solve complex problems with other norms than L_2 norms.

The error minimization in the L_p norm or the constraint minimization of the L_p norm can be formulated in CVX, a package written for MATLAB [CR12, GB08], in this way:

```
n = size(A,1); m = size(A,2);
if (n>m)
    cvx_begin
        variable x(m) complex
        minimize( norm( A * x - b , p) )
    cvx_end
else
    cvx_begin
        variable x(m) complex
        minimize( norm( x , p) )
        subject to
            A * x == b
    cvx_end
end
```

In practice, the fixed and rigorous constraint is often replaced by a a constraint allowing for small quadratic deviations β, in order to yield a more stable convergence, cf. [Sch12a]. With the relaxed constraints, the formulation becomes

```
        subject to
            sum(square_abs( A * x - b ) <= beta
```

10.2 Sound field of 1D velocity boundary condition along x

An exemplary boundary value problem for the normal derivative of the pressure in the shape of a rectangular gap function in an infinite rigid contour rquires spatial convolution with the Green's function, corresponding to the Rayleigh integral

$$p(\boldsymbol{r}) = 2\frac{\partial}{\partial y}p(x)\big|_{y=0} \star G_{\mathrm{2D}}(x,y). \tag{154}$$

With the Green's function for the considered 2D case, we obtain

$$p(\boldsymbol{r}) = \frac{\partial}{\partial y}p(x)\big|_{y=0} \star \frac{\mathrm{i}}{2} H_0^{(2)}\left(k\sqrt{y^2+x^2}\right), \tag{155}$$

and Fig. 32 shows the result.

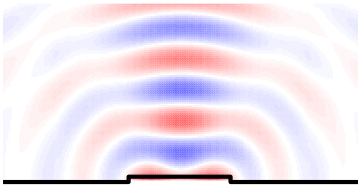

Figure 32 – 2D sound field of a rectangular gap, convolution/integral formulation.

10.3 Fourier transform for planar holophony/holography

Fast convolution: Despite plane waves have been disregarded as physical solutions before, it is still useful to use Fourier transforms for fast convolution. Despite this requires zero-padding to avoid circular convolution, which is difficult to avoid when the Green's function is actually infinite, the fast convolution was crucial to enable acoustic holography in its beginnings [Wil99, Fle88]. The double circulant matrix $\boldsymbol{G}$ of the planar holography task before (circulant in x and also in y) is diagonalized by the transform into the spatial Fourier domain. As the fast transform uses much less as operations as matrix full multiplications, and multiplication of each wave-number bin with a diagonal matrix or its inverse, i.e., component-wise multiplication/division, makes fast convolution/deconvolution efficient, however also cyclic, so not entirely accurate, in space.

10.3.1 Far-field directivity:

The far-field directivity of velocity patterns of finite extent on an otherwise infinitely large and rigid x, y plane can be approximated by the Rayleigh integral after simplificatrion $G \propto e^{\mathrm{i}\,k\,\boldsymbol{\theta}^{\mathrm{T}}\boldsymbol{r}}$. This makes the Fourier transform of the velocity countour (cf. [Mös88, Mös09, Wik10]) an estimator of the far-field directivity. Assuming the source lie in one dimension x only, i.e. along $\boldsymbol{\theta} = (1,\,0)^{\mathrm{T}}$, the exponential function remains $e^{\mathrm{i}\,k\,\cos\varphi}$. *The*

far field approximation of the sound pressure is therefore proportional to the Fourier transform of the sound particle velocity, evaluated at $k \cos\varphi$*,*

$$p_\infty(\varphi) \propto \mathcal{F}_{x,k_x=k\cos\varphi}\left\{\frac{\partial}{\partial y}p(x,y)\right\}. \tag{156}$$

10.3.2 Holographic analysis, known sound pressure along x.

In direct inversion of the boundary condition of the velocity, we obtain by spectral deconvolution of the sound pressure wiht the Fourier transformation symbol $\mathcal{F}_{x,k_x}\{\cdot\}$

$$v_y(x)\big|_{y=0} = \mathcal{F}^{-1}_{x,k_x}\left\{\frac{\mathcal{F}_{x,k_x}\left[p(x,y_0)\right]}{\mathcal{F}_{x,k_x}\left[\frac{\rho\omega}{2}H_0^{(2)}\left(k\sqrt{y_0^2+x^2}\right)\right]}\right\}. \tag{157}$$

The efficient way to calculate the discrete Fourier transform is the FFT. In any case, as with discrete-time signal processing [OSB99], the geometry of the problem gets implicitly periodic/cyclic in space.

The sound pressure evaluated at other points than measured can be obtained by inserting into Eq. (155)

$$p(\boldsymbol{r}) = \mathcal{F}^{-1}_{x,k_x}\left\{\frac{\mathcal{F}_{x,k_x}\left[p(x,y_0)\right]}{\mathcal{F}_{x,k_x}\left[H_0^{(2)}\left(k\sqrt{y_0^2+x^2}\right)\right]}\,\mathcal{F}_{x,k_x}\left[H_0^{(2)}\left(k\sqrt{y^2+x^2}\right)\right]\right\}. \tag{158}$$

Regularization (addition of small contributions to the absolute value) can be used in the denominator to limit its smallness.

10.3.3 Example: Far field holophony for finite-length linear loudspeaker array in 2D

Superimposing multiple rectangular gap functions with a spacing of Δx, we can simulate the sound field of loudspeaker arrays, see Fig. 33.

The given example essentially uses the far-field approximation with real-valued $-k \le k_x \le k$. With the phase modulation property of the Fourier transform we can achieve beamforming. Its goal usually is to excite a single beam of sound pointing to just one direction with minimized magnitude in any other direction. The directivity plot shows $\nu_y(k\,\cos(\varphi))$ for this range of k_x. It is important to know that the respective range of k_x depends on the frequency ($k = \omega/c$), whereas the pattern in k itself is frequency independent and only depends on the spatial distribution of the cap functions.

Aliasing in the far field. The second diagram in Fig.33 cuts out a part of the wave number spectrum $\nu_y(k_x)$ with $-k \le k_x \le k$ being larger, i.e. for a higher frequency. As there already is an image component of the wave number spectrum $\nu_y(k_x)$, we speak of far field *aliasing*, i.e. a non-unique directional mapping of the beam direction.

As a pre-requisite against far field aliasing there is the general constraint that there must be at least two elements per wavelength

$$k = \frac{\omega}{c} = \frac{2\pi}{\lambda} < \frac{\pi}{\Delta x}, \qquad \Rightarrow \Delta x < \frac{\lambda}{2}. \tag{159}$$

In the particular case of far field beamforming in the angle φ (enclosed angle to the y axis that is perpendicular to the array) this limit can be pushed a bit further (best case: $\varphi = 0$, worst case $\varphi = \pm\pi/2$ "'end fire direction"'), if sound waves from outside of the angles $\pm\varphi_{\max}$ can be acoustically excluded (!)

$$k(1 + |\sin(\varphi_{\max})|) < \frac{2\pi}{\Delta x}, \qquad \Rightarrow \Delta x < \frac{\lambda}{1 + |\sin(\varphi_{\max})|}.$$

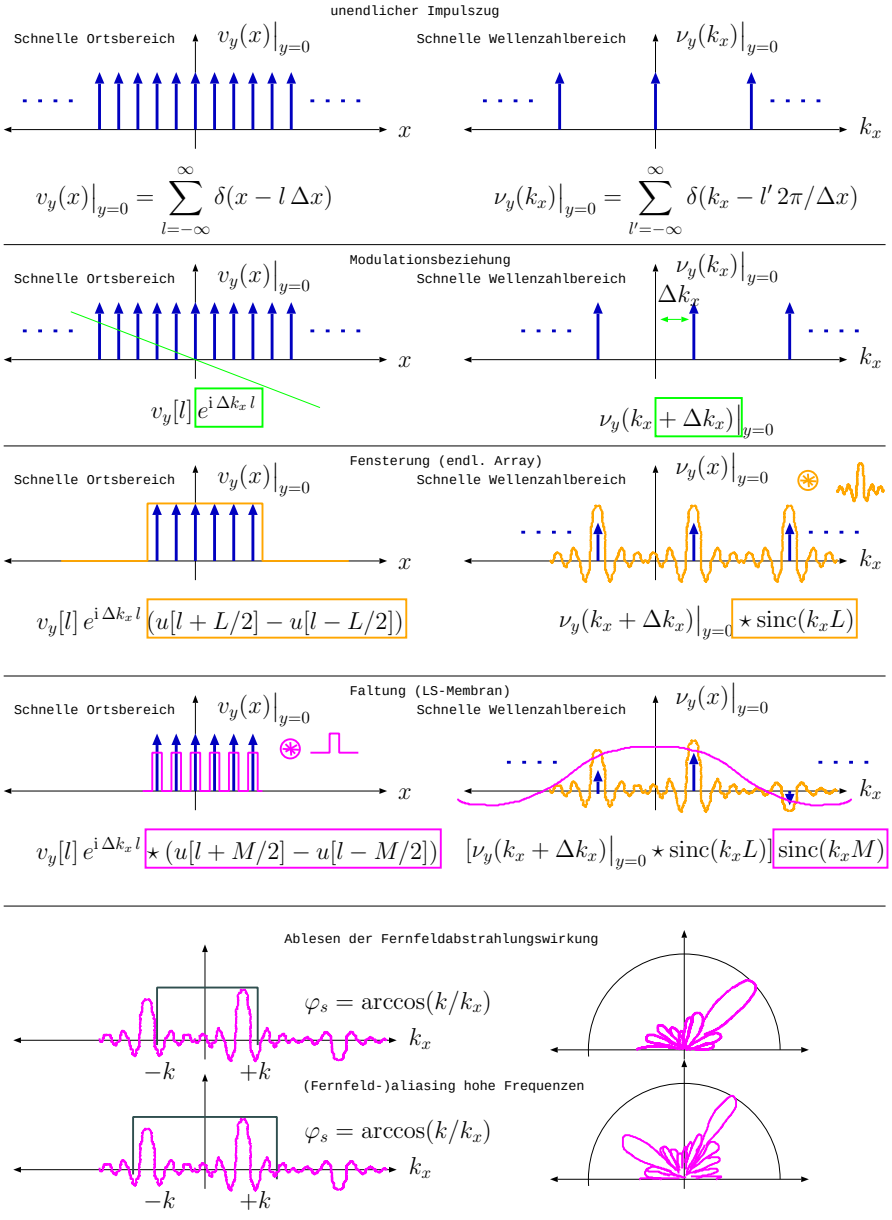

Figure 33 – Spatial signal processing for 1D loudspeaker array.

10.3.4 Example: Holography with finite-length linear microphone array in 2D

Is the sound pressure only known on discrete points $l\Delta x$ along x, the wave number spectrum becomes cyclic as above $\psi(k_x)\big|_{y=y_0}$ with the period $k_{xp} = \frac{2\pi}{\Delta x}$.

Near field aliasing. Given the assumption holds that the wave number spectum vanishes for $|k_x| > \frac{2\pi}{\Delta x}$, there are neither sampling errors nor spatial aliasing. However, the smallest wavelength depends on the sound emitting structrure and not from the far-field wavelength in the air λ.

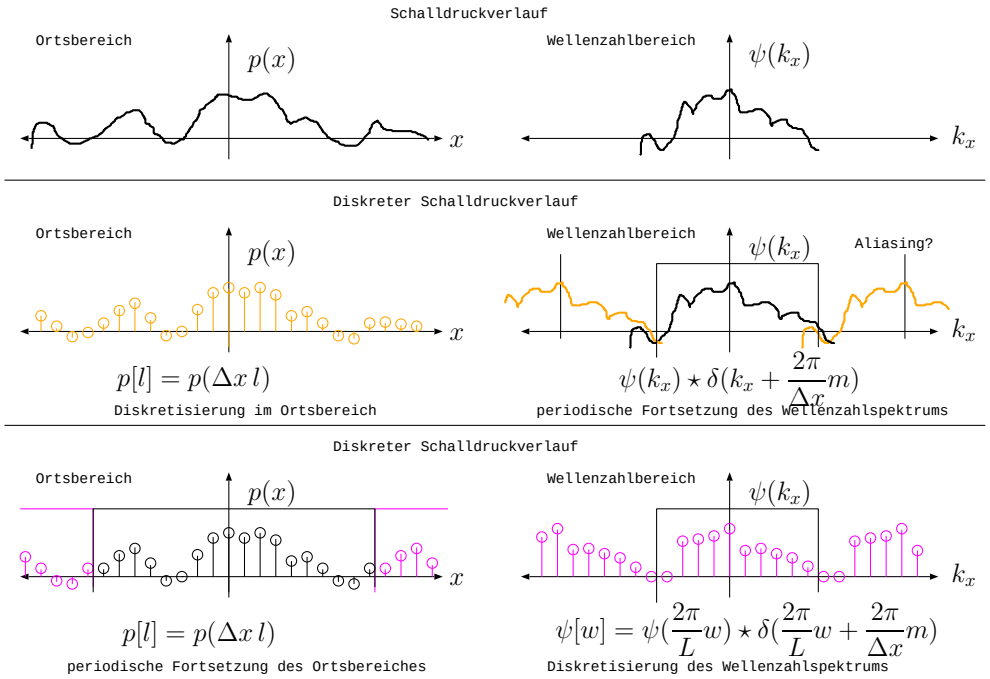

Figure 34 – Holography with discrete finite-length linear microphone array.

Using DFT/FFT to evaluate the waven umber spectrum. Given N discrete sound pressure measurements as a sequence $p[l]$, $l = 0, \ldots, \mathrm{N}-1$, we may use a DFT/FFT to calculate the wave number spectrum [4]

$$\psi[w] = \sum_{l=0}^{\mathrm{N}-1} p[l]\, e^{\mathrm{i}\,\frac{2\pi}{\mathrm{N}}\, l\, w}. \tag{160}$$

4. Usually time-domain signals use a different sign in the exponent.

The phyisical wave number k_x belonging to the discrete index w is found by discretizing the phyical plane-wave solution ($x \to \Delta x\, l$):

$$e^{\mathrm{i}\, k_x\, \Delta x\, l} \leftrightarrow e^{\mathrm{i}\, \frac{2\pi}{\mathrm{N}}\, w\, l}, \qquad \Rightarrow k_x[w] = \frac{2\pi}{\mathrm{N}\Delta x}\, w. \tag{161}$$

With this proportionality, and with the spatial propagation filters, every diskrete *wave number bin* w can be evaluated to either do far-field or near-field holography/holophony.

11 Helmholtzgleichung in Kugelkoordinaten

Die umfassenden Beschreibungen der in den Abschnitten zuvor fußen auf dem Kirchhoff-Helmholtz-Integral und besitzen oftmals aufwändige/ungünstige Darstellungen physikalischer Felder, wenngleich sich durch Faltungssätze und Fernfeldnäherungen unphysikalische ebene Wellen in einfacher Weise zur Berechnung korrekter Ergebnisse eignen.

Im gekrümmten Kugelkoordinatensystem des $\mathbb{R}^3$ ergeben sich im Wesentlichen zwei Unterscheidungsbereiche: außen und innen. Wird das Rechnen mit physikalischen Darstellungen angestrebt, sind diese entweder zur Einforderung der Ausstrahlungsbedingung, oder eines homogenen, endlichen Schallfeldes geeigneter.

Wie Abbildung 35 zeigt, sind diese zwei Grundtypen einerseits das sog. *innere Problem*, dessen Schallfeld bis zu einem Radius hin quellenfrei und endlich bleiben muss, und andererseits das *äußere Problem*, welches außerhalb eines Radius homogen und quellenfrei ist, sowie die Ausstrahlungsbedingung einhalten muss, siehe Gl. (132).

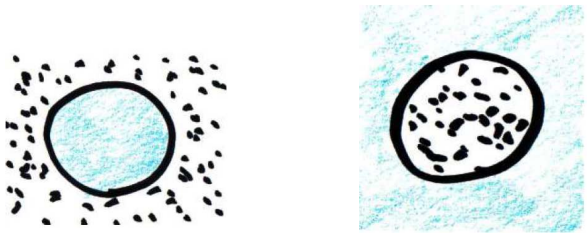

(a) (b)

Figure 35 – a) Inneres und b) äußeres Problem

Für beide dieser Typen wird nun gezeigt, wie die Lösungen der verlustlosen Wellengleichung, der Helmholtzgleichung, gefunden werden.

11.1 Ableitungsoperatoren in nichtkartesischen Koordinatensystemen

Ganz allgemein können zwei Koordinatensysteme durch ein n-tupel an Werten ausgedrückt werden. Nehmen wir an, wir haben das kartesische $(x_1, x_2, \dots)$ und ein anderes Koordinatensystem $(u_1, u_2, \dots)$ zum Beschreiben eines Punktes im beliebigdimensionalen Raum. Jeder Raumpunkt sollte in beiden Systemen erreichbar sein und eine umkehrbare Abbildungen dazwischen existieren, z.B. $u_j = u_j(x_1, x_2, \dots)$. Eine einzelne Ableitung, sagen wir nach der Komponente x_i, lässt sich über die Kettenregel durch eine Summe gewichteter Ableitungen nach u_j ausdrücken:

$$\frac{\partial}{\partial x_i} = \sum_j \frac{\partial u_j}{\partial x_i} \frac{\partial}{\partial u_j}. \tag{162}$$

Vektoriell geschrieben werden Ableitungen des Gradienten $\nabla = \frac{\partial}{\partial \boldsymbol{x}}$ mit $\frac{\partial}{\partial \boldsymbol{u}}$ zu:

$$\nabla = \frac{\partial \boldsymbol{u}^{\mathrm{T}}}{\partial \boldsymbol{x}} \frac{\partial}{\partial \boldsymbol{u}} := \boldsymbol{J}_{\partial u/\partial x} \frac{\partial}{\partial \boldsymbol{u}}, \tag{163}$$

wobei die allgemein von $\boldsymbol{x}$ oder $\boldsymbol{u}$ abhängige Jacobi-Matrix $\boldsymbol{J}_{\partial u/\partial x} = \left[\frac{\partial u_j}{\partial x_i}\right]_{ij}$ alle partiellen Ableitungen der Umrechnungsvorschrift enthält. Es gibt sie auch für die Umkehrvorschrift $\boldsymbol{J}_{\partial x/\partial u} = \left[\frac{\partial x_i}{\partial u_j}\right]_{ji}$. Vollwertig ist das Koordinatensystem $\boldsymbol{u}_j$ aber nur, wenn die Determinante überall verschieden von null ist $|\boldsymbol{J}| \neq 0$.

Bei orthogonalen Koordinatensystemen ist $\boldsymbol{J}^{\mathrm{T}}\boldsymbol{J}$ eine Diagonalmatrix. Mit $\boldsymbol{J}_{\partial x/\partial u} = \frac{\partial \boldsymbol{x}^{\mathrm{T}}}{\partial \boldsymbol{u}}$ ist das leicht zu sehen: die differentielle Ortsänderungen $\partial \boldsymbol{x}/\partial u_j$ jeder nichtkartesischen Koordinate u_j bilden im Raum ein orthogonales Koordinatenkreuz, das abhängig vom Ort freie Ausrichtung und Schenkellängen haben darf.

Viel interessanter als der Gradient ist der Laplace-Operator; er ist allgemein $\triangle = \sum_i \frac{\partial^2}{\partial x_i^2}$ und mit der Kettenregel (jetzt von x_i nach u_j gerechnet)

$$\begin{aligned} \triangle &= \sum_i \frac{\partial}{\partial x_i}\left(\frac{\partial}{\partial x_i}\right) = \sum_i \frac{\partial}{\partial x_i}\left(\sum_j \frac{\partial u_j}{\partial x_i}\frac{\partial}{\partial u_j}\right) \\ &= \sum_{i,j} \frac{\partial^2 u_j}{\partial x_i^2}\frac{\partial}{\partial u_j} + \sum_{i,j,k} \frac{\partial u_j}{\partial x_i}\frac{\partial u_k}{\partial x_i}\frac{\partial^2}{\partial u_j \partial u_k}, \end{aligned} \tag{164}$$

$$\text{wobei } \sum_{i,j,k} \frac{\partial u_j}{\partial x_i}\frac{\partial u_k}{\partial x_i}\frac{\partial^2}{\partial u_j \partial u_k} = \frac{\partial}{\partial \boldsymbol{u}^{\mathrm{T}}}\Big] \underbrace{\boldsymbol{J}^{\mathrm{T}}\boldsymbol{J}}_{\text{ortho: diag}} \Big[\frac{\partial}{\partial \boldsymbol{u}} = \sum_{i,j}\left(\frac{\partial u_j}{\partial x_i}\right)^2 \frac{\partial^2}{\partial u_j^2}.$$

Die Verwendung orthogonaler Koordinatensysteme vereinfacht ihn stark (letzte Zeile), sodass er bloß aus einfachen und sortenreinen doppelten Ableitungen des neuen Koordinatensystems besteht. Beide sind mit den partiellen Ableitungen der Koordinaten gewichtet. Für jedes u_j gibt es im Laplace-Operator einen Summenterm

$$\triangle = \sum_j \triangle_{u_j}, \qquad \text{wobei } \triangle_{u_j} = \left[\sum_i \frac{\partial^2 u_j}{\partial x_i^2}\right]\frac{\partial}{\partial u_j} + \left[\sum_i \left(\frac{\partial u_j}{\partial x_i}\right)^2\right]\frac{\partial^2}{\partial u_j^2}. \tag{165}$$

11.2 Helmholtzgleichung des $\mathbb{R}^3$ in Kugelkoordinaten

In drei räumlichen Dimensionen hat das Kugelkoordinantensystem abgesehen vom Radius zwei Winkel, den Azimutwinkel φ, der auf der Projektion auf die xy-Ebene gegen den Uhrzeigersinn den Abstand zur x-Achse angibt, und den Zenitwinkel ϑ, der den Winkel zur z-Achse misst.

11.2.1 Kugelkoordinaten

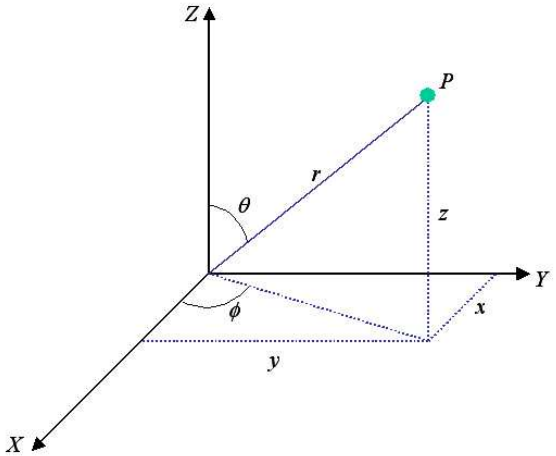

Figure 36 – Kugelkoordinaten

$$
\begin{aligned}
x &= r\cos\varphi\sin\vartheta & r &= \sqrt{x^2+y^2+z^2}\\
y &= r\sin\varphi\sin\vartheta & \varphi &= \arctan\left(\frac{x}{y}\right)\\
z &= r\cos\vartheta & \vartheta &= \arccos\left(\frac{z}{r}\right)\\
x,y,z &\in [-\infty,\infty] & r &\in [0,\infty]\,,\ \varphi\in[0,2\pi]\,,\ \vartheta\in[0,\pi]
\end{aligned}
$$

11.2.2 Laplace-Operator in Kugelkoordinaten

Bei der Berechnung des Laplace-Operators Kugelkoordinaten ergibt sich, vgl. Anhang P,

$$\triangle = \left(\frac{\partial^2}{\partial r^2}+\frac{2}{r}\frac{\partial}{\partial r}\right)+\frac{1}{r^2\sin\vartheta}\frac{\partial}{\partial\vartheta}\left(\sin\vartheta\frac{\partial}{\partial\vartheta}\right)+\frac{1}{r^2\sin^2\vartheta}\frac{\partial^2}{\partial\varphi^2}\,. \tag{166}$$

Durch den Separationsansatz

$$p(r,\varphi,\vartheta) = R(r)\Phi(\varphi)\Theta(\vartheta) \tag{167}$$

lässt sich die Helmholtzgleichung in drei gewöhnliche DGLn überführen, vgl. Anhang Q,

$$\frac{\mathrm{d}^2\Phi}{\mathrm{d}\varphi^2} + m^2\Phi = 0 \;, \tag{168}$$

$$\frac{1}{\sin\vartheta}\frac{\mathrm{d}}{\mathrm{d}\vartheta}\left(\sin\vartheta\frac{\mathrm{d}\Theta}{\mathrm{d}\vartheta}\right) + \left[\nu\,(\nu+1) - \frac{m^2}{\sin^2\vartheta}\right]\Theta = 0 \;, \tag{169}$$

$$\frac{1}{r^2}\frac{\mathrm{d}}{\mathrm{d}r}\left(r^2\frac{\mathrm{d}R}{\mathrm{d}r}\right) + k^2R - \frac{n(n+1)}{r^2}R = 0 \;. \tag{170}$$

11.2.3 Lösung der DGL in φ, Glg. (168)

Für die Lösung im Azimutwinkel ergibt sich

$$\Phi(\varphi) = A\sin(m\varphi) + B\cos(m\varphi) \;,\; m \in \mathbb{Z} \;. \tag{171}$$

It corresponds to the harmonics used for 2D Ambisonic panning.

11.2.4 Lösung der DGL in ϑ, Glg. (169)

This differential equation is nearly the same as for the axisymmetric solution obtained for panning in 3D. Written in terms of $\frac{\mathrm{d}}{\mathrm{d}\cos\vartheta} = \frac{\mathrm{d}}{\mathrm{d}\mu}$ it becomes

$$(1-\mu^2)\frac{\mathrm{d}^2P}{\mathrm{d}\mu^2} - 2\mu\,\frac{\mathrm{d}P}{\mathrm{d}\mu} + \left[n(n+1) - \frac{m^2}{(1-\mu^2)}\right]P = 0, \tag{172}$$

and we observe the shift $-\frac{m^2}{(1-\mu^2)}$ in the factor of P is new: it is the one that we had for solving Eq. (53).

Diese DGL wird als *zugeordnete Legendre'sche* DGL bezeichnet und kann in die Hypergeometrische DGL umgeformt werden

$$z(1-z)\frac{\mathrm{d}^2w}{\mathrm{d}z^2} + [c-(a+b+1)z]\,\frac{\mathrm{d}w}{\mathrm{d}z} - abw = 0.$$

Lösungen:

$$\begin{aligned} u^{(1)}(z) &= F(a;b;c;z) \\ u^{(1)}(z) &= \frac{\Gamma(c)\Gamma(c-a-b)}{\Gamma(c-a)\Gamma(c-b)}F\left(a;b;a+b+1-c;1-z\right) \\ &\quad + \frac{\Gamma(c)\Gamma(a+b-c)}{\Gamma(a)\Gamma(b)}(1-z)^{c-a-b}F\left(c-a;c-b;1+c-a-b;1-z\right) \;, \end{aligned}$$

die Gauß'sche hypergeometrische Funktion

$$F(a;b;c;z) = \sum_{s=0}^{\infty}\frac{(a)_s(b)_s}{(c)_s}\frac{z^s}{s!} \quad , \quad |z|<1 \wedge c \notin \mathbb{Z}^- \tag{173}$$

dabei sind $(a)_s$, $(b)_s$ und $(c)_s$ steigende Faktorielle (*Pochhammer-Symbol*), mit der Definition

$$(a)_0 \equiv 1, \quad (a)_s \equiv \frac{\Gamma(a+s)}{\Gamma(a)} = a(a+1)\dots(a+s-1), \quad s \in \mathbb{Z}^+ \quad , \tag{174}$$

wobei die Gamma-Funktion

$$\Gamma(z) \equiv \int_0^\infty t^{z-1} e^{-t} \mathrm{d}t \ , \quad \Re\{z\} > 0. \tag{175}$$

Durch Rücksubstitution erhält man

$$P_\nu^\mu(\cos\vartheta) = \frac{1}{\Gamma(1-\mu)} \left(\frac{1+\cos\vartheta}{1-\cos\vartheta}\right)^{\frac{\mu}{2}} F\left(-\nu, \nu+1; 1-\mu; \frac{1-\cos\vartheta}{2}\right), \tag{176}$$

$$\begin{aligned} Q_\nu^\mu(\cos\vartheta) = {} & \frac{1}{2}\Gamma(\mu)\cos(\mu\pi)\left(\frac{1+\cos\vartheta}{1-\cos\vartheta}\right)^{\frac{\mu}{2}} F\left(-\nu, 1+\nu; 1-\mu; \frac{1-\cos\vartheta}{2}\right) \\ & + \frac{1}{2}\Gamma(-\mu)\frac{\Gamma(1+\nu+\mu)}{\Gamma(1+\nu-\mu)}\left(\frac{1-\cos\vartheta}{1+\cos\vartheta}\right)^{\frac{\mu}{2}} F\left(-\nu, 1+\nu; 1+\mu; \frac{1-\cos\vartheta}{2}\right) \ , \end{aligned} \tag{177}$$

$$\Theta(\vartheta) = C P_\nu^\mu(\cos\vartheta) + D Q_\nu^\mu(\cos\vartheta) \ . \tag{178}$$

Die Lösungen $P_\nu^\mu(\cos\vartheta)$ und $Q_\nu^\mu(\cos\vartheta)$ werden als zugeordnete Legendre-Funktionen der 1. und 2. Art bezeichnet und ergeben sich wie folgt:

Physikalisch sinnvoll sind nur Lösungen bei denen der Schalldruck endliche Werte annimmt, daher $|\Theta(\vartheta)| < \infty$, d.h. $\nu = n \in \mathbb{N}_0$, vgl. Abb. 37. Damit ergibt sich für Lösungen in ϑ

$$\Theta(\vartheta) = C P_n^m(\cos\vartheta) \tag{179}$$

Für $n \in \mathbb{N}_0$ bricht die hypergeometrische Reihe in $P_n^m(\cos\vartheta)$ für Potenzen $s > n$ ab, man bezeichnet diese Funktionen auch als zugeordnete Legendre-Polynome:

$$P_0^0(\cos\vartheta) = 1$$

$$P_1^0(\cos\vartheta) = \cos\vartheta$$

$$P_1^1(\cos\vartheta) = -\sin\vartheta$$

$$P_2^0(\cos\vartheta) = \tfrac{1}{2}(3\cos^2\vartheta - 1)$$

$$P_2^1(\cos\vartheta) = -3\cos\vartheta\sin\vartheta$$

$$P_2^2(\cos\vartheta) = 3\sin^2\vartheta$$

$$P_3^0(\cos\vartheta) = \tfrac{1}{2}(5\cos^3\vartheta - 3\cos\vartheta)$$

$$P_3^1(\cos\vartheta) = -\tfrac{3}{2}(5\cos^2\vartheta - 1)\sin\vartheta$$

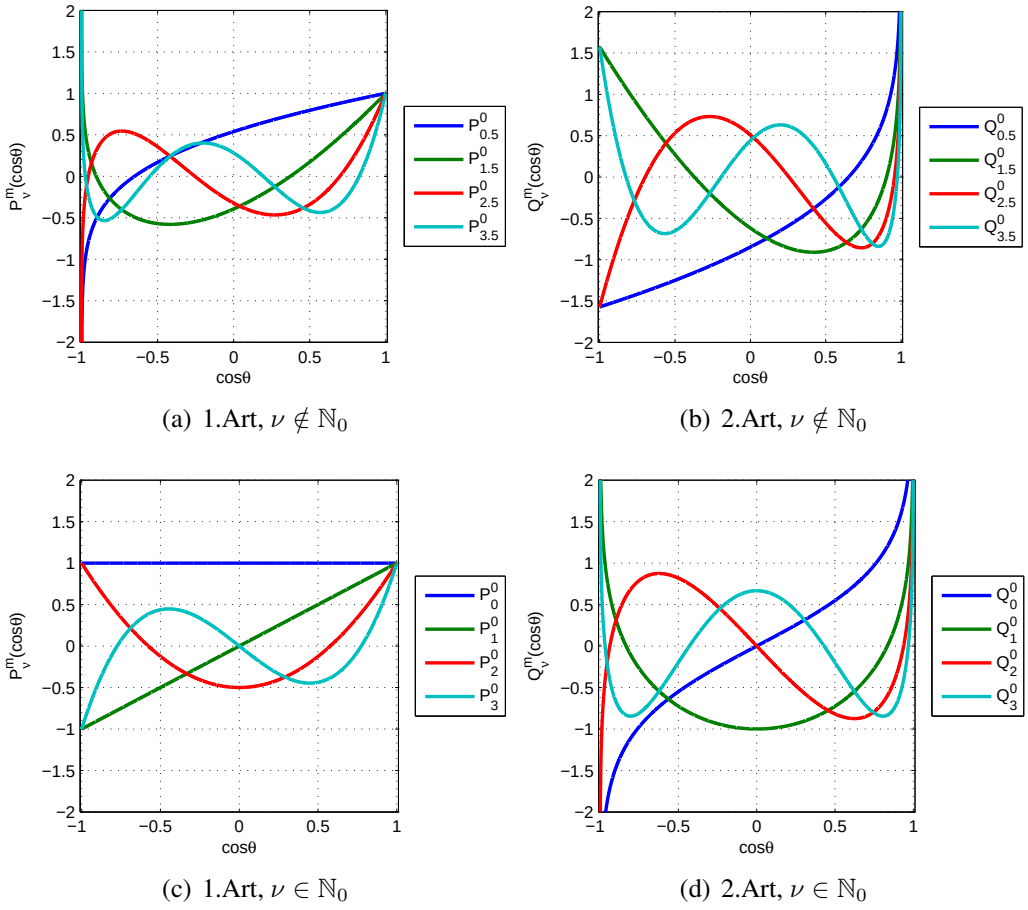

(a) 1.Art, $\nu \notin \mathbb{N}_0$ (b) 2.Art, $\nu \notin \mathbb{N}_0$

(c) 1.Art, $\nu \in \mathbb{N}_0$ (d) 2.Art, $\nu \in \mathbb{N}_0$

Figure 37 – zugeordnete Legendre-Funktionen

$$
\begin{aligned}
P_3^2(\cos\vartheta) &= 15\cos\vartheta\sin^2\vartheta \\
P_3^3(\cos\vartheta) &= -15\sin^3\vartheta \\
P_4^0(\cos\vartheta) &= \tfrac{1}{8}(35\cos^4\vartheta - 30\cos\vartheta^2 + 3) \\
P_4^1(\cos\vartheta) &= -\tfrac{5}{2}(7\cos^3\vartheta - 3\cos\vartheta)\sin\vartheta \\
P_4^2(\cos\vartheta) &= \tfrac{15}{2}(7\cos^2\vartheta - 1)\sin^2\vartheta \\
P_4^3(\cos\vartheta) &= -105\cos\vartheta\sin^3\vartheta \\
P_4^4(\cos\vartheta) &= 105\sin^4\vartheta \\
&\vdots
\end{aligned}
$$

Rekurrenzbeziehungen

$$
\begin{aligned}
P_0^0(\xi) &= 1 \\
P_n^n(\xi) &= -(2n-1)\,P_{n-1}^{n-1}(\xi)\sqrt{1-\xi^2} \qquad \forall n \in \mathbb{Z} : n > 0
\end{aligned}
$$

$$\begin{aligned} P_n^{n-1}(\xi) &= (2n-1)\,\xi P_{n-1}^{n-1}(\xi) \qquad \forall n \in \mathbb{Z} : n > 0 \\ (n-m)\,P_n^m(\xi) &= (2n-1)\,\xi P_{n-1}^m(\xi) - (n+m-1)\,P_{n-2}^m(\xi) \\ &\qquad \forall n, m \in \mathbb{Z} : n \geq 3;\ 0 \leq m \leq n-2 \end{aligned}$$

11.2.5 Lösung der DGL in r, Glg. (170)

Allgemeine Lösung, vgl. Appendix **??**

$$R(r) = E j_n(kr) + F y_n(kr) \tag{180}$$

mit $j_n(kr) = \sqrt{\frac{\pi}{2kr}}\, J_{n+\frac{1}{2}}(kr)$ und $y_n(kr) = \sqrt{\frac{\pi}{2kr}}\, Y_{n+\frac{1}{2}}(kr)$. Die Funktionen $j_n(kr)$, $y_n(kr)$ werden als sphärische Bessel- bzw. Neumann-Funktionen bezeichnet. Die radiale

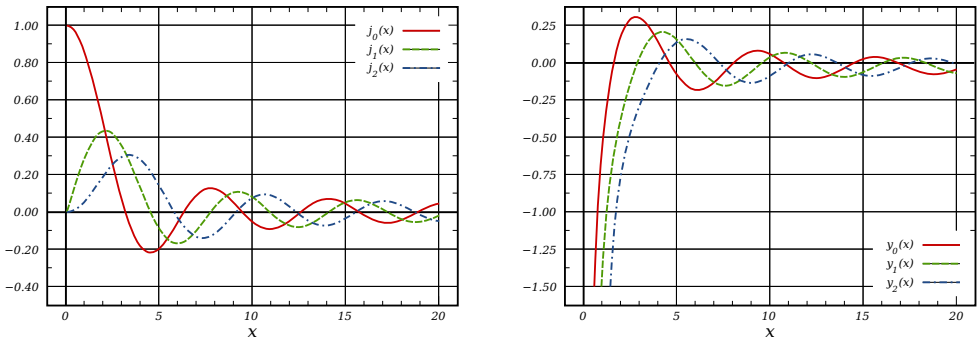

(a) 1.Art (b) 2.Art

Figure 38 – sphärische Bessel-Funktionen

Lösung kann alternativ wieder mit komplexwertigen Funktionen dargestellt werden

$$R(r) = \tilde{E}\, h_n^{(1)}(kr) + \tilde{F}\, h_n^{(2)}(kr)\ ,$$

wobei $h_n^{(1,2)}(kr)$ als sphärische Hankel-Funktionen der 1. bzw. 2. Art bezeichnet werden:

$$\begin{aligned} h_n^{(1)}(kr) &= j_n(kr) + \mathrm{i} y_n(kr) \\ h_n^{(2)}(kr) &= j_n(kr) - \mathrm{i} y_n(kr). \end{aligned}$$

11.3 Lösungen für inneres und äußeres Problem im $\mathbb{R}^3$

Inneres Problem Von $j_n(kr)$ und $y_n(kr)$ bleibt nur $j_n(kr)$ um $kr < a$, $a > 0$ endlich. Daher kommt nur $j_n(kr)$ für innere Probleme infrage:

$$R(r) = E j_n(kr)$$

Eingesetzt in den Produktansatz ist eine physikalische Lösung des inneren Problems:

$$p_{nm}(r, \varphi, \vartheta) = E\, j_n(kr)\; C\, P_n^m(\cos\vartheta)\, (A \sin(m\varphi) + B\cos(m\varphi))\,.$$

Mit der Summe über alle Moden ergibt sich mit normierten Kugelflächenfunktionen

$$p(r, \varphi, \vartheta) = \sum_{n=0}^{\infty} \sum_{m=-n}^{n} b_{nm}\, j_n(kr) \underbrace{\sqrt{\frac{(n-|m|)!(2-\delta_m)}{4\pi(n+|m|)!}}}_{:=N_n^{|m|}} P_n^{|m|}(\cos\vartheta) \begin{cases} \cos(m\varphi) & ,\, m \geq 0 \\ \sin(m\varphi) & ,m < 0 \end{cases},$$

Äußeres Problem Sommerfeld'sche Ausstrahlungsbedingung für den dreidimensionalen Raum:

$$\lim_{r\to\infty} r \left(\frac{\partial}{\partial r} + \mathrm{i}k \right) R(r) = 0\,.$$

Es zeigt sich, dass nur $h_n^{(2)}(kr)$ diese Bedingung erfüllt und die Lösung für den Schalldruck des ausstrahlendenden Feldes ergibt

$$p(r, \varphi, \vartheta) = \sum_{n=0}^{\infty} \sum_{m=-n}^{n} c_{nm}\, h_n^{(2)}(kr)\, N_n^{|m|}\, P_n^{|m|}(\cos\vartheta) \begin{cases} \cos(m\varphi) & ,\, m \geq 0 \\ \sin(m\varphi) & ,m < 0 \end{cases}.$$

11.3.1 Sphärische Basislösungen

Die anwendungsfertigen Lösungen sehen zusammen wie folgt aus

$$p(r, \varphi, \vartheta) = \sum_{n=0}^{\infty} \sum_{m=-n}^{n} \left(b_{nm}\, j_n(kr) + c_{nm}\, h_n^{(2)}(kr) \right) Y_n^m(\varphi, \vartheta).$$

Damit können wieder alle Arten von homogenen Schallfeldern durch bekannte Koeffizienten (*Wellenspektren*) b_{nm}, c_{nm} dargestellt werden. Die winkelabhängigen Lösungen werden als $Y_n^m(\varphi, \vartheta)$ zusammengefasst und als Kugelflächenfunktionen (engl. spherical harmonics) bezeichnet:

$$Y_n^m(\varphi, \vartheta) = N_n^{|m|}\, P_n^{|m|}(\cos\vartheta) \begin{cases} \cos(m\varphi) & ,\, m \geq 0 \\ \sin(m\varphi) & ,m < 0 \end{cases}. \tag{181}$$

Diese Funktionen sind normiert bezgl. ihrer quadratischen Summe auf der Einheitskugel und gehorchen der Orthogonalitätsbeziehung

$$\int_{\vartheta=0}^{\pi}\int_{\varphi=0}^{2\pi} Y_n^m\, Y_{n'}^{m'}\, \sin\vartheta\,\mathrm{d}\vartheta\,\mathrm{d}\varphi = \delta_{nn'}\,\delta_{mm'}. \tag{182}$$

Weiters erlaubt die *Orthogonalitätsbeziehung* die Definition des Transformationsintegrals in Kugelflächenfunktionen

$$f(\varphi,\vartheta) = \sum_{n=0}^{\infty}\sum_{m=-n}^{n} \phi_{nm}\, Y_n^m(\varphi,\vartheta) \qquad \left| \int Y_{n'}^{m'},\ \int Y_{n'}^{m'} Y_n^m = \delta_{n'n}\delta_{m'm} \right.$$

$$\Rightarrow \phi_{nm} = \iint f(\varphi,\vartheta)\, Y_n^m(\varphi,\vartheta)\,\mathrm{d}\varphi\,\sin(\vartheta)\,\mathrm{d}\vartheta. \tag{183}$$

Die unendliche Reihe an Kugelflächenfunktionen ist vollständig, daher gelingt es mit $\phi_{nm} = \iint \delta(\varphi-\varphi_0)\,\delta(\cos\vartheta-\cos\vartheta_0)\,Y_n^m(\varphi,\vartheta)\,\mathrm{d}\varphi\,\sin(\vartheta)\,\mathrm{d}\vartheta = Y_n^m(\varphi_0,\vartheta_0)$ auch, eine sphärische Dirac Deltafunktion an beliebigen Winkeln darzustellen

$$\sum_{n=0}^{\infty}\sum_{m=-n}^{n} Y_n^m(\varphi_0,\vartheta_0)\, Y_n^m(\varphi,\vartheta) = \delta(\varphi-\varphi_0)\,\delta(\cos\vartheta-\cos\vartheta_0). \tag{184}$$

11.3.2 Lösung der kugelförmigen Quellverteilung in Kugelkoordinaten 3D

Wird die Helmholtzgleichung von einer kugelförmigen Quellanordnung am Radius r_0 mit einer richtungsabhängigen Amplitudenverteilung $f(\boldsymbol{\theta})$ angeregt

$$\left(\triangle + k^2\right) p = -\frac{1}{r_0^2}\delta(r-r_0)\, f(\boldsymbol{\theta}), \tag{185}$$

so ist es geschickt, die Amplitundenverteilung in Kugelflächenfunktionen zerlegt anzugeben (hier vereinfacht mit der Abhängigkeit $\boldsymbol{\theta}$ anstelle von φ, ϑ notiert):

$$f(\boldsymbol{\theta}) = \sum_{n=0}^{\infty}\sum_{m=-n}^{n} \phi_{nm}\, Y_n^m(\boldsymbol{\theta}). \tag{186}$$

Weil sich der Richtungsanteil der Helmholtzgleichung vom kr-abhängigen Anteil separiert, muss der Koeffizient ϕ_{nm} im Lösungsansatz vorkommen. Gesucht wird eine Funktion $g_n(kr)$ in kr gesucht

$$G = \sum_{n=0}^{\infty}\sum_{m=-n}^{n} g_n(kr)\ \phi_{nm}\, Y_n^m(\boldsymbol{\theta}). \tag{187}$$

Die Kugelflächenfunktionen sind auch Eigenfunktionen des Laplace-Operators $\triangle = \frac{2}{r}\frac{\partial}{\partial r} + \frac{\partial^2}{\partial r^2} + \frac{1}{r^2\sin\vartheta}\frac{\partial}{\partial\vartheta}\left(\sin\vartheta\frac{\partial}{\partial\vartheta}\right) + \frac{1}{r^2\sin^2\vartheta}\frac{\partial^2}{\partial\varphi^2}$, weswegen seine Anwendung ergibt (Eigenwert entspricht der Separationskonstante winkelabhängiger Terme) $\triangle\, Y_n^m = -n(n+1)/r^2\, Y_n^m$. Eingesetzt und mit der Orthogonalitätsbeziehung Gl. (182) erhalten wir

$$\left(\frac{2}{r}\frac{\partial}{\partial r} + \frac{\partial^2}{\partial r^2} + k^2 - \frac{n(n+1)}{r^2}\right) g_n(kr) = -\frac{\delta(r-r_0)}{r_0^2} \tag{188}$$

Lösung der inhomogenen sphärischen Bessel-Differentialgleichung. Wie in Kreyszig [Kre99] beschrieben, kann diese inhomogene Gleichung mit der *Variation der Konstanten* gelöst werden, bzw. wie in [Ger07], unter der Verwendung der beiden Lösungen $h_n^{(2)}(kr)$ und $j_n(kr)$ für den Radius, und mit $\mathrm{d}kr/\mathrm{d}r = k$:

$$g_n(kr) = h_n^{(2)}(kr) \int_0^r \frac{j_n(kr)}{W} \frac{\delta(r-r_0)}{r_0^2} \frac{\mathrm{d}kr}{k} + j_n(kr) \int_r^\infty \frac{h_n^{(2)}(kr)}{W} \frac{\delta(r-r_0)}{r_0^2} \frac{\mathrm{d}kr}{k}.$$

Darin drückt Wronski-Determinante W, ein Exprodukt, das hier verschieden von 0 ist, die Unabhängigkeit beider Lösungen aus, siehe [AS64]

$$W = \begin{vmatrix} j_n(kr) & j_n'(kr) \\ h_n^{(2)}(kr) & h_n'^{(2)}(kr) \end{vmatrix} = j_n(kr) h_n'^{(2)}(kr) - j_n'(kr) h_n^{(2)}(kr) = -\frac{\mathrm{i}}{(kr)^2}. \tag{189}$$

Folgende Lösung erhalten wir:

$$g_n(kr) = -\mathrm{i}\,k \begin{cases} j_n(kr_0)\, h_n^{(2)}(kr), & \text{für } r \geq r_0, \\ h_n^{(2)}(kr_0)\, j_n(kr) & \text{für } r \leq r_0. \end{cases} \tag{190}$$

Die Quellenverteilung auf der Kugel ergibt daher das Feld

$$G = -\mathrm{i}\,k \sum_{n=0}^{\infty} \sum_{m=-n}^{n} \phi_{nm}\, Y_n^m(\boldsymbol{\theta}) \begin{cases} j_n(kr_0)\, h_n^{(2)}(kr), & \text{für } r \geq r_0, \\ h_n^{(2)}(kr_0)\, j_n(kr) & \text{für } r \leq r_0. \end{cases} \tag{191}$$

mit den normierten Kugelflächenfunktionen $Y_n^m(\boldsymbol{\theta})$ aus Gl. (181).

11.3.3 Punktquelle in 3D

Für eine Punktquelle an der Richtung $\boldsymbol{\theta}_0$ ist der richtungsabhängige Anteil $\phi_{nm} = Y_n^m(\boldsymbol{\theta}_0)$

$$G = -\mathrm{i}\,k \sum_{n=0}^{\infty} \sum_{m=-n}^{n} Y_n^m(\boldsymbol{\theta}_0)\, Y_n^m(\boldsymbol{\theta}) \begin{cases} j_n(kr_0)\, h_n^{(2)}(kr), & \text{für } r \geq r_0, \\ h_n^{(2)}(kr_0)\, j_n(kr) & \text{für } r \leq r_0. \end{cases} \tag{192}$$

Punktquelle 3D im Ursprung. Für den Radius $r_0 = 0$ und mit $j_{|n|}(0) = \delta_n$ erhalten wir mit $Y_0^0\, \phi_{00} = \frac{1}{4\pi}$ und $h_0(kr) = \frac{e^{-\mathrm{i}\,k\,r}}{-\mathrm{i}\,k\,r}$ die bekannte Formel der Green'schen Funktion

$$G = -\mathrm{i}\,k\, \frac{1}{4\pi}\, h_0(kr) = -\mathrm{i}\,k\, \frac{1}{4\pi}\, \frac{e^{-\mathrm{i}\,k\,r}}{-\mathrm{i}\,k\,r} = \frac{e^{-\mathrm{i}\,k\,r}}{4\pi\, r}. \tag{193}$$

11.4 Kugelförmige Mikrofon / Lautsprecherarrays

Kugelförmige Lautsprecherarrays sind den StudentInnen des Instituts für Elektronische Musik und Akustik bereits in Form des IEM-CUBE bekannt [Son00, MN02, Dan00].

Damit werden einfallende Wellenfelder - so gut es mit der begrenzten Anzahl von Lautsprechern geht - synthetisiert.

Es gibt aber auch eine Fülle ganz neuer, spannender Arbeiten zu kugelförmigen Mikrofonarrays für einfallende Schallfelder [ME02, Li05, Raf05], und abstrahlende Schallfelder [WA80, ZH07, Hoh09, Deb10]. Zusätzlich bedient sich auch das aktuellere Feld der kompakten Kugellautsprecheranordnungen der selben theoretischen Grundlage [WDC97, KW04, Beh06, AFKW06, ZH07, ZN07, ZPS08, Pom08, Pol07, Ple09, Zot09a, Ker10, Pas10].

Der wesentliche Vorteil von kugelförmigen Arrays ist, dass eine umfassende Analyse/Synthese für alle Raumrichtungen des Kugelkoordinatensystems möglich ist. Damit gibt es auch keine Vorne/Hinten Ambiguität für Arrays dieser Art.

Verwendete Lösungen. Wie oben gezeigt, wird die Wellengleichung in Kugelkoordinaten mit einem Produktansatz $p_h = R(r)\,\Phi(\varphi)\,\Theta(\vartheta)$ und Separation der Variablen gelöst. Die Separationskonstanten beinhalten die Indizes n, m, die - wie oben gezeigt - ganzzahlig sein müssen. Letztendlich ergeben sich mit allen vorausgesetzten Bedingungen (Quellenfreiheit des einstrahlenden Feldes, Sommerfeld'sche Ausstrahlungsbedingung für ausstrahlende Wellen, Kausalität, Periodizität um φ) die Lösungen

$$p_h = \sum_{n=0}^{\infty} \sum_{m=-n}^{n} \left(b_{nm} j_n(kr) + c_{nm} h_n(kr)\right) Y_n^m(\varphi,\vartheta)\,, \tag{194}$$

$$\text{bzw. } v_h = \frac{\mathrm{i}}{\rho_0 c} \sum_{n=0}^{\infty} \sum_{m=-n}^{n} \left(b_{nm} j_n'(kr) + c_{nm} h_n'(kr)\right) Y_n^m(\varphi,\vartheta)\,, \tag{195}$$

wobei der Index n oft Ordnung genannt wird, m Grad, $Y_n^m(\varphi,\vartheta)$ die Kugelflächenfunktionen (*spherical Harmonics*), $j_n(kr)$ die sphärischen Besselfunktionen und $h_n(kr)$ die sphärischen Hankelfunktionen, sowie $j_n'(kr)$, $h_n'(kr)$ deren Ableitungen sind.

Wellenspektrum. b_{nm}, c_{nm} sind Koeffizienten der einfallenden, bzw. auslaufenden Wellen und werden Wellenspektren genannt. b_{nm} beschreibt Wellen, die am Koordinatenursprung quellenfrei sind und dort keine Unendlichkeitsstellen besitzen dürfen. c_{nm} beschreibt Wellen, die vom Koordinatenursprung auslaufen, und dort $n+1$ Unendlichkeitsstellen besitzen.

Diese *sphärischen Basislösungen* behalten ihre Form im Winkel stets bei und bleiben bei Einstrahlung/Abstrahlung unabhängig voneinander. Sie werden nur durch die jeweilige radiale Funktion $j_n(kr)$ oder $h_n(kr)$ in Amplitude und Phase verändert. Der Lösungsraum besitzt keine so einfache Interpretation wie jener des ebenen Koordinatensystems. Ein wesentlicher Vorteil dieser Beschreibung liegt aber in der gleichmäßigen Auflösung im gesamten Raum, die aufgrund seiner Form vorne und hinten nicht verwechselt (ggf. Inneres mit Äußerem).

Kugelflächenfunktionen. Kugelflächenfunktionen sind der *anguläre* Anteil, der in beiden Arten von Basislösungen gleichermaßen auftritt. Am leichtesten lassen sie sich als

Schallschnelle vorstellen, d.h. als Schwingungen einer Kugeloberfläche für eine gedachte Kugel mit bestimmten Radius vorstellen. Diese Kugelmoden bekommen mit zunehmender Ordnungszahl n mehrere *Knotenkreise*, wobei die Gradzahl m dem Betrage nach die Knotenkreise durch Nord- und Südpol der Kugel zählt. Als Kugelflächenfunktionen beschreiben sie die Fourier-Zerlegung der Kugeloberfläche.

Sphärische Bessel / Neumannfunktionen. Die sphärischen Bessel- und Neumannfunktionen beschreiben die radiale Ausbreitung von Schallfeldern in Kugelflächenfunktionen, siehe Abb. 39. Die sphärische Hankelfunktion setzt sich zusammen aus

$$h_n\left(kr\right) = j_n\left(kr\right) - iy_n\left(kr\right). \tag{196}$$

und besitzt daher mit den Neumannfunktionen eine Unendlichkeitsstelle bei $r = 0$. Die Besselfunktionen beschreiben einfallende Wellenfelder, die in den sphärischen Basislösungen betrachtet stehende Wellenfelder sind.[5] (Die abgeleiteten Funktionen werden zur

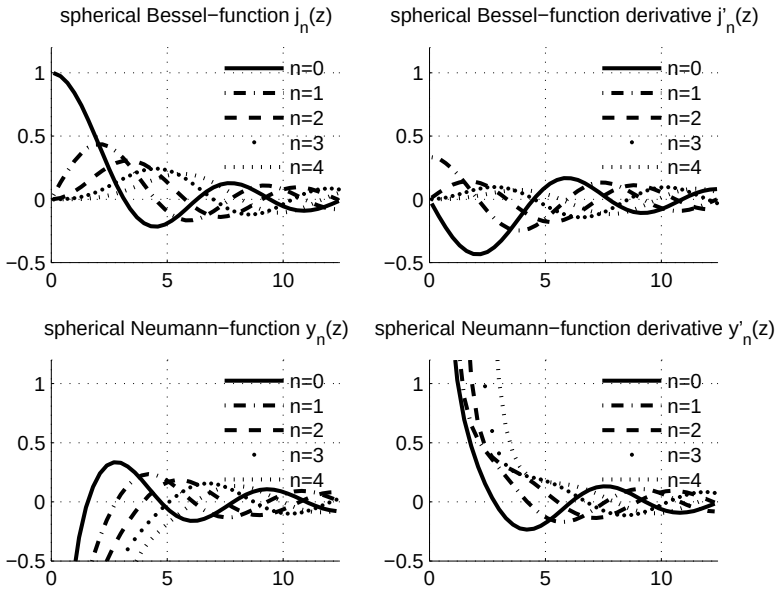

Figure 39 – Sphärische Bessel und Neumannfunktionen

Beschreibung der Schallschnelle verwendet.)

11.5 Matrixnotation von kugelförmigen Aufgaben

Mit einer geeigneten Reihenfolge, in welcher die Kugelflächenfunktionen der Indizes n und m in einen Vektor geschrieben werden, lässt sich die Doppelsumme in Gl. (194) als

5. Ebene Wellen sind einstrahlende Felder, aber an sich keine Stehwellen. Sie lassen sich aber aus entsprechender komplexwertiger Linearkombination der Stehwellenlösungen darstellen.

Skalarprodukt anschreiben. Typischerweise wird n ab dem Index N abgebrochen, um endliche Vektorlängen zu erhalten. Damit, und mit dem komponentenweisen Hadamardprodukt für Vektoren $\boldsymbol{a}\cdot\boldsymbol{b} = \mathrm{diag}\{\boldsymbol{a}\}\,\boldsymbol{b}$, wird $p = \sum\sum Y_n^m(\varphi,\vartheta)\,(b_{nm} j_n(kr) + c_{nm} h_n(kr))$ zu

$$\begin{aligned} p(kr,\varphi,\vartheta) &= \boldsymbol{y}_{\mathrm{N}}^{\mathrm{T}}(\varphi,\vartheta)\big(\mathrm{diag}\{\boldsymbol{j}_{\mathrm{N}}(kr)\}\,\boldsymbol{b}_{\mathrm{N}} + \mathrm{diag}\{\boldsymbol{h}_{\mathrm{N}}(kr)\}\,\boldsymbol{c}_{\mathrm{N}}\big), \\ v(kr,\varphi,\vartheta) &= \frac{\mathrm{i}}{\rho_0 c}\boldsymbol{y}_{\mathrm{N}}^{\mathrm{T}}(\varphi,\vartheta)\big(\mathrm{diag}\{\boldsymbol{j}'_{\mathrm{N}}(kr)\}\,\boldsymbol{b}_{\mathrm{N}} + \mathrm{diag}\{\boldsymbol{h}'_{\mathrm{N}}(kr)\}\,\boldsymbol{c}_{\mathrm{N}}\big). \end{aligned} \tag{197}$$

Mit der Definition der Vektorisierung von n und m zu $q = n^2 + n + m + 1$ werden die Einzelausdrücke zu

$$\boldsymbol{b}_{\mathrm{N}} := \begin{pmatrix} b_{0,0} \\ b_{1,-1} \\ b_{1,0} \\ b_{1,1} \\ b_{2,-2} \\ \vdots \\ b_{\mathrm{N},\mathrm{N}} \end{pmatrix}, \quad \boldsymbol{j}_{\mathrm{N}}(kr) := \begin{pmatrix} j_0(kr) \\ j_1(kr) \\ j_1(kr) \\ j_1(kr) \\ j_2(kr) \\ \vdots \\ j_{\mathrm{N}}(kr) \end{pmatrix}, \quad \boldsymbol{y}_{\mathrm{N}}(\varphi,\vartheta) := \begin{pmatrix} Y_0^0(\varphi,\vartheta) \\ Y_1^{-1}(\varphi,\vartheta) \\ Y_1^0(\varphi,\vartheta) \\ Y_1^1(\varphi,\vartheta) \\ Y_2^{-2}(\varphi,\vartheta) \\ \vdots \\ Y_{\mathrm{N}}^{\mathrm{N}}(\varphi,\vartheta) \end{pmatrix}. \tag{198}$$

Wellenspektrum. Das Wellenspektrum $\boldsymbol{b}_{\mathrm{N}}$ reicht aus, um einfallende Schallfelder zu beschreiben, eine vollständige Beschreibung erhalten wir im Falle $\mathrm{N} \to \infty$. Umgekehrt beschreibt das Wellenspektrum $\boldsymbol{c}_{\mathrm{N}}$ ausstrahlende Felder, auch vollständig für $\mathrm{N} \to \infty$.

Sphärisches Wellenspektrum. Wird auf die Rücktransformation in den Winkelbereich verzichtet, so ergibt sich das *sphärisches Wellenspektrum*[6]. Die sphärischen Wellenspektren für Schalldruck und radiale Schallschnelle lauten:

$$\begin{aligned} \boldsymbol{\psi}_{\mathrm{N}}(kr) &= \mathrm{diag}\{\boldsymbol{j}_{\mathrm{N}}(kr)\}\,\boldsymbol{b}_{\mathrm{N}} + \mathrm{diag}\{\boldsymbol{h}_{\mathrm{N}}(kr)\}\,\boldsymbol{c}_{\mathrm{N}}, \\ \boldsymbol{\nu}_{\mathrm{N}}(kr) &= \frac{\mathrm{i}}{\rho_0 c}\big(\mathrm{diag}\{\boldsymbol{j}'_{\mathrm{N}}(kr)\}\,\boldsymbol{b}_{\mathrm{N}} + \mathrm{diag}\{\boldsymbol{h}'_{\mathrm{N}}(kr)\}\,\boldsymbol{c}_{\mathrm{N}}\big). \end{aligned} \tag{199}$$

Zur Vollständigkeit: in den Ortsbereich gelangt man durch Rücktransformation, vgl. Gl. (197)

$$\begin{aligned} p(kr,\varphi,\vartheta) &= \boldsymbol{y}_{\mathrm{N}}^{\mathrm{T}}(\varphi,\vartheta)\;\boldsymbol{\psi}_{\mathrm{N}}(kr), \\ v(kr,\varphi,\vartheta) &= \boldsymbol{y}_{\mathrm{N}}^{\mathrm{T}}(\varphi,\vartheta)\;\boldsymbol{\nu}_{\mathrm{N}}(kr). \end{aligned} \tag{200}$$

11.6 Theorie zur Messung der Schallabstrahlung

Zur holografischen Bestimmung der Schallabstrahlung müssen die Koeffizienten $\boldsymbol{c}_{\mathrm{N}}$ ermittelt werden. Dazu wird im Winkel eine streng begrenzte Auflösung angenommen. Zudem wird angenommen, dass es keine Schalleinstrahlung gibt, also $c_{nm} = 0 : n > \mathrm{N}$, $b_{nm} = 0$. Vorerst können wir das sphärische Wellenspektrum $\boldsymbol{\psi}_{\mathrm{N}}(kR)$ aus dem Verlauf

6. Im Gegensatz zu den *Wellenspektren* für ein/auslaufende Wellen $\boldsymbol{b}_{\mathrm{N}}$, $\boldsymbol{c}_{\mathrm{N}}$, beziehen sich sph. Wellenspektren für Schalldrücke/Schallschnellen auf einen bestimmten Radius r, vgl. [Wil99].

Figure 40 – Kugelförmige Mikrofonanordnung zur Messung der Schallabstrahlung.

des Schalldruckes an einer Kugeloberfläche mit dem Radius R berechnen, wovon diskrete Messwerte an den Winkelpaaren $\{\varphi_l, \vartheta_l\}$ mit $l = 1 \dots \mathrm{L}$ vorliegen. Schreibt man die Zusammensetzung aller L Schalldrücke aus dem sphärischen Wellenspektrum $\boldsymbol{\psi}_\mathrm{N}(kR)$ untereinander an, ergeben sich L gleichzeitige Forderungen aus Gl. (200)

$$\begin{pmatrix} p(\varphi_1, \vartheta_1) \\ p(\varphi_2, \vartheta_2) \\ \vdots \\ p(\varphi_\mathrm{L}, \vartheta_\mathrm{L}) \end{pmatrix} = \begin{pmatrix} \boldsymbol{y}_\mathrm{N}^\mathrm{T}(\varphi_1, \vartheta_1) \\ \boldsymbol{y}_\mathrm{N}^\mathrm{T}(\varphi_2, \vartheta_2) \\ \vdots \\ \boldsymbol{y}_\mathrm{N}^\mathrm{T}(\varphi_\mathrm{L}, \vartheta_\mathrm{L}) \end{pmatrix} \boldsymbol{\psi}_\mathrm{N}(kR), \tag{201}$$

Kompakt angeschrieben

$$\boldsymbol{p} = \boldsymbol{Y}_\mathrm{N}\, \boldsymbol{\psi}_\mathrm{N}(kR). \tag{202}$$

(Hyper-)Interpolation. Gilt oben genannte Annahme der begrenzten Winkelauflösung (anguläre Bandbegrenzung), und lässt sich $\boldsymbol{Y}_\mathrm{N}^{-1}$ bilden, siehe Abschn. 11.9, so lässt sich ein diskret gemessenes Schalldruckmuster $\boldsymbol{p}$ durch Inversion von Gl. (202) in ein sphärisches Wellenspektrum umrechnen, und mit Gl. (200) beliebig fein interpolieren

$$\begin{aligned} \boldsymbol{\psi}_\mathrm{N}(kR) &= \boldsymbol{Y}_\mathrm{N}^{-1}\, \boldsymbol{p}, \\ \Rightarrow p(kR, \varphi, \vartheta) &= \boldsymbol{y}_\mathrm{N}^\mathrm{T}(\varphi, \vartheta)\, \boldsymbol{\psi}_\mathrm{N}(kR). \end{aligned} \tag{203}$$

Holografische Extrapolation. Zum Wellenspektrum $\boldsymbol{c}_\mathrm{N}$ gelangt man, indem der Ausbreitungsterm $h_n(kR)$ aus dem sphärischen Wellenspektrum $\boldsymbol{\psi}_\mathrm{N}(kR)$ heraus dividiert wird. Die reziproken Vektoreinträge werden einfach als invertierte Diagonalmatrix angeschrieben

$$\boldsymbol{c}_\mathrm{N} = \mathrm{diag}\left\{\boldsymbol{h}_\mathrm{N}(kR)\right\}^{-1}\, \boldsymbol{\psi}_\mathrm{N}(kR). \tag{204}$$

Von $\boldsymbol{c}_\mathrm{N}$ ausgehend ist es mit $b_{nm} = 0$ und Gl. (199) möglich, einen beliebigen Radius r einzusetzen, der alle im Schallfeld enthaltenen Quellen (inkl. Spiegelquellen) einschließen muss, um den Schalldruck zu bestimmen

$$\boldsymbol{\psi}_\mathrm{N}(kr) = \mathrm{diag}\left\{\boldsymbol{h}_\mathrm{N}(kr)\right\}\ \boldsymbol{c}_\mathrm{N}.$$

Die Formel gilt im Frequenzbereich, da $k = \omega/c$. In Vektornotation voll ausgeschrieben, ergibt sich für den diskreten Schalldruck die Interpolation im Winkel und Extrapolation im Radius

$$p(kr, \varphi, \vartheta) = \boldsymbol{y}_\mathrm{N}^\mathrm{T}(\varphi, \vartheta)\, \mathrm{diag}\left\{\boldsymbol{h}_\mathrm{N}(kr)\right\} \mathrm{diag}\left\{\boldsymbol{h}_\mathrm{N}(kR)\right\}^{-1}\ \boldsymbol{Y}_\mathrm{N}^{-1}\, \boldsymbol{p}. \tag{205}$$

Für Interessierte: Fabian Hohl hat die Messkugel am Institut gebaut und einige Instrumente auf Ähnlichkeiten ihrer Teiltonabstrahlungen untersucht [Hoh09]. Daniel Deboy hat in seiner Diplomarbeit untersucht, inwieweit Schallquellen in der Messkugel lokalisiert werden können, und ihre Orientierung verfolgt werden kann [Deb10]. Wie die Abtastung der Kugel funktioniert ist in [Zot09b] zu finden.

11.7 Theorie zur Erzeugung von Schallabstrahlung

Zur holofonen Synthese von Schallabstrahlung wird angenommen, dass eine kompakte kugelförmige Anordnung von Lautsprechern, vgl. Abb. 41, im geschlossenen Kugelgehäuse eine Randbedingung der Schallschnelle für das äußere Schallfeld darstellt. Dazu werden einzelne Lautsprechermembranen als Kugelkappe einer festen Kugel betrachtet, die im Unterschied zu unbewegten festen Kugelteilen ($v(\varphi,\vartheta) = 0$), jeweils eine konstante Amplitude und Phase an der Position l der Membranen als Oberflächenschnelle einprägt $v(\varphi,\vartheta) = v^{(l)}$.

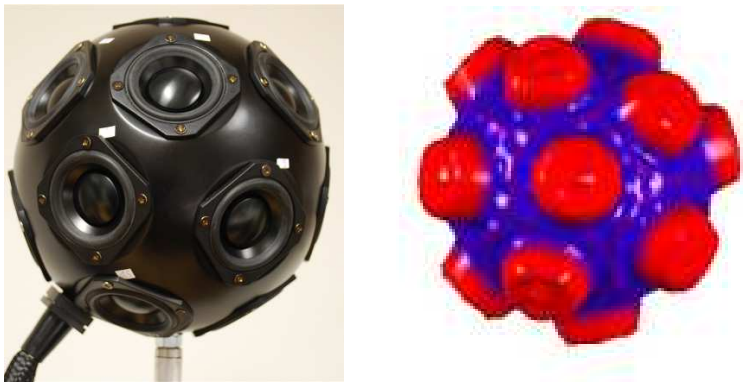

Figure 41 – Links: kompakte kugelförmige Lautsprecheranordnung zur Synthese variabler Schallabstrahlung (akustische Holofonie), rechts: Kappenmodell mit allen Membranschnellen auf 1 gesetzt. Abbildungen aus [Ker10].

11.7.1 Kugelkappenmodell durch Faltung auf der Kugel

Zur Darstellung aller kugelkappenförmig verteilten Schallschnellen in Kugelflächenfunktionen muss eine große Winkelauflösung $\mathrm{Q} \to \infty$ verwendet werden, um scharfen Grenzen der Membranen abzubilden. Zur Berechnung wird die Geometrie der Membranen von ihrer steuerbaren Schnelle getrennt formuliert. Die Oberflächenschnelle des Gesamtsystems wird zur Summe L gewichteter *Aperturfunktionen* $a^{(l)}$ mit den Membranschnellen $v^{(l)}$

$$v(\varphi,\vartheta) = \sum_{l=1}^{\mathrm{L}} a^{(l)}(\varphi,\vartheta)\, v^{(l)}.$$

Diese Aperturfunktionen werden mit dem Faltungssatz auf der Kugel [DH94] und aus der Transformierten einer Dirac-Deltaverteilung in die Kugelflächenfunktionen gebildet. Dabei wird eine Nordpolkappe des entsprechenden Öffnungswinkels α

$$a^{(nordp.)}(\vartheta) = 1 - u(\vartheta - \alpha/2)$$

durch Faltung mit der Deltadistributionen eines Lautsprechermittelpunktes an die richtige Stelle auf der Kugel gefaltet. Für den l-ten Lautsprecher ist das symbolisch:

$$a^{(l)}(\varphi,\vartheta) = a^{(\mathrm{nordp.})}(\vartheta) \star \delta(\varphi - \varphi_l)\delta(\vartheta - \vartheta_l).$$

Die sphärischen Spektren

$$a_n^{(\mathrm{nordp.})} = \sqrt{\frac{2n+1}{2}}\pi\,\delta_m \begin{cases} \cos(\alpha/2)\,P_n(\cos(\alpha/2)) - P_{n-1}(\cos(\alpha/2)), & n>0 \\ 1-\cos(\alpha/2), & n=0 \end{cases}$$

und $Y_n^m(\varphi_l,\vartheta_l)$, Gl.(**??**), ergeben das Spektrum der Apertur (Faltungssatz auf der Kugel)

$$a_{nm}^{(l)} = a_n^{(\mathrm{nordp.})}\,Y_n^m(\varphi_l,\vartheta_l).$$

Das gesamte Oberflächenschnellemuster transformiert in Kugelflächenfunktionen kann folglich als Matrix-Vektorprodukt angeschrieben werden, mit $\boldsymbol{A}_\mathrm{Q} = \mathrm{diag}_\mathrm{Q}\{\boldsymbol{a}_\mathrm{Q}^{(nordp.)}\}\boldsymbol{Y}_\mathrm{Q}^\mathrm{T}$ und den Schnellen $\boldsymbol{v} = [v^{(1)}\ldots v^{(\mathrm{L})}]^\mathrm{T}$

$$\boldsymbol{\nu}_\mathrm{Q} = \mathcal{SHT}\{v(\varphi,\vartheta)\} = \boldsymbol{A}_\mathrm{Q}\,\boldsymbol{v}. \tag{206}$$

11.7.2 Randwertproblem: Wellenspektrum des Kugelkappenmodells

Über das Wellenspektrum $\boldsymbol{c}_\mathrm{N}$ in Bezug auf Schallschnelle und Schalldruck, Gl. (199), berechnet sich das sphärische Wellenspektrum des Schalldruckes zu

$$\boldsymbol{\psi}_\mathrm{Q}(r) = \frac{\rho_0 c}{\mathrm{i}}\,\mathrm{diag}\,\{\boldsymbol{h}_\mathrm{Q}(kr)\}\,\mathrm{diag}\,\{\boldsymbol{h}'_\mathrm{Q}(kR)\}^{-1}\,\boldsymbol{A}_\mathrm{Q}\,\boldsymbol{v}. \tag{207}$$

Zur Steuerung wird in vorhandenen Literaturquellen der Vektor $\boldsymbol{v}$ mit den Eingangsspannungen der Lautsprecher elektroakustisch ins Verhältnis gesetzt. Ziel dabei ist, jede einzelne Komponente in $\boldsymbol{\psi}_\mathrm{N}$ zu steuern, wobei zur Steuerbarkeit in jedem Fall $\mathrm{N} \le \sqrt{L}-1$ gelten muss. Ordnungen größer als N werden nicht gesteuert, können deshalb bei hohen Frequenzen räumliches Aliasing beinhalten.

Wird - zur groben Vereinfachung - der Vektor mit den Membranschnellen als Eingangsgröße betrachtet, so ergibt sich die Ansteuerung mit $\boldsymbol{v}$ für ein gewünschtes sphärisches Wellenspektrum $\boldsymbol{\psi}_\mathrm{N}|_{r_p}$ aus der Inversion der oberen Gleichung zu

$$\boldsymbol{v} = \frac{\mathrm{i}}{\rho_0 c}\boldsymbol{A}_\mathrm{N}^{-1}\,\mathrm{diag}\,\{\boldsymbol{h}'_\mathrm{N}(kR)\}\,\mathrm{diag}\,\{\boldsymbol{h}_\mathrm{N}(kr_p)\}^{-1}\,\boldsymbol{\psi}_\mathrm{N}|_{r_p}. \tag{208}$$

Der daraus berechnete Schalldruck mit Gl. (207) beinhaltet dann auch räumliche Aliase.

Für Interessierte: Die radiale Scharfstellung mit dem Term $\frac{h'_n(kR)}{h_n(kr_p)}$ erfolgt über IIR Filter aus der Diplomarbeit von Hannes Pomberger [ZN07, Pom08], die genaue Form von $\boldsymbol{A}_\mathrm{Q}$ ist in [ZH07, Pol07, Zot09a, Ker10, Pas10] ersichtlich. Elektroakustische Modelle finden sich in [ZPS08, Zot09a, Pas10].

11.8 Theorie zur Erzeugung von Schalleinstrahlung

Zur holofonen Erzeugung von Schalleinstrahlung ($c_{nm} = 0 : \forall n$ und $b_{nm} = 0 : \ n > \mathrm{N}$) wäre es ungünstig, wie zuvor feste unbewegliche kugelförmige Wände zu bauen und darin nach innen weisende Lautsprecher zu montieren. Abgesehen vom konstruktiven Nachteil ergibt sich ein handfester Nachteil: So ein Raum hätte stark ausgeprägte Resonanzen. Mathematisch betrachtet müsste folglich die Erzeugung einfallender Moden an bestimmten Frequenzen daran scheitern, dass die Einstrahlungsfunktion für bestimmte Frequenzen an der Raumoberfläche $j_n'(kR) = 0$ bleiben muss. Die betroffene Ordnung n, kann als ganzes nicht reproduziert werden.

Holofone Erzeugung von Schalleinstrahlung verwendet einen anderen Ansatz: Am Radius R befindet sich eine kugelförmige Anordnung von Quellen, die im Gegensatz zu einer Randbedingung kein Hindernis für die Schallausbreitung sind. Die mathematische Formulierung geschieht über eine Verteilung mit dem Quellsignal $f(\varphi, \vartheta)$ an der Stelle R, welche die Helmholtzgleichung anregt [ZPF09]

$$(\Delta + k^2)\, p = -f(\varphi, \vartheta)\, \frac{\delta(r - R)}{r^2}. \tag{209}$$

Das entspricht einer kontinuierlichen kugelförmigen Fläche aus Punktquellen mit individuellen Signalen (Quellstärkeverteilung, *source-strength distribution*); man könnte dabei an eine verteilte Vielzahl an Lautsprecher denken.

Die Lösung dieser inhomogenen Helmholtzgleichung in Kugelkoordinaten verwendet die Quellstärkeverteilung im Bereich der Kugelflächenfunktionen transformiert

$$\boldsymbol{\phi}_\mathrm{Q} = \iint f(\varphi, \vartheta)\, \boldsymbol{y}_\mathrm{Q}(\varphi, \vartheta)\, \mathrm{d}\varphi\, \sin(\vartheta)\, \mathrm{d}\vartheta \tag{210}$$

und ergibt das Wellenspektrum

$$\boldsymbol{b}_\mathrm{Q} = -\mathrm{i}k\, \mathrm{diag}\left\{\boldsymbol{h}_\mathrm{Q}(kR)\right\} \boldsymbol{\phi}_\mathrm{Q}. \tag{211}$$

Durch das Wellenspektrum $\boldsymbol{b}_\mathrm{Q}$ ist der Schalldruck an jedem Punkt innerhalb $r < R$ beschrieben

$$p(kr, \varphi, \vartheta) = \boldsymbol{y}_\mathrm{Q}^\mathrm{T}(\varphi, \vartheta)\, \mathrm{diag}\{\boldsymbol{j}_\mathrm{Q}(kr)\}\, \boldsymbol{b}_\mathrm{Q}. \tag{212}$$

Quellstärkeverteilung Punktquelle. Wird eine Punktquelle mit Einheitsamplitude an den Koordinaten $r_0, \varphi_0, \vartheta_0$ angenommen, so berechnet sich ihre Quellstärkeverteilung in Kugelflächenfunktionen aus Gl.(**??**) zu

$$f(\varphi, \vartheta) = \delta(\varphi - \varphi_0)\delta(\vartheta - \vartheta_0), \tag{213}$$

$$\boldsymbol{\phi}_\mathrm{Q} = \iint \boldsymbol{y}_\mathrm{Q}(\varphi, \vartheta)\, \delta(\varphi - \varphi_0)\delta(\vartheta - \vartheta_0)\, \mathrm{d}\varphi\, \sin(\vartheta)\, \mathrm{d}\vartheta = \boldsymbol{y}_\mathrm{Q}(\varphi_0, \vartheta_0). \tag{214}$$

Diese Transformation ist auch brauchbar, um später virtuelle Punktquellen formulieren zu können, bzw. um Lautsprecher als Punktquellen zu modellieren. Die Punktquelle hat also ein Wellenspektrum

$$\boldsymbol{b}_\mathrm{Q} = -\mathrm{i}k\, \mathrm{diag}\left\{\boldsymbol{h}_\mathrm{Q}(kr_0)\right\} \boldsymbol{y}_\mathrm{Q}(\varphi_0, \vartheta_0). \tag{215}$$

Diskrete Lautsprecherverteilung im Winkel. Liegt eine diskrete Quellverteilung in Form einer umgebenden kugelförmigen Lautsprecheranordnung an den Winkelpaaren $\{\varphi_l, \vartheta_l\}_{l=1\ldots \mathrm{L}}$ und dem Radius R vor, und es gibt einen Ansteuerungsvektor $\boldsymbol{g}$, so lässt sich f angeben als

$$\hat{f}(\varphi,\vartheta) = \begin{pmatrix} \delta(\varphi-\varphi_1)\delta(\vartheta-\vartheta_1) \\ \delta(\varphi-\varphi_2)\delta(\vartheta-\vartheta_2) \\ \vdots \\ \delta(\varphi-\varphi_\mathrm{L})\delta(\vartheta-\vartheta_\mathrm{L}) \end{pmatrix}^\mathrm{T} \boldsymbol{g}, \tag{216}$$

$$\hat{\boldsymbol{\phi}}_\mathrm{Q} = \iint \boldsymbol{y}_\mathrm{Q}(\varphi,\vartheta)\, \hat{f}(\varphi,\vartheta)\, d\varphi\, \sin(\vartheta)\, d\vartheta = \boldsymbol{Y}_\mathrm{Q}^\mathrm{T}\, \boldsymbol{g}. \tag{217}$$

Damit ergibt sich das Wellenspektrum der diskreten Quellverteilung zu

$$\hat{\boldsymbol{b}}_\mathrm{Q} = -\mathrm{i}k\, \mathrm{diag}\,\{\boldsymbol{h}_\mathrm{Q}(kR)\}\, \boldsymbol{Y}_\mathrm{Q}^\mathrm{T}\, \boldsymbol{g}. \tag{218}$$

Ambisonics und Anpassung der Wellenspektren. Der Ambisonics-Ansatz versucht nun, die Wellenspektren $\hat{\boldsymbol{b}}_\mathrm{Q}$ mit einer gewünschten, beliebigen Quellstärkeverteilung, z.B. jener einer Punktquelle $\boldsymbol{b}_\mathrm{Q}$, in Übereinstimmung zu bringen.

Ambisonics nimmt dazu an, dass es günstig ist, die Steuerung von $\hat{\boldsymbol{\phi}}_\mathrm{Q}$ aus Gl. (217) zu berechnen, indem nur eine geglättete Winkelauflösung betrachtet wird, also eine begrenzte Ordnung N. Damit wird verhindert, dass Richtungsinformation in der diskreten Darstellung verloren geht.

Somit ergibt sich die Steuerung von $\boldsymbol{g}$ aus Gln. (215)(218) zu

$$\boldsymbol{g} = \left(\boldsymbol{Y}_\mathrm{N}^\mathrm{T}\right)^{-1} \mathrm{diag}\,\{\boldsymbol{h}_\mathrm{N}(kr_0)\}\, \mathrm{diag}\,\{\boldsymbol{h}_\mathrm{N}(kR)\}^{-1}\, \boldsymbol{y}_\mathrm{N}(\varphi_0,\vartheta_0), \tag{219}$$

worin $\left(\boldsymbol{Y}_\mathrm{N}^\mathrm{T}\right)^{-1}$ der sog. *Dekoder* [Dan00], siehe Abschn. 11.9, der Ambisonicsanordnung ist und $\frac{h_n(kr_0)}{h_n(kR)}$ die sog. *Distanzkodierung* [Dan00] und $\boldsymbol{y}_\mathrm{N}(\varphi_0,\vartheta_0)$ die *Enkodierung* einer Punktquelle sind. Diese Art der Steuerbarkeit ist nur mit gleichmäßigen, vollständigen Lautsprecheranordnungen möglich, wobei die Einschränkung der Winkelauflösung $\mathrm{N} \leq \sqrt{L}-1$ gilt.

Wird die Distanzkodierung weggelassen, so wird die Gleichung unabhängig von der Frequenz und virtuelle Quellen sind am Radius der Lautsprecheranordnung angeordnet. Räumliche Aliase sind die Komponenten für $n > \mathrm{N}$, welche außerhalb des sog. *sweet-spot* Gewicht bekommen. Das ist ein zentraler Bereich, der nur etwa $\mathrm{N}/3$ Wellenlängen durchmisst. Warum Ambisonics dennoch nicht nur für binaurale Anwendungen gut funktioniert ist eine offene Frage der Psychoakustik.

Diese Theorie ist auch zur Interpolation und Extrapolation von Richtwirkungsmustern bei der Vermessung von Mikrofonen anwendbar.

Alternativen für unvollständige Lautsprecheranordnungen und weniger perfekte Dekodierung können in [Pom08] gefunden werden.

11.9 Diskrete Zerlegung und Erzeugung von Kugelflächenfunktionen

In den vorigen Abschnitten wurden bereits Zerlegung und Erzeugung von Kugelflächenfunktionen angewendet. Der Zusammenhang kommt in der Fachliteratur relativ kurz, benötigt aber Erläuterung. Allgemein betrachtet, wird dabei ein sphärisches Spektrum γ_{nm} mit einem diskreten Muster g_l, das an verschiedenen diskreten Winkeln auf einem Radius existiert, rechnerisch in Beziehung gesetzt. Am einfachsten wird das diskrete Muster g_l als Vektor $\boldsymbol{g} = (g(\boldsymbol{\theta}_1), \cdots, g(\boldsymbol{\theta}_\mathrm{L}))^\mathrm{T}$ geschrieben. In [Zot09b, Zot09a] werden

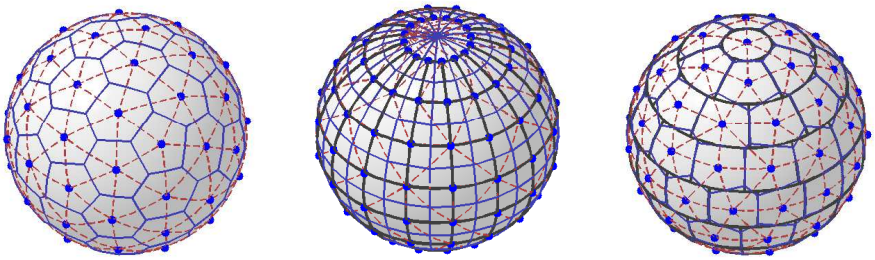

(a) Hyperinterpolation (*hi*) L = 64 (b) Gauss-quadrature (*gl*) L = 128 (c) Equal area partitions (*eq*) L = 75

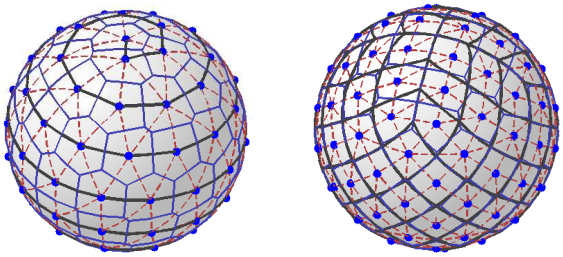

(d) Spiral points (*sp*) L = 76 (e) HEALPix (*hp*) L = 108

Figure 42 – Beispiele für verschiedene Abtastungsstrategien der Kugel [Zot09b].

einige Diskretisierungsarten auf der Kugel zitiert, zu sehen in Abb. 42.

11.9.1 Zerlegung: ortsdiskretisierte Kugelflächenfunktionenreihe

Eine kontinuierliche Funktion $\boldsymbol{g}(\boldsymbol{\theta})$ kann aus einer unendlichen Summe der mit dem sphärischen Spektrum gewichteter Kugelflächenfunktionen zusammengesetzt werden. Wir drücken diese als Inprodukt zweier unendlich langer Vektoren $\boldsymbol{y}(\boldsymbol{\theta}) = (Y_{0,0}(\boldsymbol{\theta}), \cdots, Y_{\mathrm{NN}}(\boldsymbol{\theta}), \cdots)^\mathrm{T}$ und $\boldsymbol{\gamma} = (\gamma_{0,0}, \cdots, \gamma_{\mathrm{NN}}, \cdots)^\mathrm{T}$ aus

$$\boldsymbol{g}(\boldsymbol{\theta}) = \boldsymbol{y}(\boldsymbol{\theta})^\mathrm{T}\, \boldsymbol{\gamma}.$$

Diskretisieren wir diese im Winkel, erhalten wir ein ortsdiskretes Muster $\boldsymbol{g}$

$$\boldsymbol{g} = \boldsymbol{Y}\,\boldsymbol{\gamma}, \qquad \text{mit } \boldsymbol{Y} = \begin{bmatrix} \boldsymbol{y}^{\mathrm{T}}(\boldsymbol{\theta}_1) \\ \vdots \\ \boldsymbol{y}^{\mathrm{T}}(\boldsymbol{\theta}_{\mathrm{L}}) \end{bmatrix}. \tag{220}$$

Zur Zerlegung eines allgemeinen Musters $\boldsymbol{g}$ müsste das unendlich große Gleichungssystem Gl. (220) invertiert werden, um das sphärische Spektrum zu erhalten. *Die Annahme eines in der Ordnung*[7] *begrenzten Musters* $\boldsymbol{g} = \boldsymbol{g}_{\mathrm{N}} = \boldsymbol{Y}_{\mathrm{N}}\,\boldsymbol{\gamma}_{\mathrm{N}}$ *erlaubt die Inversion. Demnach dürfen nur Kugelflächenfunktionen begrenzter Ordnung am Entstehen des Musters beteiligt sein.*

11.9.2 Erzeugung: Steuerung sphärischer Spektren mit gesteuerten Punkten

Typischerweise ist zur Erzeugung von Mustern aus Kugelflächenfunktionen die Ansteuerung diskreter Punkte nötig. Als Steuergrößen haben diese Punkte sphärische Spektren, die bekannt sind.

Das sphärische Spektrum $\boldsymbol{\gamma}$ eines Punktes an $\boldsymbol{\theta}_0$ entspricht (siehe Gln. (183)(214)) $\boldsymbol{\gamma} = \boldsymbol{y}(\boldsymbol{\theta}_0)$. Wird ein System aus Punkten mit Gewichten $\boldsymbol{g}$ gesteuert, ergibt sich das Spektrum:

$$\boldsymbol{\gamma} = \boldsymbol{Y}^{\mathrm{T}}\,\boldsymbol{g}. \tag{221}$$

Zur Erzeugung eines gewünschten Spektrums $\boldsymbol{\gamma}$ müssten die Punkte mit dem inversen unendlich großen Gleichungssystem Gl. (221) angesteuert werden. *Dazu wird das System* $\boldsymbol{\gamma}_{\mathrm{N}} = \boldsymbol{Y}_{\mathrm{N}}^{\mathrm{T}}\,\boldsymbol{g}_{\mathrm{N}}$ *der Punktspektren als im Winkel bandbegrenzt angenommen und invertiert. Diese Bandbegrenzung im Winkel sollte bei der Synthese eingefordert werden.*

7. Man spricht von „im Winkel bandbegrenzt“.

11.9.3 Inversion

Für oben genannte Fälle ist entweder die Inversion von $\boldsymbol{Y}_\mathrm{N}$, oder von $\boldsymbol{Y}_\mathrm{N}^\mathrm{T}$ erforderlich. Die muss nicht unbedingt trivial sein. Sollte sie gelingen, gelten die Formeln der folgenden zwei Absätze.

Minimierung der Fehlerquadrate zur diskreten Kugelflächenfunktionenanalyse

Wenn keine extremalen Punkte zur Hyperinterpolation verwendet werden, gibt es keine Inverse, nur eine Linksinverse. Bei der Analyse stehen mehr Messwerte zur Verfügung als Spektralkoeffizienten geschätzt werden sollen. Das Ergebnis entspricht der Minimierung der Fehlerquadrate, vgl. [HG06]:

$$J(\boldsymbol{\gamma}_\mathrm{N}) = \|\boldsymbol{g} - \boldsymbol{Y}_\mathrm{N}\boldsymbol{\gamma}_\mathrm{N}\|^2 \to \min \qquad \Rightarrow \frac{\partial}{\partial \boldsymbol{\gamma}_\mathrm{N}^\mathrm{T}} J(\boldsymbol{\gamma}_\mathrm{N}) = \boldsymbol{Y}_\mathrm{N}^\mathrm{T}\,\boldsymbol{g} - \boldsymbol{Y}_\mathrm{N}^\mathrm{T}\,\boldsymbol{Y}_\mathrm{N}\,\boldsymbol{\gamma}_\mathrm{N} \stackrel{!}{=} 0,$$

$$\Longrightarrow \boldsymbol{\gamma}_\mathrm{N} = \underbrace{\left(\boldsymbol{Y}_\mathrm{N}^\mathrm{T}\,\boldsymbol{Y}_\mathrm{N}\right)^{-1}\boldsymbol{Y}_\mathrm{N}^\mathrm{T}}_{:=\boldsymbol{Y}_\mathrm{N}^\dagger}\,\boldsymbol{g}. \tag{222}$$

Die Verteilung der Abtastpunkte ist entscheidend für die gute Invertierbarkeit der Matrix $\boldsymbol{Y}_\mathrm{N}^\mathrm{T}\boldsymbol{Y}_\mathrm{N}$, d.h. alle Singulärwerte sind dann groß genug, $\mathrm{K} = (\mathrm{N}+1)^2$. Fehler kommen nur durch Muster zustande, die nicht in Kugelflächenfunktionen begrenzter Ordnung ausgedrückt $\boldsymbol{g} \neq \boldsymbol{Y}_\mathrm{N}\,\boldsymbol{\gamma}_\mathrm{N}$ bzw. in solche umgedeutet werden können. Sind die Abtastpunkte ungleich verteilt, so werden solche Zerlegungsfehler (etwa durch Rauschen der Mikrofone) auf der Kugelfläche ungleich verteilt.

Bedingte Minimierung der Quadrate zur Kugelflächenfunktionensynthese

Wenn keine Punkte für Hyperinterpolation verwendet werden, gibt es keine Inverse, nur eine Rechtsinverse. Für die Synthese stehen dann mehr Steuerungspunkte als die Anzahl an bandbegrenzten Kugelflächenfunktionen, die erzeugt werden sollen, zur Verfügung. Die Gleichheit der (im Bandbegrenzten) erzeugten Spektren kann auf viele Arten erreicht werden. Für eine eindeutige Lösung wird deshalb nicht nur Gleichheit gefordert, sondern auch die Energie der Gewichte $\|\boldsymbol{g}\|^2$ minimiert

$$\|\boldsymbol{g}\|^2 \to \min. \tag{223}$$

$$\text{subject to: } \boldsymbol{\gamma}_\mathrm{N} \stackrel{!}{=} \boldsymbol{Y}_\mathrm{N}^\mathrm{T}\,\boldsymbol{g}, \qquad \Rightarrow J(\boldsymbol{g},\boldsymbol{\lambda}) = \|\boldsymbol{g}\|^2 + (\boldsymbol{\gamma}_\mathrm{N}^\mathrm{T} - \boldsymbol{g}^\mathrm{T}\boldsymbol{Y}_\mathrm{N})\,\boldsymbol{\lambda},$$

worin der Optimierungsfehler $J(\boldsymbol{g},\boldsymbol{\lambda})$ ist und die Lagrange-Multiplikatoren $\boldsymbol{\lambda}$ sind. Optimierung ergibt (vgl. [HG06]):

$$I: \ \frac{\partial}{\partial \boldsymbol{g}^\mathrm{T}} J(\boldsymbol{g},\boldsymbol{\lambda}) = \boldsymbol{g}_\mathrm{opt} - \boldsymbol{Y}_\mathrm{N}\,\boldsymbol{\lambda} \stackrel{!}{=} 0, \qquad \Rightarrow \boldsymbol{g}_\mathrm{opt} = \boldsymbol{Y}_\mathrm{N}\,\boldsymbol{\lambda}$$

$$II: \ \frac{\partial}{\partial \boldsymbol{\lambda}^\mathrm{T}} J(\boldsymbol{g},\boldsymbol{\lambda}^\mathrm{T}) = \boldsymbol{\gamma}_\mathrm{N} - \boldsymbol{Y}_\mathrm{N}^\mathrm{T}\,\boldsymbol{g} \stackrel{!}{=} 0, \quad \stackrel{\text{mit } \boldsymbol{g}_\mathrm{opt} \text{ aus I}}{\Rightarrow} \boldsymbol{\lambda}_\mathrm{opt} = (\boldsymbol{Y}_\mathrm{N}^\mathrm{T}\,\boldsymbol{Y}_\mathrm{N})^{-1}\,\boldsymbol{\gamma}_\mathrm{N},$$

$$\Longrightarrow \boldsymbol{g} = \boldsymbol{Y}_\mathrm{N}(\boldsymbol{Y}_\mathrm{N}^\mathrm{T}\,\boldsymbol{Y}_\mathrm{N})^{-1}\,\boldsymbol{\gamma}_\mathrm{N}. \tag{224}$$

Die Matrix $\boldsymbol{Y}_\mathrm{N}(\boldsymbol{Y}_\mathrm{N}^\mathrm{T}\,\boldsymbol{Y}_\mathrm{N})^{-1}$ wird in Ambisonics *Dekoder* genannt.

Verallgemeinerte Inverse: Pseudoinverse durch Singulärwertzerlegung

Die Struktur der Signulärwertzerlegung [8] (SVD) bietet Hilfe bei der Inversion, indem $\boldsymbol{Y}_\mathrm{N} = \boldsymbol{U}\ \boldsymbol{S}\ \boldsymbol{V}^\mathrm{T}$ in eine Diagonalmatrix mit Singulärwerten $\boldsymbol{S} = \mathrm{diag}\{\boldsymbol{s}\}$ und zwei orthogonalen Matrizen $\boldsymbol{U}$ und $\boldsymbol{V}$ mit den Links- und Rechtseigenvektoren zerlegt wird. Die SVD kann für eine regularisierte Inverse $\boldsymbol{Y}_\mathrm{N}^\dagger = \tilde{\boldsymbol{V}}\ \tilde{\boldsymbol{S}}^{-1}\ \tilde{\boldsymbol{U}}^\mathrm{T}$ benützt werden, indem nur die K ausreichend großen Singulärwerte aus $\tilde{\boldsymbol{S}}$ behalten werden und der Rest - auch aus den orthogonalen Matrizen - verworfen wird. Man könnte K als die *mit sinnvollem Aufwand steuerbaren* Freiheitsgrade bezeichnen.

Die regularisierte Pseudoinverse nach [GK65] ergibt für Gl. (220) einerseits das aus beliebigen Mustern $\boldsymbol{g}$ geschätzte Spektrum $\boldsymbol{\gamma}_\mathrm{N}$, bzw. für Gl. (221) die Gewichte $\boldsymbol{g}_\mathrm{N}$ für das Wunschspektrum $\boldsymbol{\gamma}_\mathrm{N}$

$$\text{Analyse: } \boldsymbol{\gamma}_\mathrm{N} = \boldsymbol{Y}_\mathrm{N}^\dagger\, \boldsymbol{g}, \qquad\qquad \text{Synthese: } \boldsymbol{g}_\mathrm{N} = (\boldsymbol{Y}_\mathrm{N}^\mathrm{T})^\dagger\, \boldsymbol{\gamma}_\mathrm{N}. \tag{225}$$

Durch das Verwerfen kleiner Singulärwerte, wird die Division durch Null, also eine Zerlegung in Muster, die schwer zu trennen und daher störanfällig [9] sind, vermieden. Die Eigenschaft der Inversen bestimmt sich aus den Dimensionen von $\boldsymbol{Y}_\mathrm{N}$ und der Anzahl K:

1. *Diskrete Kugelflächenfunktionenanalyse/-synthese:* Spektren werden durch die Pseudoinverse exakt bestimmt, wenn die Bandbegrenzung im Winkel eingehalten wird und alle Spektralkomponenten bestimmt/überbestimmt sind $\mathrm{K} = (\mathrm{N}+1)^2 \leq \mathrm{L}$.
2. *Diskrete Kugelflächenfunktioneninterpolation:* Muster/Gewichte $\boldsymbol{g} = \boldsymbol{g}_\mathrm{N}$ stimmen durch die Pseudoinverse exakt überein, wenn die Punkte bestimmt/überbestimmt sind $\mathrm{K} = \mathrm{L} \leq (\mathrm{N}+1)^2$.
3. *Kugelflächenfunktionenapproximation:* Wenn $\mathrm{K} < \min[(\mathrm{N}+1)^2, \mathrm{L}]$, ergibt die Pseudoinverse weder Interpolation noch Analyse und kann nur als Näherung verwendet werden.

Im ersten Fall, der Analyse/Synthese erhält man stets exakt bestimmte sphärische Spektren begrenzter Ordnung, die gegebenen Mustern/Gewichten entsprechen. Diese Zerlegungsart ist für Holografie und Holofonie nützlich. Bei der Analyse liest sie sich als $(\boldsymbol{Y}_\mathrm{N}^\mathrm{T}\boldsymbol{Y}_\mathrm{N})^{-1}\boldsymbol{Y}_\mathrm{N}^\mathrm{T}$ und invertiert $\boldsymbol{Y}_\mathrm{N}$ von der linken Seite. (Bei der Synthese invertiert $\boldsymbol{Y}_\mathrm{N}^\mathrm{T}(\boldsymbol{Y}_\mathrm{N}^\mathrm{T}\boldsymbol{Y}_\mathrm{N})^{-1}$ die Matrix $\boldsymbol{Y}_\mathrm{N}^\mathrm{T}$ von rechts.).

Im zweiten Fall erhält man stets exakt bestimmte diskrete Muster, die sphärischen Spektren begrenzter Ordnung entsprechen. Im dritten Fall sind sowohl für die Analyse, als auch die Interpolation zu wenige Signulärwerte/Freiheitsgrade übrig. Jedoch liefert die Pseudoinverse laut [GK65] die bestmögliche Zwischenlösung: *sie findet den kürzesten Lösungsvektor $\boldsymbol{\gamma}_\mathrm{N}$, der den Abstand zwischen $\boldsymbol{Y}_\mathrm{N}\,\boldsymbol{\gamma}_\mathrm{N}$ und $\boldsymbol{g}$ minimiert.*

Abb. 43 klassifiziert einige Abtastungsstrategien der Kugel in das dreiteilige Schema. Als Ordnung wird für alle $\mathrm{N} = 9$ verwendet, und die Anzahl der Abtastpunkte wird variiert:

8. singular-value decomposition
9. Im Audiobereich sind vermutlich Singulärwerte von $0 \cdots -20$dB noch praktisch.

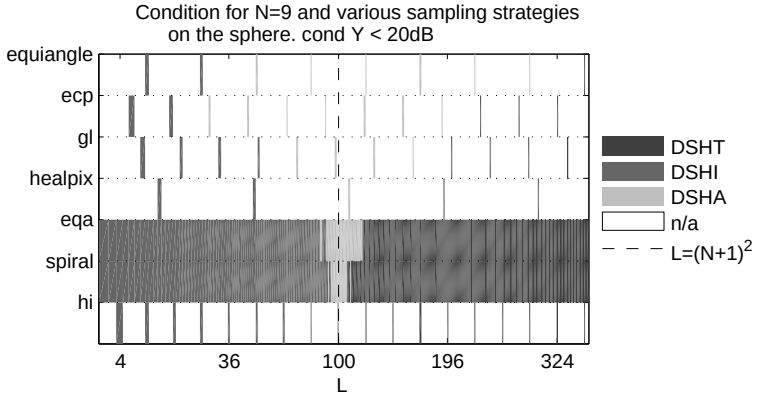

Figure 43 – Bekannte Abtungsstrategien sind zur Interpolation (pseudo-spectral analysis [Boy00]), Approximation oder Transformation (spectral analysis [Boy00]) geeignet. Um $\mathrm{L} = (\mathrm{N}+1)^2$ gelten die meisten nur für Approximation; Hyperinterpolation ist beides: Interpolation und Transformation.

extremale Punkte für Hyperinterpolation [SW04] (*hi*), Spiralpunkte [RSZ95] (*sp*), Gleichflächige Zerlegung [SK97] (*eqa*), HEALPix [GHB+05], Gauß-Legendre-Raster [Sne94] (*gl*), Gleichwinkeliges zylindrisches Raster [Sne94] (*ecp*), gleichwinkeliges Raster [DH94].

Bei der Ambisonicswiedergabe ist oft keine Holofonie möglich und die verallgemeinerte Inverse leistet bei ausreichender Regularisierung gute Dienste. Warum das Resultat für das Gehör oftmals ausreicht, ist Gegenstand der Dissertation von Matthias Frank [Fra13b]. Verallgemeinerte Dekodierungsstrategien sind in [ZPN12, ZF12, **?**].

11.10 Theorie zur Messung der Schalleinstrahlung

Mit kompakten kugelförmigen Mikrofonanordnungen lässt sich das rundum einfallende Schallfeld aufnehmen. Im Bereich der Kugelflächenfunktionen lässt sich auch in diesem Fall akustische Holografie machen (Extrapolation des aufgenommenen Schallfeldes auf einen anderen Radius).

Wie oben wird $c_{nm} = 0 : \forall n$ und $b_{nm} = 0 : \ n > \mathrm{N}$ angenommen, d.h. ein Schallfeld mit begrenzter Richtungsauflösung und ohne Quellen am Koordinatenursprung. Die sphärischen Wellenspektren von Schalldruck und Schallschnelle an einem Radius R sind somit

$$\boldsymbol{\psi}_\mathrm{N}(kR) = \mathrm{diag}\{\boldsymbol{j}_\mathrm{N}(kR)\}\,\boldsymbol{b}_\mathrm{N}, \tag{226}$$

$$\boldsymbol{\nu}_\mathrm{N}(kR) = \frac{\mathrm{i}}{\rho_0 c}\,\mathrm{diag}\{\boldsymbol{j}'_\mathrm{N}(kR)\}\,\boldsymbol{b}_\mathrm{N}. \tag{227}$$

Weil der vom Radius abhängige Teil in beiden Gleichungen 0 werden kann, sind reine Drucksensoren, bzw Radialschnellesensoren alleine nicht zielführend. Typischerweise gibt es 2 Lösungsstrategien: die Verwendung von Nierenmikrofonen am Radius R, oder der Einsatz von Druckmikrofonen auf einer festen Kugel mit dem Radius R.

Kompakte kugelförmige Mikrofonanordnung mit fester Oberfläche. An einer festen Kugeloberfläche gilt die Bedingung einer verschwindenden Schallschnelle in Oberflächennormalrichtung $\boldsymbol{\nu}_\mathrm{N}(kR) = 0$. Das wird in der Literatur [Li05, Raf05, Pet04, Mor06] erreicht, indem das ausstrahlende Wellenspektrum $\boldsymbol{c}_\mathrm{Q}$ des gebeugten Schallfeldes berechnet wird:

$$\boldsymbol{\nu}_\mathrm{Q}(kR) = \frac{\mathrm{i}}{\rho_0 c}\left(\mathrm{diag}\{\boldsymbol{j}'_\mathrm{Q}(kR)\}\,\boldsymbol{b}_\mathrm{Q} + \mathrm{diag}\{\boldsymbol{h}'_\mathrm{Q}(kR)\}\,\boldsymbol{c}_\mathrm{Q}\right) \stackrel{!}{=} 0, \tag{228}$$

$$\Rightarrow \boldsymbol{c}_\mathrm{Q} = -\mathrm{diag}\left\{\boldsymbol{j}'_\mathrm{Q}(kR)\right\}\mathrm{diag}\left\{\boldsymbol{h}'_\mathrm{Q}(kR)\right\}^{-1}\,\boldsymbol{b}_\mathrm{Q}. \tag{229}$$

Es ergibt sich eine neue Gleichung für das Wellenspektrum des Schalldruckes

$$\begin{aligned}\boldsymbol{\psi}_\mathrm{Q}(kR) &= \mathrm{diag}\left\{\boldsymbol{j}_\mathrm{Q}(kR)\right\} - \mathrm{diag}\{\boldsymbol{h}_\mathrm{Q}(kR)\}\mathrm{diag}\{\boldsymbol{j}'_\mathrm{Q}(kR)\}\mathrm{diag}\{\boldsymbol{h}'_\mathrm{Q}(kR)\}^{-1}\,\boldsymbol{b}_\mathrm{Q}\\ &= \frac{1}{\mathrm{i}(kR)^2}\,\mathrm{diag}\left\{\boldsymbol{h}'_\mathrm{Q}(kR)\right\}^{-1}\,\boldsymbol{b}_\mathrm{Q}.\end{aligned} \tag{230}$$

Zur Zeile 2 gelangt man über die Wronski-Determinante sphärischer Besselfunktionen $j_n(kr)\,h'_n(kr) - j'_n(kr)\,h_n(kr) = 1/\mathrm{i}(kr)^2$. Das bemerkenswerte an obiger Gleichung ist, dass zur Berechnung von $\boldsymbol{b}_\mathrm{Q}$ durch keine Nullfaktoren mehr dividiert werden muss. Diese Filterfrequenzgänge sind zur Kartierung von Quellstärkeverteilungen geeignet. Wie oben, ist das Wellenspektrum einer Quellstärkeverteilung $\boldsymbol{\phi}_\mathrm{Q}$ am Radius r_p definiert als

$$\boldsymbol{b}_\mathrm{Q} = -\mathrm{i}k\,\mathrm{diag}\left\{\boldsymbol{h}_\mathrm{Q}(kr_p)\right\}\,\boldsymbol{\phi}_\mathrm{Q}. \tag{231}$$

Beschränkt man sich auf eine endliche Ordnung $n \le \mathrm{N} < \mathrm{Q}$, bildet das Wellenzahlspektrum $\boldsymbol{\psi}_\mathrm{N}(kR) = \boldsymbol{Y}_\mathrm{N}^{-1}\,\boldsymbol{p}$, mutmaßt mit Quellen am Radius r_p, so kann Gl. (231) in Gl. (230) eingesetzt und durch Inversion die Quellstärkeverteilung $\boldsymbol{\phi}_\mathrm{N}$ kartieren werden:

$$\boldsymbol{\phi}_\mathrm{N} = -\mathrm{diag}\{(kR)^2\,\boldsymbol{h}'_\mathrm{N}(kR)\}\mathrm{diag}\{k\,\boldsymbol{h}_\mathrm{N}(kr_p)\}^{-1}\,\boldsymbol{Y}_\mathrm{N}^{-1}\,\boldsymbol{p}. \tag{232}$$

Im Winkel aufgetragen ist das dann

$$f(\varphi,\vartheta) = \boldsymbol{y}_{\mathrm{N}}^{\mathrm{T}}(\varphi,\vartheta)\,\boldsymbol{\phi}_{\mathrm{N}}. \tag{233}$$

Für Interessierte: In der Diplomarbeit von Peter Plessas [Ple09], Svend-Oscar Petersen [Pet04], Munhum Park [PR05] und Adam O'Donovan [ODZ08] sind gute Beispiele dieser Art für Richtungskartierung von Schallfeldern zu finden.

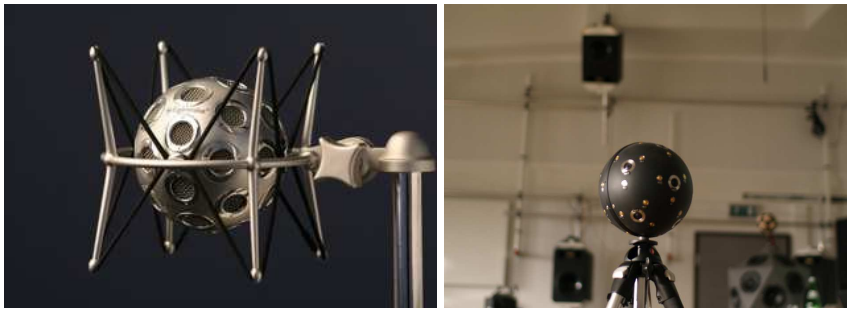

Figure 44 – Kugelförmige Mikrofonanordnung von mhacoustics und Bruel und Kjær.

11.11 Radiale Scharfstellfilter / Holografiefilter

Wie oben, tritt bei hohen Frequenzen räumliches Aliasing auf. Aufgrund der Abtastung allerdings, weist dieses in der Regel keine bekannte Regelmäßigkeit auf. Zudem sind, ähnlich wie bei der Nahfeldholografie, die Filterausdrücke, z.B. $\frac{(kR)^2 h_n'(kR)}{k\, h_n(kr_p)}$, bei den tiefen Frequenzen extrem groß und daher Störgeräuschanfällig.

Sphärische Hankelfilter

Bis auf einen Verzögerungsfaktor $e^{-\mathrm{i}kr}$ lassen sich die sphärischen Hankelfunktionen $h_n(kr)$ und ihre Ableitung $h_n'(kr)$ als fraktionale Polynome von $\mathrm{i}kr$ darstellen

$$h_n(kr) = \mathrm{i}^{n+1}\frac{e^{-\mathrm{i}kr}}{kr}\sum_{l=0}^{n}\frac{(n+l)!}{l!(n-l)!}\frac{1}{(2\mathrm{i}kr)^l}, \quad h_n'(kr) = -\frac{n+1}{kr}h_n(kr) + h_{n-1}(kr).$$

Da $kr = \omega/c\,r$ von der Frequenz und dem Radius abhängt, die Laplace-Frequenzdomäne aber unempfindlich gegenüber Frequenzskalierung reagiert [10], können wir Hankelfunktionen direkt als Hankelfilter normierten Radius $r = c$ im Laplace-Bereich anschreiben (auf einen Nenner gebracht)

$$h_n(s) = -\mathrm{i}^n\frac{\sum_{l=0}^{n}\alpha_n[l]s^l}{s^{n+1}}\,e^{-s}, \qquad h_n'(s) = \mathrm{i}^{n+1}\frac{\sum_{l=0}^{n}\beta_n[l]s^l}{s^{n+2}}\,e^{-s},$$

10. Die Impulsantwort wird einfach mit dem reziproken Skalierfaktor in der Zeit gestaucht.

wobei $\alpha_n[l], \beta_n[l]$ bloß irgendwelche rationalen Koeffizienten sind. Mit der Zergliederung in Filterstufen 2. Ordnung, der entsprechenden Skalierung für die Radien, und der Impulsinvarianztransformation erhalten wir wunderbare digitale IIR-Filter für die Berechnung aller holografischen Filterungen, siehe [Pom08].

Holografiefilter

Die radialen Filter besitzen einfache asymptotische Darstellungen, aus welchen sie konstruiert werden können.

Der Absolutbetrag aller Hankelfunktionen verläuft oberhalb des Argumentes $kr \gg 1$ asymptotisch gleich und fällt mit dem Faktor $\frac{1}{kr}$. Unterhalb verlaufen Hankelfunktionen höherer Ordnung steiler $\frac{1}{(kr)^{n+1}}$ und haben höhere Beträge.

Beträge abgeleiteter Hankelfunktionen verhalten sich ähnlich, sind für kleine Argumente $kr \ll 1$ aber noch steiler $\frac{1}{(kr)^{n+2}}$ und höher.

Aus diesem Verhalten lassen sich Verläufe in Abb. 45 leichter verstehen. Sie zeigt die radialen Scharfstellfilter für die oben diskutierten kugelförmigen Probleme.

Die enorm hohen (zum Teil bei 0Hz instabilen) Verstärkugen der holografischen Filter bei tiefen Frequenzen führt in der Praxis zu technischen Problemen. Störgeräusche und Fehlpositionierungen aller Art, sowie zu physikalisch nicht schaffbare Lautstärken, wirken sich stark aus, oder der numerisch auflösbare Dynamikbereich wird im interessanten Frequenzband verlassen.

In der Praxis müssen zur Einschränkung der Frequenzgänge Filter eingesetzt werden. Das bedeutet meistens, dass bei tiefen Frequenzen die Richtungsauflösung reduziert wird. Dazu werden von den Ambisonics-Kanälen der höchsten Ordnung beginnend, tieffrequente Signale durch Hochpassfilterung entfernt. Bei Kanälen niedrigerer Ordnung reicht ein Hochpass tieferer Grenzfrequenz aus. Weil durch den Ausfall der hohen Ordnungen Amplitudenverluste entstehen würden, wurden in [Ker10] die übrig gebliebenen Komponenten durch Schelvingfilter angehoben, siehe Abb. 46.

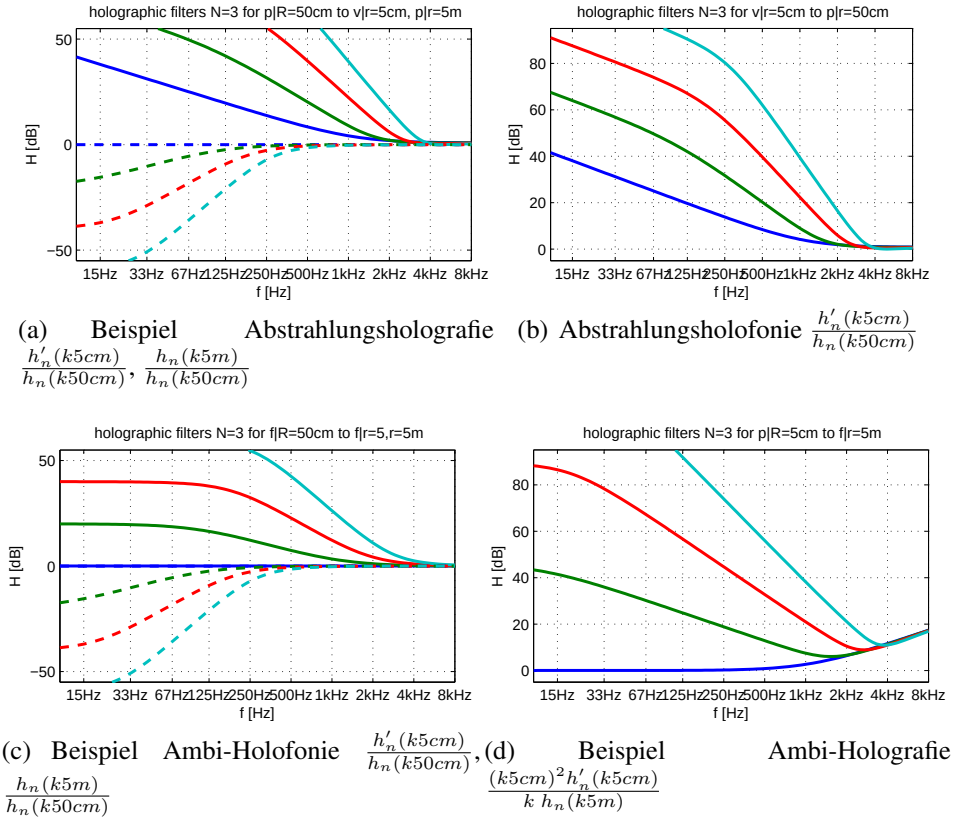

(a) Beispiel Abstrahlungsholografie $\frac{h_n'(k5cm)}{h_n(k50cm)}$, $\frac{h_n(k5m)}{h_n(k50cm)}$ (b) Abstrahlungsholofonie $\frac{h_n'(k5cm)}{h_n(k50cm)}$

(c) Beispiel Ambi-Holofonie $\frac{h_n'(k5cm)}{h_n(k50cm)}$, $\frac{h_n(k5m)}{h_n(k50cm)}$ (d) Beispiel Ambi-Holografie $\frac{(k5cm)^2 h_n'(k5cm)}{k\ h_n(k5m)}$

Figure 45 – Holografische Filter (zum radial Scharfstellen) für unterschiedliche Anwendungen. Knicke bei niedrigen Frequenzen sind jeweils durch den kleineren der beiden Radien bestimmt, Knicke bei hohen Frequenzen durch den größeren.

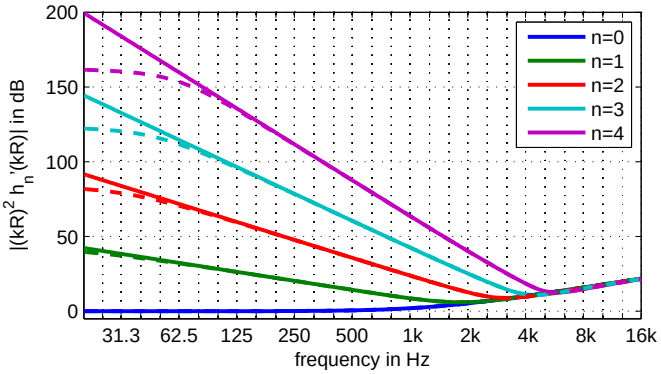

(a) Theoretical filters

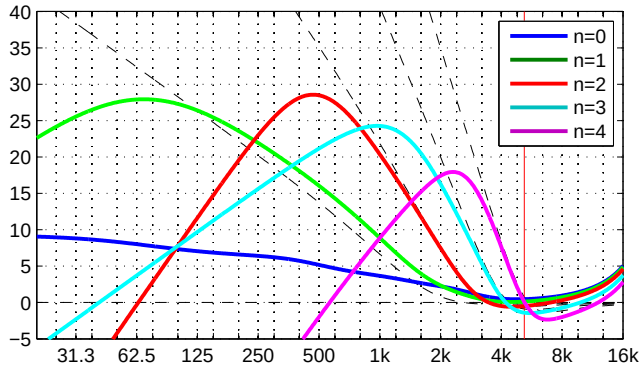

(b) Diffuse-field compensated filters limited at fc={20,59,612,1534,2742} Hz for the successive maximum orders $N = 0, 1, 2, 3, 4$

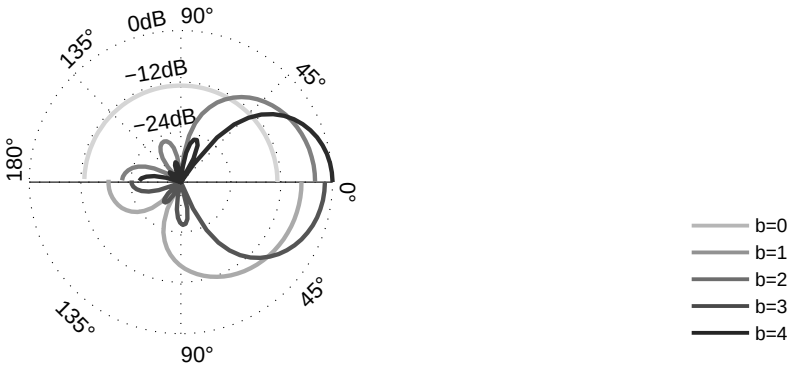

(c) Diffuse-field equalized max-rE point-spread functions

Figure 46 – Radial filter design presented in [LZ15] based on a filter bank that splits the Ambisonic signals into bands, in which individual sidelobe-cancelling $\mathrm{max} - \boldsymbol{r}_{\mathrm{E}}$ weights are applied and diffuse-field equalized wrt. each other.

12 Ambisonic Effects

12.1 Mirror

12.2 Rotation

12.3 Warping

12.4 Widening (Distance/diffuseness/early lateral reflections)

12.5 Directional audio coding

12.6 Reverberation and spatial decomposition method

12.7 Artificial convolution reverberation

12.8 Feedback delay network for diffuse reverberation

13 Compact spherical loudspeaker arrays (IEM IKO)

13.1 Spherical cap model

13.2 Control + Measurement

13.3 Listening experiments

13.3.1 Distance control (Laitinen+Wendt)

13.3.2 Auditory event placement

13.4 Archives of Acoustics

13.5 CMJ

14 5D room impulse responses + virtual IKO

14.1 Compact Ambisonic microphone and loudspeaker array measurement

14.2 Simple model

14.3 Direction/frequency vs. time resolution uncertainty

14.4 Virtual IKO

14.5 Double SDM

15 Holographic sound images of instruments

15.1 Fingering dependency in wood instruments

15.2 Interpolation in spherical harmonics

15.3 Acoustic centering problem + rotation tracking

16 Old holography/holophony lecture notes as appendix

A Level differences on pairwise horizontal loudspeaker pairs

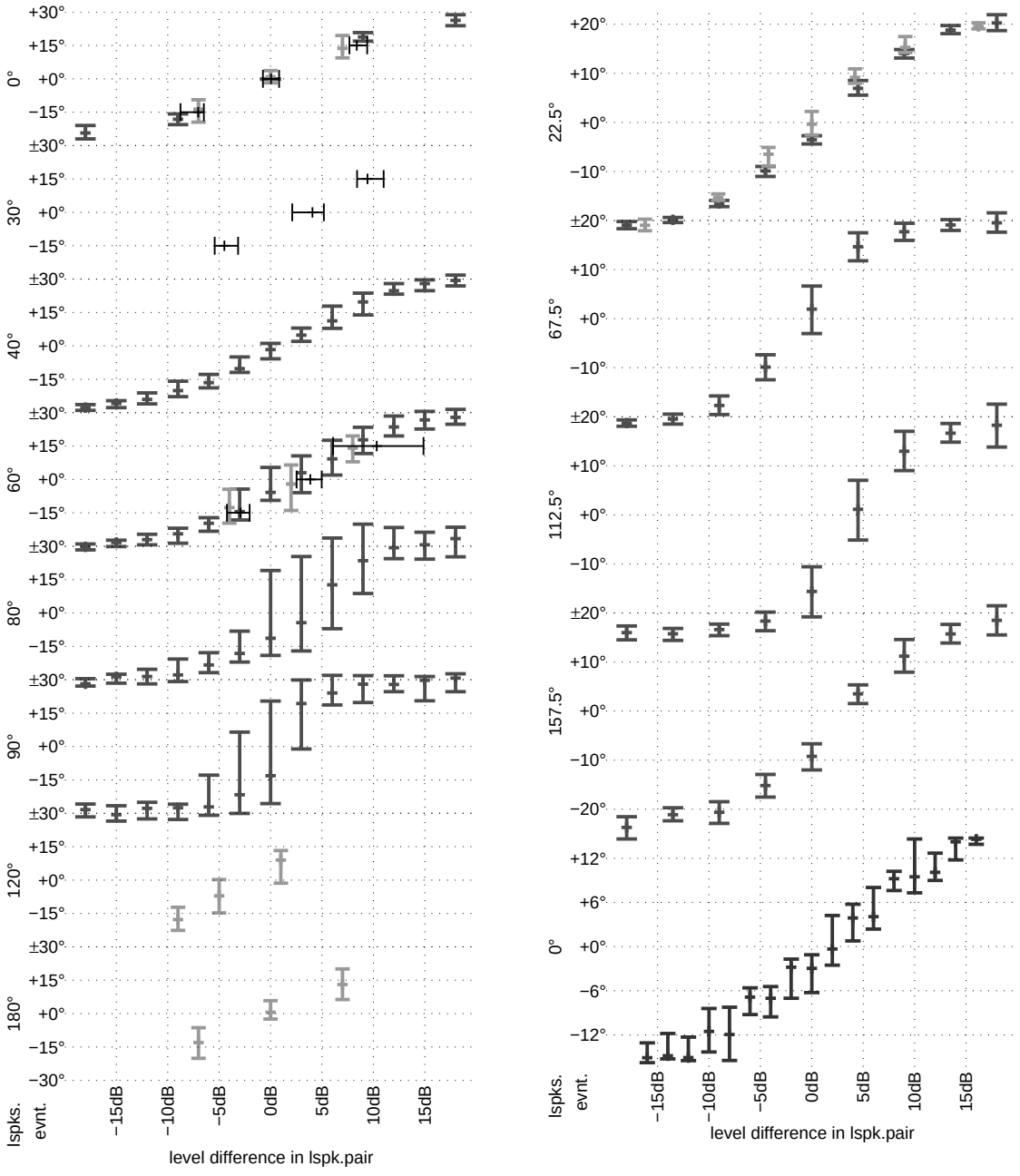

Figure 47 – Results of several listening esperiments about pairwise level differences of loudspeakers on the horizon; left $\pm 30°$: Theile et al. [TP77] first experiment in dark gray and thick, second experiment in light gray and thick, Pulkki [Pul03] in black and thin; right $\pm 22.5°$: Simon et al. [SMR09] dark gray and thick (1…4), Frank [Fra13b] light gray and thick, Martin [MWCQ99] black and thick.

B Sine and Tangent Law

The sine and tangent law [CDV58] observes the sound pressure of plane waves at to locations $x = 0$, $y = \pm d$ at ear distance in order to simulate the ear signals. A plane wave from the left half of the room from the angle $\varphi > 0$ first arrives at the left ear $p_{\text{left}} = e^{\mathrm{i}\,kd\,\sin\varphi}$ and later on the right one $p_{\text{right}} = e^{-\mathrm{i}\,kd\,\sin\varphi}$. The phase difference is $\Phi_\varphi = 2\,kd\,\sin\varphi$.

A superimposed pair of plane waves from the directions $\pm\alpha$ arrives at the left eare as $p_{\text{left}} = g_1\,e^{\mathrm{i}\,kd\,\sin\alpha} + g_2\,e^{-\mathrm{i}\,kd\,\sin\alpha}$, right as $p_{\text{right}} = g_1\,e^{-\mathrm{i}\,kd\,\sin\alpha} + g_2\,e^{\mathrm{i}\,kd\,\sin\alpha} = p^*_{\text{left}}$. The phase difference $\Phi_{\pm\alpha} = 2\angle p_{\text{left}} = 2\,\arctan\frac{(g_1-g_2)\,\sin(kd\,\sin\alpha)}{(g_1+g_2)\,\cos(kd\,\sin\alpha)}$ can be linearized for long wave lengths $kd \to 0$ to $\Phi_{\pm\alpha} \approx 2\,\arctan\left(kd\,\frac{g_1-g_2}{g_1+g_2}\,\sin\alpha\right) \approx 2\frac{g_1-g_2}{g_1+g_2}\,kd\,\sin\alpha$.

Comparing the phase difference of the single plane wave with the one of the superimposed pair, $2\,kd\,\sin\varphi = 2\,kd\,\frac{g_1-g_2}{g_1+g_2}\,\sin\alpha$, one arrives at the sine law

$$\sin\varphi = \frac{g_1-g_2}{g_1+g_2}\,\sin\alpha.$$

If we claim our hearing to posess the ability to not only estimate the interaural phase difference Φ but also its derivative with regard to head rotation $\frac{\partial\Phi}{\partial\delta}$, we arrive at a value pair of binaural features $(\Phi_\varphi, \frac{\partial\Phi_\varphi}{\partial\delta}) = 2\,kd\,(\sin\varphi, \cos\varphi)$ than should match the one of the plane wave pair. For this pair, the phase difference derived with regard to head rotation is $2\,kd\,\frac{\partial}{\partial\delta}\Phi_{\pm\alpha} \approx 2\,kd\,\frac{g_1\,\frac{\partial}{\partial\delta}\sin(\alpha+\delta)|_{\delta=0} + g_2\,\frac{\partial}{\partial\delta}\sin(-\alpha+\delta)|_{\delta=0}}{g_1+g_2} = 2\,kd\,\frac{g_1+g_2}{g_1+g_2}\cos\alpha = 2\,kd\,\cos\alpha$, which yields the value pair $(\Phi_{\pm\alpha}, \frac{\partial\Phi_{\pm\alpha}}{\partial\delta}) = 2\,kd\,(\frac{g_1-g_2}{g_1+g_2}\,\sin\alpha,\,\cos\alpha)$. In polar coordinates, the radius of both value pairs differs. While the plane wave yields a value pair at the radius $2\,kd$ in the binaural feature space, the plane wave pair is of the radius $2\,kd$ only between $\pm\alpha$, at which one of the two gains must vanish, and amplitude panning can be used to connect these two points $2kd\,(\pm\sin\alpha,\,\cos\alpha)$ by a straight line. The plane wave with the most similar feature pair musst lie on the same polar angle. We may equate the tangents of both points $\frac{\Phi_\varphi}{\frac{\partial\Phi_\varphi}{\partial\delta}} = \frac{\Phi_{\pm\alpha}}{\frac{\partial\Phi_{\pm\alpha}}{\partial\delta}}$ and obtain the tangent law:

$$\tan\varphi = \frac{g_1-g_2}{g_1+g_2}\,\tan\alpha.$$

If instead of the angle of a plane wave with the closest features to those of a given amplitude difference is searched, but the closest features of an amplitude difference matching those of a given plane wave, then the sine law is the best match, even in the two-dimensional feature space.

C 2D Ambisonic panning in terms of a Fourier series

C.1 Panning function as Fourier series

Assuming that we first try to find a continuous panning function, we can regard the Fourier series as suitable means to express this function. The Fourier coefficient $a_{|m|}\, e^{-\mathrm{i}m\varphi_\mathrm{s}}$ is able to control the direction and length of the $\boldsymbol{r}_\mathrm{E}$- and $\boldsymbol{r}_\mathrm{V}$ vector perfectly:

$$g(\varphi) = \frac{1}{2\pi} \sum_{m=-\infty}^{\infty} a_{|m|}\, e^{-\mathrm{i}m\varphi_\mathrm{s}}\, e^{\mathrm{i}m\varphi}. \tag{234}$$

While $a_{|m|} = 1$, yields a directional Dirac Delta function $g(\varphi) = \delta(\varphi - \varphi_\mathrm{s})$, values for $a_{|m|}$ tending to zero for large $|m|$ yield a smoother curve $g(\varphi)$ that is easier to sample.

Before looking into sampling the panning function at the loudspeaker positions, we seek whether the definitions of the linear and quadratic loudness and vector models are invariant with regard to the panning direction φ_s, and what their relation is to $a_{|m|}$.

For the loudness models, this is easily shown by replacing the integration variable φ by $\phi = \varphi - \varphi_\mathrm{s}$, and for the quadratic measure by considering orthogonality:

$$P = \int_{-\pi}^{\pi} g(\varphi)\,\mathrm{d}\varphi = \sum_{m=-\infty}^{\infty} \frac{a_m}{2\pi} \underbrace{\int_{-\pi-\varphi_\mathrm{s}}^{\pi-\varphi_\mathrm{s}} e^{\mathrm{i}m\phi}\,\mathrm{d}\phi}_{:=2\pi\,\delta_{m0}} = a_0, \tag{235}$$

$$E = \int_{-\pi}^{\pi} |g(\varphi)|^2\,\mathrm{d}\varphi = \sum_{m'=-\infty}^{\infty} \sum_{m=-\infty}^{\infty} \frac{a_m a_{m'}^*}{(2\pi)^2} \underbrace{\int_{-\pi-\varphi_\mathrm{s}}^{\pi-\varphi_\mathrm{s}} e^{\mathrm{i}(m-m')\phi}\,\mathrm{d}\phi}_{:=2\pi\,\delta_{mm'}} = \sum_{m=-\infty}^{\infty} \frac{|a_m|^2}{2\pi}. \tag{236}$$

Obviously the quadratic loudness measure involves all of the Fourier terms a_m (Parseval's theorem) while the linear one only considers a_0.

For the vector models, the notation of the vectors involved as complex scalars (x component as real and y component as imaginary part of the complex Gaussian number plane) simplifies the calculations a lot, i.e. using $\boldsymbol{\theta} = e^{\mathrm{i}\varphi}$. Again, the orthogonality relation helps simplifying the expressions:

$$\boldsymbol{r}_\mathrm{V} = \frac{\int_{-\pi}^{\pi} g(\varphi)\, e^{\mathrm{i}\varphi}\,\mathrm{d}\varphi}{V} = \frac{\sum_m \frac{a_m}{2\pi}\, e^{-\mathrm{i}m\varphi_\mathrm{s}} \overbrace{\int_{-\pi}^{\pi} e^{\mathrm{i}(m+1)\varphi}\mathrm{d}\varphi}^{2\pi\delta_{m+1,0}}}{a_0} = \frac{a_1}{a_0} e^{\mathrm{i}\varphi_\mathrm{s}}, \tag{237}$$

$$\boldsymbol{r}_\mathrm{E} = \frac{\int_{-\pi}^{\pi} |g(\varphi)|^2\, e^{\mathrm{i}\varphi}\,\mathrm{d}\varphi}{E} = \frac{\sum_{m,m'} \frac{a_m a_{m'}^*}{(2\pi)^2}\, e^{-\mathrm{i}(m-m')\varphi_\mathrm{s}} \overbrace{\int_{-\pi}^{\pi} e^{\mathrm{i}(m-m'+1)\varphi}\mathrm{d}\varphi}^{2\pi\delta_{m-m'+1,0}}}{\sum_m \frac{|a_m|^2}{2\pi}}$$

$$= \frac{\sum_{m=-\infty}^{\infty} a_m a_{m+1}^*}{\sum_{m=-\infty}^{\infty} |a_m|^2} \, e^{\mathrm{i}\varphi_\mathrm{s}}. \tag{238}$$

In all of the above results, the vectors point exactly into the desired direction. The vector component $e^{-\mathrm{i}m\varphi_\mathrm{s}}$ just undergoes a sign change but remains untouched otherwise. Note that this is largely fulfilled independently of what the weights a_m exactly look like.

The lengths of both vectors is independent of the panning direction φ_s. This can also be logically concluded from two facts, see Sec. C.2: (1) $g(\varphi)$ is symmetric around φ_s, (2) and its shape is preserved under rotation. The length $\|\mathrm{r_V}\|$ only depends on the weights a_0 and a_1, while the length $\|\boldsymbol{r}_\mathrm{E}\|$ depends on all the Fourier coefficient weights a_m involved, which seems to be important as the $\boldsymbol{r}_\mathrm{E}$ vector was an excellent predictor in the listening experiments about direction and width.

Surely, both the quadratic criteria, E and $\boldsymbol{r}_\mathrm{E}$ are the more critical ones when considering the continuous panning function as they involve all of the weights a_m.

C.2 Finite-order Fourier series

Rotation invariant shape. The represented shape of a 2π-periodic function in a finite-order Fourier series is rotation-invariant. For $2\pi\, g(\varphi) = \sum_{m=-\mathrm{N}}^{\mathrm{N}} a_{|m|}\, e^{\mathrm{i}m(\varphi-\varphi_\mathrm{s})}$ with arbitrary aiming φ_s, rotation by $-\varphi_\mathrm{s}$ is losslessly expressed by modified coefficients $a_{|m|}\, e^{+\mathrm{i}m\varphi_\mathrm{s}}$ (*shift theorem*), proved by $\sum_{m=-\mathrm{N}}^{\mathrm{N}} a_{|m|}\, e^{\mathrm{i}m\varphi_\mathrm{s}}\, e^{\mathrm{i}m(\varphi-\varphi_\mathrm{s})} = \sum_{m=-\mathrm{N}}^{\mathrm{N}} a_{|m|}\, e^{\mathrm{i}m\varphi}$, which obviously is $2\pi\, g(\varphi+\varphi_\mathrm{s})$, the shape of the original function rotated to aim at 0.

Symmetry. A real-valued and symmetric Fourier coefficient $a_{|m|} = \Re\{a_{\pm m}\}$ yields a symmetric real shape $\sum_{m=-\mathrm{N}}^{\mathrm{N}} a_m\, e^{\mathrm{i}m\phi} = a_0\, e^{\mathrm{i}0\phi} + \sum_{m=1}^{\mathrm{N}} \left(a_{-m}\, e^{-\mathrm{i}m\phi} + a_m\, e^{\mathrm{i}m\phi}\right)$. Symmetry yields for the second term $\sum_{m=1}^{\mathrm{N}} 2a_m \Re\{e^{-\mathrm{i}m\phi}\} = \sum_{m=1}^{\mathrm{N}} 2a_m \cos(m\phi)$. Such a cosine series is symmetric around $\phi = \varphi - \varphi_\mathrm{s}$, i.e. around the panning direction.

Is $\gamma_m = a_{|m|}$ a symmetric rectangular function, the finite geometric sum lets us obtain

$$g(\varphi) = \frac{1}{2\pi} \sum_{m=-N}^{N} e^{\mathrm{i}m\phi} = \frac{e^{-\mathrm{i}m\phi} - e^{\mathrm{i}(m+1)\phi}}{1 - e^{\mathrm{i}\phi}} = \frac{\sin[(m+\frac{1}{2})\phi]}{2\pi \sin\frac{\phi}{2}}, \tag{239}$$

the periodic sinc function shifted to φ_s. However, there are better ways to define $a_{|m|}$.

C.3 Finite-order series with maximum r_E vector length

The maximization of the $\boldsymbol{r}_\mathrm{E}$ vector length by optimal Fourier weights a_m yields a narrower perceived width and beneficial sidelobe suppression [DRP99]. For this purpose, the length $r_\mathrm{E} = \frac{\sum_{m=-\infty}^{\infty} a_m a_{m+1}}{\sum_{m=-\infty}^{\infty} a_m^2}$ is differentiated with regard to the weight a_m and equated to zero.

The numerator can be re-written to $\sum_{m=-\infty}^{\infty} a_m a_{m+1} = \sum_{m'=0}^{\infty} a_{m'} a_{m'+1} + a_{m'} a_{m'-1}$. Formally, the differentiated fraction equated to zero $r_\mathrm{E} = \frac{A}{B}$ can be simplified to $r'_\mathrm{E} =$

$\frac{A'}{B} - \frac{AB'}{B^2} = \frac{A'}{B} - \frac{r_\mathrm{E}\,B'}{B}$, and we may require $A' - r_\mathrm{E}\,B' = 0$

$$\frac{\partial}{\partial a_m}\left(\sum_{m'=0}^{\infty} a_{m'}a_{m'+1} + a_{m'}a_{m'-1}\right) - r_\mathrm{E}\,\frac{\partial}{\partial a_m}\left(\sum_{m'=-\infty}^{\infty} a_{m'}^2\right) = 0$$

$$a_{m+1} + a_{m-1} - 2\,r_\mathrm{E}\,a_m = 0. \qquad (240)$$

As a result to our optimization problem we obviously got a recurrence relation for both a_m and the minimum r_E. We find a recurrence in [OBC00, Eq. 18.9.1], Tab. 1, as a recurrence defining the Chebyshev polynomials ($T_m(\cos\varphi) = \cos m\varphi$) from lower-order ones,

$$T_{m+1}(x) + T_{m-1}(x) - 2x\,T_m(x) = 0,$$

and by comparison we find for a_m and r_E: $r_\mathrm{E} = x$, $a_m = T_m(r_\mathrm{E})$. As a boundary condition, we want to require $a_0 = 1$, what is fulfilled automatically by $T_0(x) = 1$, and we require that the term after the highest order N should vanish, hence $a_{\mathrm{N}+1} = T_{\mathrm{N}+1}(r_\mathrm{E}) = 0$. A suitable length for r_E must lie within the interval $[-1;1]$, so that we may substitute r_E by the cosine of a dispersion angle σ_E that should correspondingly be as small as possible and be a zero crossing of the $\mathrm{N}+1$ order term $T_{\mathrm{N}+1}(\cos\sigma_\mathrm{E}) = \cos[(\mathrm{N}+1)\sigma_\mathrm{E}] = 0$, hence must become $\sigma_\mathrm{E} = \frac{\pi}{2}(\mathrm{N}+1)$. The required $\max - \boldsymbol{r}_\mathrm{E}$ weight consequently is a $\cos$ half-wave window

$$a_m = \cos(\tfrac{\pi}{2}\tfrac{m}{\mathrm{N}+1}). \qquad (241)$$

C.4 Optimally arranged surround loudspeaker ring

We are looking for a discretization with L an optimal loudspeaker setup, characterized by the angles φ_l. For such a setup, the panning-invariant properties P, E, r_V, r_E and the accurate directions of $\boldsymbol{r}_\mathrm{V}$ and $\boldsymbol{r}_\mathrm{E}$ should stay preserved

$$P = \int_{-\pi}^{\pi} g(\varphi)\,\mathrm{d}\varphi = \tfrac{2\pi}{\mathrm{L}}\sum_{l=1}^{\mathrm{L}} g(\varphi_l), \qquad \boldsymbol{r}_\mathrm{V} = \frac{\int_{-\pi}^{\pi} g(\varphi)\,e^{\mathrm{i}\varphi}\,\mathrm{d}\varphi}{V} = \frac{\frac{2\pi}{\mathrm{L}}\sum_{l=1}^{\mathrm{L}} g(\varphi_l)\,e^{\mathrm{i}\varphi_l}}{V},$$

$$E = \int_{-\pi}^{\pi} |g(\varphi)|^2\,\mathrm{d}\varphi = \tfrac{2\pi}{\mathrm{L}}\sum_{l=1}^{\mathrm{L}} |g(\varphi_l)|^2, \quad \boldsymbol{r}_\mathrm{E} = \frac{\int_{-\pi}^{\pi} |g(\varphi)|^2\,e^{\mathrm{i}\varphi}\,\mathrm{d}\varphi}{E} = \frac{\frac{2\pi}{\mathrm{L}}\sum_{l=1}^{\mathrm{L}} |g(\varphi_l)|^2\,e^{\mathrm{i}\varphi_l}}{E}.$$

What would be an optimal arrangement that can be defined without needing to prove all of the four equivalences?

D Laplacian in axisymmetric coordinates

The generalized chain rule yields

$$\triangle = \sum_j \frac{\partial^2}{\partial x_j^2} = \sum_j \frac{\partial}{\partial x_j}\left(\frac{\partial\mu}{\partial x_j}\frac{\mathrm{d}}{\mathrm{d}\mu}\right) = \sum_j \frac{\partial^2\mu}{\partial x_j^2}\frac{\mathrm{d}}{\mathrm{d}\mu} + \sum_j \left(\frac{\partial\mu}{\partial x_j}\right)^2 \frac{\mathrm{d}^2}{\mathrm{d}\mu^2}. \qquad (242)$$

The derivative of one over the r often appears. It is with regard to any of the coordinates

$$\frac{\partial}{\partial x_j}\frac{1}{r} = -\frac{1}{r^2}\frac{\partial r}{\partial x_j} = -\frac{1}{r^2}\frac{\partial[\sum_j x_j^2]^{\frac{1}{2}}}{\partial x_j} = -\frac{1}{r^2}\frac{[\sum_j x_j^2]^{-\frac{1}{2}}}{2}\frac{\partial \sum_j x_j^2}{\partial x_j} = -\frac{1}{r^3}\frac{1}{2}2x_j = -\frac{x_j}{r^3}. \tag{243}$$

The derivatives of μ are for $j \neq 1$:

$$\frac{\partial \mu}{\partial x_j} = \frac{\partial}{\partial x_j}\frac{x_\mathrm{D}}{r} = -\frac{x_\mathrm{D}\, x_j}{r^3}, \tag{244}$$

$$\frac{\partial^2 \mu}{\partial^2 x_j} = -\frac{\partial}{\partial x_j}\frac{x_\mathrm{D}\, x_j}{r^3} = -\frac{x_\mathrm{D}}{r^3} + 3\frac{x_\mathrm{D} x_j^2}{r^5} = \frac{3x_\mathrm{D}x_j^2 - r^2 x_\mathrm{D}}{r^5}. \tag{245}$$

The first derivative of μ to x_D involves one more term depending on x_D that we could skip in the product rule before:

$$\frac{\partial \mu}{\partial x_\mathrm{D}} = \frac{\partial}{\partial x_\mathrm{D}}\frac{x_\mathrm{D}}{r} = -\frac{x_\mathrm{D}^2}{r^3} + \frac{1}{r} = \frac{r^2 - x_\mathrm{D}^2}{r^3} = \frac{\sum_{j\setminus \mathrm{D}} x_j^2}{r^3} = \frac{r_{\mathrm{D}-1}^2}{r^3}, \tag{246}$$

$$\frac{\partial^2 \mu}{\partial x_\mathrm{D}^2} = \frac{\partial}{\partial x_\mathrm{D}}\frac{r_{\mathrm{D}-1}^2}{r^3} = \frac{-3\, x_\mathrm{D}\, r_{\mathrm{D}-1}}{r^5}. \tag{247}$$

We obtain for the factors involved in front of the second and first-order derivatives of the axisymmetric Laplacian:

$$\sum_j \left(\frac{\partial \mu}{\partial x_j}\right)^2 = \frac{r_{\mathrm{D}-1}^4}{r^6} + \frac{x_\mathrm{D}^2 \sum_{j\setminus \mathrm{D}} x_j^2}{r^6} = \frac{(r^2 - x_\mathrm{D}^2) r_{\mathrm{D}-1}^2}{r^6} + \frac{x_\mathrm{D}^2 r_{\mathrm{D}-1}^2}{r^6} = \frac{r^2 r_{\mathrm{D}-1}^2}{r^6} = \frac{r_{\mathrm{D}-1}^2}{r^4}, \tag{248}$$

$$\sum_j \frac{\partial^2 \phi}{\partial x_j^2} = \frac{-3x_\mathrm{D}\, r_{\mathrm{D}-1}}{r^5} + \frac{3x_\mathrm{D}\sum_{j\setminus \mathrm{D}} x_j^2 - \sum_{j\setminus \mathrm{D}} r^2 x_\mathrm{D}}{r^5} = -(\mathrm{D}-1)\frac{x_\mathrm{D}}{r^3}. \tag{249}$$

Considering $\frac{x_\mathrm{D}}{r} = \mu$ and $\frac{r_{\mathrm{D}-1}}{r} = \sqrt{1-\mu^2}$, i.e., $\frac{x_\mathrm{D}}{r^3} = \frac{\mu}{r^2}$ and $\frac{r_{\mathrm{D}-1}^2}{r^4} = \frac{1-\mu^2}{r^2}$, the axisymmetric Laplacian $\triangle_\mu$ becomes

$$r^2 \triangle_\mu = (1-\mu^2)\frac{\mathrm{d}^2}{\mathrm{d}\mu^2} - (\mathrm{D}-1)\,\mu\,\frac{\mathrm{d}}{\mathrm{d}\mu}. \tag{250}$$

We can re-write the axisymmetric Laplacian (which can be proven using the chain rule), involving the definition $\alpha = \frac{\mathrm{D}-3}{2}$, and $w(\mu) = (1-\mu^2)^\alpha$, see Sec. E

$$r^2 \triangle_\mu\ f = (1-\mu^2)\frac{\mathrm{d}^2}{\mathrm{d}\mu^2} - 2(\alpha+1)\,\mu\,\frac{\mathrm{d}}{\mathrm{d}\mu} \tag{251}$$

$$= \frac{1}{(1-\mu^2)^\alpha}\frac{\mathrm{d}}{\mathrm{d}\mu}\left[(1-\mu^2)^{\alpha+1}\frac{\mathrm{d}}{\mathrm{d}\mu}f\right] = \frac{1}{w(\mu)}\frac{\mathrm{d}}{\mathrm{d}\mu}\left[(1-\mu^2)\,w(\mu)\,\frac{\mathrm{d}}{\mathrm{d}\mu}f\right]. \tag{252}$$

E Jacobi determinant of axisymmetric coordinates

For the axisymmetric coordinate μ, we re-write the integration constants $\prod_{j=1}^{\mathrm{D}} \mathrm{d}x_j = |\boldsymbol{J}|\,\mathrm{d}\mu \prod_{j=1}^{\mathrm{D}-1} \mathrm{d}\tilde{x}_j$ with the determinant of the *Jacobian* matrix that describes how the surface element is stretched. The Jacobi matrix is filled with derivatives of the old coordinates with regard to the new ones. One of the new coordinates is μ that defines $x_{\mathrm{D}} = r\,\mu$. The other $\mathrm{D}-1$ coordinates are just copies of x_j but normalized to preserve the information about the radius as the new radius $r = \sqrt{\sum_i \tilde{x}_i^2}$ of the $(\mathrm{D}-1)$-dimensional subspace. This defines

$$x_{\mathrm{D}} = \mu\, r, \qquad\qquad x_j = \tilde{x}_j \sqrt{1-\mu^2}, \tag{253}$$

and herewith the derivatives for $\boldsymbol{J}$ are

$$\boldsymbol{J} = \begin{bmatrix} \left[\frac{\partial x_j}{\partial \tilde{x}_i}\right]_{i,j<\mathrm{D}}, & \left[\frac{\partial x_{\mathrm{D}}}{\partial \tilde{x}_i}\right]_{i<\mathrm{D}} \\ \left[\frac{\partial x_j}{\partial \mu}\right]_{j<\mathrm{D}} & \frac{\partial x_{\mathrm{D}}}{\partial \mu} \end{bmatrix} = \begin{bmatrix} \mathbf{I}\sqrt{1-\mu^2}, & \left[\frac{\mu\,\tilde{x}_i}{r}\right]_{i<\mathrm{D}} \\ \left[-\frac{\tilde{x}_j\,\mu}{\sqrt{1-\mu^2}}\right]_{j<\mathrm{D}} & r \end{bmatrix}, \tag{254}$$

which makes the determinant particularly simple to calculate: (i) the determinant of a product of matrices is the product of the determinantes, (2) for a block-triangular matrix, the product of the diagonal blocks would be the determinant. A block-matrix $\boldsymbol{E}$ can be made block-triangular by LU decomposition

$$\boldsymbol{J} = \begin{bmatrix} \boldsymbol{A} & \boldsymbol{B} \\ \boldsymbol{C} & \boldsymbol{D} \end{bmatrix} = \begin{bmatrix} \boldsymbol{A} & \boldsymbol{0} \\ \boldsymbol{C} & \boldsymbol{I} \end{bmatrix} \begin{bmatrix} \boldsymbol{I} & \boldsymbol{A}^{-1}\boldsymbol{B} \\ \boldsymbol{0} & \boldsymbol{D} - \boldsymbol{C}\boldsymbol{A}^{-1}\boldsymbol{B} \end{bmatrix},$$
$$\text{so that } \det \boldsymbol{J} = \det \boldsymbol{A}\, \det(\boldsymbol{D} - \boldsymbol{C}\boldsymbol{A}^{-1}\boldsymbol{B}). \tag{255}$$

We get the weight of the integration constant $|\boldsymbol{J}|\,\mathrm{d}\mu$:

$$|\boldsymbol{J}| = \sqrt{1-\mu^2}^{\mathrm{D}-1} \left(r + \frac{1}{\sqrt{1-\mu^2}} \sum_j \frac{\mu\,\tilde{x}_j}{r} \frac{\mu\,\tilde{x}_j}{\sqrt{1-\mu^2}} \right) \tag{256}$$

$$= \frac{\sqrt{1-\mu^2}^{\mathrm{D}-1}}{r} \left(1 + \frac{\mu^2 r^2}{r^2(1-\mu^2)} \right) = \frac{\sqrt{1-\mu^2}^{\mathrm{D}-3}}{r} = \frac{w(\mu)}{r}. \tag{257}$$

F Axisymmetric solutions with Frobenius approach

With $\alpha = \frac{\mathrm{D}-3}{2}$, the Laplacian differential equation for purely axisymmetric functions

$$(1-\mu^2)\frac{\mathrm{d}^2 f}{\mathrm{d}\mu^2} - 2(\alpha+1)\,\mu\,\frac{\mathrm{d}f}{\mathrm{d}\mu} + \lambda\, f = 0$$

is solved for functions that are power series (Frobenius Ansatz)

$$f = \sum_{k=0}^{\infty} c_k\, \mu^k.$$

Inserted into the differential equation, we can simplify, shift the indices k to fit the powers μ^k, and find by comparison of coefficients.

$$(1-\mu^2)\sum_{k=2}^{\infty} c_k\, k\,(k-1)\,\mu^{k-2} - 2(\alpha+1)\,\mu\sum_{k=1}^{\infty} c_k\, k\,\mu^{k-1} + \lambda\sum_{k=0}^{\infty} c_k\,\mu^k = 0$$

$$\sum_{k=2}^{\infty} c_k\, k\,(k-1)\,\mu^{k-2} - \sum_{k=2}^{\infty} c_k\, k\,(k-1)\,\mu^{k} - 2(\alpha+1)\sum_{k=1}^{\infty} c_k\, k\,\mu^{k} + \lambda\sum_{k=0}^{\infty} c_k\,\mu^k = 0$$

$$\sum_{k=0}^{\infty} c_{k+2}\,(k+1)\,(k+1)\,\mu^{k} - \sum_{k=2}^{\infty} c_k\, k\,(k-1)\,\mu^{k} - 2(\alpha+1)\sum_{k=1}^{\infty} c_k\, k\,\mu^{k} + \lambda\sum_{k=0}^{\infty} c_k\,\mu^k = 0$$

$$\sum_{k=0}^{\infty}\Big\{\big[\lambda - k\,(k-1)\,u[k-2] - 2(\alpha+1)\,k\,u[k-1]\big]\,c_k + (k+1)\,(k+2)\,c_{k+2}\Big\}\mu^k = 0$$

$$c_{k+2} = \frac{2(\alpha+1)\,k + k\,(k-1) - \lambda}{(k+1)(k+2)}\,c_k. \quad \text{for } k \geq 2$$

$$\Longrightarrow c_{k+2} = \frac{k(k+2\alpha+1)\,k - \lambda}{(k+1)(k+2)}\,c_k. \quad \text{for } k \geq 2$$

Choosing $\lambda = \lambda_n = n(n+2\alpha+1)$, the series terminates at $k = n$. The recurrence of the coefficients for a certain n can be re-written to

$$c^{(n)}_{k+2} = \frac{k^2 + (2\alpha+1)\,k - n^2 - (2\alpha+1)n}{(k+1)(k+2)}\,c_k = \frac{(k-n)(k+n+2\alpha+1)}{(k+1)(k+2)}\,c^{(n)}_k.$$

For even $n = 2m$, odd-order coefficients vanish $c^{(2m)}_{2l+1} = 0$ and for odd $n = 2m+1$, coefficients of even powers vanish $c^{(2m+1)}_{2l}$. The non-zero coefficient series are composed factorials and double factorials (containing every second factor) when applying the recurrence repeatedly, and they are either based on a starting value $c^{(n)}_0$ or $c^{(n)}_1$. If we desire the polynomials to be $\mathcal{P}_n(1) = 1$, we require $\sum_{k=0}^{n} c^{(n)}_k\, 1^k = \sum_{k=0}^{n} c^{(n)}_k = 1$, what defines the common factor $c^{(n)}_{\mathrm{mod}_{n,2}}$ of the polynomial coefficients $c^{(n)}_k$.

F.1 Coefficients for a couple of Gegenbauer polynomials

Typically the first two polynomials are set to

$$\mathcal{P}_0 = 1, \qquad\qquad \mathcal{P}_1 = \mu,$$

fulfilling $\mathcal{P}_n(1) = 1$, so obviously

$$c^{(0)}_0 = 1,$$
$$c^{(1)}_1 = 1.$$

For the next polynomial we have

$$\mathcal{P}_2 = c^{(2)}_2\,\mu^2 + c^{(2)}_0\,\mu^0,$$

so for the desire $\mathcal{P}_2(1)=1$, we require $c_2^{(2)}+c_0^{(2)}=1$. Moreover the recurrence $c_{k+2}^{(n)}=\frac{(k-n)(k+n+\mathrm{D}-2)}{(k+1)(k+2)}c_k^{(n)}=-\frac{n(n+\mathrm{D}-2)-k(k+\mathrm{D}-2)}{(k+1)(k+2)}c_k^{(n)}$ for $k=0$ and $n=2$ yields

$$c_2^{(2)}+c_0^{(2)}=1,\qquad c_2^{(2)}=-\mathrm{D}\,c_0^{(2)},\qquad \Longrightarrow c_0^{(2)}=-\frac{1}{\mathrm{D}-1},\qquad c_2^{(2)}=\frac{\mathrm{D}}{\mathrm{D}-1}.$$

Doing the same for $k=1$ and $n=3$ yields

$$c_3^{(3)}+c_1^{(3)}=1,\qquad c_3^{(3)}=-\frac{\mathrm{D}+2}{3}\,c_1^{(3)},\qquad \Longrightarrow c_1^{(3)}=-\frac{3}{\mathrm{D}-1},\qquad c_3^{(3)}=\frac{\mathrm{D}+2}{\mathrm{D}-1}.$$

And with one more term for $k=0,2$ and $n=4$ this yields

$$1=c_4^{(4)}+c_2^{(4)}+c_0^{(4)},\qquad c_2^{(4)}=-2(\mathrm{D}+2)\,c_0^{(4)},\qquad c_4^{(4)}=\frac{(\mathrm{D}+2)(\mathrm{D}+4)}{3}\,c_0^{(4)}$$
$$c_0^{(4)}=-\frac{3}{(\mathrm{D}-1)(\mathrm{D}+1)},\qquad c_2^{(4)}=\frac{6(\mathrm{D}+2)}{(\mathrm{D}-1)(\mathrm{D}+1)},\qquad c_4^{(4)}=-\frac{(\mathrm{D}+2)(\mathrm{D}+4)}{(\mathrm{D}-1)(\mathrm{D}+1)}.$$

For $k=1,3$ and $n=5$ it is

$$1=c_5^{(5)}+c_3^{(5)}+c_1^{(5)},\qquad c_3^{(5)}=-\frac{2(\mathrm{D}+4)}{3}\,c_1^{(5)},\qquad c_5^{(5)}=\frac{(\mathrm{D}+4)(\mathrm{D}+6)}{15}\,c_1^{(5)}$$
$$c_1^{(5)}=\frac{15}{(\mathrm{D}-1)(\mathrm{D}+1)},\qquad c_3^{(5)}=-\frac{10(\mathrm{D}+4)}{(\mathrm{D}-1)(\mathrm{D}+1)},\qquad c_5^{(5)}=\frac{(\mathrm{D}+4)(\mathrm{D}+6)}{(\mathrm{D}-1)(\mathrm{D}+1)}.$$

As this way to find coefficients is a bit tedious, there are more elegant ways.

A more specific definition of $\mathcal{P}_n$ of reasonably low mathematical effort is only reasonable after discussing orthogonality of the polynomials and orthogonal polynomials in general.

G Orthogonality of axisymmetric harmonics

The axisymetric Laplacian differential equation $(1-\mu^2)\mathcal{P}_n''-(\mathrm{D}-1)\,\mu\,\mathcal{P}_n'+\lambda_n\,\mathcal{P}_n=0$ with $\lambda_n=n(n+2\alpha+1)$ can be re-written compactly as

$$\frac{1}{w(\mu)}\left[(1-\mu^2)\,w(\mu)\,\mathcal{P}_n'\right]'+\lambda_n\mathcal{P}_n=0. \tag{258}$$

Multiplied by another solution $\mathcal{P}_m$ and integrated over $w(\mu)\,\mathrm{d}\mu$ it becomes

$$\int_{-1}^{1}\left[(1-\mu^2)\,w(\mu)\,\mathcal{P}_n'\right]'\mathcal{P}_m\,\mathrm{d}\mu+\lambda_n\int_{-1}^{1}\mathcal{P}_n\,\mathcal{P}_m\,w(\mu)\,\mathrm{d}\mu=0.$$

The first expression can be dealt with using partial integration $\int f'g=fg-\int fg'$:

$$\int_{-1}^{1}\left[(1-\mu^2)\,w(\mu)\,\mathcal{P}_n'\right]'\mathcal{P}_m\,\mathrm{d}\mu=(1-\mu^2)\,w(\mu)\,\mathcal{P}_n'\,\mathcal{P}_m\Big|_{-1}^{1}-\int_{-1}^{1}(1-\mu^2)\,w(\mu)\,\mathcal{P}_n'\,\mathcal{P}_m'\,\mathrm{d}\mu.$$

In our case $\mathrm{D} > 1$, i.e. $\alpha > -1$, the first expression $(1-\mu^2)\,w(\mu) = (1-\mu^2)^{\alpha+1} = 0$ vanishes for the boundaries $\mu = \pm 1$ while the polynomial $\mathcal{P}_n'\mathcal{P}_m$ stays finite. We get

$$-\int_{-1}^{1}(1-\mu^2)\,w(\mu)\,\mathcal{P}_n'\,\mathcal{P}_m'\,\mathrm{d}\mu + \lambda_n\int_{-1}^{1}\mathcal{P}_n\,\mathcal{P}_m\,w(\mu)\,\mathrm{d}\mu = 0.$$

To show that the solutions $\mathcal{P}_n$ and $\mathcal{P}_m$ with $n \neq m$ are orthogonal, we subtract from this a similar equation, the one with the roles of $\mathcal{P}_n$ and $\mathcal{P}_m$ interchanged ($\mathcal{P}_m$ is inserted into its defining differential equation, multiplied with $\mathcal{P}_n$ and integrated). This cancels the first term and we get:

$$(\lambda_n - \lambda_m)\int_{-1}^{1}\mathcal{P}_n\,\mathcal{P}_m\,w(\mu)\,\mathrm{d}\mu = 0. \tag{259}$$

If the indices match $n = m$, the first term vanishes and the integral needs not vanish. For different indices $n \neq m$ our Eivenvalues are unique as $\lambda_n = n(n+\mathrm{D}-2)$, hence $\lambda_n \neq \lambda_m$, so the first term won't vanish, consequently the integral must vanish:

Any pair of solutions $\mathcal{P}_n$ and $\mathcal{P}_m$ with different index $n \neq m$ is orthogonal under the integration weight $w(\mu) = (1-\mu^2)^{\alpha}$.

H Orthogonal polynomials

A set of orthogonal polynomials $\mathcal{P}_n(\mu)$ sorted by their degree n, up to which they contain powers of the variable $\mathcal{P}_n = \sum_{k=0}^{n} c_{n,k}\,\mu^k$ can naturally be used to re-expand any other limited-degree polynomial $\mathscr{P}_n = \sum_{k=0}^{n} c_k\,\mu^k$:

$$\mathscr{P}_n(\mu) = \sum_{m=0}^{n}\gamma_m\,\mathcal{P}_m(\mu). \tag{260}$$

This is not surprising. What makes orthogonal polynomials useful is their orthogonality on the interval $[a,b]$:

$$\int_a^b \mathcal{P}_n(\mu)\mathcal{P}_m(\mu)\;w(\mu)\,\mathrm{d}\mu = \begin{cases} 0 & \text{for } n \neq m, \\ N_n^2 & \text{for } n = m. \end{cases} \tag{261}$$

Here, $N_n^2 = \int_a^b \mathcal{P}_n^2(\mu)\;w(\mu)\,\mathrm{d}\mu$ is the squared magnitude of each function integrated over the entire interval.

Note that by the ability of order-limited polynomials $\mathcal{P}_{m<n}$ to express any m^{th}-order polynomial with $m < n$, the orthogonality automatically extendeds to *any* lower-order polynomial $\mathscr{P}_{m<n} = \sum_{l=0}^{m}\gamma_l\,\mathcal{P}_l$

$$\int_a^b \mathcal{P}_n(\mu)\mathscr{P}_{m<n}(\mu)\;w(\mu)\,\mathrm{d}\mu = 0. \tag{262}$$

H.1 The transform integral: a benefit of orthogonality

The orthogonality allows to decompose any given function $g(\mu)$ into coefficients γ_m of the orthogonal polynomials rather easily by an integral transformation. We write down the decomposition that we desire and integrate over a test function $\mathcal{P}_n(\mu)w(\mu)\mathrm{d}\mu \int$. Orthogonality simplifies the expression that we get

$$\begin{aligned} g(\mu) &= \sum_{m=0}^{\infty} \gamma_m \, \mathcal{P}_m(\mu) \qquad\qquad \Big| \; \mathcal{P}_n(\mu) w(\mu) \mathrm{d}\mu \int_a^b \\ \int_a^b g(\mu)\, \mathcal{P}_n(\mu)\; w(\mu)\, \mathrm{d}\mu &= \sum_{m=0}^{\infty} \gamma_m \underbrace{\int_a^b \mathcal{P}_m(\mu) \mathcal{P}_n(\mu)\; w(\mu)\, \mathrm{d}\mu}_{N_n^2 \delta_{nm}} = N_n^2\, \gamma_n, \end{aligned}$$

We hereby found the expansion coefficients by the integral without matrix inversion. The transform pair is:

$$g(\mu) = \sum_{m=0}^{\infty} \gamma_m \, \mathcal{P}_m(\mu) \qquad\qquad \gamma_n = \frac{1}{N_n^2} \int_a^b g(\mu)\, \mathcal{P}_n(\mu)\; w(\mu)\, \mathrm{d}\mu. \tag{263}$$

As infinitely many orthogonal polynomials consist of any power μ^k with $k = 0, 1, 2, \ldots, \infty$, the representation is able to represent any function that can be described by an infinite power series.

H.2 Symetries and interval $-1 \le \mu \le 1$.

If $-a = b = 1$ and $w(\mu) = w(-\mu)$, the integration range and integration weight is symmetrical. We can re-write the orthogonality condition

$$\begin{aligned} \int_{-1}^{1} \mathcal{P}_n\, \mathcal{P}_m\; w\, \mathrm{d}\mu = & \int_{-1}^{0} \mathcal{P}_n(\mu)\, \mathcal{P}_m(\mu)\; w(\mu)\, \mathrm{d}\mu + \int_{0}^{1} g(\mu)\, \mathcal{P}_n(\mu)\; w(\mu)\, \mathrm{d}\mu \\ = & -\int_{0}^{-1} \mathcal{P}_n(\mu)\, \mathcal{P}_m(\mu)\; w(\mu)\, \mathrm{d}\mu + \int_{0}^{1} \mathcal{P}_n(\mu)\, \mathcal{P}_m(\mu)\; w(\mu)\, \mathrm{d}\mu \\ = & -\int_{0}^{1} \mathcal{P}_n(-\mu)\, \mathcal{P}_m(-\mu)\; w(-\mu)\, \mathrm{d}(-\mu) + \int_{0}^{1} \mathcal{P}_n(\mu)\, \mathcal{P}_m(\mu)\; w(\mu)\, \mathrm{d}\mu \\ = & \int_{0}^{1} \mathcal{P}_n(-\mu)\, \mathcal{P}_m(-\mu)\; w(\mu)\, \mathrm{d}\mu + \int_{0}^{1} \mathcal{P}_n(\mu)\, \mathcal{P}_m(\mu)\; w(\mu)\, \mathrm{d}\mu \\ = & \int_{0}^{1} \underbrace{\Big[\mathcal{P}_n(-\mu)\, \mathcal{P}_m(-\mu) + \mathcal{P}_n(\mu)\, \mathcal{P}_m(\mu)\Big]}_{=0 \text{ for } n \neq m} \; w(\mu)\, \mathrm{d}\mu = N_n^2\, \delta_{nm}. \end{aligned} \tag{264}$$

The expression in brackets $[\mathcal{P}_n(-\mu)\, \mathcal{P}_m(-\mu) + \mathcal{P}_n(\mu)\, \mathcal{P}_m(\mu)]$ vanishes whenever exclusively one of the two functions is odd, either $\mathcal{P}_n(-\mu) = -\mathcal{P}_n(\mu)$ or $\mathcal{P}_m(-\mu) = -\mathcal{P}_m(\mu)$,

while the other one is even. The highest power in a polynomial corresponds to its degree, odd powers of μ^{2k+1} to odd function, even powers of μ^{2k} to even functions, so consequently orthogonal polynomials for the interval $-1 \leq \mu \leq 1$ and weight $w(-\mu) = w(\mu)$ become alternatingly even and odd in m to obtain orthogonality: Odd-degree orthogonal polynomials contain only odd powers, even-degree orthogonal polynomials only even powers.

H.3 Three-term recurrence of orthogonal polynomials

Normally, we define $\mathcal{P}_0(\mu) = 1$ and any higher-degree polynomial by a simple recurrence relation, hence based on the lower order polynomials. Finding the recurrence relation requires some consideration.

Orthogonality yields that we don't need an orthogonal polynomial of the n^{th} degree $\mathcal{P}_n(\mu)$ to represent an arbitrary lower-degree polynomial $\mathscr{P}_{m<n}(\mu)$. This becomes clear when expanding the polynomial $\mathscr{P}_{m<n}(\mu) = \sum_{k=0}^{m<n} \beta_k \mathcal{P}_k(\mu)$ and considering the transform integral with $\mathcal{P}_n$ vanishing $\int \mathcal{P}_{k<n}\mathcal{P}_n = 0$ for every term because of orthogonality. We may write

$$\int_a^b \mathscr{P}_{m<n}(\mu)\, \mathcal{P}_n(\mu)\; w(\mu)\, \mathrm{d}\mu = 0. \tag{265}$$

After multiplication with μ, an orthogonal polynomial of degree $n-1$ becomes an n^{th}-degree polynomial

$$\mu\, \mathcal{P}_{n-1}(\mu) = \mathscr{P}_n(\mu). \tag{266}$$

We can find the expansion coefficients, β_m, thereof into orthogonal polynomials by integrating $\mu\, \mathcal{P}_{n-1}(\mu)$ over $\mathcal{P}_m(\mu)$. By applying the knowledge from above, we see which coefficients must vanish:

$$\beta_{m<n-2} = \frac{1}{N^2_{m<n-2}} \int_a^b \overbrace{\mathcal{P}_{m<n-2}(\mu)\, \mu}^{\mathscr{P}_{m<n-1}(\mu)}\, \mathcal{P}_{n-1}(\mu)\; w(\mu)\, \mathrm{d}\mu = 0,$$

$$\beta_{m>n} = \frac{1}{N^2_{m>n}} \int_a^b \mathcal{P}_{m>n}(\mu)\; \underbrace{\mu\, \mathcal{P}_{n-1}(\mu)}_{\mathscr{P}_n(\mu)}\; w(\mu)\, \mathrm{d}\mu = 0.$$

Obviously, $\mu\, \mathcal{P}_{n-1}(\mu)$ only consists of $\mathcal{P}_m(\mu)$ with $m = n-2, n-1, n$: *Any set of orthogonal polynomials obeys a three-term recurrence:*

$$\mu\, \mathcal{P}_{n-1}(\mu) = \beta_n^{(n)}\, \mathcal{P}_n(\mu) + \beta_{n-1}^{(n)}\, \mathcal{P}_{n-1}(\mu) + \beta_{n-2}^{(n)}\, \mathcal{P}_{n-2}(\mu) \tag{267}$$

that can be used as $\mathcal{P}_n(\mu) = \frac{1}{\beta_n^{(n)}} \Big[\big(\mu - \beta_{n-1}^{(n)}\big)\, \mathcal{P}_{n-1}(\mu) - \beta_{n-2}^{(n)}\, \mathcal{P}_{n-2}(\mu) \Big]$ to calculate higher-order polynomials based on the lower-order ones. The recurrence reduces for $-a = b = 1$ and $w(-\mu) = w(\mu)$ as this requires $\mathcal{P}_n$ to only contain even or odd powers of μ,

$$\mu\, \mathcal{P}_{n-1}(\mu) = \beta_n^{(n)}\, \mathcal{P}_n(\mu) + \beta_{n-2}^{(n)}\, \mathcal{P}_{n-2}(\mu). \tag{268}$$

If we normalize the polynomials to $\mathcal{P}_n(1) = 1$ for all n, this imposes the condition that $\beta_n^{(n)} + \beta_{n-2}^{(n)} = 1$, so that $\beta_{n-2}^{(n)} = 1 - \beta_n^{(n)}$. We skip the superscript and write β_n for the recurrence coefficient,

$$\mu\,\mathcal{P}_{n-1}(\mu) = \beta_n\,\mathcal{P}_n(\mu) + (1-\beta_n)\,\mathcal{P}_{n-2}(\mu). \tag{269}$$

We obtain the recurrence coefficient β_n from comparing coefficients of the highest powers in $\mathcal{P}_n$ and $\mathcal{P}_{n-1}$. This is done based on the coefficient recurrence for $c_n^{(n)}$,

$$\beta_n\,c_n^{(n)} = c_{n-1}^{(n-1)} \Longrightarrow \beta_n = \frac{c_{n-1}^{(n-1)}}{c_n^{(n)}}.$$

H.4 Squared Norm of Orthogonal Polynomials

According to Law and Sledd [LS75], the recurrence coefficient β_n can also be used to evaluate the normalization $N_n^2 = \int_{-1}^{1} \mathcal{P}_n(\mu)\,w(\mu)\,\mathrm{d}\mu$ of the polynomial recursively. This is done by re-formulating the three-term recurrence to

$$\mathcal{P}_n = (A_n\mu + B_n)\mathcal{P}_{n-1} - C_n\mathcal{P}_{n-2}. \tag{270}$$

Law and Sledd's derivation is based on explicitly evaluating only the first term of the recurrence until $\mathcal{P}_0 = 1$, while the rest must stay some polynomial of the degree $n-1$

$$\mathcal{P}_n = A_n\mu\mathcal{P}_{n-1} + \mathscr{A}_{n-1} = A_nA_{n-1}\mu^2\mathcal{P}_{n-2} + \mathscr{B}_{n-1} = A_nA_{n-1}\ldots A_1\mu^n + \mathscr{C}_{n-1},$$

or more neatly

$$\mu^n = (A_nA_{n-1}\ldots A_1)^{-1}\mathcal{P}_n + \mathscr{P}_{n-1}. \tag{271}$$

Integration over $\mathcal{P}_n\,w\,\mathrm{d}\mu$ $\int_a^b$ yields

$$\int_a^b \mu^n\mathcal{P}_n\,w\,\mathrm{d}\mu = (A_nA_{n-1}\ldots A_1)^{-1}\underbrace{\int_a^b \mathcal{P}_n^2\,w\,\mathrm{d}\mu}_{=N_n^2} + \underbrace{\int_a^b \mathscr{P}_{n-1}\,\mathcal{P}_n\,w\,\mathrm{d}\mu}_{=0}$$

$$\int_a^b \mu^n\mathcal{P}_n\,w\,\mathrm{d}\mu = (A_nA_{n-1}\ldots A_1)^{-1}\,N_n^2. \tag{272}$$

$\mu^n\mathcal{P}_n$ is re-expressed by re-arranging Eq. (270) to $\mu\mathcal{P}_n = A_{n+1}^{-1}[\mathcal{P}_{n+1} - B_{n+1}\mathcal{P}_n + C_{n+1}\mathcal{P}_{n-1}]$ and multiplication with $\mu^{n-1} = (A_{n-1}\ldots A_1)^{-1}[\mathcal{P}_{n-1}+\mathscr{P}_{n-2}]$ from Eq. (271),

$$\begin{aligned}\int_a^b \mu^n\mathcal{P}_n\,w\,\mathrm{d}\mu &= \frac{\int_a^b[\mathcal{P}_{n+1} - B_{n+1}\mathcal{P}_n + C_{n+1}\mathcal{P}_{n-1}][\mathcal{P}_{n-1} + \mathscr{P}_{n-2}]\,w\,\mathrm{d}\mu}{A_{n+1}(A_{n-1}\ldots A_1)}\\ &= \frac{C_{n+1}}{A_{n+1}(A_{n-1}\ldots A_1)}\underbrace{\int_a^b \mathcal{P}_{n-1}^2\,w\,\mathrm{d}\mu}_{=N_{n-1}^2}.\end{aligned} \tag{273}$$

Together with Eq. (272), we get

$$N_{n-1}^2 = \frac{C_{n+1}A_n}{A_{n+1}} N_{n-1}^2, \tag{274}$$

which is in our symmetric and normalized case with $\beta_n \mathcal{P}_n(\mu) = \mu\mathcal{P}_{n-1} - (1-\beta_n)\mathcal{P}_{n-2}$ hence $A_n = \frac{1}{\beta_n}$, $B_n = 0$, and $C_n = \frac{1-\beta_n}{\beta_n}$,

$$N_n^2 = \frac{1-\beta_{n+1}}{\beta_n} N_{n-1}^2. \tag{275}$$

H.5 Rodrigues' formula for Gegenbauer polynomials.

The French mathematician Rodrigues provided an formular for the Legendre polynomials that are orthogonal using the integral measure $w(\mu) = 1$. A general Rodrigues formula for a more arbitrary measure $w(\mu) = (1-\mu^2)^\alpha$ can be given to specify the corresponding orthogonal polynomials $\mathcal{P}_n$

$$\mathcal{P}_n = \frac{e_n}{w(\mu)} \frac{\mathrm{d}^n}{\mathrm{d}\mu^n} \left[w(\mu)\,(1-\mu^2)^n \right] = \frac{e_n}{(1-\mu^2)^\alpha} \frac{\mathrm{d}^n}{\mathrm{d}\mu^n} (1-\mu^2)^{\alpha+n}, \tag{276}$$

where e_n is a normalization factor.

Proof. To prove the Rodrigues formula, we substitute $y = (1-\mu^2)$ for simplification and re-formulate the fact that $\mathcal{P}_n$ is always orthogonal to any arbitrary lower-order polynomial (see Eq. (262) in Sec. H):

$$e_n \int_{-1}^{1} \mathcal{P}_n \mathscr{P}_{m<n} \underbrace{w(\mu)}_{=y^\alpha} \mathrm{d}\mu = 0. \tag{277}$$

For the proof, we insert the Rodrigues formula $\frac{1}{y^\alpha}\frac{\mathrm{d}^n}{\mathrm{d}\mu^n} y^{\alpha+n}$ without e_n, yielding

$$\int_{-1}^{1} \frac{\mathrm{d}^n}{\mathrm{d}\mu^n} y^{\alpha+n}\, \mathscr{P}_{m<n}\, \mathrm{d}\mu = 0.$$

Repeated integration by parts always causes the first term to vanish, since $\frac{\mathrm{d}^l}{\mathrm{d}\mu^l} y^{\alpha+n}$ is always zero at $\mu = \pm 1$ whenever $\alpha > 1$ and $l < n$, while $\mathcal{P}_n$ and $\mathscr{P}_{m<n}$ stay finite:

$$\begin{aligned}
\int_{-1}^{1} \frac{\mathrm{d}^n y^{\alpha+n}}{\mathrm{d}\mu^n}\, \mathscr{P}_{m<n}\, \mathrm{d}\mu &= \overbrace{\frac{\mathrm{d}^{n-1} y^{\alpha+n}}{\mathrm{d}\mu^{n-1}}\, \mathscr{P}_{m<n}\Big|_{-1}^{1}}^{=0} - \int_{-1}^{1} \frac{\mathrm{d}^{n-1} y^{\alpha+n}}{\mathrm{d}\mu^{n-1}} \frac{\mathrm{d}\mathscr{P}_{m<n}}{\mathrm{d}\mu}\, \mathrm{d}\mu \\
&= -\overbrace{\frac{\mathrm{d}^{n-2} y^{\alpha+n}}{\mathrm{d}\mu^{n-2}} \frac{\mathrm{d}\mathscr{P}_{m<n}}{\mathrm{d}\mu}\Big|_{-1}^{1}}^{=0} + \int_{-1}^{1} \frac{\mathrm{d}^{n-2} y^{\alpha+n}}{\mathrm{d}\mu^{n-2}} \frac{\mathrm{d}^2\mathscr{P}_{m<n}}{\mathrm{d}\mu^2}\, \mathrm{d}\mu = \dots \\
&= (-1)^n \int_{-1}^{1} y^{\alpha+n} \underbrace{\frac{\mathrm{d}^n \mathscr{P}_{m<n}}{\mathrm{d}\mu^n}}_{=0}\, \mathrm{d}\mu = 0.
\end{aligned}$$

The above proof means that the Rodrigues formula produces a function orthogonal to any lower-order polynomial. For formal completeness, we show $\mathcal{P}_n$ to be an n^{th} order polynomial by repeatedly deriving using $\frac{\mathrm{d}}{\mathrm{d}x}y^b = \left(\frac{\mathrm{d}y}{\mathrm{d}x}\right)\frac{\mathrm{d}}{\mathrm{d}y}y^b$

$$\begin{aligned}
\mathcal{P}_n(\mu) &= \frac{e_n}{y^\alpha}\frac{\mathrm{d}^n}{\mathrm{d}\mu^n}y^b = \frac{1}{y^\alpha}\frac{\mathrm{d}^{n-1}}{\mathrm{d}\mu^{n-1}}\left\{\left[\frac{\mathrm{d}y}{\mathrm{d}\mu}\right]\frac{\mathrm{d}y^b}{\mathrm{d}y}\right\}\\
&= \frac{e_n}{y^\alpha}\frac{\mathrm{d}^{n-2}}{\mathrm{d}\mu^{n-2}}\left\{\left[\frac{\mathrm{d}y}{\mathrm{d}\mu}\right]^2\frac{\mathrm{d}^2y^b}{\mathrm{d}y^2} + \left[\frac{\mathrm{d}}{\mathrm{d}\mu}\left[\frac{\mathrm{d}y}{\mathrm{d}\mu}\right]\right]\frac{\mathrm{d}y^b}{\mathrm{d}y}\right\}\\
&= \frac{e_n}{y^\alpha}\frac{\mathrm{d}^{n-3}}{\mathrm{d}\mu^{n-3}}\left\{\left[\frac{\mathrm{d}y}{\mathrm{d}\mu}\right]^3\frac{\mathrm{d}^3y^b}{\mathrm{d}\mu^3} + \left[\frac{\mathrm{d}}{\mathrm{d}\mu}\left[\frac{\mathrm{d}y}{\mathrm{d}\mu}\right]^2\right]\frac{\mathrm{d}^2y^b}{\mathrm{d}y^2} + \left[\frac{\mathrm{d}^2}{\mathrm{d}\mu^2}\left[\frac{\mathrm{d}y}{\mathrm{d}\mu}\right]^1\right]\frac{\mathrm{d}^1y^b}{\mathrm{d}y^1}\right\}\\
&= \frac{e_n}{y^\alpha}\sum_{k=0}^{n}\left[\frac{\mathrm{d}^k}{\mathrm{d}\mu^k}\left[\frac{\mathrm{d}y}{\mathrm{d}\mu}\right]^{n-k}\right]\frac{\mathrm{d}^{n-k}y^b}{\mathrm{d}y^{n-k}}
\end{aligned}$$

To evaluate $\frac{\mathrm{d}^k}{\mathrm{d}\mu^k}\left[\frac{\mathrm{d}y}{\mathrm{d}\mu}\right]^{n-k}$, we insert $\frac{\mathrm{d}y}{\mathrm{d}\mu} = -2\mu$ and get

$$(-2)^{n-k}\frac{\mathrm{d}^k}{\mathrm{d}\mu^k}\mu^{n-k} = \begin{cases}(-2)^{n-k}\frac{(n-k)!}{(n-2k)!}\mu^{n-2k}, & \text{if } 2k \le n\\ 0, & \text{else.}\end{cases} \tag{278}$$

The falling factorials $(a)_k = (a)\cdot(a-1)\ldots(a-k+1)$ allow to write $\frac{\mathrm{d}^k y^b}{\mathrm{d}y^k} = (b)_k y^{b-k}$, and we finally get a polynomial in which the factor $y^{-\alpha}$ reduces $y^{\alpha+n-k}$ to y^{n-k}:

$$\mathcal{P}_n(\mu) = e_n\sum_{k=0}^{\frac{n}{2}}\frac{(-2)^{n-k}(n-k)!(\alpha+n)_k}{(n-2k)!}(1-\mu^2)^{n-k}\mu^{n-2k}. \tag{279}$$

We may use the binomial coefficient $\frac{n!}{k!(n-k)!}$ to get

$$\mathcal{P}_n(\mu) = e_n(-1)^n\sum_{k=0}^{\frac{n}{2}}\frac{(-2)^k(n-k)!(\alpha+n)_k}{(n-2k)!}\sum_{l=0}^{n-k}(-1)^l\frac{(n-k)!}{l!(n-k-l)!}\mu^{2l}\mu^{n-2k} \tag{280}$$

$$= e_n\sum_{k=0}^{\frac{n}{2}}\frac{(-2)^{n-k}(n-k)!(\alpha+n)_k}{(n-2k)!}\sum_{l=0}^{n-k}(-1)^l\frac{(n-k)!}{l!(n-k-l)!}\mu^{n-2(k-l)} \tag{281}$$

Rcurrences based on Rodrigues formula.

H.6 Three-term recurrence for Gegenbauer polynomials

To obtain the missing term β_n of the general three-term recurrence for orthogonal polynomials with $w(\mu) = w(-\mu)$ and $-a = b = 1$, we need to resolve $\beta_n = \frac{c_{n-1}^{(n-1)}}{c_n^{(n)}}$. From the coefficients in Appendix F.1, we obtain

$$\beta_2 = \frac{\mathrm{D}-1}{\mathrm{D}}, \qquad \beta_3 = \frac{\mathrm{D}}{\mathrm{D}+2}, \qquad \beta_4 = -\frac{\mathrm{D}+1}{\mathrm{D}+4}, \qquad \beta_5 = -\frac{\mathrm{D}+2}{\mathrm{D}+6},$$

and we can find a dependency on n by

$$\beta_n = \frac{n-3+\mathrm{D}}{2n-4+\mathrm{D}}, \qquad (1-\beta_n) = \frac{n-1}{2n-4+\mathrm{D}}. \tag{282}$$

Using the above coefficients (please note that due to the normalization $\mathcal{P}_n(1) = 1$ our definition here differs from what can be found in textbooks), the Gegenbauer polynomials obey the following recurrence relation

$$\mu\,\mathcal{P}_{n-1}(\mu) = \frac{n-3+\mathrm{D}}{2n-4+\mathrm{D}}\,\mathcal{P}_n(\mu) + \frac{n-1}{2n-4+\mathrm{D}}\mathcal{P}_{n-2}(\mu), \tag{283}$$

of which this version is used to calculate higher-order from lower-order polynomials

$$\mathcal{P}_n(\mu) = \frac{2n-4+\mathrm{D}}{n-3+\mathrm{D}}\,\mu\,\mathcal{P}_{n-1}(\mu) + \frac{n-1}{n-3+\mathrm{D}}\,\mathcal{P}_{n-2}(\mu).$$

H.7 Derivative Recurrence of the Gegenbauer Polynomials

$$P_n' = \sum_{k=0}^{n-1} a_k^{(n)} P_k$$

$$xP_{n-1} = \beta_n P_n + (1-\beta_n)P_{n-2}$$

$$P_{n-1} + xP_{n-1}' = \beta_n P_n' + (1-\beta_n)P_{n-2}'$$

$$P_{n-1} + x\sum_{k=0}^{n-2} a_k^{(n-1)} P_k = \beta_n \sum_{k=0}^{n-1} a_k^{(n)} P_k + (1-\beta_n)\sum_{k=0}^{n-3} a_k^{(n-2)} P_k$$

$$P_{n-1} + \sum_{k=0}^{n-2} a_k^{(n-1)}[\beta_{k+1}P_{k+1} + (1-\beta_{k+1})P_{k-1}] = \beta_n \sum_{k=0}^{n-1} a_k^{(n)} P_k + (1-\beta_n)\sum_{k=0}^{n-3} a_k^{(n-2)} P_k$$

H.8 Squared Norm of Orthogonal Polynomials

According to Law and Sledd [LS75], the recurrence coefficient β_n can also be used to evaluate the normalization $N_n^2 = \int_{-1}^{1} \mathcal{P}_n(\mu)\,\sqrt{1-\mu^2}^{\mathrm{D}-3}\,\mathrm{d}\mu$ of the polynomial recursively by $N_n^2 = \frac{\mathcal{P}_n A_{n-1}}{A_n} N_{n-1}^2$ if the recurrence is denoted as $\mathcal{P}_{n+1} = (A_n\mu + B_n)\mathcal{P}_n - \mathcal{P}_n\mathcal{P}_{n-1}$. Using β_n, this becomes

$$N_n^2 = \frac{1-\beta_{n+1}}{\beta_n}\,N_{n-1}^2. \tag{284}$$

H.9 Norm of the Gegenbauer polynomials

For the transform integral, the squared norm $N_n^2 = \int_{-1}^{1} \mathcal{P}_n(\mu)\, w(\mu)\, \mathrm{d}\mu$ plays an important role for normalization. As the zeroth-order polynomial is $\mathcal{P}_0(\mu) = 1$, its norm $N_0^2 = \int_{-1}^{1} w(\mu)\, \mathrm{d}\mu$ should be easiest to find. The others follow from Eq. (284).

Finding N_0^2. Using all coordinates of the D-dimensional space, the integral over μ the last one of multiple integrals. In the sequence of the $(\mathrm{D}-1)$-fold integration over 1 to determine the surface $S_{\mathrm{D}-1}$ of the $\mathbb{S}^{\mathrm{D}-1}$ unit sphere in a D-dimensional space, the integral over μ delivers the distinguishing factor between the surfaces $S_{\mathrm{D}-1}$ and $S_{\mathrm{D}-2}$, the one of the next lower-dimensional unit sphere, cf. [HC37, vol.2, p.387],

$$S_{\mathrm{D}-1} = \underbrace{\iiint \mathrm{d}S_{\mathrm{D}-2}}_{=S_{\mathrm{D}-2}} \cdot \underbrace{\int_{-1}^{1} \sqrt{1-\mu^2}^{\mathrm{D}-3}\, \mathrm{d}\mu}_{=N_0^2}\,. \tag{285}$$

With $S_{\mathrm{D}-1} = \frac{2\sqrt{\pi}^{\mathrm{D}-1}}{\Gamma(\frac{\mathrm{D}-1}{2})}$, and the gamma function $\Gamma(n+1) = n!$ is the factorial for integers, its generalization otherwise, we conclude that

$$N_0^2 = \frac{S_{\mathrm{D}-1}}{S_{\mathrm{D}-2}} = \frac{\sqrt{\pi}\Gamma(\frac{\mathrm{D}-2}{2})}{\Gamma(\frac{\mathrm{D}-1}{2})}. \tag{286}$$

For 2 dimensions $\mathrm{D} = 2$ we get $N_0^2 = \frac{2\pi}{2} = \pi$, and for 3 dimensions $\mathrm{D} = 3$ we get $N_0^2 = \frac{4\pi}{2\pi} = 2$.

Other squared norms N_n^2. According to Eq. (284), the norm of higher-orer polynomials can be calculated from N_0^2, recursively. For the Gegenbauer polynomials, this becomes

$$N_n^2 = \frac{n(2n+\mathrm{D}-4)}{(2n+\mathrm{D}-2)(n+\mathrm{D}-3)}\, N_{n-1}^2.$$

Using $N_0^2 = \frac{S_{\mathrm{D}-1}}{S_{\mathrm{D}-2}}$ as a starting value, we get from the entire sequence

$$\begin{aligned} N_1^2 &= \frac{1}{\mathrm{D}}\, N_0^2, \quad N_2^2 = \frac{2}{(\mathrm{D}+2)(\mathrm{D}-1)}\, N_0^2, \quad N_3^2 = \frac{6}{(\mathrm{D}+4)(\mathrm{D}-1)\mathrm{D}}\, N_0^2, \\ N_n^2 &= \frac{n!}{(2n+\mathrm{D}-2)(n+\mathrm{D}-3)!}\frac{S_{\mathrm{D}-1}}{S_{\mathrm{D}-2}} \quad \text{for } n > 1, \end{aligned} \tag{287}$$

which finally yields $N_n^2 = \frac{\pi}{2-\delta_{n,0}}$ for $\mathrm{D} = 2$ and $N_n^2 = \frac{2}{2n+1}$ for $\mathrm{D} = 3$.

I Deriving the P, E, $\boldsymbol{r}_\mathrm{V}$, and $\boldsymbol{r}_\mathrm{E}$ measure of axisymmetric panning function

The panning function

$$g(\mu) = \sum_{n=0}^{\mathrm{N}} \frac{a_n}{S_{\mathrm{D}-2} N_n^2} \mathcal{P}_n(\mu) \tag{288}$$

is rotationally symmetric around the μ axis of a D-dimensional space. For the scalar measures, we integrate over μ with the surface weight $w(\mu) = \sqrt{1-\mu^2}^{\mathrm{D}-3}$, and we use the surface S_{D-2} of the unit sphere in the $(\mathrm{D}-1)$-dimensional space to denote the result of the integrals independent of μ:

$$P = S_{\mathrm{D}-2} \int_{-1}^{1} \sum_{n=0}^{\mathrm{N}} \frac{a_n}{S_{\mathrm{D}-2}\, N_n^2} \mathcal{P}_n(\mu)\, w(\mu) \mathrm{d}\mu = \sum_{n=0}^{\mathrm{N}} \frac{a_n}{N_n^2} \overbrace{\int_{-1}^{1} \mathcal{P}_n(\mu)\, w(\mu) \mathrm{d}\mu}^{N_n^2 \delta_{n0}} = a_0 \tag{289}$$

$$E = S_{\mathrm{D}-2} \sum_{n,n'} \frac{a_{n'}^*}{S_{\mathrm{D}-2} N_{n'}^2} \frac{a_n}{S_{\mathrm{D}-2} N_n^2} \overbrace{\int_{-1}^{1} \mathcal{P}_n(\mu) \mathcal{P}_{n'}(\mu)\, w(\mu) \mathrm{d}\mu}^{N_n^2 \delta_{nn'}} = \sum_{n=0}^{\mathrm{N}} \frac{|a_n|^2}{S_{\mathrm{D}-2} N_n^2}. \tag{290}$$

For rotationally symmetric shapes in space, the vector models always indicate the direction of axial symmetry. The remaining integral for $\boldsymbol{r}_\mathrm{V}$ and $\boldsymbol{r}_\mathrm{E}$ is a one-dimensional calculation along μ and determines the length.

$$r_\mathrm{V} = \frac{S_{\mathrm{D}-2} \sum_{n=0}^{\mathrm{N}} \frac{a_n}{N_n^2 S_{\mathrm{D}-2}} \overbrace{\int_{-1}^{1} \mathcal{P}_n(\mu)\, \mu\, w(\mu) \mathrm{d}\mu}^{N_1^2 \delta_{n,1}}}{V} = \frac{a_1}{a_0}. \tag{291}$$

For the $\boldsymbol{r}_\mathrm{V}$, the expression below the brace was evaluated by inserting the recurrence of the Gegenbauer polynomials $\mu \mathcal{P}_n(\mu) = \ldots$,

$$\int_{-1}^{1} [(1-\beta_{n+1}) P_{n-1}(\mu) + \beta_{n+1} P_{n+1}(\mu)] w(\mu) \mathrm{d}\mu = (1-\beta_2) N_0^2 \delta_{n,1} = N_1^2 \delta_{n,1}, \tag{292}$$

and by noticing that one can re-write $(1-\beta_2)N_0^2$ to $\beta_1 N_1^2$ because of the recurrence of the normalization in Eq. (284), $N_1^2 = \frac{1-\beta_2}{\beta_1} N_0^2$, and further to N_1^2 given that $\beta_1 = 1$.

For $\boldsymbol{r}_\mathrm{E}$, the expression with the integral yields

$$r_\mathrm{E} = \frac{S_{\mathrm{D}-2} \sum_{n,n'} \frac{a_n}{S_{\mathrm{D}-2} N_n^2} \frac{a_{n'}^*}{S_{\mathrm{D}-2} N_{n'}^2} \overbrace{\int_{-1}^{1} \mathcal{P}_n(\mu) \mathcal{P}_{n'}(\mu)\, \mu\, w(\mu)\, \mathrm{d}\mu}}{E} = \frac{\sum_n \frac{\beta_{n+1}}{N_n^2} 2\Re\{a_n a_{n+1}^*\}}{\sum_n \frac{1}{N_n^2} |a_n|^2}. \tag{293}$$

To evaluate the expression below the brace, the recurrence was used

$$\int_{-1}^{1} \mathcal{P}_n(\mu)\big[(1-\beta_{n'+1})\mathcal{P}_{n'-1}(\mu) + \beta_{n'+1}P_{n'+1}(\mu)\big]w(\mu)\mathrm{d}\mu \\ = N_n^2(1-\beta_{n'+1})\delta_{n,n'-1} + N_n^2\beta_{n'+1}\delta_{n,n'+1},$$

and re-insertion gave

$$r_\mathrm{E} = \frac{\sum_n \frac{a_n a_{n+1}^*}{S_{\mathrm{D}-2}N_{n+1}^2}(1-\beta_{n+2}) + \sum_n \frac{a_n a_{n-1}^*}{S_{\mathrm{D}-2}N_{n-1}^2}\beta_n}{E} = \frac{\sum_n \frac{a_n a_{n+1}^* + a_n^* a_{n+1}}{S_{\mathrm{D}-2}N_n^2}\beta_{n+1}}{E}, \quad (294)$$

for which Eq. (284) was used to re-write $\frac{1-\beta_{n+2}}{N_{n+1}^2} = \frac{\beta_{n+1}}{N_n^2}$ in the first numerator term, and a shift of n by one in the second one.

J Maximizing the $\boldsymbol{r}_\mathrm{E}$ vector for axisymmetric panning functions

The energy vector length is determined by the real-valued coefficients a_n in terms of $r_\mathrm{E} = \frac{\sum_n \frac{2\beta_{n+1}}{N_n^2} a_n a_{n+1}}{\sum_n \frac{1}{N_n^2} a_n^2} = \frac{A}{B}$. We may derive it with regard to a_n and equate to zero to maximize its length, yielding $r_\mathrm{E}' = \frac{A'}{B} - \frac{A}{B^2}B' = \frac{A' - r_\mathrm{E}\,B'}{B} = 0$. It is therefore sufficient to equate $A' - r_\mathrm{E}\,B' = 0$ and find the derivatives of the numerator and denominator, A', B', respectively. For the numerator A' this is

$$\frac{\partial}{\partial a_n}\sum_{n'}\frac{2\beta_{n'+1}a_{n'}a_{n'+1}}{N_{n'}^2} = \frac{2\beta_{n+1}a_{n+1}}{N_n^2} + \frac{2\beta_n a_{n-1}}{N_{n-1}^2} = \frac{2}{N_n^2}\left[\beta_{n+1}a_{n+1} + (1-\beta_{n+1})a_{n-1}\right],$$

for which the equivalence $\frac{\beta_n}{N_{n-1}^2} = \frac{1-\beta_{n+1}}{N_n^2}$ from Eq. (284) helped unify expressions. For the denominator B' we get $\frac{\partial}{\partial a_n}\sum_{n'}\frac{a_{n'}^2}{N_{n'}^2} = \frac{2}{N_n^2}a_n$, and we insert A' and B' into $A' - r_\mathrm{E}\,B' = 0$

$$\beta_{n+1}a_{n+1} + (1-\beta_{n+1})a_{n-1} - r_\mathrm{E}\,a_n = 0. \quad (295)$$

We recognize the recurrence relation $\beta_{n+1}\mathcal{P}_{n+1} + (1-\beta_{n+1})\mathcal{P}_{n-1} - \mu\,\mathcal{P}_n(\mu) = 0$ of the orthogonal polynomials and hereby find $a_n = \mathcal{P}_n(\mu)$ with $r_\mathrm{E} = \mu$, i.e. the solution

$$a_n = \mathcal{P}_n(r_\mathrm{E}). \quad (296)$$

We desire the boundary condition $a_{\mathrm{N}+1} = 0$, yielding $a_{\mathrm{N}+1} = \mathcal{P}_{\mathrm{N}+1}(r_\mathrm{E}) = 0$, which requires us to find the largest root of $\mathcal{P}_{\mathrm{N}+1}$, cf. [DRP99, Dan00], yielding the maximized length of the $\boldsymbol{r}_\mathrm{E}$ vector.

J.1 Higher-order cardioid axisymmetric panning function

The un-normalized higher-order cardioid

$$g_{\mathrm{N}}(\mu) = (1+\mu)^{\mathrm{N}} \tag{297}$$

is characterized by its flat design at $\mu = -1$, which can also be described by requiring its first $\mathrm{N}-1$ derivatives to vanish, while the N^{th} derivative must not be trivial,

$$\begin{aligned} &\frac{\mathrm{d}^l}{\mathrm{d}\mu^l} g(\mu)\Big|_{\mu=-1} = 0, \qquad\qquad \forall l = 0, \ldots, \mathrm{N}-1, \\ &\frac{\mathrm{d}^{\mathrm{N}}}{\mathrm{d}\mu^{\mathrm{N}}} g(\mu)\Big|_{\mu=-1} \neq 0. \end{aligned} \tag{298}$$

We desire the same for the expression of the axisymmetric finite-order panning function

$$g_{\mathrm{N}}(\mu) = \frac{1}{S_{\mathrm{D}-2}} \sum_{n=0}^{\mathrm{N}} \frac{a_n^{(\mathrm{N})}}{N_n^2}\, \mathcal{P}_n(\mu), \tag{299}$$

and from the definition of g_{N} we see that $g_{\mathrm{N}} = (1+\mu)\, g_{\mathrm{N}-1}$. We may set up a corresponding recurrence for the coefficients $a_n^{(\mathrm{N})}$ using

$$\begin{aligned} \sum_{n=0}^{\mathrm{N}} \frac{a_n^{(\mathrm{N})}}{N_n^2}\, \mathcal{P}_n(\mu) &= \sum_{n=0}^{\mathrm{N}-1} \frac{a_n^{(\mathrm{N}-1)}}{N_n^2}\, (1+\mu)\, \mathcal{P}_n(\mu) \\ &= \sum_{n=0}^{\mathrm{N}-1} \frac{a_n^{(\mathrm{N}-1)}}{N_n^2}\, \left[\mathcal{P}_n(\mu) + (1-\beta_{n+1})\, \mathcal{P}_{n-1}(\mu) + \beta_{n+1}\, \mathcal{P}_{n+1}(\mu)\right] \\ &= \sum_{n=0}^{\mathrm{N}-1} \left[\frac{a_n^{(\mathrm{N}-1)}}{N_n^2} \mathcal{P}_n(\mu) + \frac{a_n^{(\mathrm{N}-1)}}{N_{n-1}^2} \beta_n\, \mathcal{P}_{n-1}(\mu) + \frac{a_n^{(\mathrm{N}-1)}}{N_{n+1}^2} (1-\beta_{n+2})\, \mathcal{P}_{n+1}(\mu) \right], \end{aligned} \tag{300}$$

where the properties $(1-\beta_{n+1}) = \beta_n\, N_n^2/N_{n-1}^2$ and $\beta_{n+1} = (1-\beta_{n+2})\, N_n^2/N_{n+1}^2$ were used in the last line. Integration $w(\mu)\mathrm{d}\mu \int \mathcal{P}_m(\mu)$ yields $\int \frac{\mathcal{P}_n(\mu)\, \mathcal{P}_m(\mu)}{N_n^2} w(\mu)\, \mathrm{d}\mu = \delta_{nm}$, and we get the recurrence

$$\begin{aligned} a_m^{(\mathrm{N})} &= a_m^{(\mathrm{N}-1)} + \beta_{m+1}\, a_{m+1}^{(\mathrm{N}-1)} + (1-\beta_{m+1})\, a_{m-1}^{(\mathrm{N}-1)} \\ &= a_m^{(\mathrm{N}-1)} + \frac{n+\mathrm{D}-2}{2n+\mathrm{D}-2}\, a_{m+1}^{(\mathrm{N}-1)} + \frac{n}{2n+\mathrm{D}-2}\, a_{m-1}^{(\mathrm{N}-1)}. \end{aligned} \tag{301}$$

In terms of the coefficient notation $\mathcal{P}_n(\mu) = \sum_{k=0}^{n} c_k^{(n)}\,\mu^k$ and $\frac{\mathrm{d}^l}{\mathrm{d}\mu^l}\mu^k = \frac{k!}{(k-l)!}\mu^{k-l}$, we have

$$S_{\mathrm{D}-2}\frac{\mathrm{d}^l}{\mathrm{d}\mu^l}g(\mu)\Big|_{\mu=-1} = \sum_{n=l}^{\mathrm{N}}\frac{a_n}{N_n^2}\sum_{k=l}^{n}\frac{k!c_k^{(n)}\mu^{k-l}}{(k-l)!}\Big|_{\mu=-1} = \sum_{n=l}^{\mathrm{N}}\frac{a_n}{N_n^2}\sum_{k=l}^{n}\frac{k!c_k^{(n)}(-1)^{k-l}}{(k-l)!}.$$

For the non-trivial term with $l = \mathrm{N}$, there is only on term left

$$S_{\mathrm{D}-2}\frac{\mathrm{d}^{\mathrm{N}}}{\mathrm{d}\mu^{\mathrm{N}}}g(\mu)\Big|_{\mu=-1} = \frac{a_{\mathrm{N}}\,\mathrm{N}!c_{\mathrm{N}}^{(\mathrm{N})}}{N_{\mathrm{N}}^2} \neq 0.$$

and for $l = \mathrm{N}-1$, what remains is

$$\begin{aligned} S_{\mathrm{D}-2}\frac{\mathrm{d}^{\mathrm{N}}}{\mathrm{d}\mu^{\mathrm{N}}}g(\mu)\Big|_{-1} &= \sum_{n=\mathrm{N}-1}^{\mathrm{N}}\frac{a_n}{N_n^2}\sum_{k=\mathrm{N}-1}^{n}\frac{k!c_k^{(n)}(-1)^{k-(\mathrm{N}-1)}}{[k-(\mathrm{N}-1)]!} \\ &= \frac{a_{\mathrm{N}-1}(\mathrm{N}-1)!c_{\mathrm{N}-1}^{(\mathrm{N}-1)}}{N_{\mathrm{N}-1}^2} - \frac{a_{\mathrm{N}}\mathrm{N}!c_{\mathrm{N}}^{(\mathrm{N})}}{N_{\mathrm{N}}^2} = 0, \end{aligned}$$

which is still easy to overlook as $c_{2k}^{(2l+1)} = 0$ and $c_{2k+1}^{(2l)} = 0$. We get $a_{\mathrm{N}-1}$ from a_{N} by

$$a_{\mathrm{N}-1} = \mathrm{N}\frac{N_{\mathrm{N}-1}^2}{N_{\mathrm{N}}^2}\frac{c_{\mathrm{N}}^{(\mathrm{N})}}{c_{\mathrm{N}-1}^{(\mathrm{N}-1)}}\,a_{\mathrm{N}}.$$

We can simplify this using $\frac{1}{\beta_n} = \frac{c_n^{(n)}}{c_{n-1}^{(n-1)}} = \frac{2n+\mathrm{D}-4}{n+\mathrm{D}-3}$ and $\frac{N_{n-1}^2}{N_n^2} = \frac{(2n+\mathrm{D}-2)(n+\mathrm{D}-3)}{n(2n+\mathrm{D}-4)}$ from the recurrence relation and the recurrence of the squared norm,

$$a_{\mathrm{N}-1} = \frac{2\mathrm{N}+\mathrm{D}-2}{\mathrm{N}}\,a_{\mathrm{N}}$$

For $l = \mathrm{N}-2$, we get

$$\sum_{n=\mathrm{N}-2}^{\mathrm{N}}\sum_{k=\mathrm{N}-2}^{n}\frac{a_n}{N_n^2}\frac{k!c_k^{(n)}(-1)^{k-(\mathrm{N}-2)}}{[k-(\mathrm{N}-2)]!} =$$

$$\frac{a_{\mathrm{N}-2}(\mathrm{N}-2)!c_{\mathrm{N}-2}^{(\mathrm{N}-2)}}{N_{\mathrm{N}-2}^2} - \frac{a_{\mathrm{N}-1}(\mathrm{N}-1)!c_{\mathrm{N}-1}^{(\mathrm{N}-1)}}{N_{\mathrm{N}-1}^2} + \frac{a_{\mathrm{N}}(\mathrm{N}-2)!c_{\mathrm{N}-2}^{(\mathrm{N})}}{N_{\mathrm{N}}^2} + \frac{a_{\mathrm{N}}\mathrm{N}!c_{\mathrm{N}}^{(\mathrm{N})}}{2N_{\mathrm{N}}^2} = 0.$$

Before, the terms $B(a_{\mathrm{N}-1})$ and $A(a_{\mathrm{N}})$ had to cancel each other for $l = \mathrm{N}-1$ with $B - A = 0$. Now we can replace $-B + A/2 = -A/2$ and get

$$\frac{a_{\mathrm{N}-2}(\mathrm{N}-2)!c_{\mathrm{N}-2}^{(\mathrm{N}-2)}}{N_{\mathrm{N}-2}^2} + \frac{a_{\mathrm{N}}(\mathrm{N}-2)!c_{\mathrm{N}-2}^{(\mathrm{N})}}{N_{\mathrm{N}}^2} - \frac{a_{\mathrm{N}}\mathrm{N}!c_{\mathrm{N}}^{(\mathrm{N})}}{2N_{\mathrm{N}}^2} = 0.$$

We use $\frac{(\mathrm{N}-2)!c_{\mathrm{N}-2}^{(\mathrm{N}-2)}}{N_{\mathrm{N}-2}^2} = \frac{\mathrm{N}!}{N_{\mathrm{N}}^2(2\mathrm{N}+\mathrm{D}-2)(2\mathrm{N}+\mathrm{D}-4)}c_{\mathrm{N}}^{(\mathrm{N})}$ and $(\mathrm{N}-2)!c_{\mathrm{N}-2}^{(\mathrm{N})} = \frac{\mathrm{N}!}{2(4-\mathrm{D})}c_{\mathrm{N}}^{(\mathrm{N})}$ to get

$$\begin{aligned} \frac{a_{\mathrm{N}-2}}{(2\mathrm{N}+\mathrm{D}-2)(2\mathrm{N}+\mathrm{D}-4)} + \frac{a_{\mathrm{N}}}{2(4-\mathrm{D})} - \frac{a_{\mathrm{N}}}{2} &= 0 \\ a_{\mathrm{N}-2} = \frac{(3-\mathrm{D})(2\mathrm{N}+\mathrm{D}-2)(2\mathrm{N}+\mathrm{D}-4)}{2(4-\mathrm{D})}a_{\mathrm{N}}. & \end{aligned} \tag{302}$$

Further calculation is a bit tedious and is omitted for brevity. It is a reasonable assumption to use weights as desind by Daniel [Dan00] for in-phase weighting. As the weights were given as $a_n = \frac{N!}{(N-n)!}\frac{N!}{(N+n)!}$ for $\mathrm{D} = 2$ and $a_n = \frac{N!}{(N-n)!}\frac{(N+1)!}{(N+n+1)!}$ for $\mathrm{D} = 3$ as that the next step would yield

$$a_n = \frac{\mathrm{N!}}{(\mathrm{N}-n)!}\frac{(\mathrm{N}+\mathrm{D}-2)!}{(\mathrm{N}+n+\mathrm{D}-2)!}.$$

J.2 Particular max-rE solutions for $\mathrm{D} = 2$ and $\mathrm{D} = 3$

A fairly good approximation for practical use has been given in [ZF12] by

$$r_{\mathrm{E}} = \cos\frac{137.9^\circ}{\mathrm{N}+1.51}, \tag{303}$$

and it saves us the time for polynomial root finding.

K Laplacian in polar angle

The Laplacian $\triangle = \frac{\partial^2}{\partial x^2} + \frac{\partial^2}{\partial y^2}$ for $\mathrm{D} = 2$ is re-written to the angular dependency φ by the generalized chain rule $\frac{\partial}{\partial x} = \frac{\partial \varphi}{\partial x}\frac{\partial}{\partial \varphi}$, and $\varphi = \arctan\frac{y}{x}$, with $\arctan' u = \frac{1}{1+u^2}$,

$$\frac{\partial}{\partial x} = \frac{\partial \varphi}{\partial x}\frac{\partial}{\partial \varphi} = \frac{x^2}{x^2+y^2}\left(-\frac{y}{x^2}\right)\frac{\partial}{\partial \varphi} = -\frac{y}{r_{xy}^2}\frac{\partial}{\partial \varphi}, \qquad \frac{\partial^2}{\partial x^2} = \frac{4xy}{r_{xy}^4}\frac{\partial}{\partial \varphi} + \frac{y^2}{r_{xy}^4}\frac{\partial^2}{\partial \varphi^2},$$
$$\frac{\partial}{\partial y} = \frac{\partial \varphi}{\partial y}\frac{\partial}{\partial \varphi} = \frac{x^2}{x^2+y^2}\frac{1}{x}\frac{\partial}{\partial \varphi} = \frac{x}{r_{xy}^2}\frac{\partial}{\partial \varphi}, \qquad \frac{\partial^2}{\partial y^2} = -\frac{4yx}{r_{xy}^4}\frac{\partial}{\partial \varphi} + \frac{x^2}{r_{xy}^4}\frac{\partial^2}{\partial \varphi^2},$$

yielding in sum

$$\triangle_\varphi = \frac{\partial^2}{\partial x^2} + \frac{\partial^2}{\partial y^2} = \frac{x^2+y^2}{r_{xy}^4}\frac{\partial^2}{\partial \varphi^2} = \frac{1}{r_{xy}^2}\frac{\partial^2}{\partial \varphi^2}. \tag{304}$$

L Laplacian in azimuth and cos of zenith

The Laplacian $\triangle = \frac{\partial^2}{\partial x^2} + \frac{\partial^2}{\partial y^2} + \frac{\partial^2}{\partial z^2}$ for $\mathrm{D} = 3$ is re-written to the angular dependencies $\varphi = \arctan\frac{y}{x}$ and $\mu = \arccos\frac{z}{r}$ by the generalized chain rule $\frac{\partial}{\partial x} = \frac{\partial \varphi}{\partial x}\frac{\partial}{\partial \varphi} + \frac{\partial \mu}{\partial x}\frac{\partial}{\partial \mu}$. As shown in Sec. 11.1, the Laplacian in any orthogonal non-Cartesian coordinates, using only the angular components in φ and μ here, is

$$\triangle_{\varphi,\mu} = \left[\frac{\partial^2\varphi}{\partial x^2} + \frac{\partial^2\varphi}{\partial y^2} + \frac{\partial^2\varphi}{\partial z^2}\right]\frac{\partial}{\partial \varphi} + \left[\left(\frac{\partial\varphi}{\partial x}\right)^2 + \left(\frac{\partial\varphi}{\partial y}\right)^2 + \left(\frac{\partial\varphi}{\partial z}\right)^2\right]\frac{\partial^2}{\partial \varphi^2}$$
$$+ \left[\frac{\partial^2\mu}{\partial x^2} + \frac{\partial^2\mu}{\partial y^2} + \frac{\partial^2\mu}{\partial z^2}\right]\frac{\partial}{\partial \mu} + \left[\left(\frac{\partial\mu}{\partial x}\right)^2 + \left(\frac{\partial\mu}{\partial y}\right)^2 + \left(\frac{\partial\mu}{\partial z}\right)^2\right]\frac{\partial^2}{\partial \mu^2}.$$

The sum of the squared first-order and the second-order derivatives of $\varphi = \arctan\frac{y}{x}$ in x and y are known from above, $\left(\frac{\partial\varphi}{\partial x}\right)^2 + \left(\frac{\partial\varphi}{\partial y}\right)^2 = 0$, and $\frac{\partial^2\varphi}{\partial x^2} + \frac{\partial^2\varphi}{\partial y^2} = \frac{1}{x^2+y^2} = \frac{1}{r^2(1-\mu^2)}$, and in z they vanish $\frac{\partial\varphi}{\partial z} = 0$. The derivatives of $\mu = \frac{z}{r}$ are:

$$\frac{\partial\mu}{\partial x} = -\frac{z}{r^2}\frac{x}{r} = \frac{-xz}{r^3}, \qquad \frac{\partial^2\mu}{\partial x^2} = -\frac{z}{r^3} + 3\frac{xz}{r^4}\frac{x}{r} = \frac{z(3x^2-r^2)}{r^5},$$
$$\frac{\partial\mu}{\partial y} = -\frac{z}{r^2}\frac{y}{r} = \frac{-yz}{r^3}, \qquad \frac{\partial^2\mu}{\partial y^2} = \frac{z(3y^2-r^2)}{r^5},$$
$$\frac{\partial\mu}{\partial z} = \frac{1}{r} - \frac{z^2}{r^3} = \frac{r_{xy}^2}{r^3}, \qquad .\frac{\partial^2\mu}{\partial y^2} = -3\frac{r_{xy}^2}{r^4}\frac{z}{r} = -3\frac{z\,r_{xy}^2}{r^5}.$$

The squared first-order derivatives sum up to $\frac{(x^2+y^2)z^2+r_{xy}^4}{r^6} = \frac{r_{xy}^2z^2+r_{xy}^4}{r^6} = \frac{r_{xy}^2(r^2-r_{xy}^2)+r_{xy}^4}{r^6} = \frac{r_{xy}^2}{r^4} = \frac{1-\mu^2}{r^2}$, and the second-order derivatives sum up to $-2\frac{z}{r^3} = -2\frac{\mu}{r^2}$. Together with the derivatives for φ, the Laplacian becomes

$$r^2\triangle_{\varphi,\mu} = (1-\mu^2)\frac{\partial^2}{\partial\mu^2} - 2\mu\frac{\partial}{\partial\mu} + \frac{1}{1-\mu^2}\frac{\partial^2}{\partial\varphi^2}. \tag{305}$$

M 0D wave equation (harmonic oscillator)

As a mathematical warm-up excercise, we calculate the *oscillating* solution of the single differential segment. Along its dimension x, we only regard the two locations $(0, \Delta x)$, which we could regard making the problem dimensionless (0D) in space.

A rigid boundary condition $v(0) = 0$ on the left side clarifies the behavior of the element. $v(0)$ is therefore vanishing in the Eqs. (73)(74). Regarding Eq. (74) for the right end, we obtain the equation of the *harmonic oscillator* after omission of $(x + \Delta x)$ for easier readability:

$$m\,\ddot{v} + s\,v = \dot{F}^{\mathrm{E}}.$$

After a replacement $\omega_0 := \frac{s}{m}$ we have

$$\left(\omega_0^2 + \frac{\partial^2}{\partial t^2}\right) v = m\,\dot{F}^{\mathrm{E}}. \tag{306}$$

Homogeneous solution. Zeroing the right end, and hereby the external force, we obtain the following equation

$$\omega_0^2\,v + \ddot{v} = 0$$

of the eigenoscillations of the system. We guess an exponential solution $v_{\mathrm{h}} = e^{\lambda t}$ for the homogeneous problem and insert it, with $\frac{\partial}{\partial t^2} e^{\lambda t} = \lambda^2\,e^{\lambda t}$,

$$\begin{aligned} (\omega_0^2 + \lambda^2)\,e^{\lambda t} &= 0, \qquad \left| \frac{1}{e^{\lambda t}},\ -\omega_0^2 \right. \\ \lambda^2 &= -\omega_0^2. \end{aligned} \tag{307}$$

The equation defines λ and is called *characteristic equation*. Obviously it requires $\lambda = \pm \mathrm{i}\omega_0$, what defines both solutions in arbitrary linear combination,

$$v_{\mathrm{h}}(t) = a\,e^{\mathrm{i}\omega_0\,t} + b\,e^{-\mathrm{i}\omega_0\,t}, \tag{308}$$

which, e.g., yields $v_{\mathrm{h}}(t) = \cos(\omega_0\,t)$ with $a = b = \frac{1}{2}$.

Inhomogeneous Solution. The inhomogeneous solution requires more effort, because we require it to be causal, $v(t<0)=0$. It can therefore not be infinitely narrow-band, anymore. To describe an elementary solution, the right side of the equation is often set to a Dirac delta $m\dot{F}^{\mathrm{E}}=\delta(t)$, which yields a *Green'sche function* or impulse response as a solution. The external force then corresponds to a scaled jump $F^{\mathrm{E}}=\frac{\int_{-\infty}^{t}\delta(\tau)\,\mathrm{d}\tau}{m}=\frac{1}{m}\,u(t)$. We describe the solution as being composed of complex exponentials with unknown weighting function $\nu(\omega)$:

$$v_{\mathrm{in}}(t)=\int_{-\infty}^{\infty}e^{\mathrm{i}\omega\,t}\,\nu(\omega)\,\mathrm{d}\omega,$$

and we get upon insertion into the equation of the harmonic oscillator

$$\int_{-\infty}^{\infty}\left[\omega_0^2+(\mathrm{i}\omega)^2\right]e^{\mathrm{i}\omega\,t}\,\nu(\omega)\,\mathrm{d}\omega=\delta(t).$$

To find the explicit definition of $\nu(\omega)$, we Fourier transform over t by $\int_{-\infty}^{\infty}e^{-\mathrm{i}\omega' t}\mathrm{d}t$

$$\int_{-\infty}^{\infty}\left(\omega_0^2-\omega^2\right)\underbrace{\left(\int_{-\infty}^{\infty}e^{\mathrm{i}(\omega-\omega')\,t}\,\mathrm{d}t\right)}_{2\pi\delta(\omega-\omega')}\nu(\omega)\,\mathrm{d}\omega=\underbrace{\int_{-\infty}^{\infty}\delta(t)\,e^{-\mathrm{i}\omega' t}\mathrm{d}t}_{=1},$$

$$\Rightarrow\ \nu(\omega)=-\frac{1}{2\pi}\frac{1}{\omega^2-\omega_0^2}.$$

The frequency response $\nu(\omega)$ is obviously non-zero, however, at $\omega_0^2=\frac{s}{m}\in\mathbb{R}$ it posesses two infinite resonances. For a solution in the time domain, we need to evaluate

$$v_{\mathrm{in}}(t)=-\frac{1}{2\pi}\int_{-\infty}^{\infty}\frac{e^{\mathrm{i}\omega\,t}}{\omega^2-\omega_0^2}\,\mathrm{d}\omega. \tag{309}$$

Partial fraction expansion separates the pair of poles $\frac{1}{\omega^2-\omega_0^2}=\frac{A}{\omega-\omega_0}+\frac{B}{\omega+\omega_0}$, i.e. $1=A(\omega+\omega_0)+B(\omega-\omega_0)$, and hence $A=-B=\frac{1}{2\omega_0}$, so that we get

$$v_{\mathrm{in}}(t)=-\frac{1}{2\pi}\frac{1}{2\omega_0}\int_{-\infty}^{\infty}\left[\frac{e^{\mathrm{i}\omega\,t}}{\omega-\omega_0}-\frac{e^{\mathrm{i}\omega\,t}}{\omega+\omega_0}\right]\mathrm{d}\omega.$$

Both poles at $\pm\omega_0$ lie on the integration path. Therefore, we *regularize* the equation [KT14] by adding the imaginary expression $\mathrm{i}\epsilon$:

$$v_{\mathrm{in}}(t)=-\frac{1}{2\pi}\frac{1}{2\omega_0}\lim_{|\epsilon|\to 0}\int_{-\infty}^{\infty}\left[\frac{e^{\mathrm{i}\omega\,t}}{\omega-\omega_0-\mathrm{i}\epsilon}-\frac{e^{\mathrm{i}\omega\,t}}{\omega+\omega_0-\mathrm{i}\epsilon}\right]\mathrm{d}\omega.$$

To evaluate the improper integral, we use *Jordan's lemma*. It allows to close the improper integration path in ω using the one semicircle over the complex half-plane at infinity for which the integrand vanishes. For$t\geq 0$ the integrand $e^{\mathrm{i}\omega t}$ vanishes for $\Im\{\omega\}\to\infty$ only with the semicircle C_+ of mathematically positive orientation. For $t<0$ the semicircle C_- is used, cf. Fig. 48.

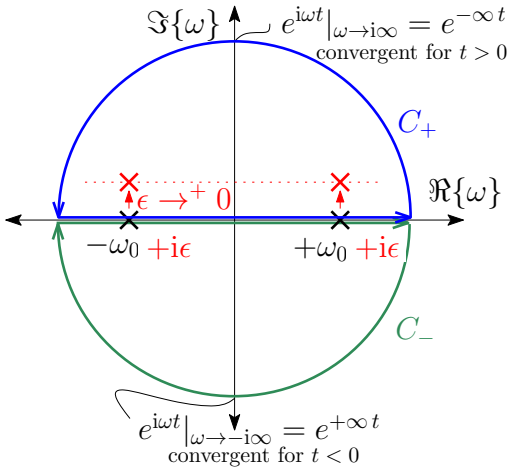

Figure 48 – Regularization of the poles for the inhomogeneous solution of the mass and spring system, and closure of the improper integration path using the path C_+ over the positive imaginary half plane for $t \geq 0$, or the negative one C_- for $t < 0$.

Cauchy's integral formula yields the value $\oint \frac{f(z)}{z-z_0} = \pm 2\pi\mathrm{i} f(z_0)$ if the for integration path surrounds the pole z_0, otherwise zero; the orientation of the path determines the sign of the result.

Requiring causality, $v_{\text{in}}(t < 0) = 0$, the path C_+ must exclusively contain both poles, so that the integral for $t < 0$ over C_- vanishes. Hence for the causal solution, ϵ is positive for both the poles:

$$\begin{aligned} v_{\text{in}}(t) &= \lim_{\epsilon\to+0} e^{-\epsilon\, t} \begin{cases} -\frac{1}{2\pi}\frac{1}{2\omega_0} 2\pi\mathrm{i}\left[e^{\mathrm{i}\omega_0\, t} - e^{-\mathrm{i}\omega_0\, t}\right] = \frac{1}{\omega_0}\sin(\omega_0 t) & \text{for } t \geq 0 \\ 0 & \text{for } t < 0 \end{cases} \\ &= \tfrac{1}{\omega_0}\sin\left(\omega_0\, t\right)\, u(t). \end{aligned} \tag{310}$$

A positive ϵ corresponds to insertion of friction in parallel to the spring. Therefore regularization is also called the method of vanishing loss [Sch12b].

N Green'sche Funktion durch richtungsunabhängiges Koordinatensystem

Die inhomogene Helmholtzgleichung in richtungsunabhängigen Koordinaten. Wir verwerfen die Richtungsabhängigkeit und setzen die Quelle in den Ursprung. In Kugelkoordinaten verallgemeinerter Dimensionszahl D bleibt der Radius als einzige räumliche Abhängigkeit $r = \sqrt{\sum_{i=0}^{\mathrm{D}-1} x_i^2}$. Der Laplaceoperator wird mit der verallgemeinerten Kettenregel in ein richtungsunabhängiges Radiuskoordinatensystem überführt:

$$\triangle = \sum_{i=0}^{\mathrm{D}-1} \frac{\partial^2}{\partial x_i^2} = \sum_{i=0}^{\mathrm{D}-1} \frac{\partial}{\partial x_i}\left(\frac{\partial}{\partial x_i}\right) = \sum_{i=0}^{\mathrm{D}-1} \frac{\partial}{\partial x_i}\left(\frac{\partial r}{\partial x_i}\frac{\partial}{\partial r}\right)$$

$$= \sum_{i=0}^{\mathrm{D}-1} \left[\left(\frac{\partial}{\partial x_i} \frac{\partial r}{\partial x_i} \right) \frac{\partial}{\partial r} + \frac{\partial r}{\partial x_i} \left(\frac{\partial}{\partial x_i} \frac{\partial}{\partial r} \right) \right]$$
$$= \sum_{i=0}^{\mathrm{D}-1} \left[\frac{\partial^2 r}{\partial x_i^2} \frac{\partial}{\partial r} + \left(\frac{\partial r}{\partial x_i} \right)^2 \frac{\partial^2}{\partial r^2} \right].$$

Mit der ersten Ableitung $\frac{\partial \sqrt{\sum_{i=0}^{\mathrm{D}-1} x_i^2}}{\partial x_i} = \frac{1}{2\sqrt{\sum_{i=0}^{\mathrm{D}-1} x_i^2}} 2\,x_i = \frac{x_i}{r}$ quadriert und der zweiten Ableitung $\frac{\partial}{\partial x_i}\frac{x_i}{r} = \frac{1}{r} - \frac{x_i}{r}\frac{x_i}{r^2}$ eingesetzt, erhalten wir

$$\triangle = \left(\frac{\mathrm{D}}{r} - \frac{\sum_{i=0}^{\mathrm{D}-1} x_i^2}{r^3} \right) \frac{\partial}{\partial r} + \left(\frac{\sum_{i=0}^{\mathrm{D}-1} x_i^2}{r^2} \right) \frac{\partial^2}{\partial r^2} = \frac{\mathrm{D}-1}{r} \frac{\partial}{\partial r} + \frac{\partial^2}{\partial r^2}. \tag{311}$$

Die Definitionsgleichung für die Green'sche Funktion ist damit

$$\left[\frac{\mathrm{D}-1}{r} \frac{\partial}{\partial r} + \frac{\partial^2}{\partial r^2} + k^2 \right] G = -\delta(r). \tag{312}$$

Transformierte Defintionsgleichung der Green'schen Funktion im Freifeld. Hoffend, damit einen schwierig beschreibbaren Teil der Lösung abspalten zu können, wählen wir den Produktansatz,

$$G = a\, g(r)\, r^{-\nu},$$

da wir uns vorstellen, dass das Feld der Green'schen Funktion radial ausklingen müsste.

Durch $\frac{1}{a}\frac{\partial}{\partial r} G = g'\, r^{-\nu} - \nu\, g\, r^{-\nu-1}$ und wiederholte Ableitung $\frac{1}{a}\frac{\partial}{\partial r}\left[g'\, r^{-\nu} - \nu\, g\, r^{-\nu-1}\right] = g'' r^{-\nu} - 2\nu\, g'\, r^{-\nu-1} - \nu(-\nu-1) g\, r^{-\nu-2}$ erhalten wir der Idee gemäß eine *transformierte Definitionsgleichung der Green'schen Funktion*

$$a\, r^{-\nu-2} \left[r^2 \frac{\partial^2}{\partial r^2} + (\mathrm{D}-1-2\nu)\, r \frac{\partial}{\partial r} - (\mathrm{D}-1-\nu-1)\nu + k^2 r^2 \right] g = -\delta(r). \tag{313}$$

Aber ist damit die Gleichung nun auch einfacher geworden?

Fernfeldnäherung der Green'schen Funktion im Freifeld. Mit $2\nu = \mathrm{D}-1$ wird die erste Klammer der transformierten Gleichung (313) null $(\mathrm{D}-1-2\nu) = 0$ und die zweite $-(\mathrm{D}-2-\nu)\nu = -\frac{\mathrm{D}-3}{2}\frac{\mathrm{D}-1}{2}$:

$$a\, r^{-\nu} \left[\frac{\partial^2}{\partial r^2} - \frac{(\mathrm{D}-3)(\mathrm{D}-1)}{4\, r} + k^2 \right] g = -\delta(r).$$

Für $\mathrm{D} = 1$ und $\mathrm{D} = 3$ entfällt der Ausdruck $\frac{(\mathrm{D}-3)(\mathrm{D}-1)}{4\, r}$ in der Mitte von selbst, ansonsten wird er für große Radien vernachlässigbar, und die verbleibende Differentialgleichung,

$$\lim_{r\to\infty}: \qquad a\, r^{-\nu} \left[\frac{\partial^2}{\partial r^2} + k^2 \right] g = -\delta(r),$$

wird, wie bereits bekannt, durch den Exponentialansatz $e^{\pm \mathrm{i}kr}$ gelöst. *Physikalisch sinnvoll* und *kausal* ist nur die auslaufende Welle $g = e^{-\mathrm{i}kr}$. Somit ist bis auf den unbestimmten Faktor a bestimmt, dass die Green'sche Funktion bei großen Radien so aussehen muss:

$$\lim_{r\to\infty} G = a\,\frac{e^{-\mathrm{i}kr}}{\sqrt{r}^{\mathrm{D}-1}}. \qquad \text{(bei D = 1 und D = 3 sogar exakt bei kleinem Radius).} \quad (314)$$

Green'sche Funktion beliebiger Dimension: Bessel'sche Differentialgleichung. Durch die Wahl des Exponenten $\nu = \frac{\mathrm{D}-2}{2}$, oder umgekehrt $\mathrm{D} = 2 + 2\nu$, erhalten wir die Konstanten der transformierten Gl. (313) zu $(\mathrm{D} - 2\nu - 1) = 1$, $(\mathrm{D} - \nu - 2) = \nu$ und damit die inhomogene Bessel'sche Differentialgleichung

$$\left(r^2\,\frac{\partial^2}{\partial r^2} + r\,\frac{\partial}{\partial r} + k^2r^2 - \nu^2\right)\,g = -\frac{\delta(r)}{a\,r^{-\nu-2}}. \quad (315)$$

Alle Besselfunktionen $J_\nu(kr)$, $Y_\nu(kr)$, $H_\nu^{(1)}(kr)$, $H_\nu^{(2)}(kr)$ kämen für g infrage. Aber nur die Hankelfunktion 2. Art $H_\nu^{(2)}(kr)$ beschreibt einen kausalen Ausbreitungsterm:

$$G = a\,\sqrt{r}^{2-\mathrm{D}}\,H^{(2)}_{\frac{\mathrm{D}-2}{2}}(kr).$$

Die Näherung $\lim_{kr\to\infty} H_\nu^{(2)}(kr) = \sqrt{2/(\pi\,kr)}\,e^{-\mathrm{i}kr-\mathrm{i}(2\nu+1)\frac{\pi}{4}}$ aus [OBC00, Eq.10.2.6] verdeutlicht das, denn im Fernfeld ergibt sich die Proportionalität aus Gl. (314)

$$\lim_{r\to\infty} a\,\sqrt{r}^{2-\mathrm{D}}\,H_\nu^{(2)}(kr) = a\,\sqrt{2/(\pi\,k)}e^{-\mathrm{i}(\mathrm{D}-1)\frac{\pi}{4}}\;\frac{e^{-\mathrm{i}kr}}{\sqrt{r}^{\mathrm{D}-1}}.$$

Nach [Som92, Anhang III, S213, Gl.12] wird die Normierung a am Grenzwert $k\mathrm{R} \to 0$ durch den Gauß'schen Integralsatz Gl. (117), $\int_V \triangle G\;\mathrm{d}\boldsymbol{r} = \int_{\partial V} \boldsymbol{\nabla}^{\mathrm{T}} G\,\mathrm{d}\boldsymbol{S}(\boldsymbol{r})$, bestimmt:

$$\lim_{\mathrm{R}\to 0}\int_{r\le\mathrm{R}} \triangle G\;\mathrm{d}\boldsymbol{r} = \lim_{\mathrm{R}\to 0}\int_{\boldsymbol{r}^{\mathrm{T}}\boldsymbol{r}=\mathrm{R}^2} \frac{\partial G}{\partial r}\,\mathrm{d}S(\boldsymbol{r}).$$

Auf der linken Seite ist das besonders einfach wegen $\lim_{k\to 0}\triangle G = -\delta - k^2 G = -\delta$ und der normierten Dirac Deltadistribution $\int_V \delta\,\mathrm{d}V(\boldsymbol{r}) = 1$. Der Integrand rechts verwendet die Nahfeldnäherung [OBC00, Eq.10.7.7] $\lim_{kr\to 0} H_\nu^{(2)}(kr) = \mathrm{i}\Gamma(\nu)/\pi\,[(kr)/2]^{-\nu}$, d.h. $G = a\,r^{-\nu}\;\mathrm{i}\Gamma(\nu)/\pi\,(k/2)^{-\nu}\,r^{-\nu}$, ihre Ableitung $\frac{\partial G}{\partial r} = -\mathrm{i}a2\nu\Gamma(\nu)/\pi\,(k/2)^{-\nu}\,r^{-2\nu-1}$, die Eigenschaft $\nu\Gamma(\nu) = \Gamma(\nu+1)$ und die Hypereinheitskugelfläche $S_\mathrm{D} = 2\sqrt{\pi}^{\mathrm{D}}/\Gamma(\frac{\mathrm{D}}{2})$ zur Definition des Flächenelements $r^{\mathrm{D}-1}\,S_\mathrm{D}$ bzw. $r^{2\nu+1}\,S_{2\nu+2} = r^{2\nu+1}\,S_{2\nu+2} = \frac{r^{2\nu+1}\,2\,\pi^{\nu+1}}{\Gamma(\nu+1)}$. Eingesetzt kürzen sich Gammafunktionen und Radiusabhängigkeit

$$-1 = -\frac{\mathrm{i}a2\,2^\nu\cancel{\Gamma(\nu+1)}}{\cancel{\pi}\,k^\nu\,\cancel{r^{2\nu+1}}}\;\frac{\cancel{r^{2\nu+1}}2\,\pi^{\nu+\cancel{1}}}{\cancel{\Gamma(\nu+1)}} = -4\mathrm{i}a\,\left(\frac{2\pi}{k}\right)^\nu,$$

$$\Rightarrow\; a = \frac{1}{4\mathrm{i}}\sqrt{\frac{2\pi}{k}}^{\mathrm{D}-2}.$$

Wir können die Green'sche Funktion des Freifeldes somit angeben zu

$$G = \frac{1}{4\mathrm{i}}\sqrt{\frac{2\pi}{kr}}^{\mathrm{D}-2} H^{(2)}_{\frac{\mathrm{D}-2}{2}}(kr). \tag{316}$$

Damit, und mit den einfachen Sonderfällen für $\mathrm{D} = 1, 3$ ergeben sich für Green'sche Funktion des Freifeldes folgende Definitionen:

$$\left[\frac{\partial^2}{\partial r^2} + k^2\right] G_{1\mathrm{D}}(r) = -\delta_{1\mathrm{D}}(r), \qquad \Rightarrow G_{1\mathrm{D}} = \frac{e^{-\mathrm{i}kr}}{2\mathrm{i}k}, \tag{317}$$

$$\left[\frac{\partial^2}{\partial r^2} + \frac{1}{r}\frac{\partial}{\partial r} + k^2\right] G_{2\mathrm{D}}(r) = -\delta_{2\mathrm{D}}(r), \qquad \Rightarrow G_{2\mathrm{D}} = \frac{1}{4\mathrm{i}} H^{(2)}_0(kr), \tag{318}$$

$$\left[\frac{\partial^2}{\partial r^2} + \frac{2}{r}\frac{\partial}{\partial r} + k^2\right] G_{3\mathrm{D}}(r) = -\delta_{3\mathrm{D}}(r), \qquad \Rightarrow G_{3\mathrm{D}} = \frac{e^{-\mathrm{i}kr}}{4\pi r}. \tag{319}$$

O Green'sche Funktion durch Residuenintegrale und auf komplexen Integrationswegen

Im Wellenzahlraum hängt der Integrand für die Green'sche Funktion

$$G = \frac{1}{(2\pi)^{\mathrm{D}}} \iint \frac{e^{\mathrm{i}\boldsymbol{k}^{\mathrm{T}}\boldsymbol{r}}}{k^2 - \frac{\omega^2}{c^2}}\,\mathrm{d}\boldsymbol{k} = \frac{1}{(2\pi)^{\mathrm{D}}} \iint \frac{e^{\mathrm{i}kr\mu}}{k^2 - \frac{\omega^2}{c^2}}\,\mathrm{d}\boldsymbol{k}.$$

offenbar nur mehr von $k\mu$ ab, was sich als letzte hypersphärische Koordinate eines mit $\boldsymbol{\theta}_r$ ausgerichteten Wellenzahlraums deuten lässt. Das zugehörige Flächenelement ist nach Hilbert und Courant [HC37, p.387] $\sqrt{1-\mu^2}^{\mathrm{D}-3}\,\mathrm{d}\mu\; k^{\mathrm{D}-1}\,\mathrm{d}k$, und die $\mathrm{D}-2$ unabhängigen Integrale ergeben den Faktor $S_{\mathrm{D}-1} = \frac{2\sqrt{\pi}^{\mathrm{D}-1}}{\Gamma(\frac{\mathrm{D}-1}{2})}$, die Fläche der Hyper-Einheitskugel im $\mathbb{R}^{\mathrm{D}-1}$. Damit bleibt dieses Zweifachintegral zu lösen

$$G = \frac{S_{\mathrm{D}-1}}{(2\pi)^{\mathrm{D}}} \iint \frac{e^{\mathrm{i}kr\mu}}{k^2 - \frac{\omega^2}{c^2}} \sqrt{1-\mu^2}^{\mathrm{D}-3}\,\mathrm{d}\mu\; k^{\mathrm{D}-1}\,\mathrm{d}k.$$

Die typische Annahme der Integrationsgrenzen $0 \le k \le \infty$ und $-1 \le \mu \le 1$ wird für eine gleichmäßige Konvergenz des Integrals verworfen, und wir verwenden stattdessen $k \in C_+$ wie in Abb. 23, worin der Bruch $\frac{1}{k^2-\omega^2c^2} = \frac{c}{2\omega}\lim_{\epsilon\to+0}\left[\frac{1}{k-\frac{\omega-\mathrm{i}\epsilon}{c}} - \frac{1}{k+\frac{\omega-\mathrm{i}\epsilon}{c}}\right]$ partialbruchzerlegt mit Verschiebung hin zu verschwindenden, kausalen Verlusten verwendet wird, siehe Abb. 23:

$$\begin{aligned} G &= \frac{S_{\mathrm{D}-1}}{(2\pi)^{\mathrm{D}}}\frac{c}{2\,\omega}\lim_{\epsilon\to+0}\oint_{C_+}\left[\int e^{\mathrm{i}kr\,\mu}\sqrt{1-\mu^2}^{\mathrm{D}-3}\,\mathrm{d}\mu\right]\left[\frac{1}{k-\frac{\omega-\mathrm{i}\epsilon}{c}} - \frac{1}{k+\frac{\omega-\mathrm{i}\epsilon}{c}}\right] k^{\mathrm{D}-1}\,\mathrm{d}k \\ &= -\frac{S_{\mathrm{D}-1}}{2(2\pi)^{\mathrm{D}-1}}\mathrm{i}(-1)^{\mathrm{D}-1}\left(\frac{\omega}{c}\right)^{\mathrm{D}-2}\int e^{-\mathrm{i}\frac{\omega}{c}r\,\mu}\sqrt{1-\mu^2}^{\mathrm{D}-3}\,\mathrm{d}\mu \\ &= -\frac{S_{\mathrm{D}-1}}{2(2\pi)^{\mathrm{D}-1}}\mathrm{i}(-1)^{\mathrm{D}-1}k^{\mathrm{D}-2}\int e^{-\mathrm{i}kr\,\mu}\sqrt{1-\mu^2}^{\mathrm{D}-3}\,\mathrm{d}\mu. \end{aligned}$$

Da die Wellenzahl nicht notwendigerweise reellwertig ist, darf für ein konvergentes Integral in μ der veränderte Integrationspfad in Anlehnung an Weyl [Wey19] das Integral in μ verwendet werden, [OBC00, Eq.10.9.21]:

$$\frac{\sqrt{\pi}^3}{\Gamma(\frac{1}{2}-\nu)\left(\frac{kr}{2}\right)^\nu}\, H_\nu^{(2)}(kr) = \int_{1-\mathrm{i}\infty}^{1} e^{-\mathrm{i}kr\mu}\sqrt{1-\mu^2}^{2\nu-1}\,\mathrm{d}\mu.$$

Mit $\nu = \frac{\mathrm{D}-2}{2}$ zurückeingesetzt ergibt sich mit $S_{\mathrm{D}-1} = \frac{2\sqrt{\pi}^{\mathrm{D}-1}}{\Gamma(\frac{\mathrm{D}-1}{2})}$ und die Reflexionseigenschaft [OBC00, Eq.5.5.3] $\Gamma(1-z)\Gamma(z) = \frac{\pi}{\sin\pi z}$ der Gammafunktion

$$\begin{aligned} G &= \frac{(-1)^{\mathrm{D}-1}\pi}{2\mathrm{i}\,\Gamma(1-\frac{\mathrm{D}-1}{2})\Gamma(\frac{\mathrm{D}-1}{2})}\sqrt{\frac{k}{2\pi r}}^{\mathrm{D}-2} H^{(2)}_{\frac{\mathrm{D}-2}{2}}(kr) \\ &= \frac{(-1)^{\mathrm{D}-1}\sin((\mathrm{D}-1)\frac{\pi}{2})}{2\mathrm{i}}\sqrt{\frac{k}{2\pi r}}^{\mathrm{D}-2} H^{(2)}_{\frac{\mathrm{D}-2}{2}}(kr). \end{aligned}$$

Die Abweichung dieses Ergebnisses ist wegen des Faktors $\frac{\sin((\mathrm{D}-1)\frac{\pi}{2})}{2\mathrm{i}}$ falsch, der $\frac{1}{4\mathrm{i}}$ lauten muss. Bei ungeraden D *ergibt sich null: das Integral [OBC00, Eq.10.9.21] und die Eigenschaft [OBC00, Eq.5.5.3] $\Gamma(1-z)\Gamma(z) = \frac{\pi}{\sin\pi z}$ dürfen nicht verwendet werden…*

Wird für μ der Integrationsweg $0 \le \mu \le 1$ verwendet, also einer über ebene Wellen, würde sich statt $H_\nu^{(2)}(kr)$ die Besselfunktion $J_\nu(kr)$ ergeben, und es würden sich statt ausbreitungsfähigen Feldern Stehwellen mit ortsfesten Nullstellen ergeben.

P Laplace-Operator in Kugelkoordinaten

In Kugelkoordinaten ist der Laplace-Operator

$$\begin{aligned} \triangle &= \triangle_r + \triangle_\varphi + \triangle_\vartheta, \qquad (320)\\ \triangle_r &= \left[\frac{\partial^2 r}{\partial x^2}+\frac{\partial^2 r}{\partial y^2}+\frac{\partial^2 r}{\partial z^2}\right]\frac{\partial}{\partial r} + \left[\left(\frac{\partial r}{\partial x}\right)^2+\left(\frac{\partial r}{\partial y}\right)^2+\left(\frac{\partial r}{\partial z}\right)^2\right]\frac{\partial^2}{\partial r^2}\\ \triangle_\varphi &= \left[\frac{\partial^2 \varphi}{\partial x^2}+\frac{\partial^2 \varphi}{\partial y^2}+\frac{\partial^2 \varphi}{\partial z^2}\right]\frac{\partial}{\partial \varphi} + \left[\left(\frac{\partial \varphi}{\partial x}\right)^2+\left(\frac{\partial \varphi}{\partial y}\right)^2+\left(\frac{\partial \varphi}{\partial z}\right)^2\right]\frac{\partial^2}{\partial \varphi^2}\\ \triangle_\vartheta &= \left[\frac{\partial^2 \vartheta}{\partial x^2}+\frac{\partial^2 \vartheta}{\partial y^2}+\frac{\partial^2 \vartheta}{\partial z^2}\right]\frac{\partial}{\partial \vartheta} + \left[\left(\frac{\partial \vartheta}{\partial x}\right)^2+\left(\frac{\partial \vartheta}{\partial y}\right)^2+\left(\frac{\partial \vartheta}{\partial z}\right)^2\right]\frac{\partial^2}{\partial \vartheta^2}. \end{aligned}$$

Die Ableitungen von $r = \sqrt{x^2+y^2+z^2}$ sind (vgl. Polarkoordinatensystem in $\mathbb{R}^2$)

$$\begin{aligned} \frac{\partial r}{\partial x} &= \frac{x}{r}, & \frac{\partial r}{\partial y} &= \frac{y}{r}, & \frac{\partial r}{\partial z} &= \frac{z}{r},\\ \frac{\partial^2 r}{\partial^2 x} &= \frac{1}{r}-\frac{x^2}{r^3}, & \frac{\partial^2 r}{\partial y^2} &= \frac{1}{r}-\frac{y^2}{r^3}, & \frac{\partial^2 r}{\partial z^2} &= \frac{1}{r}-\frac{z^2}{r^3}. \end{aligned}$$

Damit ist $\triangle_r$

$$\triangle_r = \left(\frac{3}{r} - \frac{\cancel{x^2+y^2+z^2}}{\cancel{r^3}}\right)\frac{\partial}{\partial r} + \frac{\cancel{x^2+y^2+z^2}}{\cancel{r^2}}\frac{\partial^2}{\partial r^2} = \frac{2}{r}\frac{\partial}{\partial r} + \frac{\partial^2}{\partial r^2}. \tag{321}$$

Die Ableitungen von $\varphi = \arctan\frac{y}{x}$ sind gleich wie im Polarkoordinatensystem des $\mathbb{R}^2$ mit $r_{xy} := \sqrt{x^2+y^2}$

$$\frac{\partial\varphi}{\partial x} = -\frac{y}{r_{xy}^2}, \qquad \frac{\partial\varphi}{\partial y} = \frac{x}{r_{xy}^2}, \qquad \frac{\partial\varphi}{\partial z} = 0,$$
$$\frac{\partial^2\varphi}{\partial x^2} = \frac{xy}{r_{xy}^3}, \qquad \frac{\partial^2\varphi}{\partial y^2} = -\frac{xy}{r_{xy}^3}, \qquad \frac{\partial^2\varphi}{\partial z^2} = 0.$$

Damit ergibt sich $\triangle_\varphi$ zu

$$\triangle_\varphi = \frac{xy - xy\cancel{\frac{\partial}{\partial\varphi}}}{\cancel{r_{xy}^3}} + \frac{\cancel{r_{xy}^2}}{\cancel{r_{xy}^2}}\frac{\partial^2}{\partial\varphi^2} = \frac{1}{r_{xy}^2}\frac{\partial^2}{\partial\varphi^2} = \frac{1}{r^2\sin^2\vartheta}\frac{\partial^2}{\partial\varphi^2}. \tag{322}$$

Die Ableitungen von $\vartheta = \arccos\frac{z}{r}$ sind mit $\arccos'\zeta = \frac{1}{\sqrt{1-\zeta^2}}$

$$\frac{\partial\vartheta}{\partial x} = \frac{r}{\sqrt{r^2-z^2}}\left(-\frac{z}{r^2}\right)\frac{x}{r} = -\frac{zx}{r_{xy}\,r^2}, \qquad \frac{\partial\vartheta}{\partial y} = -\frac{zy}{r_{xy}\,r^2},$$
$$\frac{\partial\vartheta}{\partial z} = \frac{r}{r_{xy}}\frac{1}{r} - \frac{r}{r_{xy}}\frac{z}{r^2}\frac{z}{r} = \frac{r^2-z^2}{r_{xy}\,r^2} = \frac{r_{xy}}{r^2}.$$

Die Summe der quadrierten ersten Ableitungen ist also

$$\left(\frac{\partial\vartheta}{\partial x}\right)^2 + \left(\frac{\partial\vartheta}{\partial y}\right)^2 + \left(\frac{\partial\vartheta}{\partial z}\right)^2 = \frac{z^2\cancel{(x^2+y^2)}}{\cancel{r_{xy}^2}\,r^4} + \frac{r_{xy}^2}{r^4} = \frac{z^2+r_{xy}^2}{r^4} = \frac{1}{r^2}.$$

Die zweiten Ableitungen sind:

$$\frac{\partial}{\partial x}\left(-\frac{zx}{r_{xy}\,r^2}\right) = -\frac{z}{r_{xy}\,r^2} + \frac{zx}{r_{xy}^2\,r^2}\frac{x}{r_{xy}} + \frac{2zx}{r_{xy}\,r^3}\frac{x}{r}$$
$$= z\frac{-r^2\,r_{xy}^2 + r^2\,x^2 + 2x^2\,r_{xy}^2}{r_{xy}^3\,r^4},$$
$$\frac{\partial}{\partial y}\left(-\frac{zy}{r_{xy}\,r^2}\right) = z\frac{-r^2\,r_{xy}^2 + r^2\,y^2 + 2y^2\,r_{xy}^2}{r_{xy}^3\,r^4},$$
$$\frac{\partial}{\partial z}\left(\frac{r_{xy}}{r^2}\right) = -\frac{2\,r_{xy}}{r^3}\frac{z}{r} = -z\frac{2r_{xy}^4}{r_{xy}^3\,r^4}.$$

In Summe werden sie zu

$$\frac{\partial^2\vartheta}{\partial^2 x} + \frac{\partial^2\vartheta}{\partial^2 y} + \frac{\partial^2\vartheta}{\partial^2 z} = z\frac{-2r^2\,r_{xy}^2 + r^2\,r_{xy}^2 + 2r_{xy}^4 - 2r_{xy}^4}{r_{xy}^3\,r^4} = -\frac{z}{r_{xy}\,r^2} = -\frac{\cos\vartheta}{r^2\,\sin\vartheta}.$$

Der Bestandteil $\triangle_\vartheta$ des Laplace-Operators ist also

$$\triangle_\vartheta = -\frac{\cos\vartheta}{r^2\sin\vartheta}\frac{\partial}{\partial\vartheta} + \frac{1}{r^2}\frac{\partial^2}{\partial\vartheta^2}. \tag{323}$$

Das negative Vorzeichen wird vereinfacht, weil die entsprechende Negation von ϑ unbedeutend ist. Schließlich ist der Laplace-Operator aus Gln. (321), (322) und (323),

$$\triangle = \triangle_r + \triangle_\varphi + \triangle_\vartheta = \frac{2}{r}\frac{\partial}{\partial r} + \frac{\partial^2}{\partial r^2} + \frac{1}{r^2\sin^2\vartheta}\frac{\partial^2}{\partial\varphi^2} + \frac{\cos\vartheta}{r^2\sin\vartheta}\frac{\partial}{\partial\vartheta} + \frac{1}{r^2}\frac{\partial^2}{\partial\vartheta^2}$$

$$= \frac{1}{r^2}\frac{\partial}{\partial r}\left(r^2\frac{\partial}{\partial r}\right) + \frac{1}{r^2\sin^2\vartheta}\frac{\partial^2}{\partial\varphi^2} + \frac{1}{r^2\sin\vartheta}\frac{\partial}{\partial\vartheta}\left(\sin\vartheta\frac{\partial}{\partial\vartheta}\right). \tag{324}$$

Q Separation der Helmholtzgleichung in Kugelkoordinaten

Mit dem Laplace-Operator in Kugelkoordinaten, vgl. Glg. (166), ergibt die Helmholtz-Differentialgleichung, vgl.Glg. (93),

$$\frac{\partial^2 p(\boldsymbol{r})}{\partial r^2} + \frac{2}{r}\frac{\partial p(\boldsymbol{r})}{\partial r} + \frac{1}{r^2\sin\vartheta}\frac{\partial p(\boldsymbol{r})}{\partial\vartheta}\left(\sin\vartheta\frac{1}{r^2\sin^2\vartheta}\right) + \frac{1}{r^2\sin^2\vartheta}\frac{\partial^2 p(\boldsymbol{r})}{\partial\varphi^2} + k^2 p(\boldsymbol{r}) = 0\,.$$

Produktansatz Durch Einsetzen des Ansatzes, vgl. Glg. (167), erhält man

$$\Phi\Theta\frac{d^2R}{dr^2} + \Phi\Theta\frac{2}{r}\frac{dR}{dr} + \frac{1}{r^2}R\Phi\frac{d^2\Theta}{d\vartheta^2} + \frac{\cos\vartheta}{r^2\sin\vartheta}R\Phi\frac{d\Theta}{d\vartheta} + \frac{R\Theta}{r^2\sin\vartheta}\frac{d^2\Phi}{d\varphi^2} + k^2 + R\Phi\Theta = 0 \;\Big|\cdot\frac{r^2\sin^2\vartheta}{R\Phi\Theta}$$

$$\frac{r^2\sin^2\vartheta}{R}\frac{d^2R}{dr^2} + \frac{2r\sin^2\vartheta}{R}\frac{dR}{dr} + \frac{\sin\vartheta}{\Theta}\frac{d^2\Theta}{d\vartheta} + \frac{\cos\vartheta\sin\vartheta}{\Theta}\frac{d\Theta}{d\vartheta} + \frac{1}{\Phi}\frac{d^2\Phi}{d\varphi^2} + k^2r^2\sin^2\vartheta = 0\,.$$

Separation von φ Bringt man die von ϑ und r abhängigen Terme der Gleichung auf die rechte Seite, so ergibt sich

$$\frac{1}{\Phi}\frac{d^2\Phi}{d\varphi^2} = -\frac{r^2\sin^2\vartheta}{R}\frac{d^2R}{dr^2} - \frac{2r\sin^2\vartheta}{R}\frac{dR}{dr} - \frac{\sin\vartheta}{\Theta}\frac{d^2\Theta}{d\vartheta} - \frac{\cos\vartheta\sin\vartheta}{\Theta}\frac{d\Theta}{d\vartheta} - k^2r^2\sin^2\vartheta \stackrel{!}{=} \text{const.} \tag{325}$$

Die linke Seite von Glg. (325) ergibt mit $-\mu^2$ als Seperationskonstante gewöhnliche Differentialgleichung 2.Ordnung mit konstanten Koeffizienten, vgl. Glg. (168),

$$\frac{1}{\Phi}\frac{d^2\Phi}{d\varphi^2} = -\mu^2\,.$$

Separation von ϑ und r Die rechte Seite von Glg. (325) ergibt mit $-\mu^2$ als Seperationskonstante

$$\frac{r^2\sin^2\vartheta}{R}\frac{d^2R}{dr^2}+\frac{2r\sin^2\vartheta}{R}\frac{dR}{dr}+\frac{\sin\vartheta}{\Theta}\frac{d^2\Theta}{d\vartheta}+\frac{\cos\vartheta\sin\vartheta}{\Theta}\frac{d\Theta}{d\vartheta}+k^2r^2\sin^2\vartheta-\mu^2=0 \;\Big|:\sin^2\vartheta$$
$$\frac{r^2}{R}\frac{d^2R}{dr^2}+\frac{2r}{R}\frac{dR}{dr}+\frac{1}{\Theta\sin\vartheta}\frac{d^2\Theta}{d\vartheta}+\frac{\cos\vartheta}{\Theta\sin\vartheta}\frac{d\Theta}{d\vartheta}+k^2r^2-\frac{\mu^2}{\sin^2\vartheta}=0\,.$$

Bringt man die von ϑ abhängigen Terme der Gleichung auf die rechte Seite, so ergibt sich

$$\frac{r^2}{R}\frac{d^2R}{dr^2}+\frac{2r}{R}\frac{dR}{dr}+k^2r^2=-\frac{1}{\Theta\sin\vartheta}\frac{d^2\Theta}{d\vartheta}-\frac{\cos\vartheta}{\Theta\sin\vartheta}\frac{d\Theta}{d\vartheta}+\frac{\mu^2}{\sin^2\vartheta}\stackrel{!}{=}\text{const.} \qquad (326)$$

Die rechten Seite von Glg. (326) ergibt mit $\nu(\nu+1)$ als Seperationskonstante und nach Multiplikation mit Θ die zugeordnete Legendre'sche Differentialgleichung, vgl. Glg. (169),

$$\nu(\nu+1)\Theta=-\frac{1}{\sin\vartheta}\frac{d^2\Theta}{d\vartheta}-\frac{\cos\vartheta}{\sin\vartheta}\frac{d\Theta}{d\vartheta}+\frac{\mu^2}{\sin^2\vartheta}\Theta\,.$$

Die linke Seite von Glg. (326) ergibt mit $\nu(\nu+1)$ als Seperationskonstante und nach Multiplikation mit $\frac{R}{r^2}$ die sphärische Bessel'sche Differentialgleichung, vgl. Glg. (170),

$$\frac{d^2R}{dr^2}+\frac{2}{r}\frac{dR}{dr}+k^2R=\frac{\nu(\nu+1)}{r^2}R\,.$$

References

[AFKW06] R. Avizienis, A. Freed, P. Kassakian, and D. Wessel, "A compact 120 independent element spherical loudspeaker array with programmable radiation patterns," in *120th AES Convention*, Paris, France, 2006.

[AS64] M. Abramowitz and I. A. Stegun, *Handbook of Mathematical Functions*, 1964. [Online]. Available: http://www.math.hkbu.edu.hk/support/aands/toc.htm

[BC39] B. B. Baker and E. T. Copson, *The Mathematical Theory of Huygens' Principle*, 3rd ed. Chelsea Publishing, American Mathematical Society 2001, 1987 (1st edition 1939).

[Beh06] G. Behler, "Sound source with adjustable directivity," in *4th joint ASA ASJ meeting*, Honolulu, Hawaii, 2006.

[Blu33] A. D. Blumlein, "Improvements in and relating to sound-transmission, sound-recording and sound-reproducing systems," *GB patent 394325*, 1933.

[BM71] A. J. Burton and G. F. Miller, "The Application of Integral Equation Methods to the Numerical Solution of Some Exterior Boundary-Value Problems," *Proceedings of the Royal Society of London A*, vol. 323, no. 1553, pp. 201–210, 1971. [Online]. Available: http://rspa.royalsocietypublishing.org

[Boy00] J. P. Boyd, *Chebyshev and Fourier Spectral Methods*. DOVER Publications, 2000.

[Cap69] J. Capon, "High-resolution frequency-wavenumber spectrum analysis," in *Proceedings of the IEEE*, 1969.

[CDV58] H. Clark, G. Dutton, and P. Vanerlyn, "The 'stereosonic' recording and reproduction system," *reprinted in the Journal of the Audio Eng. Soc., from Proceedings of the Institution of Electrical Engineers, 1957*, vol. 6, no. 2, pp. 102–117, 1958.

[CG77] P. Craven and M. A. Gerzon, "Coincident microphone simulation covering three dimensional space and yielding various directional outputs," *U.S. Patent*, no. 4,042,779, 1977.

[CR12] I. CVX Research, "CVX: Matlab software for disciplined convex programming, version 2.0," http://cvxr.com/cvx, Aug. 2012.

[CS72] D. H. Cooper and T. Shiga, "Discrete-matrix multichannel stereo," *J. Audio Eng. Soc.*, vol. 20, no. 5, pp. 346–360, 1972.

[Dan00] J. Daniel, *Représentation des champs acoustiques, application à la transmission et à la reproduction de scènes sonores complexes dans un contexte multimédia*. Thèse de doctorat, 2000.

[Deb10] D. Deboy, "Acoustic centering and rotational tracking in surrounding spherical microphone arrays," Master's thesis, Kunstuni/TU Graz, 2010.

[DGS77] P. Deslarte, J.-M. Goethals, and J. J. Seidel, "Spherical codes and designs," *Geometriae Dedicata*, vol. 6, no. 3, 1977.

[DH94] J. R. Driscoll and D. M. J. Healy, "Computing fourier transforms and convolutions on the 2-sphere," *Advances in Applied Mathematics*, vol. 15, 1994.

[DRP99] J. Daniel, J.-B. Rault, and J.-D. Polack, "Acoustic properties and perceptive implications of stereophonic phenomena," in *AES 6th Int. Conf.: Spatial Sound Reproduction*, 1999.

[Duf01] D. G. Duffy, *Green's Functions with Applications*. CRC Press, 2001.

[EJZ14] N. Epain, C. T. Jin, and F. Zotter, "Ambisonic decoding with constant angular spread," *Acta Acustica united with Acustica*, vol. 100, no. 5, 2014.

[Faz10] F. Fazi, "Sound field reproduction," Ph.D. dissertation, ISVR, University of Southampton, 2010.

[Fel74] P. Felgett, "Ambisonic reproduction of directionality in surround-sound systems," *Nature*, vol. 252, pp. 534–538, 1974.

[Fle88] H. Fleischer, *Fourier-Akustik: Beschreibung der Schallstrahlung von ebenen Schwingern mit Hilfe der räumlichen Fourier-Methode*, ser. Fortschritt-Berichte VDI, Reihe 11, Schwingungstechnik, Nr. 101. VDI-Verlag, 1988.

[FN12] F. M. Fazi and P. A. Nelson, "Nonuniqueness of the solution of the sound field reproduction problem with boundary pressure control," *Acta Acustica united with Acustica*, vol. 98, no. 1, pp. 1–14, 2012. [Online]. Available: http://www.ingentaconnect.com/content/dav/aaua

[Fra13a] M. Frank, "Source width of frontal phantom sources: Perception, measurement, and modeling," *Archives of Acoustics*, vol. 38, no. 3, pp. 311–319, 2013.

[Fra13b] ——, "Phantom sources using multiple loudspeakers in the horizontal plane," PhD Thesis, Kunstuni Graz, 2013.

[Fra14a] ——, "How to make ambisonics sound good," in *Forum Acusticum, Krakow*, 2014.

[Fra14b] ——, "Localization using different amplitude-panning methods in the frontal horizontal plane," in *EAA Symposium on Auralization and Ambisonics, Berlin*, 2014.

[FSZ08] M. Frank, A. Sontacchi, and F. Zotter, "Localization experiments using different 2d ambisonic decoders," in *25th Tonmeistertagung*, 2008.

[FZ17] M. Frank and F. Zotter, "Exploring the perceptual sweet area in ambisonics," in *AES 142nd Conv.*, 2017.

[GB08] M. Grant and S. Boyd, "Graph implementations for nonsmooth convex programs," in *Recent Advances in Learning and Control*, ser. Lecture Notes in Control and Information Sciences, V. Blondel, S. Boyd, and H. Kimura, Eds. Springer-Verlag Limited, 2008, pp. 95–110, http://stanford.edu/~boyd/graph_dcp.html.

[Ger75] M. A. Gerzon, "The design of precisely coincident microphone arrays for stereo and surround sound," in *prepr. L-20 of 50th Audio Eng. Soc. Conv.*, 1975.

[Ger92] M. Gerzon, "General metatheory of auditory localization," in *prepr. 3306, Conv. Audio Eng. Soc.*, 1992.

[Ger07] U. H. Gerlach, *Linear Mathematics in Infinite Dimensions: Signals, Boundary Value Probelems, and Special Functions*. Beta Edition online, 2007. [Online]. Available: http://www.math.ohio-state.edu/~gerlach/math/BVtypset/

[GHB+05] K. M. Górski, E. Hivon, A. J. Banday, B. D. Wandelt, F. K. Hansen, M. Reinecke, and M. Bartelmann, "Healpix: A framework for high-resolution discretization and fast analysis of data distributed on the sphere," *The Astrophysical Journal*, vol. 622, pp. 759–771, 2005. [Online]. Available: http://healpix.jpl.nasa.gov

[GK65] G. Golub and W. Kahan, "Calculating the singular values and pseudo-inverse of a matrix," *SIAM Numer. Anal.*, vol. 2, no. 2, pp. 205–224, 1965.

[GP11] M. Gräf and D. Potts, "On the computation of spherical designs by a new optimization approach based on fast spherical fourier transforms," *Numer. Math.*, vol. 119, 2011. [Online]. Available: http://homepage.univie.ac.at/manuel.graef/quadrature.php

[Gre28] G. Green, *An Essay on the Application of mathematical Analysis to the theories of Electricity and Magnetism*, Facsimile-Druck in 100

Exemplaren, Berlin, 1889 ed. Nottingham, 1828. [Online]. Available: http://books.google.at/books

[HC37] D. Hilbert and R. Courant, *Methoden der mathematischen Physik II*. Springer Berlin, 1937.

[HG06] A. Hjørunges and D. Gesbert, "Complex-valued matrix differentiation: Techniques and key results," *IEEE Transaction on Signal Processing*, 2006.

[Hoh09] F. Hohl, "Kugelmikrofonarray zur abstrahlungsvermessung von musikinstrumenten," Master's thesis, Kunstuni/TU Graz, 2009.

[HS96] R. H. Hardin and N. J. A. Sloane, "Mclaren's improved snub cube and other new spherical designs in three dimensions," *Discrete and Computational Geometry*, vol. 15, pp. 429–441, 1996. [Online]. Available: http://neilsloane.com/sphdesigns/dim3/

[Huy90] C. Huygens, *Traité de la Lumière*. Gauthier-Villars Et C-ie Editeurs, Paris, 1920 (reprint of original 1690), gallica, Bibliotèque Numérique. [Online]. Available: http://galicia.bnf.fr

[Jes73] M. Jessel, *acoustique théorique: propagation et holophonie*. Paris: Masson, 1973.

[Juh93] P.-M. Juhl, "The boundary element method for sound field calculations," PhD Thesis, University of Denmark, 1993.

[KA12] T. Kimura and H. Ando, "Listening test for three-dimensional audio system based on multiple vertical panning," in *Aoustics-12, Hong Kong*, 2012.

[KA14] ——, "3d audio system using multiple vertical panning for large-screen multiview 3d video display," *ITE Transactions on Media Technology and Applications*, vol. 2, no. 1, pp. 33–45, January 2014.

[Ker10] M. Kerscher, "Compact spherical loudspeaker array for variable sound-radiation," Master's thesis, Kunstuni/TU Graz, 2010.

[Kir83] G. R. Kirchhoff, "Zur Theorie der Lichtstrahlen," *Annalen der Physik*, vol. 254, no. 4, 1883, Universal Multimedia Electronic Library (UrMEL), Thüringer Universitäts- und Landesbibliothek Jena (ThULB). [Online]. Available: http://zs.thulb.uni-jena.de/

[Kre99] E. Kreyszig, *Advanced Engineering Mathematics*, 8th ed. Wiley, 1999.

[KT14] A. Komnik and E. G. Tsitsishvili, Eds., *Komplexe Integration*. Springer Berlin Heidelberg, 2014.

[KW04] P. Kassakian and D. Wessel, "Characterization of spherical loudspeaker arrays," San Francisco, CA, 2004, p. Convention paper #1430.

[LC57] D. M. Leakey and E. C. Cherry, "Influence of noise upon the equivalence of intensity differences and small time delays in two-loudspeaker systems," *J. Acoust. Soc. Am.*, no. 29, pp. 284?–286, 1957.

[Li05] Z. Li, "The capture and recreation of 3d auditory scenes," PhD Thesis, University of Maryland, College Park, 2005.

[LR13] H. Lee and F. Rumsey, "Level and time panning of phantom images for musical sources," *J. Audio Eng. Soc.*, vol. 61, no. 12, pp. 978–988, 2013.

[LS75] A. G. Law and M. B. Sledd, "Normalizing orthogonal polynomials by using their recurrence coefficients," *Proc. American Mathematical Society*, vol. 48, no. 2, pp. 505–507, 1975.

[LZ15] S. Lösler and F. Zotter, "Comprehensive radial filter design for practical higher-order ambisonic recording," in *Fortschritte der Akustik – DAGA Nürnberg*, 2015.

[ME02] J. Meyer and G. Elko, "A highly scalable spherical microphone array based on an orthonormal decomposition of the soundfield," in *Acoustics, Speech, and Signal Processing, 2002. Proceedings.(ICASSP'02). IEEE International Conference on*, vol. 2, Orlando, FL, USA, 2002.

[MN02] P. Majdak and M. Noisternig, *Implementation Kopfpositionsbezogener Binauraltechnik*. Diplomarbeit, 2002.

[Mor06] S. Moreau, "Étude et réalisation d'outils avancés d'encodage spatial pour la technique de spatialisation sonore Higher Order Ambisonics: microphone 3d et contrôle de distance," PhD Thesis, Université du Maine, 2006.

[Mös88] M. Möser, *Analyse und Synthese akustischer Spektren*. Springer-Verlag, 1988.

[Mös09] M. Möser, *Technische Akustik*. Springer, 2009.

[MWCQ99] G. Martin, W. Woszczyk, J. Corey, and R. Quesnel, "Sound source localization in a five-channel surround sound reproduction system," in *prepr. 4994, Conv. Audio Eng. Soc.*, 1999.

[OBC00] F. W. J. Olver, R. F. Boisvert, and C. W. Clark, Eds., *NIST Handbook of Mathematical Functions*. Cambridge, UK: Cambridge University Press, 2000, http://dlmf.nist.gov, accessed June 2012.

[ODZ08] A. O'Donovan, R. Duraiswami, and D. Zotkin, "Imaging concert hall acoustics using visual and audio cameras," in *Proceedings of the ICASSP*, 2008.

[OSB99] A. V. Oppenheim, R. W. Schafer, and J. R. Buck, *Discrete-Time Signal Processing*. Prentice Hall, 1999.

[Pas10] A. M. Pasqual, "Sound directivity control in a 3-d space by a compact spherical loudspeaker array," Ph.D. dissertation, Unicamp, Campinas, Brazil, 2010.

[Pet04] S.-O. Petersen, "Localization of sound sources using 3d microphone array," Master's Thesis, University of South Denmark, Odense, Sept 2004. [Online]. Available: oscarpetersen.dk

[Ple09] P. Plessas, "Rigid sphere microphone arrays for spatial recording and holography," Master's thesis, Kunstuni/TU Graz, 2009.

[Pol05] M. A. Poletti, "Three-dimensional surround sound systems based on spherical harmonics," *Journal of the Audio Engineering Society*, 2005.

[Pol07] M. Pollow, "Variable directivity of dodecahedron louspeakers," M. Thesis, Institut für Technische Akustik, RWTH-Aachen, Aachen, D, 2007.

[Pol16] A. Politis, "Microphone array processing for parametric spatial audio techniques," Ph.D. dissertation, Aalto University, Helsinki, 2016.

[Pom08] H. Pomberger, "Angular and radial directivity control for spherical loudspeaker arrays," Thesis, Institut für Elektronische Musik und Akustik, Kunstuni Graz, Technical University Graz, Graz, A, 2008.

[PR05] M. Park and B. Rafaely, "Sound-field analysis by plane-wave decomposition using spherical microphone array," *Journal of the Acoustical Society of America*, vol. 118, pp. 3094–3103, Aug 2005.

[Pul97] V. Pulkki, "Virtual sound source positioning using vector base amplitude panning," *J. Audio Eng. Soc.*, vol. 45, no. 6, pp. 456–466, 1997.

[Pul99] ——, "Uniform spreading of amplitude panned virtual sources," in *Proc. Applications of Signal Processing to Audio and Acoustics, IEEE*, 1999.

[Pul01] ——, "Localization of amplitude-panned virtual sources ii: Two- and three-dimensional panning," *J. Audio Eng. Soc.*, vol. 49, no. 9, pp. 753–767, 2001.

[Pul03] ——, "Compensating displacement of amplitude-panned virtual sources," in *22nd Conf. Audio Eng. Soc.*, 2003.

[Raf05] B. Rafaely, "Analysis and design of spherical microphone arrays," *IEEE Transactions on Speech and Audio Processing*, 2005.

[RFZN16] M. Romanov, M. Frank, F. Zotter, and T. Nixon, "Manipulations improving amplitude panning on small standard loudspeaker arrangements for surround with height," in *Tonmeistertagung*, 2016.

[RSZ95] E. A. Rakhmanov, E. B. Saff, and Y. M. Zhou, "Electrons on the sphere," *Computational Methods and Function Theory*, 1995.

[SBvW14] P. Stitt, S. Bertet, and M. v. Walstijn, "Off-centre localisation performance of ambisonics and hoa for large and small loudspeaker array radii," *Acta Acustica united with Acustica*, vol. 100, no. 5, pp. 937–944, 2014.

[Sch68] H. A. Schenck, "Improved Integral Formulation for Acoustic Radiation," *Journal of the Acoustical Society of America*, vol. 44, no. 1, pp. 41–58, 1968. [Online]. Available: http://asadl.org/jasa

[Sch12a] P. Schmidt, "Improvements in localisation of planar acoustic holography," Master's thesis, University of Music and Performing Arts, Graz, 2012.

[Sch12b] B. Schnizer, *Analytische Methoden in der Physik*. Vorlesung an der TU Graz, Institut für Technische Physik, 2012. [Online]. Available: http://itp.tugraz.at/~schnizer/AnalyticalMethods/

[SK97] E. Saff and A. B. J. Kuijlaars, "Distributing many points on a sphere," *The Mathematical Intelligencer*, vol. 19, pp. 523–538, 1997.

[SMR09] L. Simon, R. Mason, and F. Rumsey, "Localisation curves for a regularly-spaced octagon loudspeaker array," in *prepr. 7015, Conv. Audio Eng. Soc.*, 2009.

[Sne94] N. Sneeuw, "Global spherical harmonic analysis by least-squares and numerical quadrature methods in historical perspective," *Geophysical Journal International*, vol. 118, pp. 707–716, 1994.

[Som92] A. Sommerfeld, *Vorlesungen über Theoretische Physik (Band 6) Partielle Differentialgleichungen in der Physik*, 6th ed. Harri-Deutsch, 1978 (reprint 1992).

[Son00] A. Sontacchi, *Neue Ansätze der Schallfeldreproduktion*. Dissertation, 2000.

[SRA08] S. Spors, R. Rabenstein, and J. Ahrens, "The theory of wave field synthesis revisited," in *124th AES Convention, Amsterdam*, 2008.

[SW04] I. H. Sloan and R. S. Womersley, "Extremal systems of points and numerical integration on the sphere," *Advances in Computational Mathematics*, vol. 21, pp. 107–125, 2004.

[SZ15] S. Spors and F. Zotter, "Foundations and practical aspects of sound field synthesis," in *Tutorial 138th AES Convention*, 2015.

[TP77] G. Theile and G. Plenge, "Localization of lateral phantom sources," *J. Audio Eng. Soc.*, vol. 25, no. 4, pp. 96–200, 1977.

[vH60] H. von Helmholtz, "Theorie der Luftschwingungen in Röhren mit offenen Enden," *Journal für die reine und angewandte Mathematik*, no. 57, pp. 1–72, 1860, niedersächsische Staats- und Universitätsbibliothek, Digitalisierungszentrum, 37070 Göttingen. [Online]. Available: http://gdz.sub.uni-goettingen.de

[WA80] G. Weinreich and E. B. Arnold, "Method for measuring acoustic radiation fields," *Journal of the Acoustical Society of America*, vol. 68, 08/1980 1980.

[WDC97] O. Warusfel, P. Derogis, and R. Causse, "Radiation synthesis with digitally controlled loudspeakers," in *103rd AES Convention, Paris*, 1997.

[Wen63] K. Wendt, "Das Richtungshören bei Überlagerung zweier Schallfelder bei Intensitäts- und Laufzeitsterophonie," Ph.D. dissertation, RWTH-Aachen, 1963.

[Wen13] F. Wendt, "Untersuchung von phantomschallquellen vertikaler lautsprecheranordnungen," Master's thesis, Kunstuni Graz, 2013.

[Wey19] H. Weyl, "Ausbreitung elektromagnetischer wellen über einem ebenen leiter," *Annalen der Physik*, 1919.

[WFZ13] F. Wendt, M. Frank, and F. Zotter, "Panning with height on 2, 3, and 4 loudspeakers," in *Proc. ICSA, Erlangen*, 2013.

[Wik10] "Bessel function," 2010. [Online]. Available: http://en.wikipedia.org/wiki/Bessel_function

[Wil99] E. G. Williams, *Fourier Acoustics*. Academic Press, 1999.

[ZF12] F. Zotter and M. Frank, "All-round ambisonic panning and decoding," *Journal of the Audio Eng. Soc.*, 2012.

[ZF15] ——, "Generalized tangent law for horizontal pairwise amplitude panning," in *Proc. of the 3rd ICSA, Graz*, 2015.

[ZH07] F. Zotter and R. Höldrich, "Modeling radiation synthesis with spherical loudspeaker arrays," in *Proceedings of the ICA*, Madrid, 02/09/2007 2007.

[ZN07] F. Zotter and M. Noisternig, "Near- and far-field beamforming using spherical loudspeaker arrays," in *Proc. of the 3rd Alps Adria Acoustics Congress*, Graz, 27/09/2007 2007.

[Zot09a] F. Zotter, *Analysis and Synthesis of Sound-Radiation with Spherical Arrays*. Doktorarbeit, 2009.

[Zot09b] ——, "Sampling strategies for acoustic holography/holophony on the sphere," in *NAG-DAGA, Rotterdam*, 2009.

[ZPF09] F. Zotter, H. Pomberger, and M. Frank, "An alternative ambisonics formulation: Modal source-strength matching and the effect of spatial aliasing," in *126th AES Convention, Munich*, 2009.

[ZPN12] F. Zotter, H. Pomberger, and M. Noisternig, "Energy preserving ambisonic decoding," *Acta Acustica United with Acustica*, 2012.

[ZPS08] F. Zotter, H. Pomberger, and A. Schmeder, "Efficient directivity pattern control for spherical loudspeaker arrays," in *ACOUSTICS08*, 2008.

[ZS13] F. Zotter and S. Spors, "Is sound field control determined at all frequencies? how is it related to numerical acoustics?" in *52nd AES Conf., Sound Field Control*, Guildford, 2013.